universität
wien

DISSERTATION

Titel der Dissertation

SEDIMENTOLOGY AND BASIN ANALYSIS OF THE THAKKHOLA-MUSTANG GRABEN, CENTRAL NEPAL

Verfasser

Basanta Raj ADHIKARI, M. Sc.

angestrebter akademischer Grad

Doktor der Naturwissenschaften (Dr. rer. nat.)

Om Mani Padme Hum

"Purity must be achieved by an indivisible unity of method and wisdom, symbolized by the final syllable hum, which indicates indivisibility"

ACKNOWLEDGEMENT

DEDICATION

This dissertation is dedicated to my grandmother; Tilottama Adhikari, my parents; Lok Raj Sharma Adhikari and Sharada Biddhya Adhikari, and my sisters; Kalpana and Srijana, for their patience, love and unconditional support.

CONTENTS

LIST OF ABBREVIATIONS

$\delta^{18}O$ = Stable Oxygen isotope ratio

$\delta^{13}C$ = Stable Carbon isotope ratio

SH = Sub-Himalaya

LH = Lesser Himalaya

HHC = Higher Himalayan Crystalline

TTZ = Tibetan Tethys Zone

ITSZ =Inuds-Tsangpo Suture Zone

STDS = South Tibetan Detachment System

MSL = Means sea level

MFT = Main Frontal Thrust

MBT = Main Boundary Thrust

MCT = Main Central Thrust

XRD = X-ray diffraction

VPDB = Vienna PeeDee Belemnite

LM = Light microscope

SEM = Scanning Electron Microscope

LIST OF FIGURES

CHAPTER FOUR
FACIES ANALYSIS

CHAPTER FIVE
PETROGRAPHY AND MINERALOGY

CHAPTER SIX

STABLE ISOTOPE ANALYSIS

CHAPTER SEVEN

HEAVY MINERAL ANALYSIS

CHAPTER EIGHT

POLLEN ANALYSIS

CHAPTER NINE
DISCUSSION

Abstract

The Thakkhola-Mustang Graben, which reflects Neogene extensional tectonics in the Tibetan Plateau and Himalaya, lies north of the Dhaulagiri-Annapurna ranges and south of the Yarlung-Tsangpo Suture Zone. The basement to the graben comprises Tibetan-Tethyan sedimentary rocks of Paleozoic and Mesozoic ages, unconformably overlain by continental, mainly coarse-grained deposits (more than 850 m thick) of Neogene to Quaternary age. Stratigraphically, the Thakkhola-Mustang Graben sediments have been divided into five formations, namely, from the base upwards, the Tetang, Thakkhola, Sammargaon, Marpha and Kaligandaki formations. The Miocene Tetang and Thakkhola formations are disconformably overlain by the Plio-Pleistocene Sammargaon and Marpha formations. The Kaligandaki Formation, of Holocene age, has a cut-and-fill relationship with the underlying Marpha Formation. The Thakkhola and Tetang formations are separated by a low-angle (~5°) unconformity. Previous researchers studied the basement geology and stratigraphy of the Neogene sediments. However, Neogene paleoclimatic conditions, sediment provenance and the depositional environment(s) of the Neogene sediments have not been investigated in detail previously.

To address these problems, detailed field mapping was undertaken on both sides of the Kali gandaki River, in conjunction with lithostratigraphic and sedimentological logging of 22 profiles and measuring imbricate pebble orientations. Heavy mineral analyses (50 samples), stable isotope and thin-section analyses of carbonate rocks, palynological investigations (30 samples), compositional analyses of sediments and petrographic studies of sandstones for provenance analysis were also carried out. Facies analysis was done by studying vertical and lateral sedimentary variations within the basin. Provenance analysis was carried out by analyzing heavy minerals, paleocurrent analysis and bulk mineralogical analysis (using X-ray diffraction and sandstone petrography). The Neogene paleoclimate was inferred from oxygen and carbon stable isotopes from carbonate lithologies and from palynological data.

In the study area, 12 different lithofacies were found in three lithofacies associations. The associations are (1) matrix-rich conglomerate-gravelly sandstone association, (2) matrix-rich conglomerate with sandstone and mudstone and (3) massive siltstone with mudstone, alternating with carbonate layers. The investigation revealed that the sediments were deposited in alluvial fan, lacustrine, braided river and glacio-fluvial environments. Small braided river systems were dominant in the initial depositional phase of the Tetang Formation whereas a lacustrine environment was widespread in a later stage. Braided fluvial deposits and lacustrine deposits at different levels of the sedimentary succession dominate the Thakkhola Formation. The Sammargaon Formation is associated with glacial tills. The Marpha Formation is interpreted as glacio-lacustrine deposits. The Kaligandaki Formation was deposited in a fluvial environment.

The paleocurrent data of imbricate pebbles from all formations of the basin show a generally southward flow direction. At Dhi and Tange, the Thakkhola Formation consists of clasts derived mainly from the Mesozoic rock exposed to the east. In the Ghiling, Dhakmar and Chaile areas, the Thakkhola Formation is represented by the clasts of Paleozoic, Mesozoic and Tertiary rocks. They indicate the paleoflow from the north and west. The conglomerates of the Tetang Formation comprise mostly Mesozoic rocks with an easterly provenance. Minerals from low-to high-grade metamorphic sources are reflected in the heavy mineral assemblages of the Neogene deposits. Bulk compositional analysis of the sediments of the Thakkhola-Mustang Graben reflect the presence of quartz, calcite, muscovite, and chlorite with minor amounts of halite and clay minerals in some samples. Sandstones of the Thakkhola Formation are characterized by a high amount of quartz, low feldspar contents and low to moderate amounts of unstable lithic grains. Polycrystalline quartz with metamorphic rock fragments in lithic grains indicate a granitic source as well as sedimentary and low-grade metamorphic source terrains.

Pelletal, charophytic algae and oncolitic algal micritic limestones are present in the Thakkhola Formation. In the Tetang Formation micritic limestone with ostracods, micritic mudstone with roots and oncolites have been found. There appear also sporadic quartz clasts in the limestone. These features suggest that these limestones were developed in a lacustrine environment a considerable distance away from the river-mouth. Ostracods in dark micritic limestone indicate quite and calm water conditions. Although a very thick (850 m) pile of sediments was deposited in the Thakkhola-Mustang Graben, limestone microfabrices indicate a flat shallow lacustrine environment. The δ^{18}O values of the limestones from the Thakkhola-Mustang Graben are very similar to those obtained from the recent meteoric water analyzed by previous researchers from the area, indicating that the Thakkhola-Mustang Graben attained its current elevation prior to east-west tectonic extension of the Himalaya. The relatively high δ^{13}C values of the carbonates suggest that the Himalaya existed as an orthographic barrier to moisture already during the Miocene period.

A palynological study shows that the sediments of Tetang and Thakkhola formation (Miocene-Pliocene) contain pollen of dominantly alpine trees such as *Pinus, Picea, Tsuga* and *Quercus,* with some steppe elements such as *Artemisia, Compositae, Chenopodiaceae, Plantago* and *Poaceae*. These indicate a dry climate during sediment deposition. Consequently, it is presumed that the paleoclimate during the evolution of the Thakkhola-Mustang Graben was significantly warmer than the present-day climate.

Kurzfassung

Der Thakkhola-Mustang Graben, der eine neogene Extensionstektonik im Tibetischen Plateau und Himalaya belegt, liegt nördlich der Dhaulagiri-Annapurna Kette und südlich der Yarlung-Tsangpo Suturzone. Das Basement des Grabens bilden paläozoisch-mesozoische Sedimente der Tibet-Tethys Zone, die von kontinentalen, vor allem grobkörnigen Ablagerungen (über 850 mächtig) des Neogens bis Quartärs diskordant überlagert werden. Lithostratigrahisch wurden die Ablagerungen des Thakkhola-Mustang Grabens vom Liegenden zum Hangenden in 5 Formationen unterteilt: Tetang-, Thakkhola-, Sammargaon-, Marpha- und Kaligandaki-Formation. Die miozänen Tetang- und Thakkhola-Formationen werden diskordant von den plio-pleistozänen Sammargaon- und Marpha-Formationen überlagert. Die holozäne Kaligandaki-Formation hat eine scharfe erosive Basis zur unterlagernden Marpha-Formation. Die Tetang- und Thakkhola-Formationen werden durch eine flache Winkeldiskordanz (~5°) getrennt. Frühere Bearbeiter habe die Basementgeologie und die Stratigraphie der neogenen Sedimente untersucht. Detaillierte Untersuchungen zum neogenen Paläoklima, zur Sedimentherkunft und der Ablagerungsmilieus der neogenen Sedimente fehlen bisher.

Zur Durchführung dieser Untersuchungen wurden deatillierte Geländeaufnahmen an beiden Seiten des Kali gandaki Flusses durchgeführt, 22 lithostratigraphische und sedimentologische Profile aufgenommen und Geröllimbrikationen vermessen. Schwermineraluntersuchungen (50 Proben), Dünnschliffanalysen und stabile Isotopenuntersuchungen an Karbonatgesteinen, palynologische Untersuchungen (30 Proben), Komponentenbestand an Sedimenten und petrographische Untersuchungen an Sandsteinen zur Identifikation von Herkunftsgebieten durchgeführt. Eine Faziesanalyse wurde durchgeführt und vertikale und laterale Änderungen der Sedimente erfasst. Herkunftsgebiete wurden mit Hilfe von Schwermineralanalysen, Paläoströmungsmessungen und mineralogischen Analysen (Röntgendiffraktometrie, Sandsteinpetrographie) identifiziert. Information zum neogenen Paläoklima wurden aus der Analyse von Sauerstoff- und Kohlenstoffisotopen und aus den palynologischen Daten gewonnen.

Im Untersuchungsgebiet konnten 12 unterschiedliche Lithofazies in 3 Lithofaziesassoziationen unterschieden werden. Die Assoziationen sind (1) matrix-reiche Konglomerate-kiesige Sandsteine, (2) matrix-reiche Konglomerate mit Sandsteinen und Tonsteinen, und (3) massive Siltsteine mit Tonsteinen und Karbonatlagen. Die Untersuchungen zeigen, dass die Sedimente in Alluvialfächern, in Seen, in Braided Rivers und in glazio-fluviatilen Environments abgelagert wurden. Kleine Braided River Systeme dominierten die basale Ablagerungsphase der Tetang-Formation, während später lakustrine Environments vorherrschten. Braided fluviatile Ablagerungen und lakustrine Ablagerungen in verschiedenen Horizonten dominieren die Thakkhola-Formation. Die Sammargaon-Formation zeigt glazialen Till. Die Marpha-Formation wird als glazio-lakustrine Ablagerung interpretiert. Die Kaligandaki-Formation wurde in einem fluviatilen Environment abgelagert. Die Paläoströmungsdaten von Geröllimbrikationen aller Formationen zeigen generell Transportrichtungen nach Süden. Bei Dhi und Tange besteht die Thakkhola-Formation aus Geröllen mesozoischer Gesteine, die heute vorwiegend im Osten des Grabens anstehen. In

Gebiet von Ghiling, Dhakmar und Chaile wird die Thakkhola-Formation von einer Mischung aus paläozoischen, mesozoischen und tertiären Gesteinskomponenten charakterisiert. Sie weisen auf Paläotransport aus Nord bis West hin. Die Konglomerate der Tetang-Formation setzen sich vorwiegend aus mesozoischen Gesteinen mit einer Herkunft aus östlichen Gebieten zusammen. Niedrig- bis hochmetamorphe Liefergebiete zeigen die Schwermineralzusammensetzungen der neogenen Sedimente. Generell sind die Sedimente des Thakkhola-Mustang Grabens durch Quarz, Kalzit, Muskowit und Chlorit und geringen Anteilen in manchen Proben von Halit und Tonmineralen zusammengesetzt. Die Sandsteine zeigen hohe Anteile an Quarz, geringe Feldspatgehalte und geringe bis mittlere Gehalte an instabilen lithischen Fragmenten zusammen. Polykristalliner Quarz und metamorphe Gesteinsfragmente zeigen granitische Qellen sowie Sedimentgesteine und niedrig-gradig metamorphe Herkunftsgebiete.

Pellets, charophytische Algen und onkolithische Algenmikrite sind häufig in der Thakkhola-Formation. In der Tetang-Formation wurden mikritische Kalke mit Ostrakoden, mikritische Tonsteine mit Wurzelstrukturen und Onkolithe gefunden. Sporadisch treten Quarzklasten in den Kalken auf. Die Kalke entwickelten sich in einem lakustrinen Ablagerungsraum mit einiger Entfernung zu einer Flussmündung. Die Ostrakoden belegen ruhige Stillwasserbedingungen. Obwohl die Sedimentabfolge mächtig ist, werden auf Grund der Kalkmikrofazies flache lakustrine Environments interpretiert. Die δ18O Werte der Kalke des Thakkhola-Mustang Grabens sind sehr ähnlich jenen von publiziertem rezentem meteorischen Wasser des Gebietes. Das belegt, dass der Thakkhola-Mustang Graben schon vor der Ost-West-extensionsphase seine heutige Höhenlage erreicht hatte. Die relativ hohen δ13C Werte der Karbonate weisen darauf hin, dass der Himalaya im Miozän schon als orthographische Barriere gegen Feuchtigkeitstransport gewirkt hat.

Palynologische Untersuchungen zeigen, dass die Sedimente der Tetang- und Thakkhola-Formation (Miozän-Pliozän) dominant Pollen Alpiner Bäume beinhalten, u.a. *Pinus, Picea, Tsuga u*nd *Quercus,* dazu kommen Steppenelemente wie z.B. *Artemisia, Compositae, Chenopodiaceae, Plantago* und *Poaceae*. Die letzteren sprechen für ein trockenes Klima während der Ablagerung. Es wird auf ein signifikant wärmeres Paläoklima während der Sedimentation im Thakkhola-Mustang Graben im Vergleich zu heute geschlossen

CHAPTER ONE
INTRODUCTION

1.1 Introduction

The Himalaya provides an outstanding field laboratory for studies of lithospheric dynamics and of the effects of large-scale topography on the earth's atmosphere and climate. For at least 40 million years, the Indian subcontinent has been penetrating deeper and deeper into the rest of Asian landmass. Because of tectonic movement in Himalaya, many structures were formed. Tectonomorphologically, the whole Himalaya can be divided into different longitudinal units having unique stratigraphy and evolutionary characteristics (Gansser, 1964). From south to north, these different units are the Sub-Himalaya (SH), Lesser Himalaya (LH), Higher Himalayan Crystallines (HHC), Tibetan Tethyan Zone (TTZ) and Indus-Tsangpo Suture Zone (ITSZ), respectively.

Among those manifold structures, the Tibetan Plateau comprises the highest terrain in Asia and many researchers gave their attention on this part of the area because this area gives key concepts for continental dynamics. It lies between the Kunlun Mountains and the Himalaya and it is a region of tangled mountains that rises 4000 to 5000 m above the mean sea level. The plateau is nearly 80 km in thickness, which is the earth's largest and highest plateau with a flat interior disrupted by active normal faults. Tibet is no mean tribute to the Indian subcontinents strength and persistence, but the most spectacular consequence of the collision between the subcontinent and the rest of Asia is the world's tallest mountain range - the Himalaya (Molnar, 1986). Active deformation in Tibet is characterized by approximately north-striking normal faults and kinematically linked strike-slip faults (Molnar and Tapponnier, 1978; Rothery and Drury, 1984; Armijo et al., 1986, 1989).

Despite ongoing India-Asia convergence, late Cenozoic normal faults extend from the Himalaya in the south to the Kunlun fault in the north and from a long ~ 78° in the west to the Namche Barwa Syntaxis in the east (Tapponnier et al., 2001) (Fig. 2.3). Most of the Tibetan rifts are filled up with Plio-Quaternary coarse-grained deposits, and cut at high-angle older ~EW basins with Miocene deposits (Armijo et al., 1986, 1989). Garzione et al. (2000) stated that the Thakkhola-Mustang Graben developed earlier than Miocene probably in connection with strike-slip along the Karakoram and Jaili faults (Fig. 3.1).

The Thakkhola-Mustang Graben is a unique structure because this graben represents the Cenozoic extensional tectonic phase of the Tibetan Plateau and the whole Himalaya. The Thakkhola-Mustang Graben is located to the north of the Dhaulagiri and Annapurna Ranges and south of the Indus-Tsangpo Suture Zone (ITSZ) (Gansser, 1964; Hagen, 1959, 1968; Bordet et al., 1971, 1975). The graben is framed by Paleozoic and Mesozoic sediments or metasediments of the Tethyan series and is filled up by a thick sedimentary succession of probably Miocene to Plio-Pleistocene

age, mainly the Tetang and Thakkhola formations (Colchen et al., 1980, 1986; Fort et al., 1982; Yoshida et al., 1984).
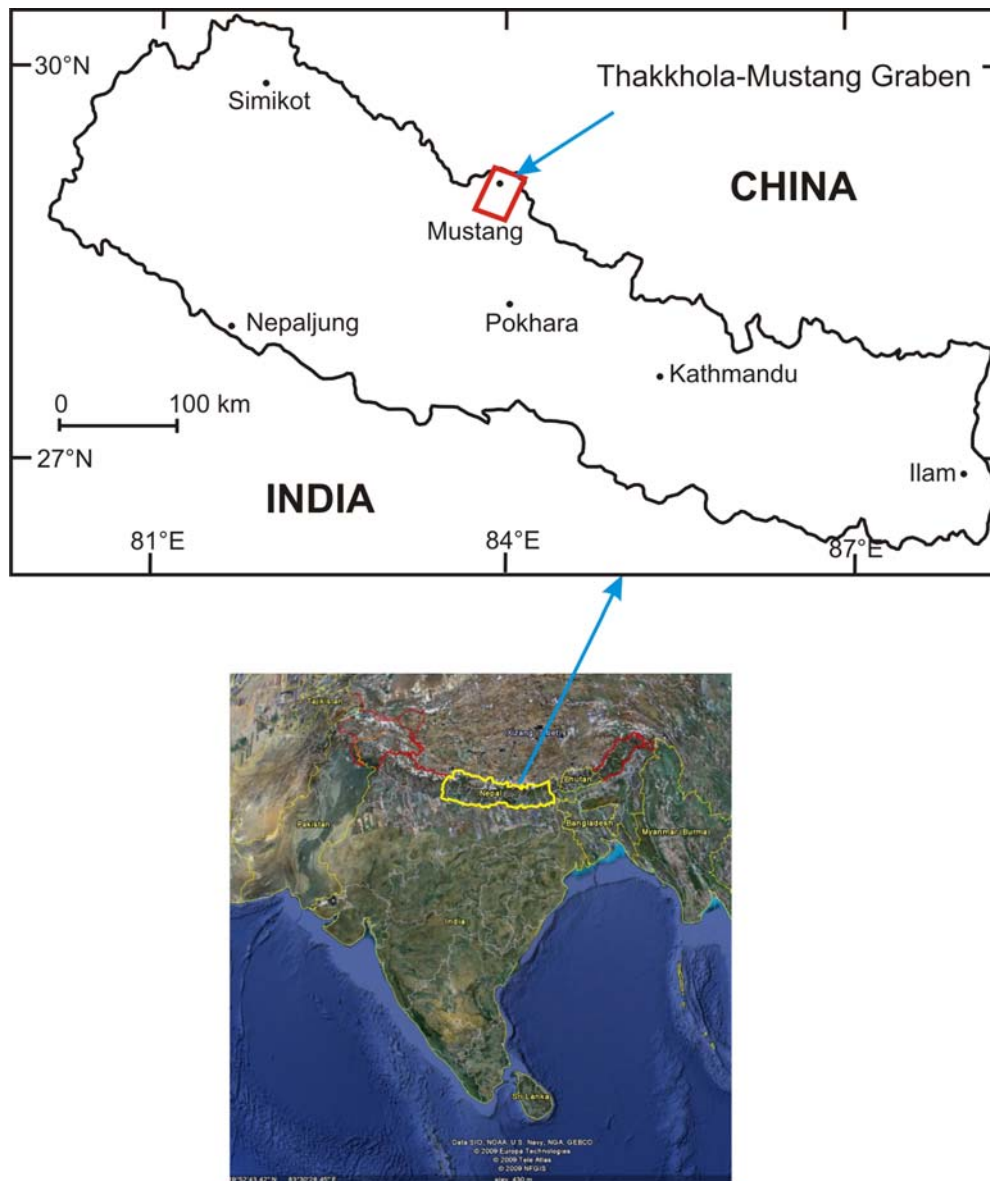
Fig. 1.1: Location map of the study area, bottom regional map taken from Google earth (2009)

Study in the Thakkhola-Mustang Graben affords many research features and themes such as the excellent exposures of the Tibetan-Tethyan succession, east-west extension of the Himalaya and the incision of the Kali Gandaki River into the basin-fill sediments, which provide excellent exposure of the depositional history of the basin. In this study, main works are related to the sedimentary depositional environmental of the basin, the provenance of the sediments and paleoclimate analysis.
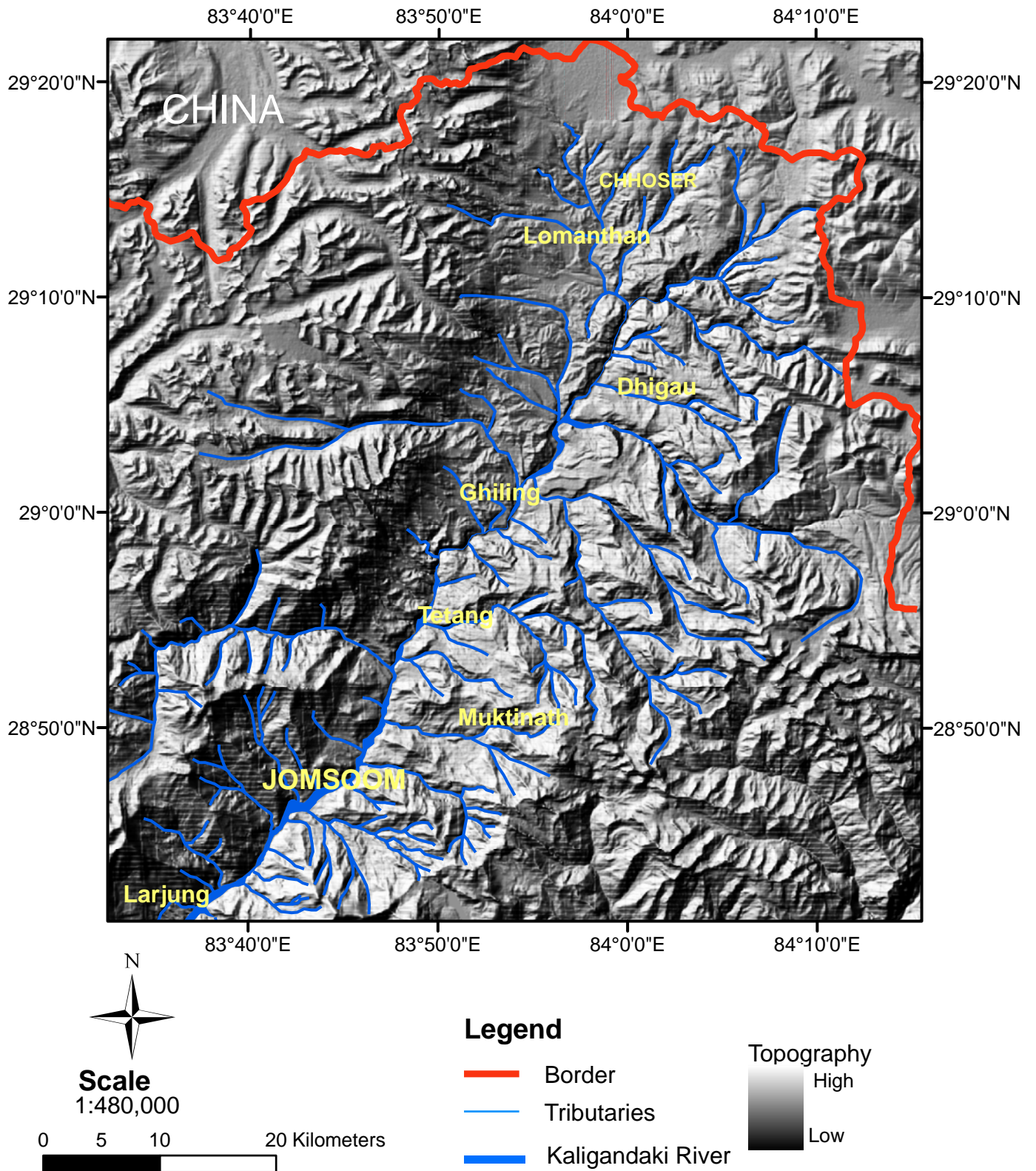
Fig. 1.1: Drainage and topograpic map of the study area (SRTM DEM from Jarvis et al. 2006)

1.2 Study area

1.2.1 Location and accessibility

The study area is located in the central development region of Nepal consisting of the Mustang District. Geographically, the study area lies between $83^{\circ}50"$-84° east longitudes and 29°-$28^{\circ}50"$ north latitudes (Fig. 1.1) Geologically, it is located in between the South Tibetan Detachment System (STDS) in the south and Indus-Tsangpo Suture Zone (ITSZ) in the north (Gansser, 1964; Hagen, 1959, 1968; Bordet et al., 1971a, 1975). It is accessible by airplane and foot trails from the Jomsoom airport.

1.2.2 Physiography and climate

Physiographically, the study area lies in the Higher Himalaya consisting of rugged glacial topography with some gentle slopes (Fig. 1.2). The graben displays a rectangular shape about 90 km long in the NE-SW direction and approximately 20 km in the NW-SE direction. This graben is situated in a region with altitude ranges from 3000 to 4000 m in the center and to more than 6000 m above mean sea level (MSL) on surrounding summits. The drainage system of the Kali Gandaki River is oriented nearly in north-south direction. The Syang Khola, Lumbuk Khola, Panda Khola, Jhon Khola, Ghilumpa Khola, Narsing Khola, Tange Khola, Charan Khola, Dhechyan, Khola, Yak Khola and the Hyujun Khola are the main tributaries of the Kali Gandaki River. All of the tributaries originate from Himalayan glaciers. The Thakkhola-Mustang Graben lies between sub-alpine and alpine regions having semiarid climate. Most of the vegetation is composed of scarce and scattered patches of thorny cushion plants (*Caragana* sp., *Astragalus* sp., *Lonicera* sp.) showing affinity with the Tibetan Plateau. Sheltered places have junipers, blue pine and birches while most ravines and riverbanks have poplars and Seabuckthorn. More than 53% of the vegetation is dominated by *Kobressia* species, which is the favorable fodder of both gazelle and domestic animals (Chetri, 2005). It remains cold throughout the year with snow cover from October to March. Days are usually windy from twelve noon onwards. Intense winds blow up in the Kali Gandaki valley. The strongest up valley winds were measured between Marpha and Chhuksang with typical speeds of 15-20 ms^{-1} (Egger et al., 2000).

1.3 Objectives

The main aim of the research was to analysis of sedimentary and depositional environments of the graben fill including the following objectives:

➢ Preparation of a geological map and columnar sections
➢ Study of the tectonic events recorded in the basin.
➢ Determination of the sedimentation history, analysis of sediment provenance and study of palaeoenvironments.
➢ Study of pollen for inferences on paleoclimate.

1.4 Previous works

There are no records of foreigners in the Mustang district before 1864. In the summer of 1865, one of the first Pundits, Mani Singh, traveled the lower part of Mustang via Muktinath and Kagbeni on return journey to Pithoragarh from Kathmandu. However, the Survey of India did not disclose his detailed report, only but a list of itinerary. Main geological works were carried out after the opening of Nepal to foreigners in 1950. Some important works related to the subject of this thesis are discussed in detail in a chronological order.

Hagen (1959, 1969), a Swiss geologist, entered Lo-Manthang for the first time after the opening of Nepal for the foreigner. He described the Thakkhola-Mustang Graben within the Langu-Manang Synclinorioum bounded by a thrust fault. The thrust fault, which is named after the Dangardzong village, is continuous for more than 80 km. He also described a fault passing through Muktinath Narsing La. The sediments of the Thakkhola-Mustang Graben belong to Thakkhola series consisting of red limestone, clays and sandstone. He compared the large area with the flysch facies of the Alps (varied deposits of clay, sandstone and shale of upper Mesozoic-Eocene Age).

Gansser (1964) described the tectonic and stratigraphic framework of the Himalayan mountain range and Paleozoic and Mesozoic sediments of the Tethyan series, which are the basement rocks of the Thakkhola-Mustang Graben. This work provides the main basis for subdivision of the Himalaya.

Bodenhausen et al. (1964) carried out a detailed work and established the basic stratigraphy of Paleozoic and Mesozoic successions of the Thakkhola-Mustang Graben in their pioneering 1962 expedition. They classified the Mesozoic strata into nine lithostratigraphic units. From bottom to top, they are as follows: Thinigaon Formation, Lower Lumachelle Formation, Jomsoom Limestone Formation, Upper Lumachelle Formation, Ferruginous beds, Checkpost Formation, Chuck Formation, Saligram Formation, and the Tangbe Formation.

Tater (1968) prepared and worked out a geological map of the Muktinath area at the scale of 1 inch to 1 mile and lithostratigraphic subdivisions of Tethyan succession. He recognized three litho-units within the Mesozoic succession, namely the Jomsoom Limestone, Saligram Formation and the Kagbeni Sandstone from bottom to top, respectively.

Bordet et al. (1971) gave the name 'Tibetan series' for the Paleozoic and Mesozoic rocks comprising the basement of the Thakkhola-Mustang Graben.

Fort (1976) studied the Quaternary deposits of the middle Kali Gandaki valley and reported three types of sedimentary basins, namely Kusma type, Ghasa type and Thakkhola type. She recognized two types of sedimentary facies, namely, thin horizontal layered beds of fine sands and silts alternately yellowish and dark colored and sand beds with oblique sedimentological features with ripple marks at the top of the beds alternating with thinner beds. From these facts, she reconstructed the ancient lake occupying an area from Larjung to north of Jomsoom.

Fort et al. (1982, 2000) described the detrital series of the Tetang and Thakkhola formations of probable Plio-Pleistocene age. They described the main structural and sedimentological characteristics of the graben-fill sediments for the first time. The deposition of alternating fluvial, lacustrine, and palustrine layers in the Tetang and Thakkhola formations indicate that the bottom of the graben was never occupied by a deep lake, but rather by a flat piedmont plain with torrential fans and small lakes. They described a northward drainage in the period of Thakkhola sedimentation. Fort (2000) described the glacier and mass wasting processes and their influence on shaping the Kali Gandaki valley. Most of the glacial evidence is best interpreted as the product of a mass wasting of considerable magnitude and probably at low frequency, a process strongly related to the very active geodynamic environment.

Colchen (1980, 1999) presented new data on the timing of the geodynamic development of southern Tibet and the northern Himalaya from Miocene to Pleistocene. The extensional stress regime during Pliocene to Pleistocene is compatible with the eastward extension that characterized southern Tibet and the northern Himalaya.

Iwata et al. (1982) carried out research on the glacial landforms and river terraces in the Thakkhola region with the following conclusions: the river terraces are grouped into three between Marpha and Kagbeni: Higher, Middle, and Lower Terraces. The longitudinal profiles of the river terraces indicate that the tectonic movements with tilting to the north have been occurring during the late Pleistocene, which suggest that the uplifting of the Great Himalayan Range is continuous at present.

Iwata (1984) also worked on the geomorphology of the Thakkhola-Mustang Graben and inferred that a glacial advance blocked the valley around Larjung before the last Interglacial period. Large-scale landslides occurred at the knick point under the influence of the regional tectonic movement as well as the gravitational instability due to the steep slope of the deep gorge and Palaeo Marpha Lake was formed.

Yoshida et al. (1984) carried out an extensive work on magnetostratigraphy and pollen studies of the Takmar series. They divided the stratigraphy of Thakkhola-Mustang Graben into three units: the Tetang Formation, the Thakkhola Formation and fluvio-glacial to glacio-lacustrine deposits. These units are subdivided into four magneto-polarity zones: the lowest normal polarity zone, lower mixed polarity zone, middle mixed polarity zone and the upper normal polarity zone. They concluded that the paleoclimate during deposition of the Tetang Formation was quite warmer than the present.

Garzanti and Frette (1991) carried out detailed stratigraphic work in the Thakkhola region. The stratigraphic succession begins in the Cambro-Ordovician with thick shallow-water carbonates followed by Siluro-Devonian units deposited in deeper-water environments. After the onset of collision between India and Asia, the sedimentary units were involved in fold-thrust deformation at high to medium metamorphic grade followed by uplift and formation of the Thakkhola-Mustang Graben with thick Plio-Pleistocene fluvio-lacustrine sediments.

Gradstein et al. (1989, 1992) worked out on the structure, tectonics, stratigraphy, fossil content, sedimentology, palaeoenvironment and evolution of the Mesozoic strata of the Thakkhola region. Their work was mainly focused on paleomagnetism, macro and micro fauna, organic debris, clay minerals and thin-section petrography.

von Rad et al. (1994) studied the Mesozoic sediments of the Thakkhola-Mustang Graben and found strikingly similarities over a distance of several thousand kilometers to Ladakh in the west and to the paleogeographically adjacent north-west Australian margin and Timor in the east. They described an almost uninterrupted about 2 km thick sequence of syn-rift sediments. These sediments were deposited on a slowly subsiding shelf and slope from Early Triassic to late Valanginian time.

Ogg and von Rad (1994) compiled paleomagnetic data of Permian, Triassic and early Jurassic from the reconstructed Gondwana blocks. These data indicated that the margin of the Tethys Sea was progressively shifting northward into more tropical latitudes. The Thakkhola region was approximately 55° S during Late Permian, 40° S during Early Triassic, 30°S during Middle Triassic and 25° S during Late Triassic. They suggested that this paleolatitude change produce a general increase in the relative importance of carbonate deposition through the Triassic on the Himalaya and Australian margins.

Garzione et al. (2000a, 2000b, 2003) described the Thakkhola-Mustang Graben in different aspects. The $\delta^{18}O$ values of carbonates in the Thakkhola-Mustang Graben ranges from -16 ‰ to -23 ‰ and reflect meteoric water values similar to modern values. They suggested that the southern Tibetan Plateau attained its current elevation prior to east-west extension. Initiation of Thakkhola-Mustang Graben extension was between 10 and 11 Ma, based on magnetostratigraphy of the older Tetang Formation. The $\delta^{13}C$ values of the soil carbonates suggest an age younger than 8 Ma for the base of the Thakkhola Formation. In the Tetang Formation, the abundance of lacustrine facies with pollen record, and the absence of paleosol carbonate suggest that condition were more humid than during subsequent deposition of the Thakkhola Formation.

Hurtado et al. (2001) described the neotectonics of the Thakkhola-Mustang Graben relating with Dangardzong fault in the western margin of the basin. Geomorphic data from the neotectonic features in the Thakkhola-Mustang Graben demonstrate important crosscutting relationships between river terraces and the Dangardzong fault, which shows displacement occurred during the Pleistocene. The termination of the Dangardzong fault at the trace of the Dhumpu detachment implies that east-west extension in the Thakkhola-Mustang Graben is confined to the hanging wall of the South Tibetan Fault System.

Saijo et al. (2002) worked on the paleosol of middle Holocene age in the Thakkhola basin and concluded that the paleosols were buried by surficial deposits of eolian and/or colluvial origin. Paleosols are rich in humus in comparison with the underlying and overlying deposits with abundant inorganic matter.

Godin (2003) showed that the Tethyan sedimentary sequence of central Nepal had been affected by three phases of folding (D1, D2 and D4) with contrasting vergence,

interspersed by two major extensional events (D3 and D5). The youngest extensional event (D5) marks the initiation and eventual southward propagation of Thakkhola-Mustang Graben. A northeast-dipping normal Lupra fault, which had been acting as a southern termination of the graben system, dropped down the Cretaceous rocks and high-level structural features in its hanging wall.

Chamlagain and Hayashi (2005) worked on the numerical simulation of the fault development of (as they call it) the Thakkhola half graben and concluded that gravitational collapse driven by the excess gravitational potential energy can explain the viable mechanism for development of north-south trending graben in southern half of the Tibet and the Himalaya. The extension caused by topographical loading and its excess gravitational potential energy could be the major factors for the development of the faults within the graben.

1.5 Overview
The dissertation is organized into 10 chapters.

Chapter 1 includes introduction, location, physiography and previous works.

Chapter 2 reviews the general geology of the Himalaya, emphasizing a broad overview of the region where samples were collected for the further analysis (Thakkhola-Mustang Graben). This chapter also reviews the basement rocks of the Thakkhola-Mustang Graben.

Chapter 3 describes the basin fill stratigraphy including some data on neotectonic features within the Thakkhola-Mustang Graben. Neogene sediments have been classified into five formations: the Tetang Formation, the Thakkhola Formation, the Sammargaon Formation, the Marpha Formation and the Kaligandaki Formation. This graben is bounded by Dangardzong fault in the west and Muktinath fault in the east.

Chapter 4 describes the facies and palaeocurrent analysis. 12 distinct facies with 3 lithofacies associations are described in this chapter. Sediments were deposited in alluvial fan, braided river and lacustrine environments.

Chapter 5 describes petrography of sandstones and limestones including compositional analysis of pebbles and bulk compositional analysis of sediments using X-ray diffraction in the conglomerate beds of Thakkhola-Mustang Graben. Both shallow and deep-water lacustrine/palustrine carbonates are present within the graben sediments.

Chapter 6 discusses about the carbon and oxygen stable isotopes analysis and $CaCO_3$ analysis of carbonate layers. The value of $\delta^{18}O$ is decreasing with increasing altitude in most of the cases with some exception within a small altitudinal difference. High $\delta^{13}C$ values strongly indicate that these carbonates were formed in the methanogenic zone. The value of $\delta^{18}O$ is almost constant whereas the values of $\delta^{13}C$ vary largely.

Chapter 7 describes the provenance analysis based on heavy mineral study. All the sediments are derived from the surrounding rocks of the Thakkhola-Mustang Graben. Low to high-grade metamorphic rock complexes comprising mica schists and related

metamorphic rocks were present on the source area. Presence of stable heavy minerals like zircon, rutile and apatite clearly indicate a granitoid source terrain.

Chapter 8 deals with the paleoclimate investigation with the help of pollen analysis. The results show that the southern part of Tibet was covered mainly by steppe vegetation during the depositional time indicating dry climate. It is presumed that the climate during the deposition of sediment in the Thakkhola-Mustang Graben was warmer than the present-day climate.

Chapter 9 includes the discussion of results and the inferences for the basin evolution. The graben developed in different successive stages from Miocene to present time. Basin evolution is presented in schematic graphic representations based on this present work and literature data.

Chapter 10 is the conclusions section of the dissertation including the main conclusions on the Thakkhola-Mustang Graben based on the present study.

CHAPTER TWO
GEOLOGICAL SETTING AND BASEMENT GEOLOGY

2.1 Geology of Himalaya

The Himalayan arc extends about 2400 km from Nanga Parbat (8138 m) in the west to Namche Barwa (7756 m) in the east with 230 to 350 km width (Le Fort, 1996). The Himalaya occupies a unique physiographic and geological setting between the Indian subcontinent with normal crustal thickness in the south and the Tibetan Plateau with a double crustal thickness in the north. Because of collision between the Indian continent with the Asian landmass, different slivers were produced along their principle thrusts. The continental slivers were stacked one over the other propagating southward and building the architecture of the Himalaya (Molnar, 1984). This mountain belt includes Nepal, Bhutan and as well as parts of Pakistan, India, and China. The whole Himalaya is divided geographically and geologically into five sections from west to east (Gansser, 1964) (Fig. 2.1).

    a) Punjab Himalaya
    a) Kumaon Himalaya
    b) Nepal Himalaya
    c) Sikkim-Bhutan Himalaya
    d) North Eastern Frontier Areas (NEFA) Himalaya

2.1.1 Punjab Himalaya

This 550 km long section of the Himalayan chain is bordered in the west by the Indus River and in the east by Sutlej River. It includes Kashmir and Spiti regions.

2.1.2 Kumaon Himalaya

From the Sutlej River eastwards this section stretches 320 km to the Kali River on the west boundary of Nepal. It includes the Garhwal Himalaya and parts of southern Tibet.

2.1.3 Nepal Himalaya

Nepal Himalaya extends from the Kali River in the west to the Mechi River in the east covering the whole length of Nepal. This part of the Himalaya is characterized by the presence of the eight highest peaks among the 15 peaks of the world exceeding 8000 m. These peaks are Sagarmatha, Kanchanjanga, Lotse, Makalu, Chou, Dhaulagiri, Manaslu, and Annapurna I.
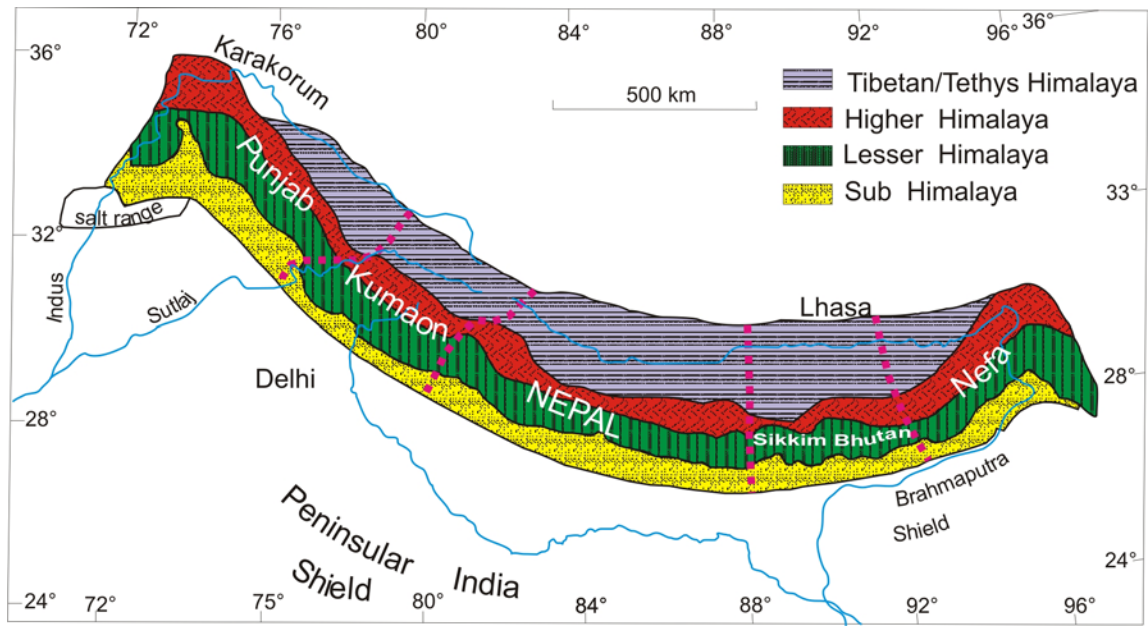
Fig. 2.1: Subdivision of Himalaya from west to east (after Gansser, 1964)
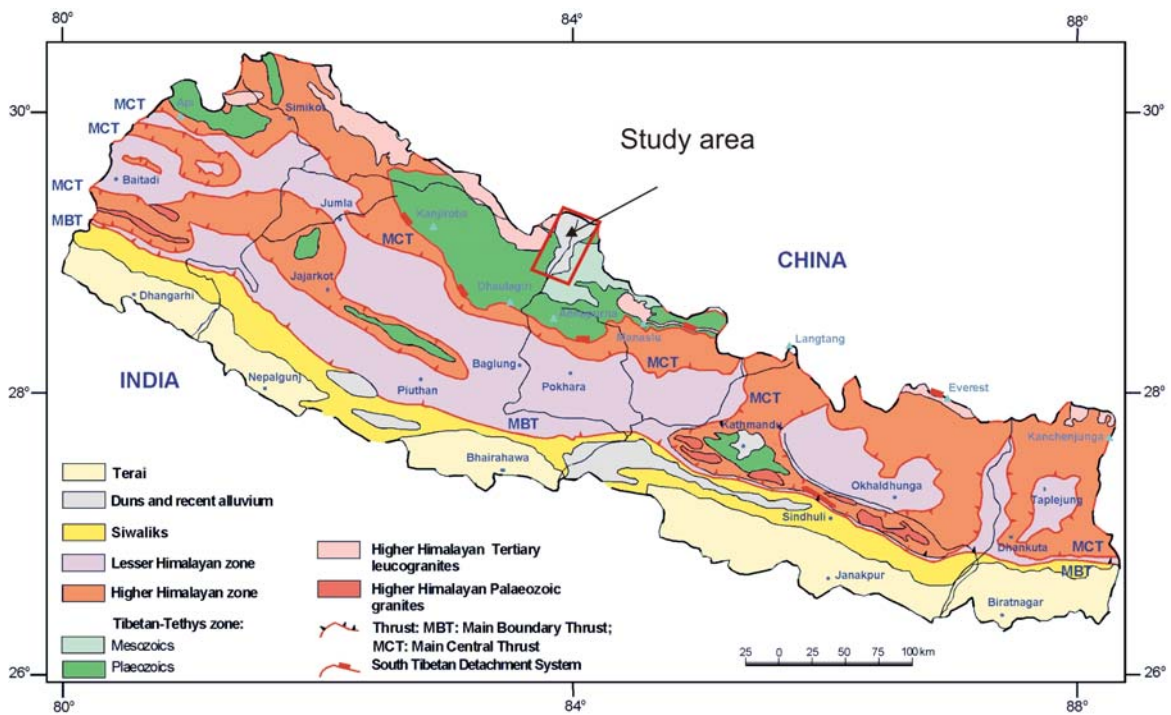
Fig. 2.2: Geological map of Nepal showing the study area (modified from Amatya and Jnawali, 1994).

2.1.4 Sikkim-Bhutan Himalaya

This part of the Himalayan range covered by the Sikkim and Bhutan (400 km), which lies between Mechi River in the west and Bhutan in the east.

2.1.5 NEFA Himalaya

This eastern part of the Himalayan range is about 400 km long. It extends from eastern boundary of Bhutan to the Tsangpo-Brahmaputra cross-gorges.

2.2 Geology of Nepal Himalaya

The Nepal Himalaya lies in the central part of the Himalayan arc, which covers nearly one third of the whole Himalaya. Geographically, the Nepal Himalaya is bounded by latitudes 26° 2' and 30° 27' N and longitudes 80° 11' E and 88° 27' E. The Nepal Himalaya can be divided longitudinally into five tectonic zones from south to north based on geological evolution (Fig. 2.2). The tectonic zones are separated from each other by the principal Himalayan thrust faults. The tectonic zones are nearly parallel and are characterized by their lithology and stratigraphy, tectonics, structure and geological history. These zones are described shortly below.

2.2.1 Terai Zone

The southernmost tectonic division of the Nepal Himalaya, Terai, represents the northern edge of the Indo-gangetic alluvial deposits having an elevation from 100 to 200 m above the mean sea level. The Main Frontal Thrust (MFT) separates it from the Sub-Himalaya (Fig. 2.2). The Terai plain is made of Pleistocene to recent alluvium with an average thickness of ~1500 m and it is already showing a significant proportion of current Himalayan stress accumulation, as is manifest in the development of thrusts and thrust-propagated folds beneath the sediments (Upreti, 1999). It can be easily differentiated from the coarser 'Bhawar Zone' by having finer-grained sediments. Rocks below the alluvium far south of the mountain front are experiencing tectonic activity and a number of thrusts and thrust-propagated folds have been recognized (Bashyal, 1998; Mugnier et al., 1999). Colluvial and alluvial fans are confined to the northern margin of the plain.

2.2.2 Sub-Himalayan Zone (Siwaliks)

The foothill ranges of the Himalaya are called the Siwaliks and comprise the southernmost tectonic zone of Nepal Himalaya, which is also called the Sub-Himalayan Zone. The Siwaliks are bounded to the south by the MFT, and by the Main Boundary Thrust (MBT) to the north (Fig. 2.2). A standard stratigraphy of the Siwalik Group has been established in Pakistan based on lithology and the paleomagnetic record (Johnson et al., 1982; Opdyke et al., 1982). Auden (1935), Sharma (1977), Tokuoka et al. (1986), Sah

et al. (1994), Dhital et al. (1995) and Nakayama and Ulak (1999) have established the stratigraphy of the Siwalik Group in Nepal. The Siwalik Group consists of an about 5 km thick upward coarsening sequence of mudstone, sandstone and conglomerate. The Siwalik Group consists of three informal units, which are the lower, middle and upper member (Tokuoka et al., 1986). The Siwalik Group can be regarded as fluvial deposits, which are strongly influenced by Himalayan uplift and climatic change through the development of the Indian monsoon (e.g. Clift et al., 2008).

2.2.3 Lesser Himalayan Zone (LHZ)

The Lesser Himalaya lies between the Siwalik foothills and the Higher Himalaya. It is bounded by MBT to the South and the Main Central Thrust (MCT) in the north. The Lesser Himalayan Zone constitutes a relatively broad tectonic zone in western Nepal Himalaya. It is sandwiched between the Churia range in the south and the High Himalaya in the north. The Lesser Himalayan Zone displays a relatively subdued and mature geomorphology (Upreti, 1999). Numerous workers (Frank and Fuchs, 1970; Upreti 1996, 1999; Decells et al., 2001) have documented the stratigraphy and tectonics of the western Nepal. This zone is composed of two principal components: sedimentaries and low-grade meta-sedimentaries including quartzite, limestone, slate, siltstone; and crystalline thrust sheets comprising metamorphic rocks like schist, gneiss, marble and granites ranging in age from Precambrian to Eocene.

2.2.4 Higher Himalayan Zone (HHZ)

The South Tibetan Detachment System (STDS) bounds the Higher Himalayan Zone in the north and MCT to the south (Fig. 2.2). A ten to twelve kilometers thick succession of high-grade metamorphic rocks of this HHZ is known as Tibetan Slab (Le Fort, 1975). The Higher Himalayan Zone is separated from the Tethyan sedimentary rocks by intervening bodies of Tertiary leucogranites forming the Higher Himalayan Granites along the Himalayan range in many areas (Upreti, 1999). It consists of high-grade crystalline rocks including various kinds of gneisses, schists and migmatites extending continuously along the entire length of the Nepal Himalaya. Two types of granites, older granites from 500 and 1800 million years ago and the younger leucogranites from 15 to 20 million years ago are associated with metamorphic rocks (Le Fort, 1981).

2.2.5 Tibetan Tethyan Zone (TTZ)

The Tibetan Tethyan Zone is the northernmost tectonic zone of the Nepal Himalaya, which occupies a wide belt consisting of sedimentary rocks. It is approx. 40 km wide unit made of a synclinorial pile of Upper Precambrian–Lower Paleozoic to Upper Cretaceous rocks. This zone is well exposed in the Marsyangdi, Kaligandaki River and Manang area. In spite of the pioneer work of Hagen (1968), detailed work was carried out in the

following years by many researchers (e.g. Bodenhausen et al., 1964; Fuchs, 1964, 1974, 1977; Waterhouse 1966, 1978; Bordet et al., 1971 a, b, 1975; Bassoullet and Mouterde, 1977; Colchen et al., 1986; Fuchs et al., 1988; Garzanti and Frette, 1991, Fuchs and Paudel, 1998; Hurtado et al., 2001 and Godin, 2003). This zone is composed mainly of sandstones, limestones, quartzites and shales with fossiliferous layer. The study area of the Thakkhola-Mustang Graben lies within this tectonic zone, overlying mainly rocks of the Tibetan Tethyan Zone.

2.3 The Neogene graben system in the Himalaya-Tibet region

The uplift of the Tibetan plateau is generally regarded as a response to the convective removal of the lower portion of the thick Asian lithosphere (Platt and England, 1994). This removal is also thought to be responsible for the east-west extension that took place during the India-Asia collision (Coleman and Hodges, 1995). The Cenozoic extensional tectonic phase created the many grabens in Tibet, and has affected whole Tibet and the northern part of the Himalaya. The onset of normal faulting was estimated to have commenced in southern Tibet about 14 Ma ago (Coleman and Hodges, 1995) and about 8 Ma ago (Harrison et al., 1995) and 4 Ma in central Tibet (Yin et al., 1999). However, Blisniuk et al. (2001) reported a minimum age of approximately 13.5 Ma for the onset of graben formation in central Tibet based on mineralization ages determined with Rb-Sr and ^{40}Ar-^{39}Ar data. These normal faults create numerous grabens, which are mainly distributed along the crest of Himalaya. Normal faults are striking either perpendicular to the Himalayan arc or to the north; most of them exhibit major deviations from these orientations (Kapp and Guynn, 2004). Numerous small and large grabens are present in Tibet and some of the major grabens from west to east are Burang Graben, Thakkhola-Mustang Graben, Gyirong Graben, Kungo Graben, Pum Qu Graben and Yadong Graben (Fig. 2.3). The horizontal graben spacing decreases from south to the north systematically, which reflects the northward decrease in the crustal thickness (Yin, 2000). The Thakkhola-Mustang Graben comprises one of the prominent grabens of this graben system, situated in the southern part of Tibet and central part of Nepal Himalaya.

2.4 Basement geology of the Thakkhola-Mustang Graben

The Thakkhola-Mustang Graben is an asymmetrical basin in central Nepal, which represents the Cenozoic extensional tectonic phase of the Tibetan Plateau and the whole Himalaya. This graben is a part of normal faulting system affecting the whole Tibetan Plateau (Molnar and Tapponnier, 1978). The Thakkhola-Mustang Graben lies on top of the Paleozoic to Cretaceous rocks of the Tethyan series between the South Tibetan Detachment Fault System (STDS) (Burchfiel et al., 1992) to the south and the Indus-Tsangpo Suture Zone (ITSZ) to the north. The Mustang-Mugu leucogranites massif (Le

fort and France-Lanord, 1994), which has been dated by Th-Pb monazite at 17.6 ± 0.3 Ma (Harrison et al., 1997) lies to the northwest of the graben.

The rocks of the Tibetan-Tethys Zone consist of a thick and nearly continuous lower Paleozoic to Paleogene marine sedimentary succession. These sedimentary rocks were deposited on the northern continental margin of the Indian Plate, which were crumpled, stacked and deformed as a consequence of collision between India and Eurasia in the early Eocene (Garzanti et al., 1987; Serle et al., 1987).

Bodenhausen et al. (1964) established the basic stratigraphy of the region in their pioneering 1962 expedition. The succession in the Thakkola area is comparable with the sedimentary units exposed to the west in Kumaon, Spiti and northwestern Himalaya (Zanskar Region) (Gaetani et al., 1986; Gaetani & Garzanti, 1991).

In this study, the adopted nomenclature and lithostratigraphy for the basement rocks of the Thakkhola-Mustang Graben are based mainly on Colchen et al. (1986) (Fig. 2.4). However, some of the units are also taken from different authors (Bodenhausen et al., 1964, Fuchs, 1977; Fuchs et al., 1988 and Bassoullet and Mouterde, 1977). The basement rocks comprise 16 formations, which are described shortly and presented in the Table 2.1.

Santuaire Black Formation: It is the basal part of the Tibetan-Tethys series and consists alternation of grey wacke, dolomite and phyllite of Cambrian age.

Annapurna yellow Formation: It consists of bluish grey limestone with quartzite and schists of Cambrian age.

Pi Formation: This formation is composed of interbedded black schist and calc-schists.

Nilgiri Limestone (Bordet et al., 1967): It consists of a thick succession of shallow water limestones, consisting ripple marks, cross lamination with brachipods, gastropods, bivalves, nautiloids and crinoids (Colchen et al., 1986).

North Face Quartzite (Bodenhausen et al., 1964): It consists of sandstones, siltstones and carbonates containing a brachiopod-echinoderms fauna of late Ordovician age (Bordet et al., 1971)

Sombre Formation: It is composed of alternating gritty dolomite, black shale and limestone (Silurian-Devonian), which is correlative with the Dark Band Formation of the Dolpo area (Fuchs, 1977). Dark limestones and marls in the upper part of this units yield Early Devonian monograptids and tentaculitids (Bordet, 1967, 1971).

Tilicho Pass Formation: It consists of micaceous siltstones and grey-green up to fine-grained sandstones base with lenticular or convolute lamination, which are intercalate with yellow-weathering metric carbonated beds associated with ferruginous layers.

Tilicho Lake Formation: It is composed of grey, bluish grey to black limestone and consists of fenestellid bryozoans, productid and spiriferid brachipods, corals, bivalves, crinoids, conodonts and ammonoids of Early Carboniferous age (Bordet et at., 1971; Fuchs et al., 1988).
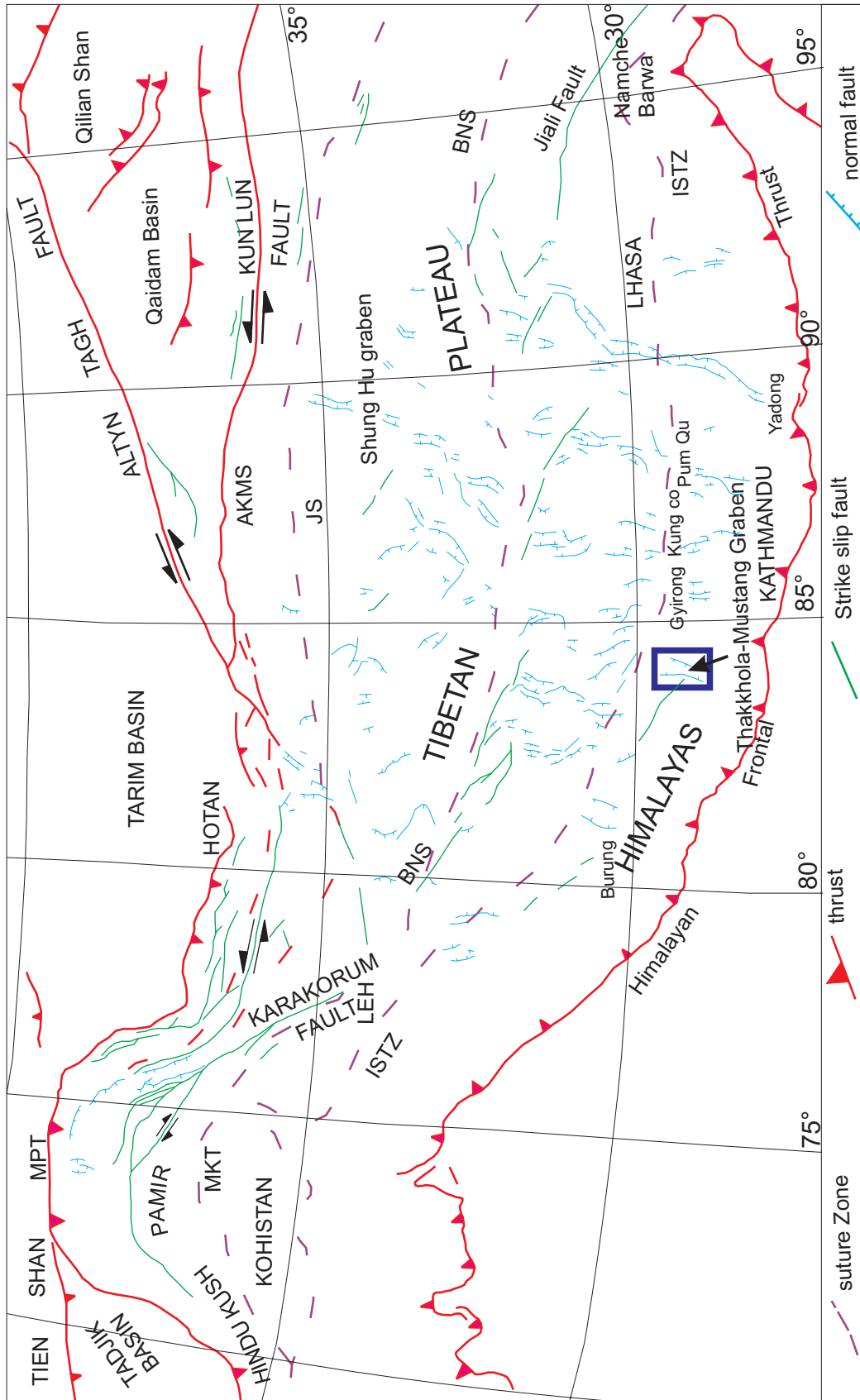
Fig. 2.3: Tectonice setting of principal active faults of Tibet and adjacent regions showing major grabens (modified from Blisniuk et al., 2001) AKMS = Ayimaqin-Kunlun-Mutztagh suture; BNS = Bangong Nujiaang SUTURE; ISTZ = Indus-Tsangpo Suture Zone; JS = Jinsha Suture; MKT = Main Karakoram Thrust; MPT = Main Pamir Thrust

Table 2.1: Lithostratigraphy of the Tibetan-Tethys Himalaya (after Colchen et al., 1986)

Formation	Nomenclature reference	Main lithology	Important Fossils	Age
Muding Formation	Bassoulet & Mouterde, 1977	Thin-bedded marls and limestone with pelagic fauna.	Hedbergella infracretacea,	Middle Cretaceous
Chuck Formation	Bodenhausen et al., 1964	Volcanic derived microconglomerate Sandstone and carbonates	Ptillophylum nepalensis, Tropaeum australe	Lower Cretaceous
Spiti Formation	Stoliczka, 1866	Dark gray to black shale with ammonites.	Kranosphinctes, ammonites, Blanfordicera	Upper Jurassic
Lumachelle Formation	Bassoullet et al., 1986	Alternationals of grey limestone with grey shale sandstone	Oyster, Lamellibranches, Bellemnopsis.	Middle Jurassic
Jomosom Limestone	Bodenhausen et al. 1964	Dark grey micrite and oolitic limestone interbeds with sandstone	Vidalina martana, Haurania, Belemnites, Macrocephalites	Lower Jurassic
Quartzite Formation	Colchen et al. 1986	Thick bedded quartzite interbed with shale	Trychyceray, Joanites, Arcestus, Arpodites, Juvavites	Upper Triassic
Thinigaon Formation	Bassoulet & Mouterde, 1977	Dark to reddish nodular limestone containing crinoids.	Meekoceras, Clyperoceras, Flemingites, Anasibirities	Lower Triassic
Thini Chu Formation	Bassoulet & Mouterde, 1977	Thick succession of quartzarenite alternating with dark pelites, limestone	Spiriferella rajah, Fenestella polyseptata	Permo carboniferous
Tilicho Lake Formation	Bordet et al., 1971	Grey, bluish grey to black limestone, calcschist and black shale	Attenuatus, Septopora cf. ekybastusica, Nekhoroshev	Early carboniferous
Tilicho Pass Formation	Bordet et al., 1967	Micaceous siltstones and grey-green up to fine grained sandstone	Monograptides, Tentaculites, Favosites	Devonian
Sombre Formation	Bordet et al., 1967	Alternating gritty dolomite, black shale and limestone	Monograptus Orthograptus bellutus, Glyptograptus	Silurian
North Face Quartzite	Bodenhausen et al, 1964)	Sandstone, siltstone and carbonate containing a brachiopod-echinoderms	Orthambonites Gyptocystidaye, Cheirocrinus	Ordovician
Nilgiri Limestone	Bordet et al., 1967	Limestones consisting of ripples marks with brachipods, gastropods	Brachiopod, Nautiloidea	Ordovician
Pi Formation	Bassoulet & Mouterde, 1977	Interbedding of black schist and calcschist	Crinoids	Ordovician
Annapurna Yellow Formation	Colchen et al. 1986	Bluish grey, limestone with quartzite and schists.	Worm traces, Trilobites	Cambrian
Santuaire Black Formation	Colchen et al. 1986	Alternation of grey wacke, Dolomite and phyllite		Cambrian

Tibetan-Tethys stratigraphy

- Muding Formation
- Chuck Formation
- Spiti Formation
- Lumechella Formation
- Jomosom Limestone
- Thini gaon Formation
- Thini Chu Formation
- Tilicho Lake Formation
- Tilicho pass Formation
- Sombre Formation
- Nilgiri Formation
- Annupurna Formation
- Santuaire Black Formation

Thakkhola-Mustang Graben sediments

- Thakkhola Formation
- Tetang Formation

- Fluvio-glacial deposits
- Glaciers
- Faults
- Rivers
- Syncline
- Anticline
- Attitude

N

0   10 km

Fig. 2.4 Geologcial map of Kaligandaki valley (modified from Colchen et al., 1986)

Thini Chu Formation: Thick succession of quarzarenite alternating with dark pelites, hybrid arenites and fossiliferous grey limestones yielding fenestellid bryzoans, spiriferid and productid brachipods, crinoids, corals and trilobites. Fine to coarse-grained snow-white quartarenites display low-angle to trough cross-lamination and herringbone structures.

Thinigaon Formation: It consists of grey to reddish nodular limestones of deep depositional environment with alternating thin-bedded marls and mainly limestone containing crinoids, brachiopods, bivalves, conodonts and ammonites. Poorly fossiliferous grey pelites interbedded with very fine-grained orange-weathering decimetric arkoses and subarkoses showing sharp base and hummocky cross-lamination present in the upper portion of the formation.

Quartzite Formation: Mainly thick-bedded quartzite interbedding with shale of the Upper Jurassic is the main lithology of the Quartzite Formation.

Jomosom limestone (Bodenhausen et al., 1964): The Jomosom limestone consists of bicalcarenites, pelletal mudstone/wackestones and oolitic grainstones. Dolomitic limestones and sandstones occur in the basal part.

Lumachelle Formation (Bassoullet et al., 1986): It consists of alternation of grey limestone with grey, shale, sandstone and marl with bivalves, gastropods, brachipods, crinoids, belemnites and rare fish fragments interbedded with hybrid arenites and grey marls.

Spiti Formation: The Spiti Formation is equivalent to the Saligram Formation of Bodenhausen et al. (1964) and equivalent to the "Spiti Shale" of Hagen (1959). It consists of dark gray to black colored shale with concretions and thin to thick-bedded sandstone and is dominated by black shale or slates. This formation consists of concretions ranges nearly from 1 cm to 50 cm and some concretions contain ammonite specimen.

Chuck Formation: It is best exposed in the several locality of Kagbeni area. The Chuck Formation is equivalent to the "Tangbe Formation" of Bodenhausen et al. (1964), "Wealdian strata" of Bordet et al. (1971), "Kagbeni Formation" of (Bassoullet & Mouterde, 1977) and "Kagbeni Unit" of Gradstein et al. (1992). It consists of volcanic-derived microconglomerates commonly rich in large intraclasts and wood fragments, sandstones and carbonaceous siltstones locally with coal lenses arranged in fining-upward sequences and deposited in a deltaic environment influenced by fluviatile process.

Muding Formation (Bassoulet & Mouterde, 1977): It consists of thin-bedded marls and marly limestones yielding a pelagic fauna. The Muding Formation is the youngest unit preserved in the Thakkhola region, where thick fluvio-lacustrine deposits of Plio-Pleistocene unconformably follow the early Cretaceous succession.

CHAPTER THREE
STRATIGRAPHY AND TECTONICS OF THE GRABEN FILL

The sedimentology and stratigraphy of the Thakkhola-Mustang Graben fill have been described by Fort et al. (1982), Colchen (1999), Bordet et al.(1971), Hutardo et al. (2001) and Garzione et al., 2003. The lithostratigraphy of the area is mainly based on the work of Fort et al. (1982) and Hurtado et al. (2001) (Fig. 3.1). Yoshida et al. (1984) worked on palynology in this area but they reported no precise biostratigraphic data. Carbonate and pollen analysis are discussed in chapter 5 and 8, respectively.

3.1 Basin fill stratigraphy

The syntectonic deposits of the Thakkhola-Mustang Graben are characterized by a thick accumulation of continental debris extending over 90 km from north to south and about 20-30 km from east to west (Colchen, 1999) (Fig. 2.4.). The graben is filled with more than 870 m of Miocene and Plio-Pleistocene sediments. The oldest sedimentary units in the Thakkhola-Mustang Graben are the middle Miocene to upper Pliocene Tetang and Thakkhola formations whereas the upper Pliocene to upper Pleistocene Sammargaon and Marpha formations overly disconformbly the Thakkhola and Tetang formations (Fig. 3.1). The best estimated age of the Tetang Formation is between ca. 11 and 9.6 Ma and the maximum age of the Thakkhola Formation is 8 Ma based on magnetostratigraphy (Garzione et al., 2000a) and the interpretation of the magnetostratigraphy as given by Yoshida et al. (1984) - they concluded that deposition of the Thakkhola Formation continued until at least 2 Ma. The two older Thakkhola- and Tetang Formation are separated by a low angle (~5°) unconformity (Fort et al., 1982). These formations lie unconformably on a substratum of the high strain rocks of the deformed Tibetan-Tethys sedimentary sequences (Fig. 2.4). The Holocene Kaligandaki Formation is in a cut-and-fill relation with these older formations.

For the study of the basins fill stratigraphy, field mapping was carried out between Lo-Manthang and Marpha village by constructing columnar sections and recording and measuring sedimentary structures.

3.1.1 Tetang Formation

The Tetang Formation is well exposed around the Tetang village along the Narsing Khola and Dhinkyo Khola. The thickness varies from few meters to more than 200 m from place to place. This formation onlaps the Cretaceous Chuck Formation (Colchen et al., 1986) (Fig. 2.1). In the southeastern part of the basin, Cretaceous rocks were slightly eroded before the Neogene deposition. Four main units within the Tetang Formation have been distinguished based on their lithostratigraphic characteristics.

20

1) Basal pebble and gravel (0-68 m): This unit is composed of quartzite, shale, sandstone and carbonate sediments derived directly from the Mesozoic bedrock, which is best exposed on the Dhinkyo Khola section (Fig. 3.2N). Some massive conglomerate beds are up-to 22 m thick with some sand lenses alternating with imbricated conglomerate beds (Fig. 3.3). Pebbles range between few cm to blocks of up to 1m in the conglomerate beds.

2) Interbedding of conglomerate bed with sand and silt layers (65-115 m): Imbricated conglomerate beds are interbedded with sand and silt layers (Fig. 3.4). Carbonate and iron concretions are present in the sandstone beds. Conglomerate beds range between few cm to 2 m while sandstone and siltstone beds are between 0.02 m to 0.3 m.

3) Sand dominated sequences (115-172 m): Sand layers are alternating with imbricated conglomerate layers and siltstone. Sand layers have mainly parallel lamination with cross bedding in some layers. Some fine-grained grey sandstone layers contain plant fossils. Mainly fining upward cycles represent this unit (Fig. 3.2M).

4) Fine siltstone with limestone beds (172-215 m): This unit is mainly dominated by fine sand and silt layers and limestone beds (Fig. 3.5). Thick siltstone beds contain sometimes plant fossils (Fig. 3.6). Limestones are very fine-grained containing ostracods.

3.1.2 Thakkhola Formation

The Thakkhola Formation crops out north of the western and eastern parts of the Tetang Formation up to Lomanthang and its extent is strictly controlled by the Dangardzong fault on the western side. The base of the Thakkhola Formation can only be seen above the Tetang Formation in the Tetang village area and Dhinkyo Khola on the eastern side. The imbricated conglomerates of the Thakkhola Formation lie just above the topmost limestone of the Tetang Formation (Fig. 3.7). The study of this formation was carried out by preparing columnar sections in Chaile, Syanboche, Ghiling, Ghami, Dhakmar, Dhi and Tange gaon. The thickness of this formation attains a maximum of more than 620 m in the Chaile section and it decreases progressively eastwards to where it lies unconformably on the Tetang Formation and further to the east upon the Mesozoic basement rocks (Fig. 3.8). The lateral facies changes from south to north and decrease in thickness are present. The formation reaches a thickness of ~ 210 m in Dhi gaon (northeastern part) (Fig. 3.1). The size of clasts in the conglomerate beds and the thickness of the conglomerate beds decrease towards the north while the frequency of silt layers increases. This formation can be subdivided in to four units based on lithological characteristic displayed in the Chaile area (Fig. 3.2L).

1) Basal conglomerates (0-182 m): This unit is mainly composed of massive conglomerate and imbricated conglomerate beds interbedded with coarse sand layers. Pebbles in the conglomerate are mainly composed of Paleozoic rocks like shale, sandstone and some Tertiary granite pebbles from the Mustang-Mugu granites. The

thicknesses of the beds are ranging from 2 m to 20 m and the average grain size is ~18 cm (Fig. 3.9).

2) Alternation of imbricated conglomerate beds with sandstone and siltstone (182-320 m): These conglomerate beds have a red matrix and are characterized by a great variety. Mainly Paleozoic clasts are present in the conglomerated beds with some Mesozoic carbonate clasts. The average clast size is ~ 3 cm. Mainly coarse to fine-grained sandstone dominate most of the sequences. Carbonate and iron rich concretions are present in the sandstone and siltstone beds whereas siltstone beds contain some plant fossils and bioturbation (Fig. 3.10).

3) Fine grained sediments (320-500 m): This unit contains various kinds of facies like lenses or beds of sandstone, polygenic pebbly conglomerate, lacustrine limestone and some silt beds. Grey to black siltstone beds are alternating with imbricated conglomerate and fine to coarse-grained sandstone. A 12 to 15 m thick siltstone is present at a level of 320 m of the sequence (Fig. 3.11). Mainly Paleozoic followed by Mesozoic and Tertiary clasts are present in the imbricated conglomerate beds. Oncolitic (Fig. 5.9A.), micritic-microsparitic detrital, micritic organic facies with several algal mats (Fig. 5.10C) are dominating in the limestone whereas bioturbation, root fragments and concretions are widespread in the siltstone beds (Fig. 3.12).

4) Upper imbricated conglomerate and sandy layers (500-623 m): Some bioturbated siltstone and massive to imbricated conglomerate beds represent this unit. Mainly Paleozoic clasts of average size of 5 cm dominate in the conglomerate beds with some Mesozoic carbonates. Carbonate and iron rich concretions are widespread in the siltstone and sandstone beds (Fig. 3.13).

3.1.3 Sammargaon Formation

This formation is unconformably overlying the Thakkhola Formation in the northern part of the Thakkhola-Mustang Graben (Fort et al., 1982). It is well exposed nearby the Tangbe village and Ghilumpa Khola (Fig. 3.1). It comprises a more than 110 m package of breccias and conglomerates that were deposited in the high relief of the Tetang and Thakkhola formations (Fig. 3.1). The basal unit consists of fine-grained sandstone with parallel laminated siltstone. Quartz and calcite are dominant minerals of the fine-grained sandstone (Fig. 5.15F). Massive conglomerate beds of average clast size 23 cm are present above the sandy layers and the imbricate clasts of conglomerate suggest southeast paleoflow (Fig. 3.2O). Some coarse grained sand layers are present in between the diamictic conglomerate of glacial till (Hurtado et al., 2001) (Fig. 3.14a). The Sammargaon Formation is also associated with glacial moraines and is interpreted to be a glacio-fluvial package deposited during middle Pleistocene glaciation (Fort et al., 1982; Fort, 1989).
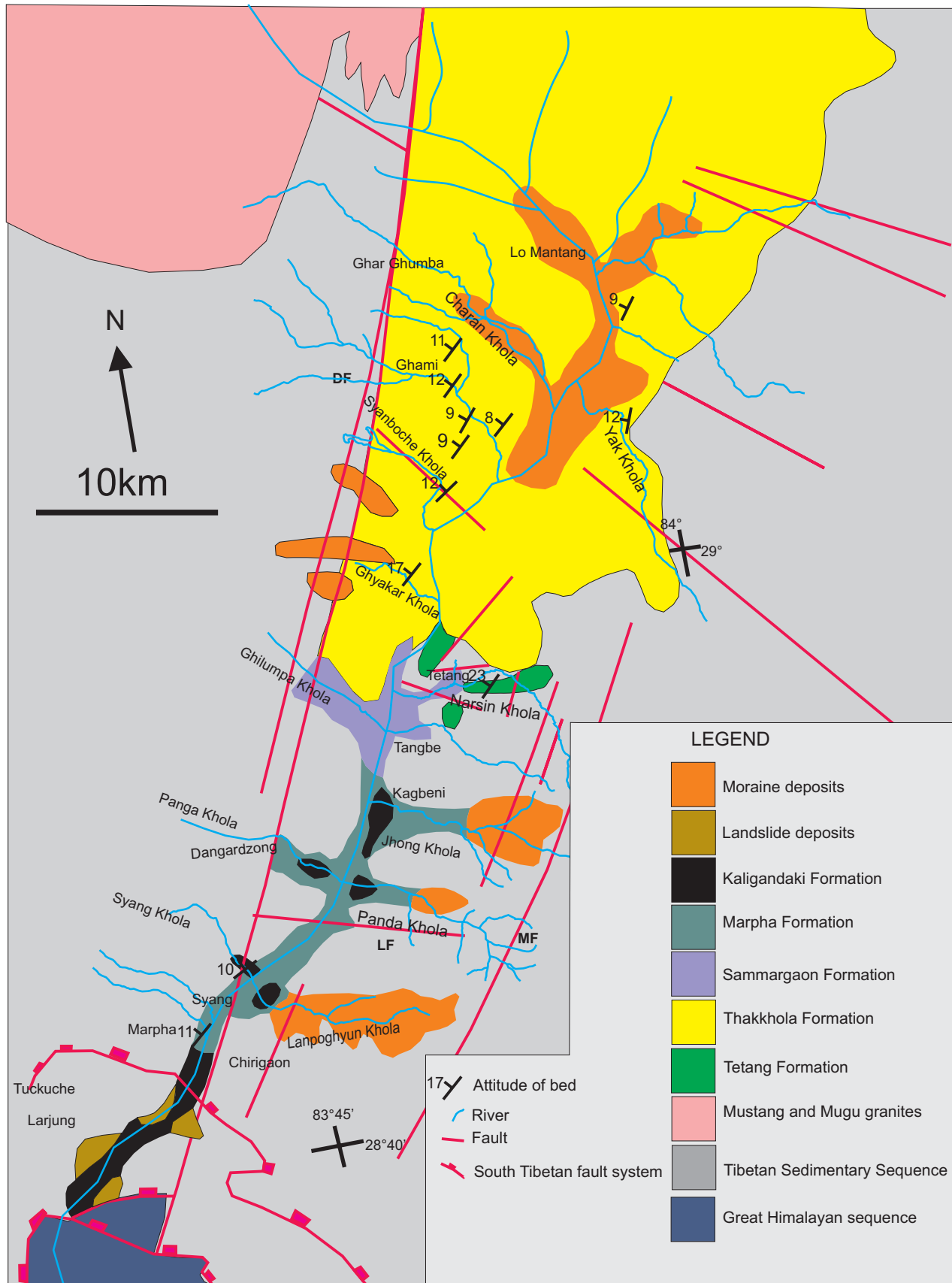
Fig. 3.1: Detailed geological map of the Thakkhola-Mustang Graben showing the basin fill units, modified from Fort et al. (1982) and Hurtardo et al. (2001) and present work. The faults which are in southern part extending east-west represent the South Tibetan fault system. DF-Dangardzong fault, MF-Muktinath fault, LF-Lupra fault.

Legend

	Limestone		Siltstone
	Sandstone		Cross bedding
	Massive conglomerate		Covered Area
	Imbricated conglomerate		Conglomerate lense in sandstone
	Pebbly Sandstone		Thinly laminated Mudstone
	Mudstone		Sand lense in conglomerate
	Shell		Plant Fossil
185	Paleocurrent direction		Root fragments
	Bioturbation		Concretion
27	Sample number	φ	Average size of the pebbles

C   S   SS   G

Clay Silt Sand Gravel

Clast composition
(each count contains ⁓50 clasts)

Tertiary clasts

Paleozoic clasts

Mesozoic clasts
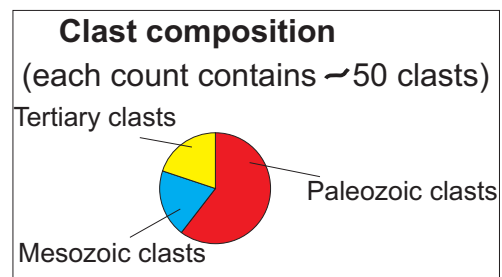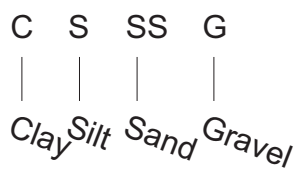
Fig. 3.2: Legend for the columnar sections

(A, B and C) Lomangthang village

N29°11'15"
E083°56'50.7"

N29°11'25.2"
E083°56'44.3"

N29°10'49.9"
E083°58'50.6"

(D) Dhakmar village

N29°05'08.3"
E083°52'53.3"

Quaternary deposits

27

φ =2.4cm

24

φ =3.9cm

7

70

6

Leg 3 start here
N29°05'26.8"
E083°53'01.1"

φ =3.1cm

73

123

φ =4.2cm

148

65

Leg 2 Start here
N29°05'10.7"
E083°52'53.5"

φ =2.3cm

5

4

3

2

1

A

B

C

D
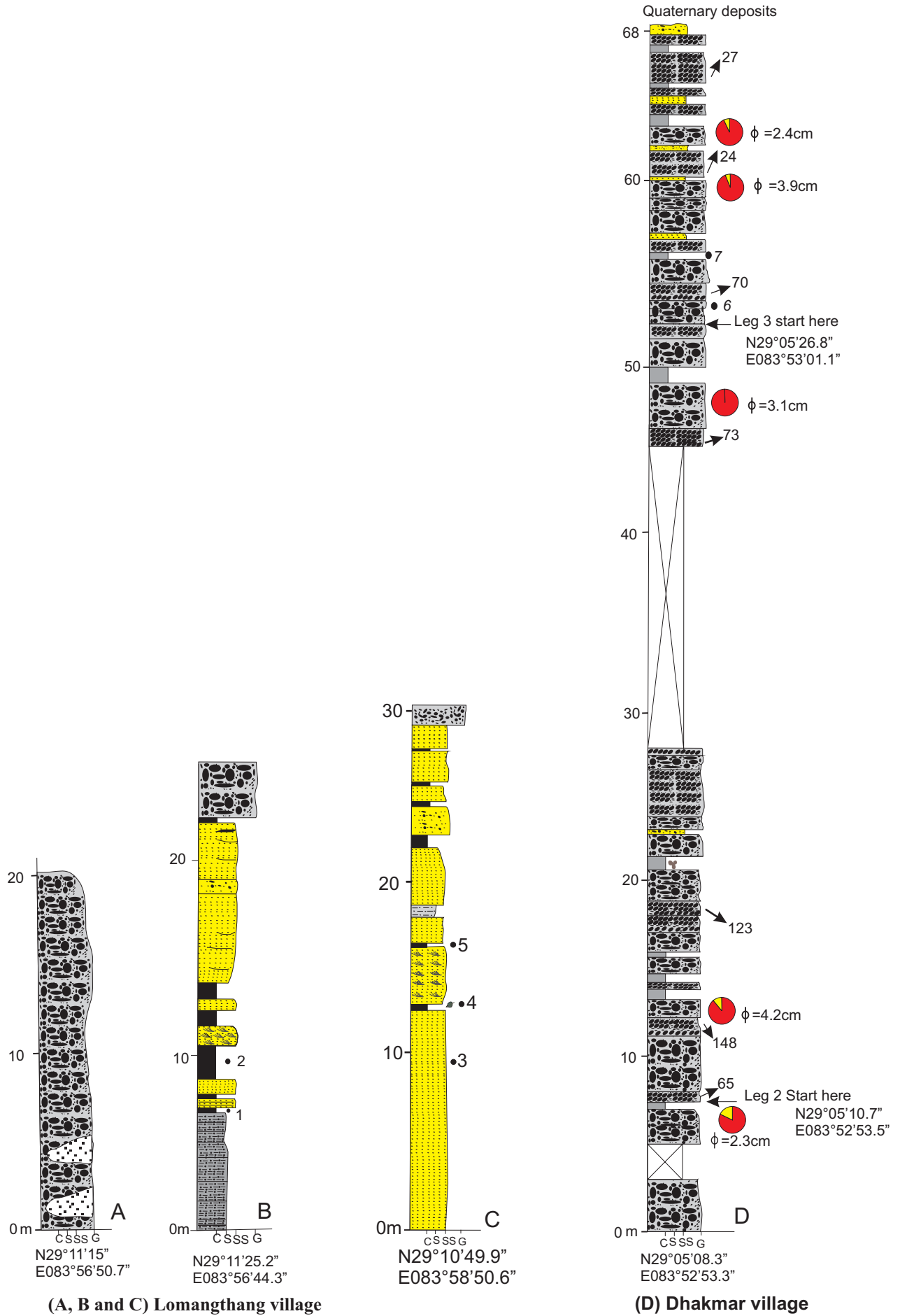
Fig. 3.2: Columnar sections of the different locations of the different formations.

(E) Dhi gaon

(F) Tange gaon

Fig. 3.2 (Continued.)

(G) Ghiling Village

N28°59'32.0"
E083°52'14.2"

φ = 5.4cm

φ = 3.4cm

φ= 2.4cm
153

A3c

A3b
136
φ = 3.7cm

A3a

φ = 6.3cm
134

CS SSG

φ = 7.01cm

145
φ = 4.7cm
Leg 2 start here
N28°59'44.7"
E083°52'07.8"

A3d

152

141

φ= 9.1cm
147

153
A3e
φ = 6.7cm
Leg 3 start here
N29°00'01.3"
E083°51'58.9"
141

135
φ = 4.2cm
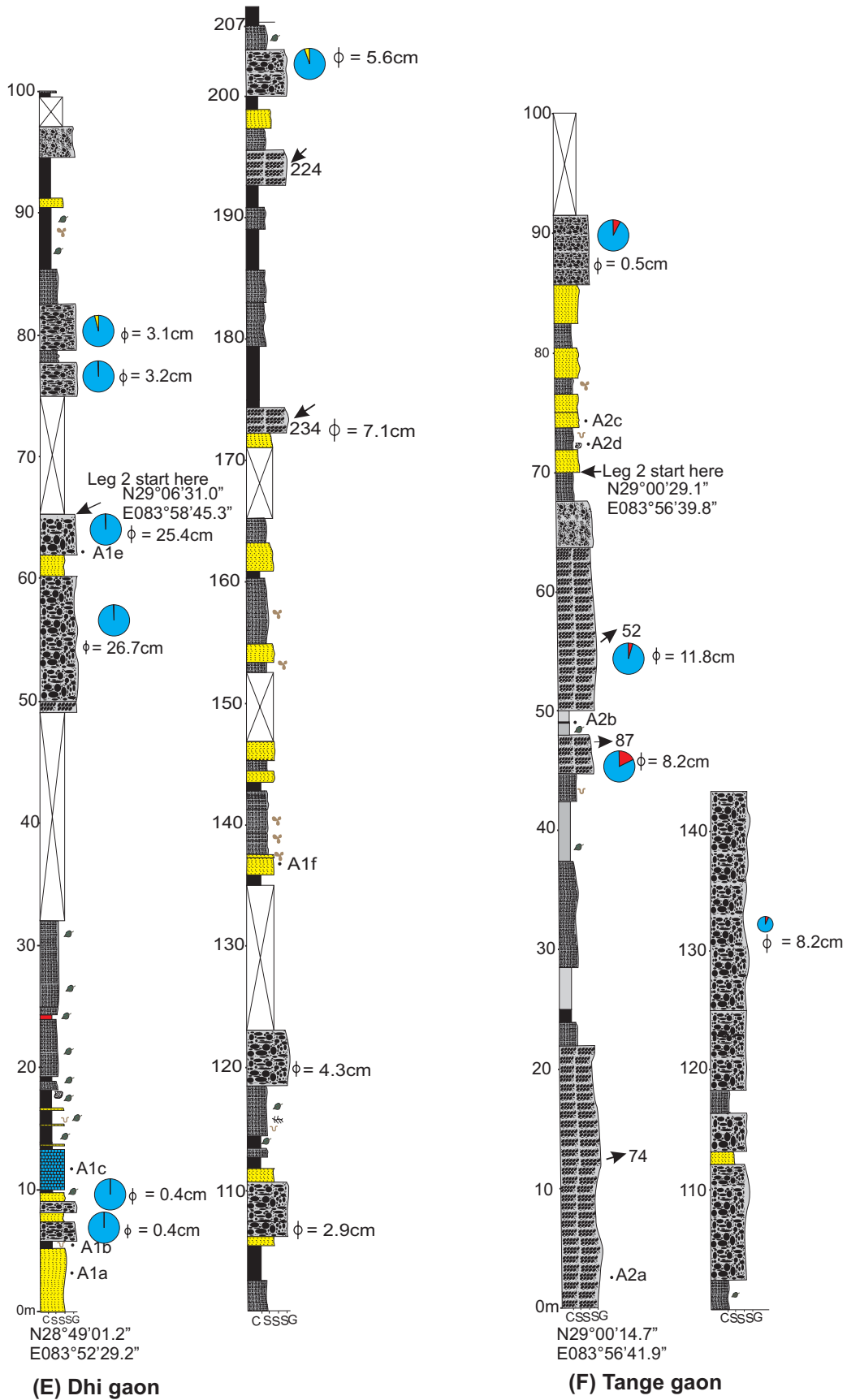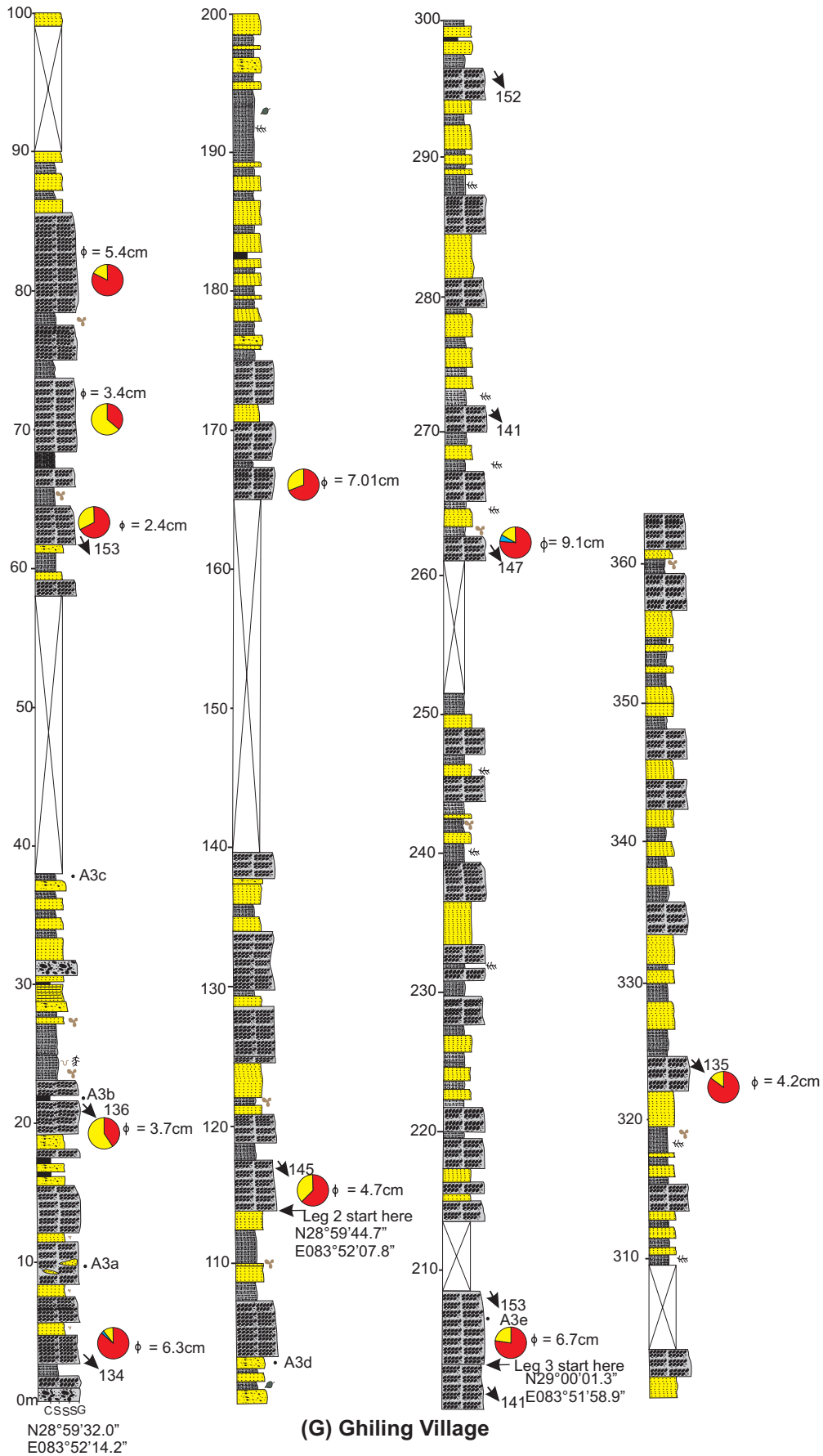
Fig. 3.2 (Continued).

Fig. 3.2 (Continued)

28

Fig. 3.2 (Continued.)

(L) Chaile

29

Fig.3.2 (Continued)

(M) Tetang Village

(N) Dhinkyo Khola
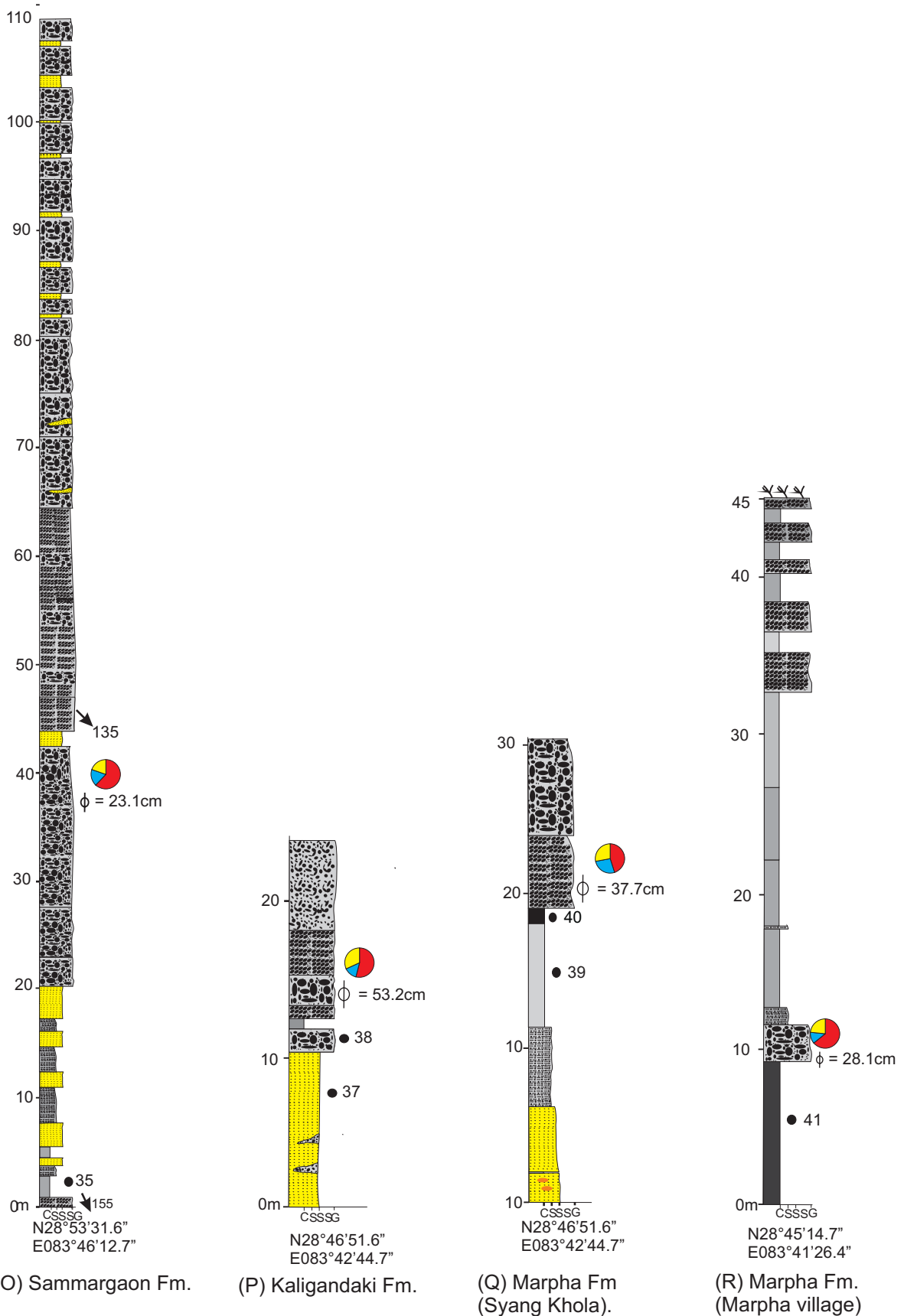
Fig. 3.2: Columnar sections of the different localities of different formations. Thakkhola Formation; (A, B, C) Lo-Manthang village, (D) Dhakmar village, (E) Dhi gaon, (F) Tange gaon, (G) Ghiling village, (H) Ghami village, (I) Chunker village, (J) Tamagaon, (K) Syanboche village, (L) Chaile village. Tetang Formation; (M) Tetang village, (N) Dhinkyo Khola. (O) Sammargaon Formation, (P) Kaligandaki Formation, Marpha Formation; (Q) Syang Khola, (R) Marpha village.

Fig. 3.3: Alternation of massive conglomerate and imbricated conglomerate beds in the Tetang Formation at Dhinkyo Khola section.
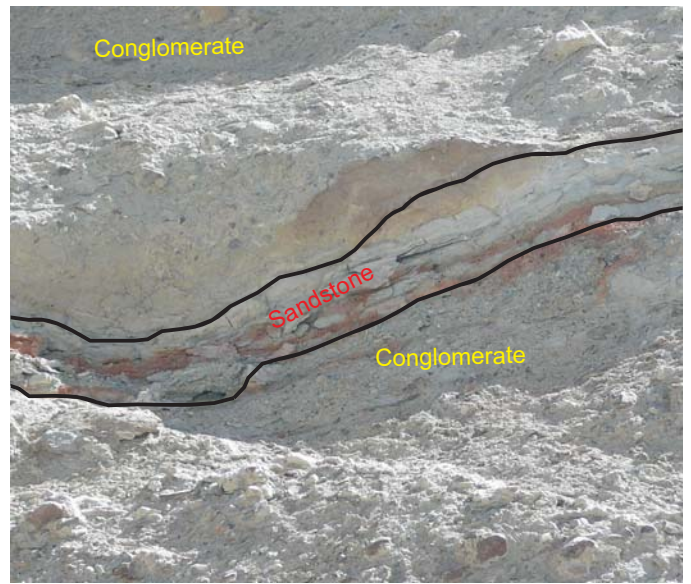
Fig. 3.4: Alternation of conglomerate and sandstone beds in the Tetang Formation at Tetang village.
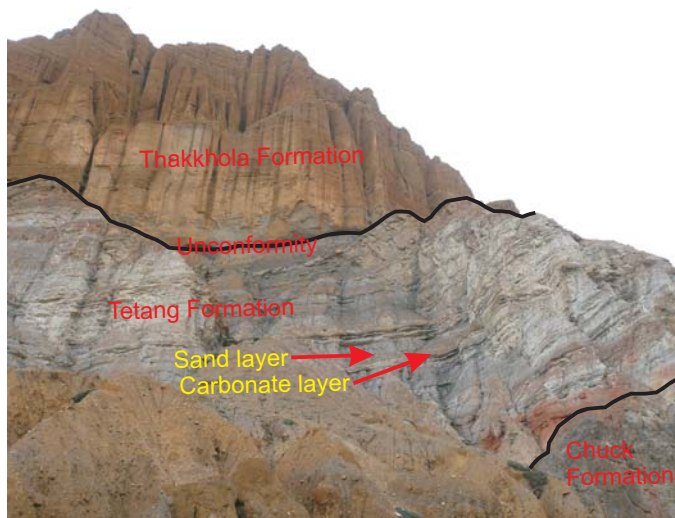
Fig. 3.5: Alternation of carbonate layers and sandstone beds in the Tetang Formation at the Tetang village. Tetang Formation lies uncomformably on the Cretaceous Chuck Formation whereas the Thakkhola Formation and the Tetang Formation are separated by an angular unconformity.
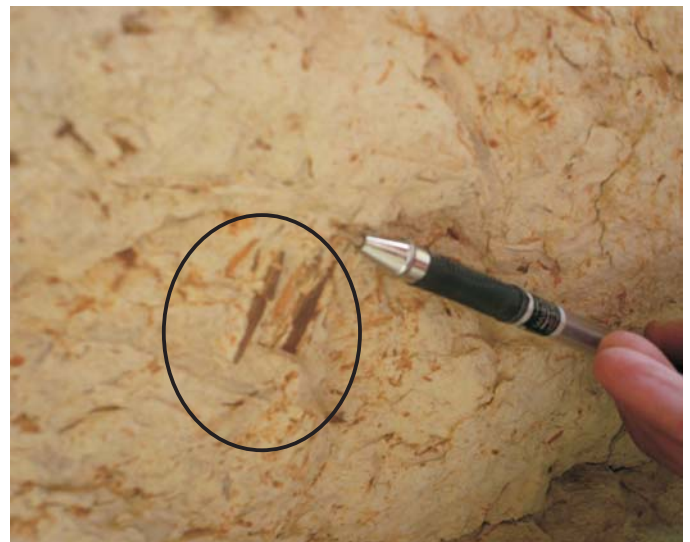
Fig. 3.6: Plant fossils in the carbonaceous silt layer on the Tetang Formation at Tetang village.

SW

NE

Braided fluvial conglomerate
(Thakkhola Formation)

Unconformity

Limestone
(Tetang Formation)

Thakkhola Formation
(Miocene-Pliocene)

Unconformity

Tetang Formation
(Miocene)

Chuck Formation
(Cretaceous)

Fig. 3.7:Thakkhola and Tetang formations are seperated by an angular unconformity. Imbricated conglomerates of the Thakkhola Formation are separated by an angular unconformity from the fine-grained limestone of the Tetang Formation at the Dhinkyo Khola section.
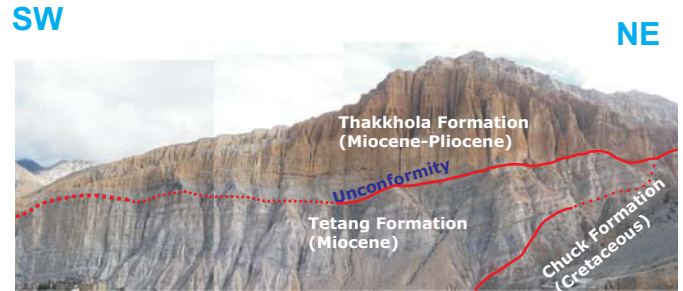
Fig. 3.8: Photo mosaic of the stratigraphic contact between the Thakkhola Formation and the Tetang Formation near Tetang village along the Narsing Khola. The Tetang Formation onlaps the Cretaceous Chuck Formation whereas an unconformity seperates the Tetang Formation and Thakkhola Formation.

Fig. 3.9: Thick conglomerate beds on the basal section of the Thakkhola Formation at Chaile section.

Fig. 3.10: Bioturbation found in the siltstone bed of the Thakkhola Formation in the Chaile section.

Fig. 3.11: Thick beds of siltstone in the Thakkhola Formation at the Chaile section on the way to Samar.

Fig. 3.12: Root fragment found in the siltstone bed of the Thakkhola Formation at Chaile section.

Fig. 3.13: Iron-rich carbonate concretions of the Thakkhola Formation at Ghiling section.

3.1.4 Marpha Formation

Glacio-lacustrine sedimentary rocks, which belong to the Marpha Formation, are well exposed in the Syang Khola and Marpha village (Fort et al., 1982; Iwata, 1984) (Fig. 3.1).The Marpha Formation comprises a more than 200 m thick succession of mudstone and siltstone intercalated with sandstone and conglomerate (Fort et al., 1982). However, it was possible only to measure a 45 m lithological succession in the studied section. The basal section is composed of fine to medium lacustrine sand with mud layers (Fig 3.2Q and R). Some slump structures are present in the sand and clay layers that were produced by the gravitational flow (Fig. 3.16). Conglomerate beds of average clast size of ca. 28 cm are interbedded with the mudstone on the upper part of the sequence (Fig. 3.17). The compositions of the clasts are mainly quartzite, sandstone, slate, granite and carbonates. These coarse sandstone grades into laminated medium-grained sandstone interbedded with thick layer of muddy conglomerate (Fig. 3.2Q).

The dipping of most beds in this formation range from 5-7 degree. At Syang Khola, the Marpha Formation is more coarse grained and consists of massive coarse-grained sandstone with a conglomerate of 37 cm clast size. Fort et al. (1982) correlate the lowermost Marpha Formation with the uppermost Sammargaon Formation based on the association of the Marpha Formation with glacial till. Previous researchers tried to calculate the age of the Marpha Formation on different basis. Iwata (1984) and Yoshida et al. (1984) assigned a late Pleistocene age (150 ka) but Hurtado et al. (2001) again reanalyzed the magnetostratigraphic data of the Yoshida et al. (1984) and assigned an age of ca. 33-37 ka to the lowermost part of the Marpha Formation.

3.1.5 Kaligandaki Formation

This formation overlies the Marpha Formation in a cut and fill relationship with the Tilicho col Formation in the Syang Khola section. The type section is more than 30 m in thickness on the western side of the Syang Khola, a tributary of Kaligandaki River. This formation can be divided in to three main units and they are distinct within and with the Marpha Formation. The basal section is composed of sandstone (KGF I), fluvial conglomerate (KGF II) and an upper debris flow breccias (KGF III) (Fig. 3.15b). Hurtado et al. (2001) correlated the fluvial conglomerate of this formation with the coarse-grained fluvial conglomerates at the mouth of the Jhong Khola at Kagbeni of age 17-5.5 ka.3.1.6.

3.1.6 Development of angular unconformity between the Tetang and the Thakkhola Formation

Fort et al. (1982) recognized an angular unconformity between the Tetang Formation and the Thakkhola Formation near the Tetang village. In this study, the same unconformity along the Tetang village as well as in the Dhinkyo Khola section was documented. The

Thakkhola Formation overlies the Tetang Formation by an angular unconformity (Fig. 3.5, 3.7, 3.8 & 3.23). 13° to 23° northwest dipping strata of the Tetang Formation are widely exposed at the Tetang village (Fig. 3.8). These strata were rotated ~ 6° westward into the Dangardzong fault before the deposition of the Thakkhola Formation (Fig. 3.14). The strata of the Thakkhola Formation just above the unconformity dip ~ 13° towards the
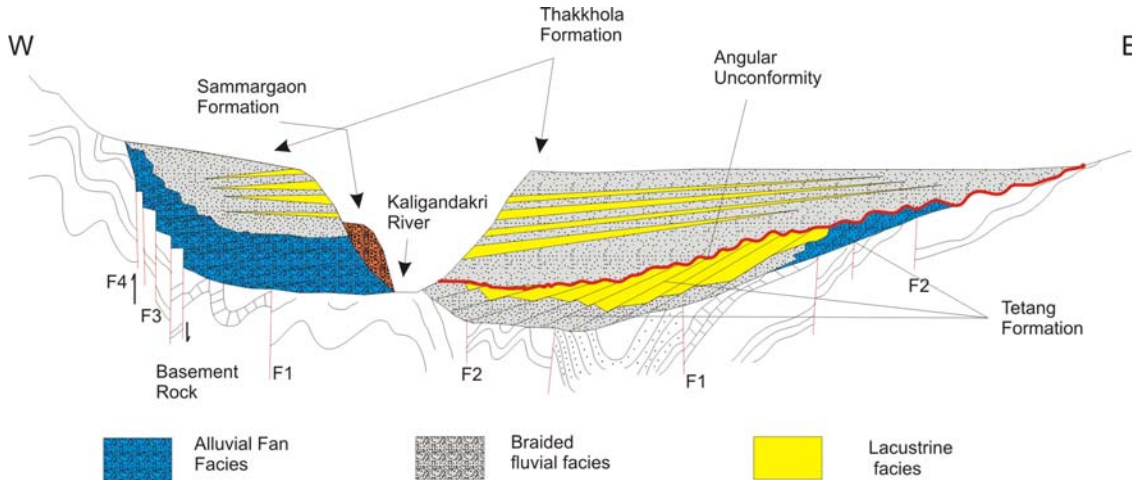
Fig. 3.14: Schematic cross section of the Thakkhola-Mustang Graben showing important tectonic features of the basin. F1, F2, F3, F4: faults of different phases in the basement rocks (modified after Fort et al., 1982).

right bank of Dhinkyo Khola section. The conglomerate bed of the Thakkhola Formation lies just above the limestone of the Tetang Formation (Fig. 3.7).

3.2 Tectonic features of the graben

The Thakkhola-Mustang Graben shows a complex kinematic and geometrical relationship with the South Tibetan Detachment System (STDS) and the Dangardzong fault. The Thakkhola-Mustang Graben is bounded by the Dangardzong fault (Hutardo et al., 2001) on its western side and Muktinath fault on the eastern side. The Dangardzong fault developed synchronous with the motion of the Annapurna detachment during Miocene times (Hutardo et al., 2001). Colchen (1999) recognized a temporal succession of compression and extensional tectonic regimes. N20°-40° trending faults are responsible for the development of the graben (Hagen, 1968) and these structures are accompanied by other faults, N0°, N115° and N150°-160° by weak folds, which affect the graben filling. Coleman (1996) observed normal faults similar to the Dangardzong fault up to 40 km to the east. Coleman and Hodges (1995) calculated the minimum age of ca. 14 Ma for the east-west extension in this graben area from the ^{49}Ar/^{39}Ar ages of hydrothermal muscovite that crystallized in one of the northeast-striking fractures. The Lupra fault is one of the most prominent east-striking types of faults (Fig. 3.1), which was interpreted by Godin (1999) as a thrust fault that was later reactivated as a normal

a

b
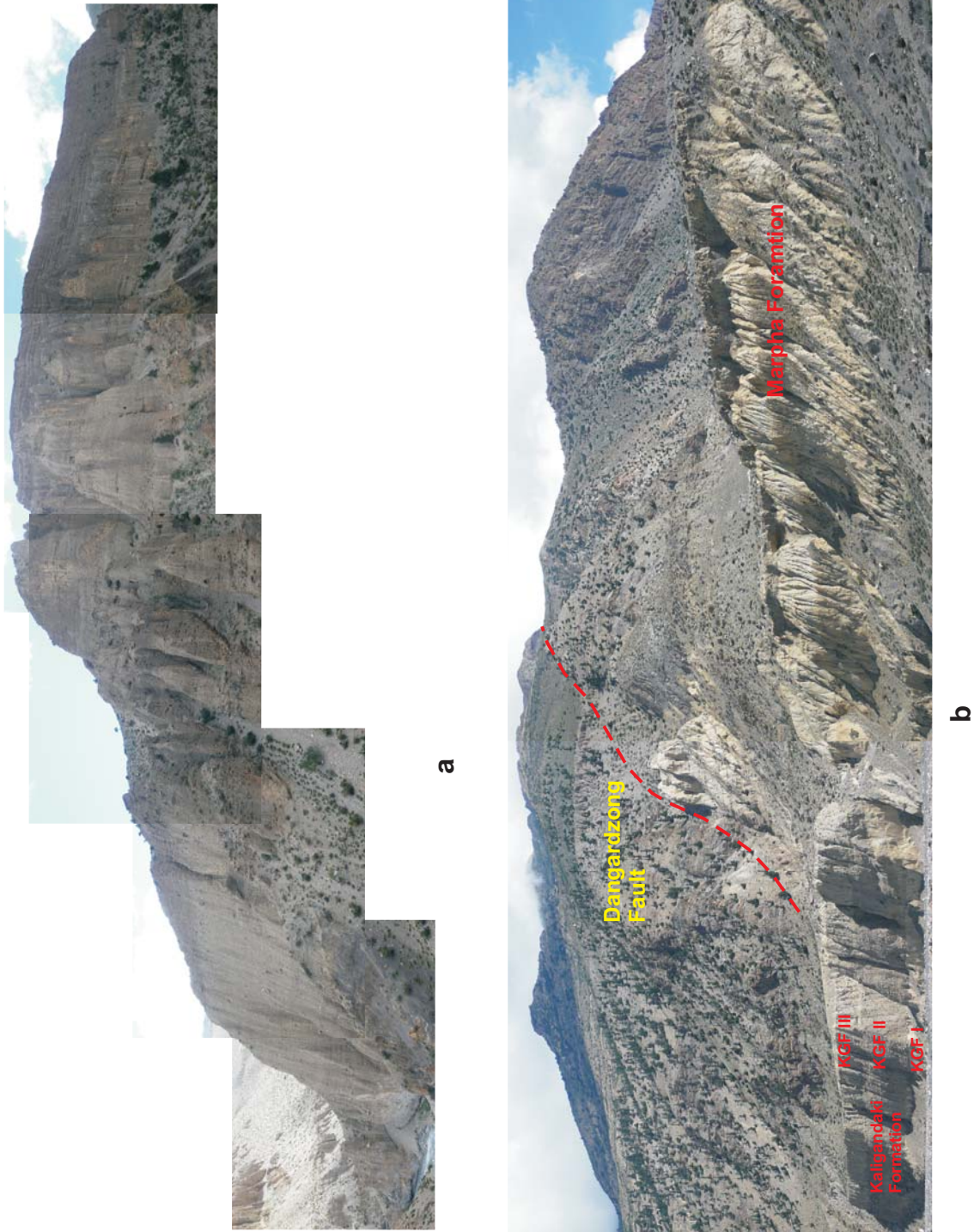
Fig. 3.15: Panoramic View of different formations. (a) Conglomerate sequences of the Sammargaon Foramtion made of glacial morains in Ghilumpa khola. (b) Marpha Formation and Kaligandaki Formation (KGFI-KGFIII) with the Dangardzong Fault on the eastern side of the Syang Khola. The Dangardzong fault does not offset the any sequences of the Kaligandaki Formation.

Fig. 3.16: Slump structure in the the basal Marpha Formation at Marpha village.

Fig. 3.17: Alternating beds of mudstone and conglomerate in the Marpha Formation at the Marpha village.
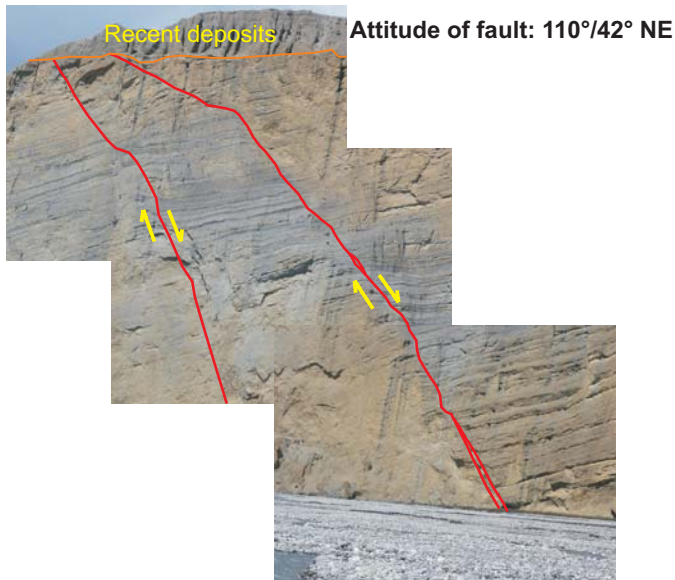
Fig. 3.18: Normal growth faults in the Thakkhola Formation in the Tange area.
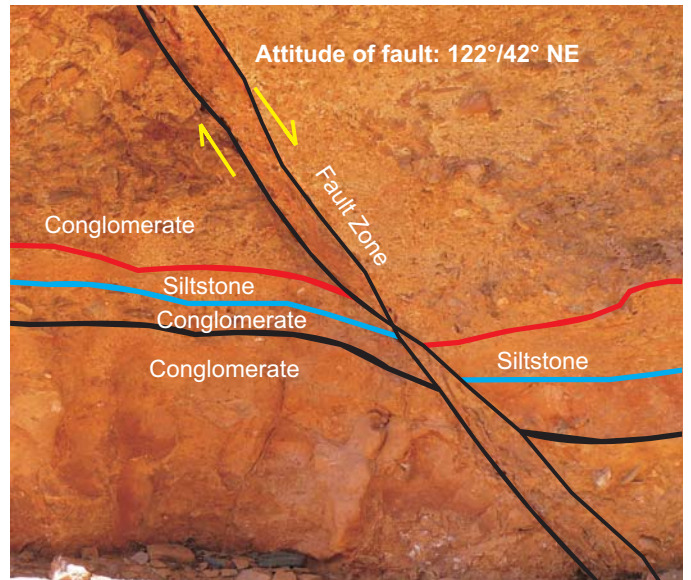
Fig. 3.19: Normal growth faults in the Thakkhola Formation in the Dhakmar area.

fault during development of the Thakkhola-Mustang Graben. Garzione et al. (2003) and Hurtado et al. (2001) mapped east striking normal faults in the Tetang area. There are numerous small-scale faults throughout the basin fill sediments, which are interpreted as a syndepositional growth faults. NE striking faults are present in the Tange area, which displace the sediments of the Thakkhola Formation. Quaternary deposits cover and seal the upper part of the fault, which suggest that the tectonic activities were mainly active in the depositional time of the Thakkhola Formation (Fig. 3.18). In the Dhakmar area, the NE striking growth fault displaces the massive conglomerate about 50 cm (Fig. 3.19). A Small-scale normal fault striking NE displaces the subsequent beds about 150 cm in the Tetang Formation, which indicates the onset of east-west extension (Fig. 3.20). Two east and west dipping two growth faults are clearly seen in the Dhinkyo Khola section (Fig. 3.21). These two faults displaced the imbricated conglomerate beds of the Thakkhola Formation and reach up to the unconformity between Thakkhola and Tetang formations.

3.2.1 Mapping of Dangardzong Fault

The Dangardzong fault, a N20°-40°E striking, steeply (~50°) dipping fault system, bounds the graben on the western side and was the main principle growth fault in this graben (Hagen, 1968, Bordet et al., 1971; Colchen, 1980) (Fig 3.1).

The fault is marked by a clear topographic depression from north to south, and it appears as a cluster of faults. On the northern end of the graben, this fault curves towards the west (strike ~ 170°) around the Mustang and Mugu plutons (Fig. 3.1). There is no trace of the Dangardzong fault north of the Indus-Tsangpo suture (Hurtado et al. 2001). The fault itself separates Tibetan Sedimentary Sequences and the basin fill of the Thakkhola-Mustang Graben, but it cuts through the Greater Himalayan Sequence on the southern part. The slip of the Dangardzong fault is decreases from the center of the graben towards the south (Fort et al. 1982), the amplitude varies from 4000 m (vertical slip) and 8 km (horizontal slip) at Sammargaon to a few tens of meters near Lete at 50 km to the south (Fort et al., 1982). Hurtado et al. (2001) noted a progressive decrease in the metamorphic grade of the footwall along the Dangardzong fault, from the biotite zone of greenschist facies at the latitude of Tangbe village to the chlorite zone and lower south of Dangardzong village, which suggest a decrease of footwall exhumation towards the south. Paleozoic and Triassic rocks on the western blocks along this fault are affected by a slight alpine metamorphism characterized by newly formed biotite and chlorite whereas the eastern block was not affected by this alpine metamorphism (Fort et al., 1982). The Dangardzong fault was studied in detail five places along its strike from north to south along the Charan Khola near Ghar Ghumba, Sammargaon, Ghilumpa Khola, Dangardzong village and Syang Khola. Detailed descriptions of these locations are given below:

Ghar Ghumba: The Dangardzong fault is exposed near the Ghar Ghumba on the Charan Khola, an east flowing tributary of the Kali Gandaki River, which is 500 m NE from the present Ghar Ghumba. Steep Paleozoic rocks (brownish quartzite) are present in the northern side whereas fault breccias are present at the Charan Khola. Deformed quartzites
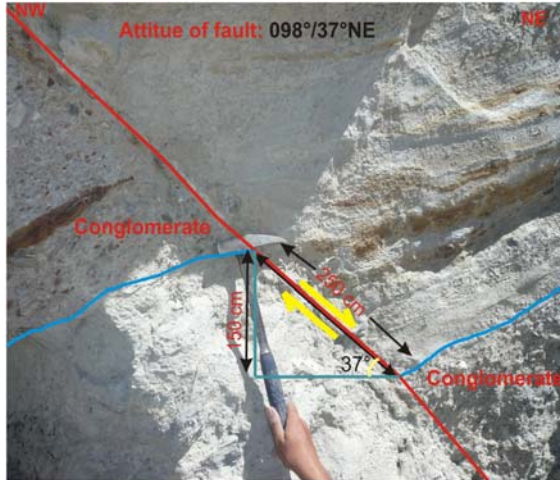
Fig. 3.20: Normal growth fault in the Tetang Formation in the Tetang village

Fig. 3.21: Normal growth fault in the Thakkhola Formation in the Dhinkyo Khola

were found along the fault line (strike is around 186°). Landslide deposits are dominating at the base of the steep quartzite terrain, which enclose very large sized angular boulders of quartzite. The Charan Khola sharply bends along the strike of the Dangardzong fault. River offset is due to young activity of the fault (Fig. 2.22A).

Sammargaon village: On the eastern side of the Samar village, fault breccias can be seen. Paleozoic rocks, which are in strong contrast to the layers of the graben fill within the fault zone, are deformed and crushed. They are nearly horizontal or only slightly folded near the fault zone (Fig. 3.22B).

Ghilumpa Khola: The Dangardzong fault is exposed at the head of the Ghilumpa Khola at an alleviated section and east flowing tributary of Kali Gandaki River (Fig. 3.22C). The Ghilumpa Khola suddenly bends southward and flows along the strike of the fault, which turns again eastward up to Kaligandaki River. The length of the river offset is about 100 m. The fault places gray fine-grained schists of the Tilicho Pass Formation on the footwall while Cretaceous quartzite of the Chuck Formation are present in the hanging wall. The river cuts the bedrock, which makes a canyon of approx. 100 m deep. The river flows downward gently depositing alluvium after the canyon. The 100 m wide fault zone consists of fault gauge. The fault is striking N 57° E and dipping 55° SE. Hurtado et al. (2001) explained that the kinematic indicators in the bedrock show normal-sense movement and the right-lateral bed in the Ghilumpa Khola coincident with the fault trace, which suggest dextral strike-slip displacement.
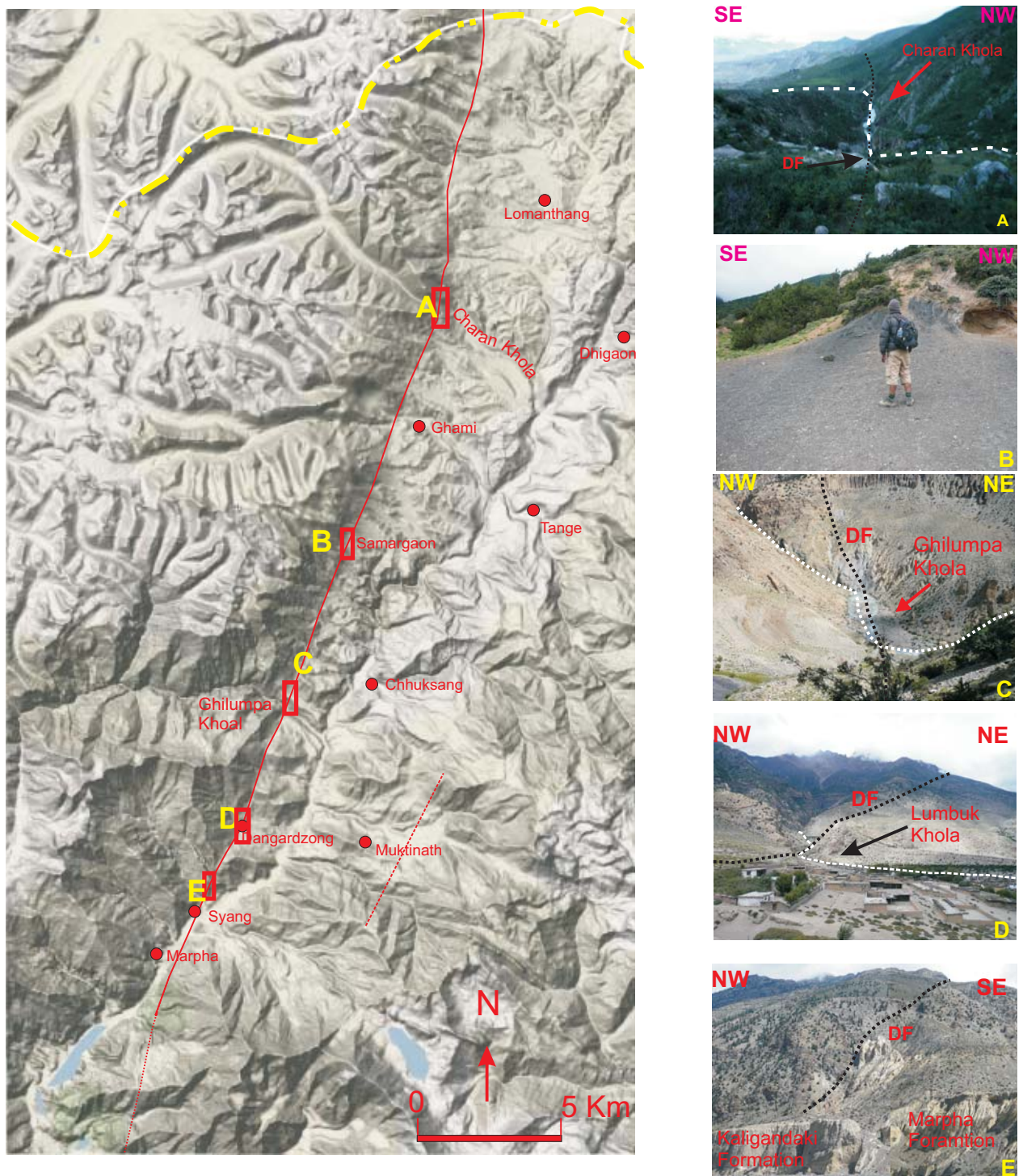
**Fig. 3.22: Trace of Danerdzong fault in google image in different place along the strike of the fault.
(A) The deflection of the Charan Khola near Ghar Ghumba (white dotted line is the trace of fault
while the dotted black line represents the path of khola), (B) fault breccia along the fault in
Samargaon, (C) Sharp bending of the Ghilumpa Khola along the strike of fault, (D) just north from
the Dangardzong Khola on the Lumbuk Khola, (E) the fault developed on the Kaligandaki Formation
and the Marpha Formation near the Syang Village on the eastern side of the Syang Khola.**
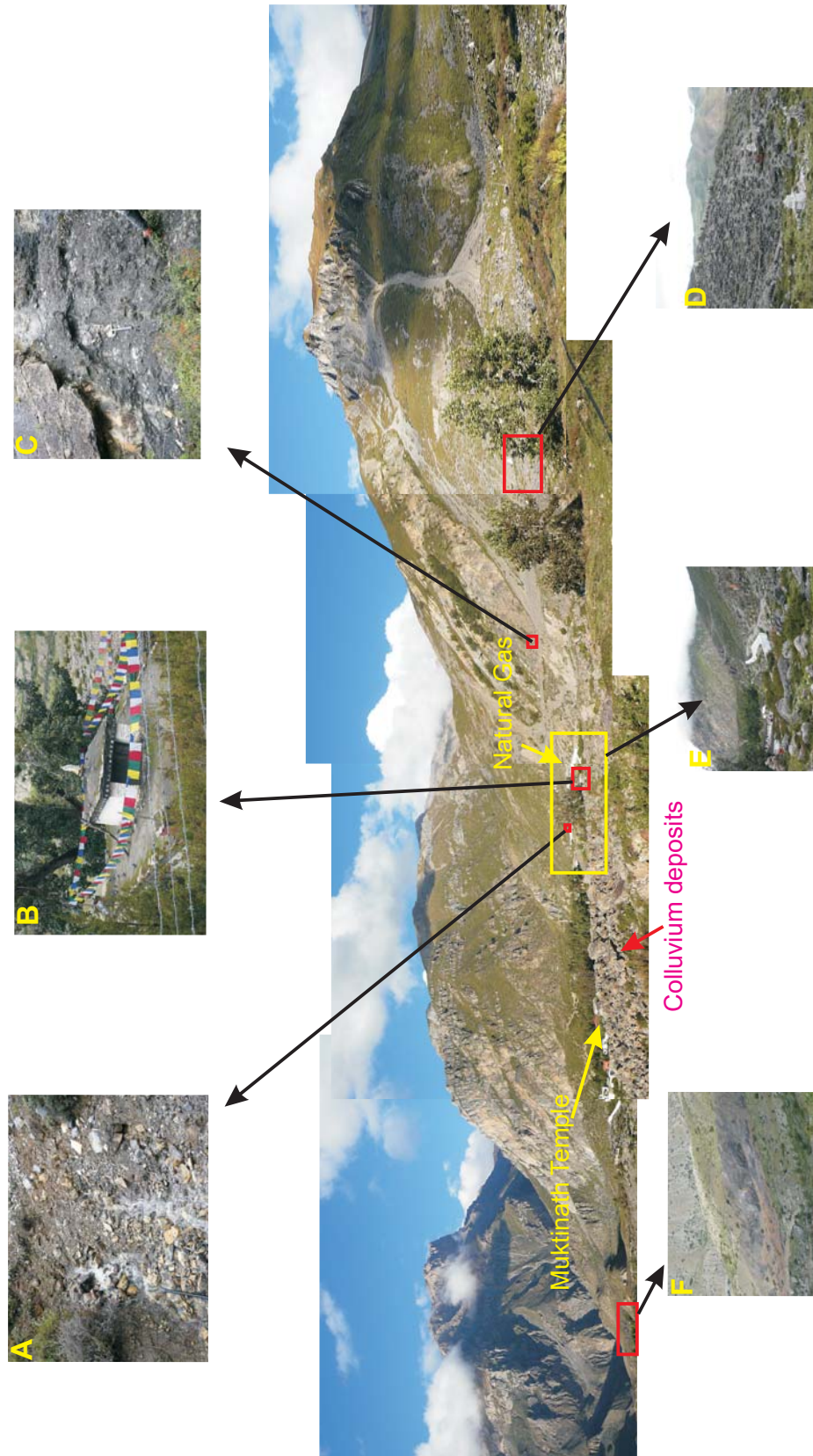
Fig. 3.23: Possible area of Muktinath Fault. Mesozoic rocks are on the bed rock and colluvium deposits around the Muktinath Temple. (A) Natural spring on the scarp north of Muktinath Temple, (B) Natural gas flame (not allowed to take pic of flame which is inside the Temple), (C) distrubed scarp of the mesozoic rock, (D) Colluvium deposit east of the Muktinath Temple, (E) Colluvium on closer view, (F) disturbed lithology with black color, possible area of Muktinath fault.

Dangardzong village: Hurtado et al. (2001) named the Dangardzong fault after the Dangardzong village. The fault is exposed on the sharp bend of the Pan Khola, a small east flowing tributary of Kaligandaki River, ca. 1 km NW of the Dangardzong Village (Fig. 3.22D). The fault places black schist and quartzite on the footwall and quartzite on the hanging wall. At this place, the fault strikes N26°E and dips 68° SE. Some slickensides are present on the footwall plunging 22°SE. In the upstream of the fault zone, the river made a gorge in the bedrock while deposited alluvium on the downstream. Hurtado et al. (2001) inferred that the fault activity has ceased by ca. 5.1 Ma based on the terrace chronology.

Syang village: The Dangardzong fault passes through this village. The fault places the Marpha Formation in a fault contact with the Tilicho Pass Formation (Fig. 3.22E & 3.15b). The fault is very hard to distinguish in this area; however, the presence of some brecciated footwall rocks indicate the position of the fault. The fault does not offset either Marpha and Kaligandaki or the river terraces. The minimum age for the last episode of the faulting was estimated as ca. 17.2 ka (Hurtado et al., 2001). They calculated the age with the help of stratigraphic and structural relationship between the terraces and the Marpha and Kaligandaki formations combined with ^{14}C chronology.

Hurtado et al. (2001) mapped the southern termination of the Dangardzong fault on a hill 3.5 km north-east of Lete village and 17 km southwest of Syang village near the village of Titi by using surface morphology, SPOT imagery and interpretation of talus and regolith lithologies. The faults are characterized by N10° to N25° strike and by a minor displacement and they are associated with the mylonitic zones (Fort, 1980).

3.2.2 Muktinath Fault

Bordet et al. (1971) have recognized numerous faults having minor vertical slip with sub-meridianal strike (N0°, N05°) on the northern side of the higher range. The Muktinath fault is the most important among them, which extends for several km from the NE of the Muktinath Temple to the Nilgiri range to the south. This fault is believed to be responsible for the emission of the natural gas in the famous Muktinath Temple (Hindu and Buddhist sanctuary) (Fig. 3.23B). The cliff above the Muktinath Temple, composed of Jomsoom limestone, is juxtaposed to the Spiti Formation by fault contact (Colchen et al., 1986). Natural spring water is coming from the scarp of the disturbed zone (Fig. 3.23 A). The Muktinath area consists of moraines intermixed with colluvium derived from the nearby limestone cliff. The moraine is composed of boulders intermixed with gravel, sand, silt and clay (Fig. 3.23D and E). Some black horizons are also exposed at the western side of the temple (Fig. 3.23F). However, the fault trace is not clearly visible in the field.

CHAPTER FOUR
FACIES ANALYSIS

4.1 Introduction

The term "facies" denotes a body of rocks with specified characteristics that differentiate it from others in appearance and composition. A facies is a distinctive rock unit that forms under certain conditions of sedimentation reflecting a particular process or environment. Facies based on petrological characters such as grain size and mineralogy are called lithofacies whereas facies based on fossil content are called biofacies. Lithofacies is a rock unit defined based on its distinctive lithologic features including composition, grain size, bedding characteristics and sedimentary structures.

Some attempts have already been made in order to infer the depositional environment and facies analysis of the Thakkhola-Mustang Graben. Most of previous researchers like Fort et al. (1982), Garzione et al. (2003) and Hurtado et al. (2001) reported that the Thakkhola and Tetang formations were deposited in alluvial fan, braided river and lacustrine environments. Yoshida et al. (1984) reported that the climate during deposition was quite warmer than that of present time based on polynormorphs. These polynormorphs consists of *Lonicera, Caragana, Ephedra, Artemisia* and others. They also reported that the Takmar Series (Thakkhola and Tetang formations) can be correlated with the Tatrot and Pinjor formations of the Siwalik Group (Jonnson et al., 1982) though the lower part of the series may be much older.

4.2 Methods

In this study, an attempt has been made to recognize the lithofacies types, their distribution and to interprete the depositional environment of the Tetang and Thakkhola formations in detail. A modified lithofacies and architectural classification from Miall (1996) was used in this study and presented in Table 4.1 and 4.2. Detailed columnar sections were made on the basis textures and sedimentary structures (Fig. 3.2A, B, C, D, E, F G, H, I, J, K, L, M, N, O, P, Q and R). Twelve distinct sedimentary facies based on lithology, bed-geometry and internal structure are identified within the sedimentary succession of the Tetang, Thakkhola, Sammargaon and Marpha formations and these can be classified into three facies associations (Table 4.3).

4.3 Facies association I: Matrix-rich conglomerate-gravelly sandstone association

4.3.1 Description

This type of facies is exposed mainly along the eastern and western sides of the basin. Facies association I consists of four different lithofacies: A-D.

Facies A is a moderately sorted gravel-boulder (recorded longest clast diameter is 21 cm) massive conglomerate with sandy matrix (Fig. 3.2L & 3.3). This matrix rich conglomerate beds are 0.5 to 6 m in thickness. Carbonate, quartzite and slate (Fig. 4.1) represent the coarse-clast population.

Lithofacies B consists of poorly sorted clast supported cobble to boulder conglomerate (Fig. 4.2). These clasts are sub-angular to sub-rounded with a small proportion of boulders distributed with the coarse-grained sand. The compositions of the clast are similar to lithofacies A without any stratification. Thicknesses of individual beds are 0.5 to 3 m.

Imbricated to massive, moderately sorted pebble conglomerate and laterally extensive beds (Fig. 3.9 and 4.3) characterize Lithofacies C. The thickness of the beds ranges from 0.3 to 12 m. The composition of the clasts includes granite, quartzite, sandstone and slate. Lithofacies D comprises mainly poorly sorted pebble and cobble-sized conglomerate with associated lenses of reddish wedge-shaped horizontally laminated sandstone (Fig. 4.4). These coarse-grained sandstones are continuous to more than 5 m and then terminate like a wedge shape.

4.3.2 Interpretation

The wide lateral extent of moderately sorted randomly oriented clasts of massive conglomerate of lithofacies A suggests the possibility of glacial origin. However, erosive base with sandy matrix within the conglomerate suggests sheet flood to channel deposits where the water has a high strength and viscosity. The clasts of carbonate, quartzite and slates appear to be derived from the surrounding rocks. This organized clast-supported massive conglomerate (Gmm) with moderately developed clast imbrications may be a result of incised-channel gravel bed load under accreting low-to waning-energy flows (Jo et al., 1997; Blair, 1999). The bed geometry represents gravel sheets or low relief longitudinal bars.

Poorly sorted, clast supported cobble to boulder conglomerate without stratification of lithofacies B is interpreted as deposits of debris flows (Johnson, 1970, 1984; Garzione et al., 2003) of low strength. Sub angular to sub rounded clasts with a small proportion of boulders within the coarse-grained sand are deposited in linguoid bars during stream flow.

Lithofacies C is interpreted as the product of low-cohesive clast rich debris flows transitional to stream flow, which is deposited in channel fill and gravel bars geometries. Imbrications show that the sediments were transported partly in traction flows. Dasgupta (2007) suggested that these types of sediments are a product of rapid sedimentation from flows of transitional character between debris flow and hyperconcentrated flows. These types of sediments are observed generally in gravelly alluvial fan systems (Blair and McPherson, 1994).

Poorly sorted pebbles and cobbles sized conglomerate with reddish wedge shaped horizontally laminated sandstone of Facies D is deposited by sheet flow. Sediments are deposited in the longitudinal bed forms and lag deposits. Nakayama and Ulak (1999) suggested that such kinds of sediments in the Siwalik of Nepal Himalaya are deposit of gravelly braided systems.

4.4 Facies association II: Matrix rich conglomerate with sandstone and mudstone

4.4.1 Description
This lithofacies is widespread within the Thakkhola-Mustang Graben. This type of facies association comprises mainly conglomerates with sandstones and mudstones.

Lithofacies E comprises moderately thick matrix-rich conglomerates of limited extent. Clasts are well rounded to sub rounded and usually imbricated (Fig. 4.5). Conglomerate beds are 0.8 to 2 m thick, which can be traced more than 500 m laterally. Paleocurrent directions are uniform within the individual sequences. Conglomerates have a sandy matrix and erosive bases. Clast compositions are variable like granite, carbonate and calcareous sandstone.

Lithofacies F consists of coarse to very coarse grained cross-stratified sandstone (Fig. 4.6). Pebbles of different composition are aligned in the cross-stratification. The sandstone beds are 0.2 to 3 m in thickness can be traced more than 20 m laterally.

Lithofacies G is characterized by massive gray, red and sometimes black compact mudstone (Fig. 4.7). Root fragments, bioturbation and plant fossils are present. These beds are 0.1 to 2 m in thickness and can be traced more than 1 km laterally.

Lithofacies H is composed of mainly of well-sorted pebble and cobble-sized conglomerate interbedded with laminated grey sandstone (Fig. 4.8). Sandstone shows iron–rich carbonates concretions (Fig. 3.13). The conglomerate beds are 0.1 to 3 m thick with some mud lenses. Erosion surfaces are common in the sandstone beds.

4.4.2 Interpretation
Lithofacies E is interpreted as longitudinal bar deposits of stream-flow rivers. Some erosion features of imbricated conglomerate imply that relatively shallow and/or unstable channels characterized the system. Some normal grading in the beds may have been developed during waning flow stages (Garzione et al., 2003). Rounded to subrounded and imbricated conglomerates originated from the bed load of a gravelly river deposits.

Coarse to very coarse cross-stratified sandstone of lithofacies F deposited as a sheet flow to channel deposits. The sheet-like geometry of sandstones and pebbly sandstones and the development of planar cross-stratification and the less clear upward-fining succession are

Table 4.1: Description of sedimentary facies classification (after Miall, 1996)

Facies code	Facies	Sedimentary structures	Interpretation
Gmm	Matrix-supported, massive gravel	Weak grading	Plastic debris flow (high-strength, viscous)
Gmg	Matrix-supported gravel	Inverse to normal grading	Pseudoplastic debris flow (low strength, viscous)
Gci	Clast-supported gravel	Inverse grading	Clast-rich debris flow (high strength), or Pseudoplastic debris flow (low strength)
Gcm	Clast supported. Massive gravel	-	Pseudoplastic debris flow (intertial bedload, turbulent flow)
Gh	Clast-supported, curdly bedded gravel	Horizontal bedding, imbrications	Longitudinal bed forms, lag deposits, sieve deposits
Gt	Gravel, stratified	Trough cross beds	Minor channel fills
Gp	Gravel, stratified	Planner cross beds	Transverse bed forms, deltaic growths from older bar remnants.
St	Sand, fine to v. coarse, may be pebbly	Solitary or grouped trough cross beds	Minor channel fills
Sp	Sand, fine to v. coarse may be pebbly	Solitary or grouped planar cross beds	Sinuously crested and linguoid (3-D) dunes
Sr	Sand, very fine to coarse	Ripple cross-lamination	Ripples (Lower flow regime)
Sh	Sand, v. fine to coarse may be pebbly	Horizontal lamination, parting or streaming lineation	Plane-bed flow (critical flow)
Sl	Sand, v. fine to coarse. May be pebbly	Low angle (<15°) cross beds	Scour fills, humpback or washed-out dunes, antidunes.
Ss	Sand, fine to v. coarse, may be pebbly	Broad, shallow scours	Scour fill
Sm	Sand, fine to coarse	Massive, or faint lamination	Sediment-gravity flow deposits
Fl	Sand, silt, Mud	Fine lamination, v. small ripples	Overbank, abandoned channel, or waning flow deposits
Fsm	Silt, Mud	Massive	Back swamp or abandoned channel deposits
Fm	Mud, silt	Massive, desiccation cracks	Overbank, abandoned channel, or drape deposits
Fr	Mud, silt	Massive, roots, bioturbation	Root bed, incipient
C	Coal, carbonaceous mud,	Plant, mud films	Vegetated swamp deposits
P	Paleosol carbonate	Pedogenic features	Soil with chemical properties.

Table 4.2: Architectural elements in fluvial deposits (after Miall, 1985 & 1996)

Element	Symbol	Principal lithofacies assemblages	Geometry and relationships
Channels	CH	any combination	Finger, lens or sheet; concave-up erosional base; scale and shape highly variable; internal concave-up secondary erosion
Gravel bars and bed forms	GB	Gmm, Gp, Gt	Lens, blanket: usually tabular bodies; commonly interbedded with Sandy bed forms
Sandy bed forms	SB	St, Sp, Sh, Sl, Sr, Ss	Lens, sheet, blanket, wedge; occurs as channel fills, crevasses splays, minor bars.
Foreset macro-forms	FM	St, Sp, Sh, Sl, Sr, Ss	Lens resting on flat or channeled base, with convex-up second-order internal erosion surfaces and upper bounding surface.
Lateral accretion deposits	LA	St, Sp, Sh, Sl, Sr, Ss; less commonly Gm, Gt, Gp.	Wedge, sheer, lobe; characterized by internal lateral accretion surfaces.
Sediment gravity flows	SG	Gmg, Gmm	Lobe, sheet; typically interbedded with gravel bars and bedforms
Laminated sand sheets	LS	Sh, Sl; minor St, Sp, Fl	Sheet, blanket
Overbank fines	OF	Fm, Fl	Thin to thick blankets; commonly interbedded with sandy bedforms; may fill abandoned channels

characteristics of the classic 'Platte-type' braided river deposits (Smith, 1972; Miall, 1978).

Massive gray, red and sometimes black compact mudstone of lithofacies G indicates standing water and perhaps lakes in flood-plain environments. Root fragments, bioturbation and some plant fossils suggest that the riverbanks were stable over a longer period. The red color of the sediments at the Dhakmar area could be related to the chemical weathering developed under warm and humid condition before the formation of the graben (Fort et al., 1982).

Lithofacies H is interpreted as an overbank deposit, abandoned channel, waning flow deposit or sheet flow. The pebbly conglomerate grades upward into laminar grey sandstone. The presence of granular interlayers indicates that the pebbly conglomerates are the product of a heavily sediment laden turbulent flow. The stratified character of the fine-grained conglomerate-granular and sandstone without distinct bedding surface can be attributed to continuous traction carpet deposition. Sohn (1997) described similar type of interlayer as a product of traction carpet sedimentation.

Table 4.3: Facies association and their occurrences in the Thakkhola-Mustang Graben. (facies are adapted from Miall 1996)

Facies associat ion	Lithofacies type	Facies code	Stratigraphic units	Description	Architect ural element	Interpretation
I	Matrix-supported, massive gravel (Facies A)	Gmm	Tetang, Thakkhola, Sammargoan	Moderately sorted, gravel, massive conglomerate, with sandy matrix, gravels up to 21 cm, erosive base, units up to 6 m thick.	GB, CH, LA	Longitudinal bars, sheet flood to channel deposits (high-strength, viscous)
I	Clast-supported gravel (Facies B)	Gci	Tetang, Thakkhola, Sammargoan	Poorly sorted, clast supported , cobble to boulder conglomerate, units up to 0.5 to 3 m.	GB, CH, LA	Linguoid bars or Pseudoplastic debris flow (low strength, viscous)
I	Matrix-supported gravel (Facies C)	Gmg	Tetang, Thakkhola	Imbricated to massive, moderately sorted pebble to gravel conglomerate and laterally extensive beds.	GB, CH, LA	Clast-rich debris flow (high strength), or Pseu-doplastic debris flow (low strength
I	Clast-supported, curdly bedded gravel (Facies D)	Gh	Tetang, Thakkhola	Poorly sorted pebble and cobble sized conglomerate with associated lenses of reddish-wedged shaped horizontally laminated sandstone.	GB, CH, LA	Longitudinal bedforms, lag deposits, sieve deposits, Sheet flows.
II	Gravel, stratified (Facies E)	Gt	Tetang, Thakkhola	Moderately thick matrix-rich conglomerate of limited extend with sandy matrix.	GB, LA, CH	Minor channel fills and transverse bars.
II	Sand, fine to v. coarse may be pebbly (Facies F)	Sp	Thakkhola	Coarse to very coarse grained cross-stratified sandstone. Pebbles of different composition are aligned in the cross-stratification.	CH, SB	Sinuously crested and linguoid (3-D) dunes, sheet flow to channel deposits
II	Mud, silt (Facies G)	Fr	Tetang, Thakkhola	Massive gray, red and sometimes black compact mudstone with root fragments, biotubation and plant fossils.	OF	Root bed, incipient
II	Sand, silt, Mud (Facies H)	Fl	Thakkhola, Marpha	Well sorted pebbly conglomerate with laminar grey sandstone.	LS, OF, SB	Overbank, abandoned channel, or waning flow deposits or sheet flow deposits
III	carbonaceous mud (Facies I)	C	Thakkhola	Poorly consolidated laminated to massive carbonaceous mud	OF	Vegetated swamp deposits, open lacustrine
III	Silt, Mud (Facies J)	Fsm	Tetang, Thakkhola	Comprises of organic layers with plant fossils	OF, SB	Back swamp or abandoned channel deposits
III	Clast supported. Massive gravel (Facies K)	Gcm	Tetang, Thakkhola	Structureless conglomerate within the mudstone and siltstone beds with lenses of conglomerate.	GB, CH, LA	Pseudoplastic debris flow (intertial bedload, turbulent flow)
III	carbonate (Facies L)	P	Tetang, Thakkhola	Laminated, yellow color, micritic matrix, with ostracods, overlained by claystone and organic layers.	LS, CH	Soil with chemical properties. Palustrine

Table: 4.4: Description and interpretation of fluvial architectural elements recognized in the Thakkhola-Mustang Graben.

Architectural element	Grain size	Description	Interpretation
Channel-fill complex (CH)	Pebble to cobble conglomerate, fine- to coarse-grained sandstone with mudclasts	Lenticular, multi-and single-storeys, sharp concave-up erosive base. Gmm, Gci, Gmg, Gh, Gt, Sp, Gcm, P.	Growth of gravelly and sandy channel fills
Gravel bars (GB)	Clast-supported granules to cobble conglomerate interbedded with sandstone	Sheet-like and lens, more than 50 m lateral extend. Gmm, Gci, Gmg, Gh, Gt, Gcm	Gravel sheets and lens, relative low-relief longitudinal bars
Sandy bedforms (SB)	Fine- to coarse-grained sandstone	Lens, sheet, blanket, wedge with erosional surface, lateral extent more than 100 m. Sp, Fl, Fsm	Channel fills, crevasses splays and minor bars
Lateral accretion (LA)	Granule to pebble conglomerate, fine-to coarse-grained sandstone	Wedge, sheet with lateral extent more than 5m. Gmm, Gci, Gmg, Gh, Gt, Gcm.	Internal lateral accretion of gravel and sand bars
Laminated sand sheet (LS)	Very fine-to medium grained sandstone	Sheet, blanket, erosive base. Fl, P.	Crevasse splay, flash flood deposits
Overbank fines (OF)	Mudstone and very-to fine-grained sandstone	Sheet-like, lateral extent for more than 1 km. Fr, C, Fsm.	Overbank and flood plain

4.5 Facies association III. Massive siltstone with mudstone- carbonate

4.5.1 Description

Thick mudstone, marls, carbonate beds and some structureless pebbly conglomerate characterized this type of facies association.

Facies I is characterized by poorly consolidated laminated to massive carbonate mud (Fig. 4.9). This type of facies was found in the Dhi section of the Thakkhola Formation. This facies is up to 3 m thick, which contains mainly algal mat, carbonate nodules and bioturbation.

Facies J comprises of carbonaceous layer (Fig. 4.16). This facies is distributed around the Dhi gaon, Tange gaon, Chaile and Tetang village. Plant fossils are widespread in this facies. Root horizons have been observed at the bottom of the organic layer.

Facies K is composed of structureless conglomerate within mudstone and siltstone beds, which is distributed in the Thakkhola Formation (Fig. 4.11). Laminated to massive siltstone beds with some erosional feature rest upon this type of facies.

Fig. 4.1: Massive conglomerate of Facies A showing the different clast composition near the Dhinkyo Khola section in the Thakkhola Formation. White arrow shows the scour surface (Facies A).

Fig. 4.2: Cobble to boulder massive conglomerate of facies B near the Dhinkyo Khola section in the Thakkhola Formation (Facies B).

Fig. 4.3: Imbricated conglomerate of the Thakkhola Formation in the Tange section (Facies C)

Fig. 4.4: Channel cutting sandstones alternating with conglomerate beds of the Thakkhola Formation at the Chaile section (Facies D)

Fig. 4.5: Matrix supported conglomerate of Thakkhola Formation at Ghiling section (Facies E)

Fig. 4.6: Cross lamination found in the sandstone of the Thakkhola Formation at Ghiling section (Facies F)

Fig. 4.7: Thick Mudstone beds in Tetang Formation in Tetang area (Facies G).

Fig. 4.8: Well sorted pebble and cobble conglomerate with fine-grained sandstone and some iron nodules in Ghiling area of Thakkhola Formation (Facies H).

Facies L consists of carbonate beds, which are laterally continuous to more than 100 m. This type of facies is present in the Chaile and Tetang area in both Tetang and Thakkhola formations (Fig. 4.12 and 3.5).

4.5.2 Interpretation

Lithofacies I is interpreted as vegetated swamp or open lacustrine deposits. Massive gray marl is interpreted as deposits of suspended fine-grained mixed sediment under a lacustrine water column (Ramos-Guerrer et al., 2000). Some algal mats are present in the marl, which suggest the existence of a stable oxygenated lacustrine water column. Organic layers with plant fossils of the lithofacies J are interpreted as back swamp deposits of abandoned channel deposits. Garzione et al. (2003) interpreted the similar types of sediments as profundal lacustrine deposits with seasonal accumulation of phytoplankton that remained unoxidized because of stagnant bottom condition.

Lithofacies K is interpreted as a pseudoplastic debris flow or suspended sediment carried by the stream into the lakes or as low-sinuosity river deposits. The uneven boundary between the siltstone and conglomerate with lacustrine sediments indicates that it was deposited probably by in turbidity flows within the lakes.

Lithofacies L is interpreted as a shallow lacustrine facies of a palustrine system. Similar limestones are interpreted as a shallow lacustrine marginal to palustrine system on the edge of a possible larger freshwater carbonate lake or part of shallow ponds situated as a distal environment in the alluvial plain (Gierlowski-Kordesch, 1998).

4.6 Paleocurrent analysis

Sedimentary particles of many clastic sediments posses a preferred orientation, imposed by the hydrodynamic forces acting during the deposition (Rees, 1965). Analysis of particle orientation is very useful for different aspects of the sedimentary structure but the most obvious application for the orientation analysis is towards the finding of paleocurrent directions. The preferred orientation of the longest a-axis of the clast is either perpendicular or parallel to the current direction over a wide range of condition. Mainly paleocurrent analysis was done to identify the direction of local or regional paleoslope, direction of sediment supply, geometry and trend of lithologic units and depositional environment (Miall, 1996).

4.6.1 Method

Twelve outcrop localities, which showed relatively well-developed imbrications of pebbles in conglomerate beds were chosen for paleocurrent analyses. Imbricate pebbles (2400) were measured by counting imbricate pebbles (20) from every possible imbricated bed of different formations. The dip direction and dip amount of the longest a-axis and intermediate b-axis of the pebbles were measured to calculate the paleoflow direction (Fig. 3.36). The clasts measured for the analysis ranges from 3 cm to 32 cm in diameter.
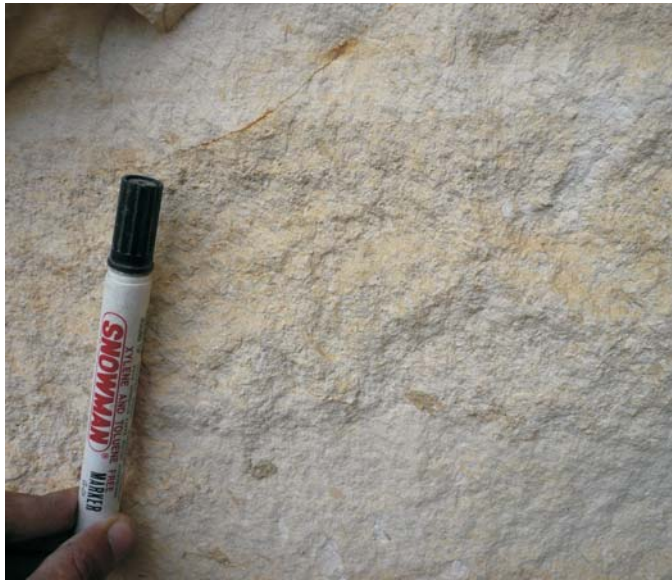
Fig. 4.9: Laminated to massive calcareous mud beds (marl) of the Thakkhola Formation in Dhi section (Facies I)

Fig. 4.10: Laminated carbonaceous layers with massive conglomerate beds of the Thakkhola Formation in Dhi section (Facies J).
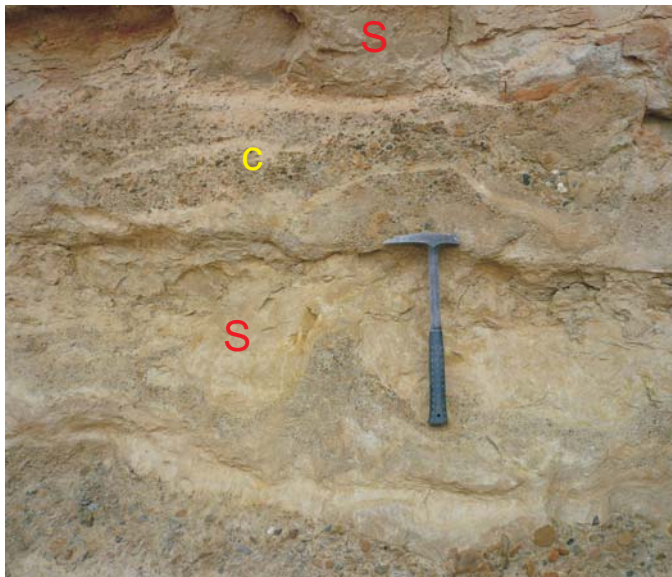
Fig. 4.11: Conglomerate beds are within the siltstone beds of Thakkhola Formation in the Chaile section (Facies K). S= Siltstone, C= Conglomerate

Fig. 4.12: Limestone bed of Thakkhola Foramtion in Chaile section (Facies L).

Fig. 4.13: Measuring the pebble imbrication in the Tetang Formation on the Tetang village.

Fig. 4.14: Imbricated comglomerate showing the paleoflow towards SE direction in the Tetang Formation at Tetang village.

Fig. 4.15: Cross stratification with imbricated coglomerate showing SE paloeflow direction of the Thakkhola Formation at Ghiling village.

Fig. 4.16: Alternation of sandstone and clast supported conglomerate of Thakkhola Formation at Ghami village. The pebbles show SE paleoflow.
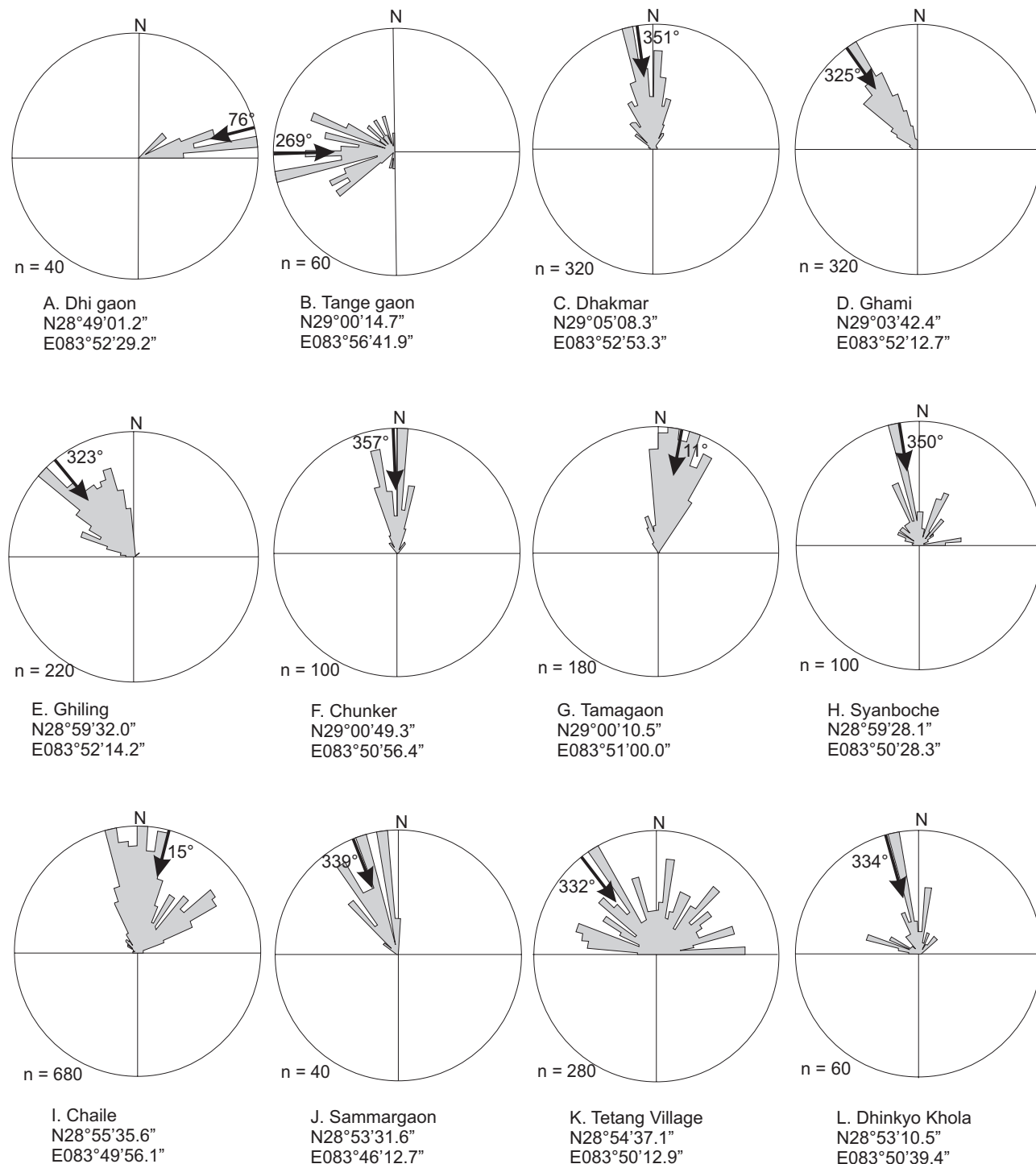
Fig. 4.17: Imbrication analysis of the gravel at the twelve sites. Arrows are the directions of the vector mean calculated by the method of Potter and Pettiohn (1977),which is the river flow directions. Rose diagrams of the orientation of pebbles in the imbricated conglomerate beds. n = number of pebbles.
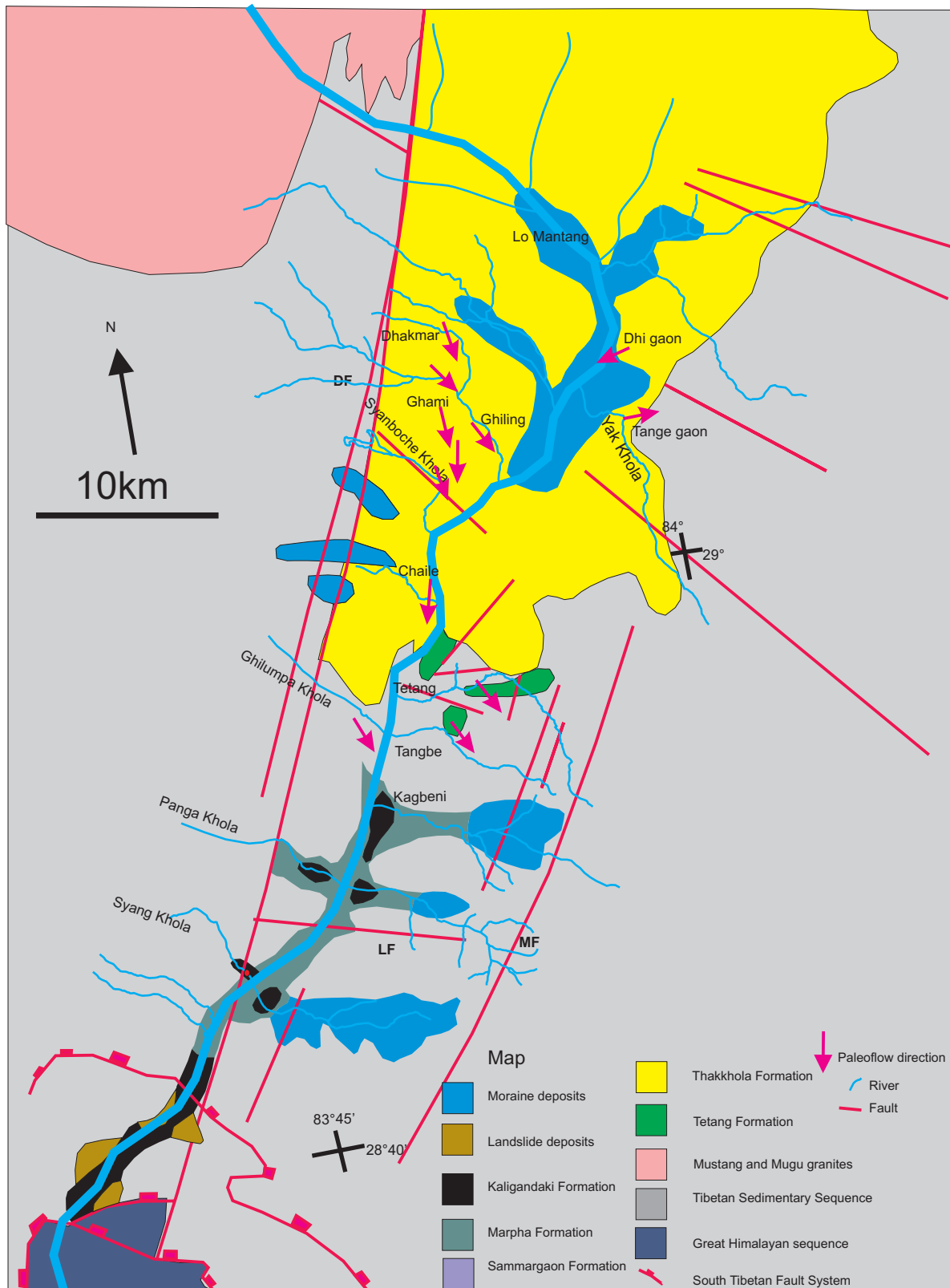
Fig. 4.18: Map showing the paleoflow direction in different formations of the Thakkhola-Mustang Graben. Map modified from Fort et al., 1982 and present work..

The conglomerates are dominantly clast supported and some matrix supported (Fig. 3.37, 3.26, 3.38, and 3.39). Data were analyzed by using GEOrient software and they were corrected for tectonic deformation by rotating the beds up to horizontal. Rose diagram of the pebble imbrications of the imbricated beds are plotted (Fig. 3.40).

4.6.2 Results and discussions

The imbrications of the conglomerate in more than 12 outcrops suggest that there was a consistent paleocurrent direction in all formations except the Tange section during deposition of the sediments. All the imbricated conglomerates of the Tetang Formation show southeast paleoflow directions except of the conglomerate bed at 38 m at the Tetang village (Fig. 3.2M and 4.17K). At the Dhinkyo Khola section, almost all imbricated pebbles show nearly southward flow direction (Fig. 3.2N and 4.17L), which are consistent with the data of Garzione et al. (2003). In Tange section, the paleo-flow is slightly NE directed (Fig. 3.41).

The general paleoflow direction of the imbricated pebbles of the Thakkhola Formation show southwest-directed paleoflow. The individual beds of the Thakkhola Formation display different paleoflow directions (Fig 3.2L) varying from bed to bed (Fig. 3.9). The paleoflow of imbricated beds up to 340 m shows southeast directed whereas the beds between 340 m and 375 m show southwest-directed paleoflow in the Chaile section. Then, it suddenly changed towards the southeast-direction and it reached up to 475 m. Then again, it changed towards the southwest-direction, which shows that the paleo Kali Gandaki River changed its course from SW to SE direction from time to time. The paleoflow directions in the Dhi area show extremely west-directed flow whereas the Tange section shows NE directions. Some local flow barrier may be the reason for the NE directed flow at Tange village. The conglomerate of the Thakkhola Formation at the middle portion of the basin (Dhakmar, Ghami, Ghiling, Chunker, Tamagaon and Syanboche) show southeast-directed paleoflow (Fig. 4.17C, D, E, F, G & H). Fort et al (1982) indicated that large parts of the Kali Gandaki River were flowing in northward direction during the Thakkhola period. This is in contradiction to most of our measurements but only the Tange area fits into this paleoflow direction.

The cobble-pebble imbricated conglomerates of the Sammargaon Formation show southeast-directed paleoflow directions (Fig. 4.17J), which are consistent with the paleoflow direction of the Thakkhola Formation measured in this work. As a summary for the paleoflow directions, most of the formations and sections of the Thakkhola-Mustang Graben show a southward-directed paleoflow and thus a similar flow as the recent fluvial system.

CHAPTER FIVE

PETROGRAPHY AND MINERALOGY

5.1 Pebble composition

For the evaluation of pebble compositions fifty pebbles were studied per possible imbricated and massive conglomerate beds in 15 locations (Fig. 5.1). Each pie diagram of clast compositions are plotted in the columnar sections of the different locations (Fig. 3.2). Average clast composition was calculated for each location (Fig. 3.41). In general, pebbles include metamorphic, igneous and sedimentary rocks.

Mainly carbonate rocks followed by sandstone, quartzite, shale and slate are dominant in the Tetang Formation (Fig. 4.2). Most of the clasts are derived from the surrounding rocks, which are confirmed from the paleocurrent direction. 78% of the Paleozoic clasts and 28% of the Mesozoic clasts are present in the Tetang village area whereas 98% of Mesozoic clasts are found in the Dhinkyo Khola section (Fig. 5.2). It reflects that at the eastern outcrop belt, the clasts were derived from the eastern side of the graben where Mesozoic rocks are present (Fig. 2.4).

On the northeastern part of the basin along the Dhi gaon and Tange area, most of the clasts are composed of Mesozoic carbonates followed by calcareous quartzite, mudstone and some granite. Paleocurrent analysis also indicates that these clasts came from the easterly neighboring Mesozoic rocks. Garzione et al. (2003) also interpreted that the possible source of these pebbles are of Mesozoic rocks exposed on the eastern footwall near Dhigaon. Sandstones, shales, slates, phyllites and mudstones of the Paleozoic rocks with granite and some Mesozoic carbonate clasts are mixed in the middle and central part of the basin but mostly Paleozoic clasts are dominant (Fig. 5.2). Granite pebbles are mainly present on the northern margin of the basin, which were derived from the Mugu and Mustang granites to the northeast. Palaeoflow directions (Fig. 4.18) confirm transport from these source areas (Fig. 4.18).

No significant differences in pebble compositions apart from local sources are reconstructed for the different formations of the Thakkhola-Mustang Graben. Mainly Paleozoic clasts are dominant in the Sammargaon Formation on the western edge of the basin followed by Tertiary granites and Mesozoic carbonates. Clasts of diverse compositions are found in the Kaligandaki and Marpha formations (Fig. 5.1). Granite clasts are more common in the Kaligandaki Formation whereas Paleozoic rocks are dominant in the Marpha Formation.

5.2 Sandstone

5.2.1 Framework components

In this study, sandstone petrography was studied in order to further investigate the provenance relations. Sand grains may indicate longer transport paths than pebble
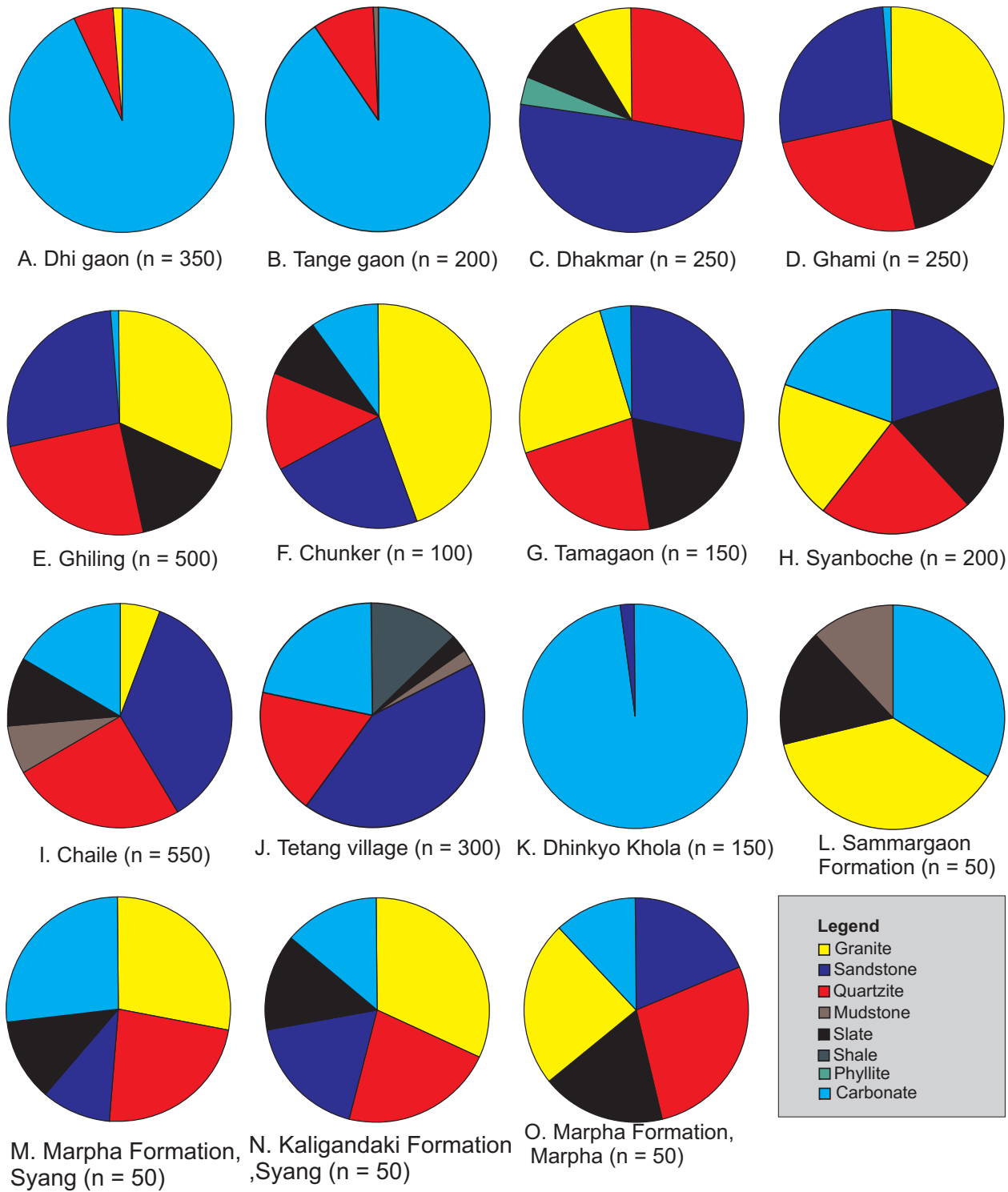
Fig. 5.1: Pie diagrams of average pebble conposition in different location of Thakkhola-Mustang Graben. Fifty pebbles were measured per possible beds in different formations.
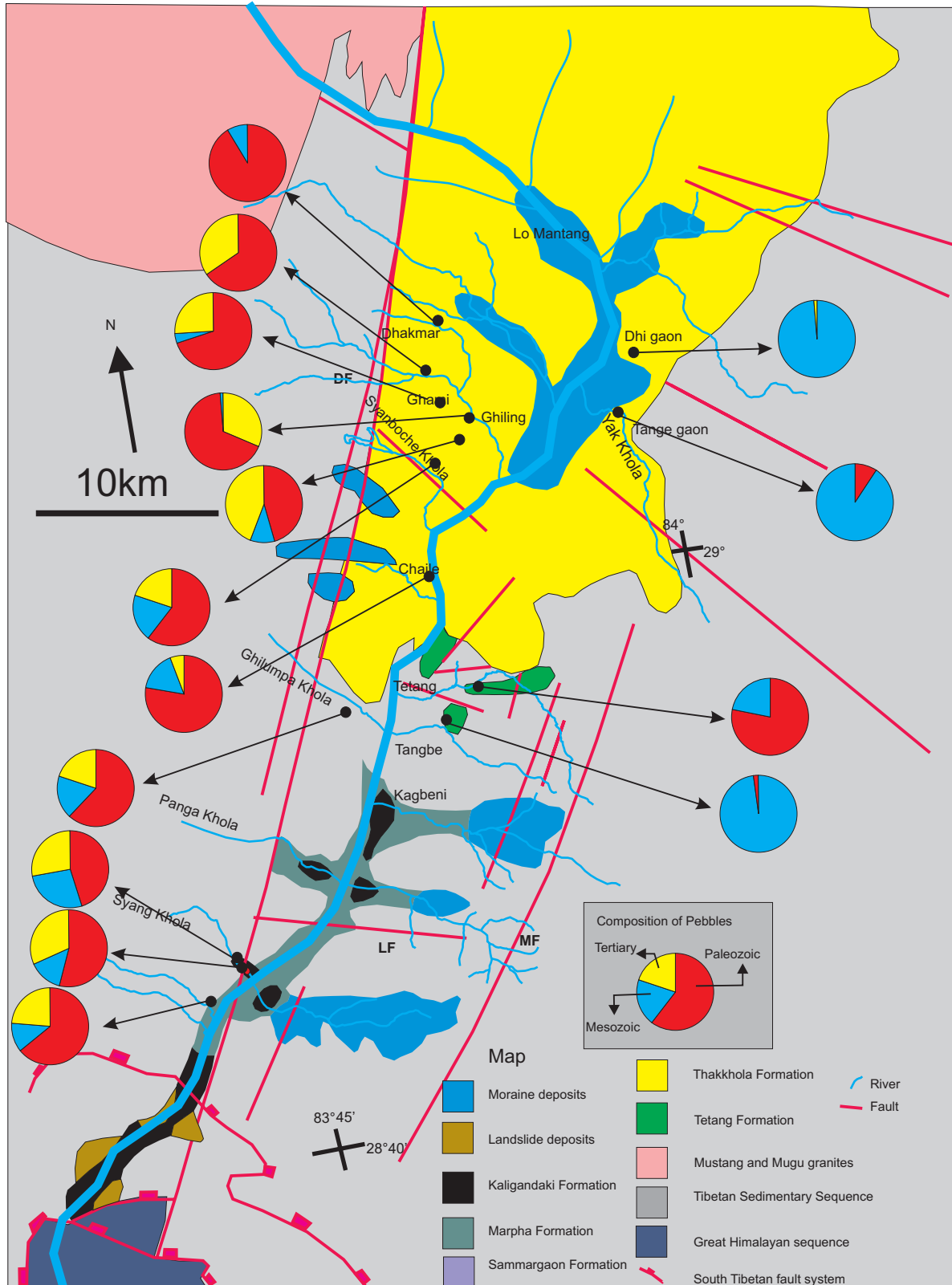
Fig. 5.2: Map showing the pebble composition generalized with ages in different formations of the Thakkhola-Mustang Graben. Map based partly on Fort et al. (1982) but pebble composition measurements from this work.

compositions and therefore may give hints to more distal source areas. The use of detrital modes to infer sandstone provenance is well-established (Dickinson & Suczek 1979). Furthermore, tectonic provenance provinces may be identified. The sandstone composition is influenced by the character of the sedimentary provenance, the nature of the sedimentary processes within the depositional basin and the kind of dispersal paths that link provenance to basin. The bulk composition of the sandstone is very useful for reconstruction of the environment during deposition at a particular time and place. Procedurally, this approach is systematically performed by the point-count determination of modes on detrital framework grain (Dickinson et al., 1983: Dickinson, 1985 and Dickinson and Suczek, 1979). Crook (1974) and Schwab (1975) have observed that quartz-rich rocks are associated with passive continental margins that quartz-poor rocks mostly of volcanogenic derivation are of magmatic island origin and that rocks of intermediate quartz content are associated mainly with active continental margins or other orogenic belts.

5.2.2 Methods
Five thin sections of sandstone from both Tetang and Thakkhola formations were used for the thin section petrographic study. The rock slices were ground to final required thickness about 30 μm. At least 300 grains were counted per thin section by the point counting method. Sandstones are classified with the help of Dott's (1964) classification.

5.2.3 Petrography of sandstones
Petrographically, sandstones are systematically analyzed by the point count determination of modes on detrital framework grains for the bulk composition of sandstones of both formations and described (Table 5.1).

Framework grains
Sandstones are characterized by mono and polycrystalline quartz, feldspar and lithic grains such as phyllitic fragments, mica, biotite, chlorite and some detrital carbonates.

Quartz
Quartz is the most prominent mineral of those sandstones and occurs as both monocrystalline and polycrystalline forms. Quartz makes up to 60% of that sandstone (Fig. 5.3B). Undulose as well as straight extension does occur in the quartz grains. Most
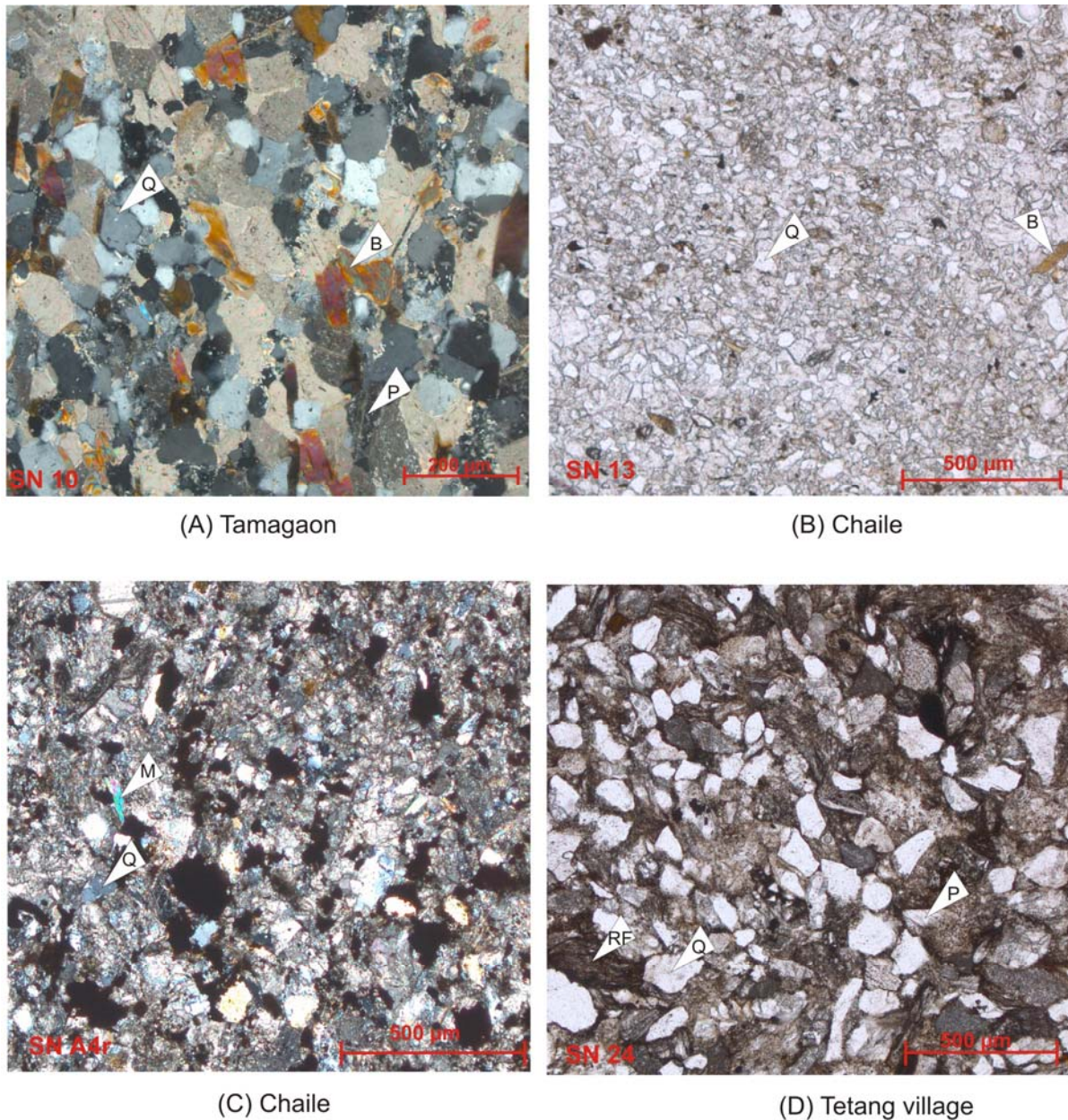
Fig. 5.3: Representative photomicrographs of sandstone of Thakkhola and Tetang formations. Q = quartz, B =biotite, M = muscovite, P= plagioclase, RF = rock fragments

of the grain boundaries are dominantly sutured with some curved boundaries (Fig. 5.3A).

Feldspar

Potassium and plagioclase feldspars are dominant on those sandstones. Orthoclase, which is identified by Carlsbad twinning, occurred mostly in feldspar with some microcline

Table 5.1: Sandstone classification

SN	%QFRF	%matrix	%Q	%F	%RF	Classification
SN 24	69	31	24	27	49	Lithic greywacke
SN 12	90	10	19	43	38	Lithic arkose
SN 10	95	5	43	31	26	Lithic arkose
SN 13	92	8	60	14	26	Feldspathic Litharenite
A4r	75	25	33	31	36	Lithic greywacke
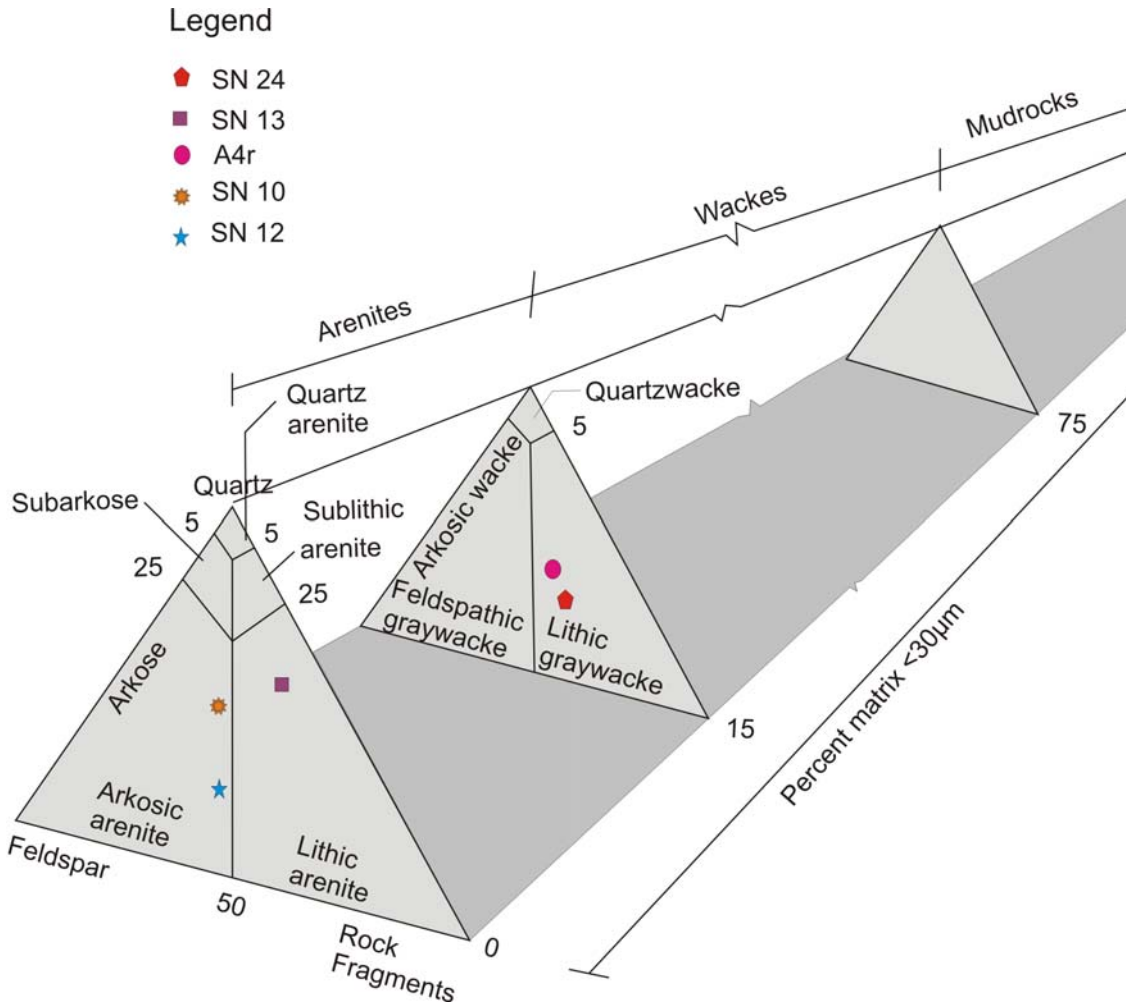
Fig. 5.4: Classification of sandstone (modified after Dott, 1964).

(Fig. 5.3A). Mostly polysynthetic twinning (Fig. 5.3A) identifies plagioclase. Feldspar makes up to 43% in some sample.

Lithic grains

Rock fragments are dominant components in most of the sandstone. In some samples, it reaches up to 49%. Lithic fragments are mostly sedimentary and metamorphic origin. Some lithic grains of metamorphic rocks include quartz-mica schist whereas sedimentary lithics include mudstone, lime mudstone and siltstone.

Mica

Muscovite and biotite occur as detrital grains. Muscovite is colorless under the plane polarized light and show high birefringence under the crossed nicols (Fig. 5.3C). Biotite is clearly brown and strongly pleochroitic (Fig. 5.3A).

Matrix

The matrix is composed of finely crystalline calcareous material. Calc-sandstone (24 % $CaCO_3$) of the Tetang Formation consists of 31 % of matrix. This matrix is acting as a cementing agent for the clastic grains. Silt sized grains of quartz and feldspar matrix dominate on the sandstone of Chile section (A4r).

Cement

Mainly fine-grained calcite cement occurs in most of the sandstones. Cement reaches up to 31% of the total composition in Sample 24.

Based on the framework composition, sandstones of the Thakkhola Formation have been classified as lithic greywacke (A4r), lithic arkose (SN12 and SN10) and feldspathic Litharenite (SN 13) whereas sandstone is classified as lithic greywacke (SN24) in the Tetang Formation using the Dott's classification (Table 5.1) (Fig. 5.4).

5.2.4 Provenance studies based on framework components

Detrital modes are recalculated to 100% as the sum of quartz (Q), feldspar (F) and lithic fragments (L). The detrital components of the compositions of the Thakkhola Formation show averaged 39% of Q (between 19% to 60%), 32% F (between 14% to 43%) and 32% L (between 26% to 38%). Sandstones of the Tetang Formation contain average 24% Q, 27% F and 49% L. Higher proportion of unstable lithics and the moderately high feldspar content of lithic arenites indicate high-relief source area (Ullah et al., 2006).

Polycrystalline quartz with more crystals is abundant in these sandstones, which is the excellent indicator for a metamorphic source (Scholle, 1978), i.e. provenance from gneisses (Blatt et al., 1980). Some polycrystalline quartz grains with straight intercrystal boundaries indicating a plutonic source do occur in less amount. Sedimentary rocks fragments such as shale, siltstone and phyllite of metamorphic rock fragments occur in lithic grains indicate a granitic source as well as sedimentary and low-grade metamorphic source terrains.

5.3 Carbonates

5.3.1 Introduction

Carbonate sediments originate on both land and sea. Today only around 10% of marine carbonate production takes place in shallow seas where as 90% carbonate production is in the deep-sea (Flügel, 2004). Terrestrial carbonates can form in different depositional environment. Carbonates of the Thakkhola-Mustang Graben were deposited in a terrestrial, mainly lacustrine to palustrine system. Freytet and Plaziat (1982) first proposed the term palustrine (derived 'paludal' meaning marshy or swampy) while describing upper Cretaceous-Paleogene limestones in southern France. Cowardin et al. (1979) defined the palustrine system as "non-tidal, perennial wetlands characterized by emergent vegetation". This system includes wetlands permanently saturated by seepage, permanently flooded wetlands and wetlands that are seasonally or intermittently flooded if the vegetative cover is predominantly hydrophytes and soils are hydric.

5.3.2 Limestone classification

There are two widely used limestone classifications, those of Dunham (1962) and Folk (1959, 1962). All the classifications are based on the distinction of three fundamental components: grains (skeletal fragments, ooids, pellets/peloids, intraclasts, and non-carbonate detritus), matrix or carbonate mud and open pores or sparry-calcite-filled primary interparticle porosity. Dunham (1962) used mud-versus grain-supported fabrics whereas Folk (1959, 1962) used the relative percentage of grains and matrix. Folk's classification is based on the relative amount of allochems, calcite cement or 'spar' and microcrystalline calcite matrix or 'micrite'. Allochems are separated into four main types; intraclasts, ooids, pellets and bioclasts (Fig. 5.5 and 5.7).

Intraclast: Intraclasts are the "intra-formational rock fragments", which can be different size ranging between 2 mm to less than few centimeter in diameter. Generally, they are cryptocrystalline to microcrystalline calcite but they can also contain small bioclasts.

Ooids: These are carbonate grains that are usually small than 1 mm in diameter spherical grains. They contain concentric laminations in cross section. Ooids have been termed as pisolites when the diameters are greater than 2 mm.

Pellets: These are cryptocrystalline to microcrystalline calcite or aragonite grains that are probably fecal origins but some have different origin such as foeces and pseudo-foeces of bivalve or gastropods. They are less than 2 mm in maximum diameter and elongated structures.

Bioclasts: Bioclasts are a test of organisms made of calcite or aragonite that lived contemporaneously with the depositional processes, which forms the sediment.

Micrite: Folk (1962) defined the micrite as a grains of smaller than 4 μm. It is carbonate mud originated by disintegration of carbonate skeletons such as calcareous algae.

Sparite: Sparite is fine- to coarse-grained calcite matrix, characterized by rather uniformly sized and generally loaf-shaped, subhedral and euhedral calcite crystals ranging above 5 to 20 μm in diameter (Flügel, 2004) but some authors described in different size of sparite like; 4-10 μm (Tucker, 1981) and 5-50 μm (Bathurst, 1975).
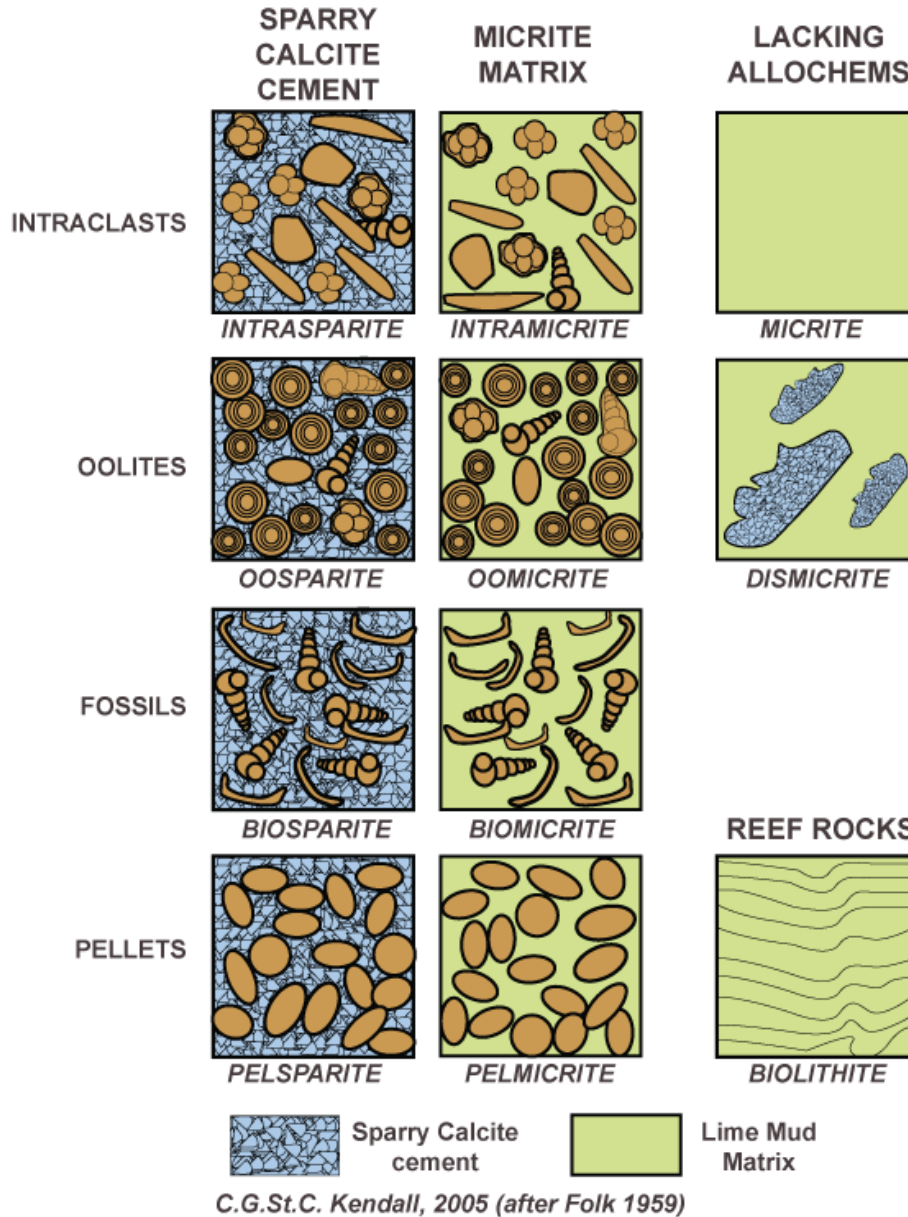
Fig. 5.5: Basic limestone types of Folk's (1959) classification

(source: http://strata.geol.sc.edu/thinsections/classification.html)

Dunham's (1962) classification is mainly based on depositional texture (Fig. 5.7). This classification is best suited for rock description that employs a hand lens or a binocular microscope.

Folk's Textural Classification of Carbonate Sediments

Percent Allochems	Over 2/3 Micrite Matrix				Subequal Spar & Micrite	Over 2/3 Spar Cement		
	0-1%	1-10%	10-50%	Over 50%		Sorting Poor	Sorting Good	Rounded & Abraded

Quiet Water Deposition ← → *Wave/Current Activity*

← *Matrix Supported Allochems*   *Grain Supported Allochems* →

Rock Names	Micrite	Fossill- iferous Biomicrite	Sparse Biomicrite	Packed Biomicrite	Poorly Washed Biosparite	Unsorted Biosparite	Sorted Biosparite	Rounded Biosparite

Lime Mud Matrix   Sparry Calcite cement

C.G.St.C. Kendall, 2005 (after Folk 1959)

Fig. 5.6: Folk's textural classification of carbonate sediments

(source: http://strata.geol.sc.edu/thinsections/classification.html)

Original components not bound together at deposition				Original components bound together at deposition. Intergrown skeletal material, lamination contrary to gravity, or cavities floored by sediment, roofed over by organic material but too large to be interstices
Contains mud (particles of clay and fine silt size)		Lacks Mud		
Mud-supported		Grain-supported		
Less than 10% Grains	More than 10% Grains			
Mudstone	Wackestone	Packstone	Grainstone	Boundstone

C. G. St. C. Kendall, 2005 (after Dunham, 1962, AAPG Memoir 1)

Fig. 5.7: Classification of limestone according to Dunham (1962)

(source: http://strata.geol.sc.edu/thinsections/classification.html)

5.3.3 Methodology

By application of the Müller Gastner Bombe-method (Müller and Gastner, 1971), the percentage of calcium carbonate was measured. Carbonate samples (29 samples) are grinded to make powder form. Ten milliliters of mixed solution of HCl and distilled water (1:1 ratio) is poured on the plastic cylinder. 1 g (1.000-1.050) of dried and ground-

up material is put with the help of gasket into the cylinder. The gasket is inserted and the cap, upon which the manometer and thumbscrew are mounted, is screwed down. A light shaking insures that all the rock powder is exposed to the acid. Calcite and aragonite react immediately by effervescing strongly. The reaction is already finished. The manometer measures the pressure in Kilo bar (Kbar) after 10 seconds. The percentage is calculated by the following formula and presented in Table 4.1.

$$\% \, CaCO_3 = \left(CaCO_3 \; manometer \; value \times \frac{100}{CaCO_3 \; (manometer \; value \; of \, the \; sandard \; sample)} \right)$$

Sixteen thin sections were studied for carbonate petrography (Fig. 4.7 and 4.8). The rock slices were ground to final required thickness about 30 μm. Limestone is classified with the help of Folk (1959) and Dunham (1962) classification (Fig. 4.4, 4.5 and 4.6).

5.3.4 Result and discussion

Percentages of $CaCO_3$ are calculated in Thakkhola, Tetang and Marpha formations in carbonaceous clay and limestone (Table 4.1). Percentage of $CaCO_3$ in limestone samples of both Thakkhola and Tetang formations range from 24 to 99.5%. $CaCO_3$ of the limestone samples in the Tetang Formation are more than 85% except in sample 24 (calc-sandstone) (Fig. 4.1D) whereas it varies in Thakkhola Formation from 45 to 99.5%. Clay samples contain very low $CaCO_3$ percentage ranging from 4 to 48%.

Petrographic analysis of the carbonate samples is an important part of this study because it allows a qualitative assessment of any potential diagenetic alternation of the carbonate fraction. The limestone analyses reveal that the microfacies are dominated by wackestone (Fig. 4.7B) and packstone (Fig. 4.7D) followed by mudstone (Fig. 4.8B). Microfabrics can be divided in two groups with seven sub-groups based on the petrographic feature and textures (Table 5.2). The first group includes shallow water carbonates microfacies while second group includes deep-water carbonates.

5.3.4.1 Shallow-water lake carbonates

5.3.4.1.1 Description

This group represents microfabrics of shallow lake water carbonates including sub-groups A, B, C and D (Fig. 5.8) of the Thakkhola Formation. These sub-groups consist of clotted matrix, rounded to elongated algal mat with fine-grained matrix with oncolitic limestone. Oncoids consist of a laminated porous microstructure with layers of micrite tubes representing the encrusted sheets of cyanobacteria or green algal filament. Some algal structures are filled with sparry calcite. Growth episodes are clearly visible in oncolitic limestone, which are separated by surface of dissolution, abrasion or breakage (Fig. 5.8F). The micritic facies includes root traces, nodules and recrytallization (Fig. 5.8D). Marl deposits in the Dhi gaon section consist of cloudy algal mat (Fig. 4.7A).

Table 5.2: CaCO$_3$ analysis of limestone and carbonaceous clay

SN No.	Location	% CaCO$_3$
	Limestone	
A$_1$c	Dhi Section (Thakkhola Fm)	45
SN9	Trail of Chunker to Syanboche (Thakkhola Fm)	77
SN10	Trail of Chunker to Syanboche (Thakkhola Fm)	95
SN12	Uphill side of the Syanboche-vena trail near Syanboche Khola (Thakkhola Fm)	63
SN13	Trail between Chaile and Samar (Thakkhola Fm)	95
SN14	Trail between Chaile and Samar (Thakkhola Fm)	99.5
A$_4$e1	Chaile section (Thakkhola Fm)	58
A$_4$g	Chaile section (Thakkhola Fm)	47
A$_4$i	Chaile section (Thakkhola Fm)	89
A$_4$k	Chaile section (Thakkhola Fm)	82
A$_4$l	Chaile section (Thakkhola Fm)	91
A$_4$r	Chaile section (Thakkhola Fm)	48
SN30	Tetang Village(Tetang Fm)	85
A$_6$u	Tetang Village (Tetang Fm).	91
SN25	Tetang Village(Tetang Fm)	94
SN24	Tetang Village(Tetang Fm)	24
A$_7$c1	Dhinkyo Khola (Tetang Fm).	92
A$_7$c	Dhinkyo Khola (Tetang Fm).	90
SN26	Dhikyo Khola(Tetang Fm)	95.5
	Carbonaceous clay	
SN8	Right side of the Ghami Khola near Ghami village (Thakkhola Fm)	8.5
SNB	Trail to Chunker to Syanboche (Thakkhola Fm)	6
SN11	Uphill side of the Syanboche-Vena trail near Syanboche Khola (Thakkhola Fm)	48
SNC	Chaile (Thakkhola Fm)	8.5
SN29	Tetang Village(Tetang Fm)	5.5
SN23	Tetang Village(Tetang Fm)	33.5
SN17	Tetang Village(Tetang Fm)	4
SND	Tetang Village(Tetang Fm)	2.5
SN40	Syang Khola (Marpha Fm)	24
SN41	Marpha(Marpha Fm)	31
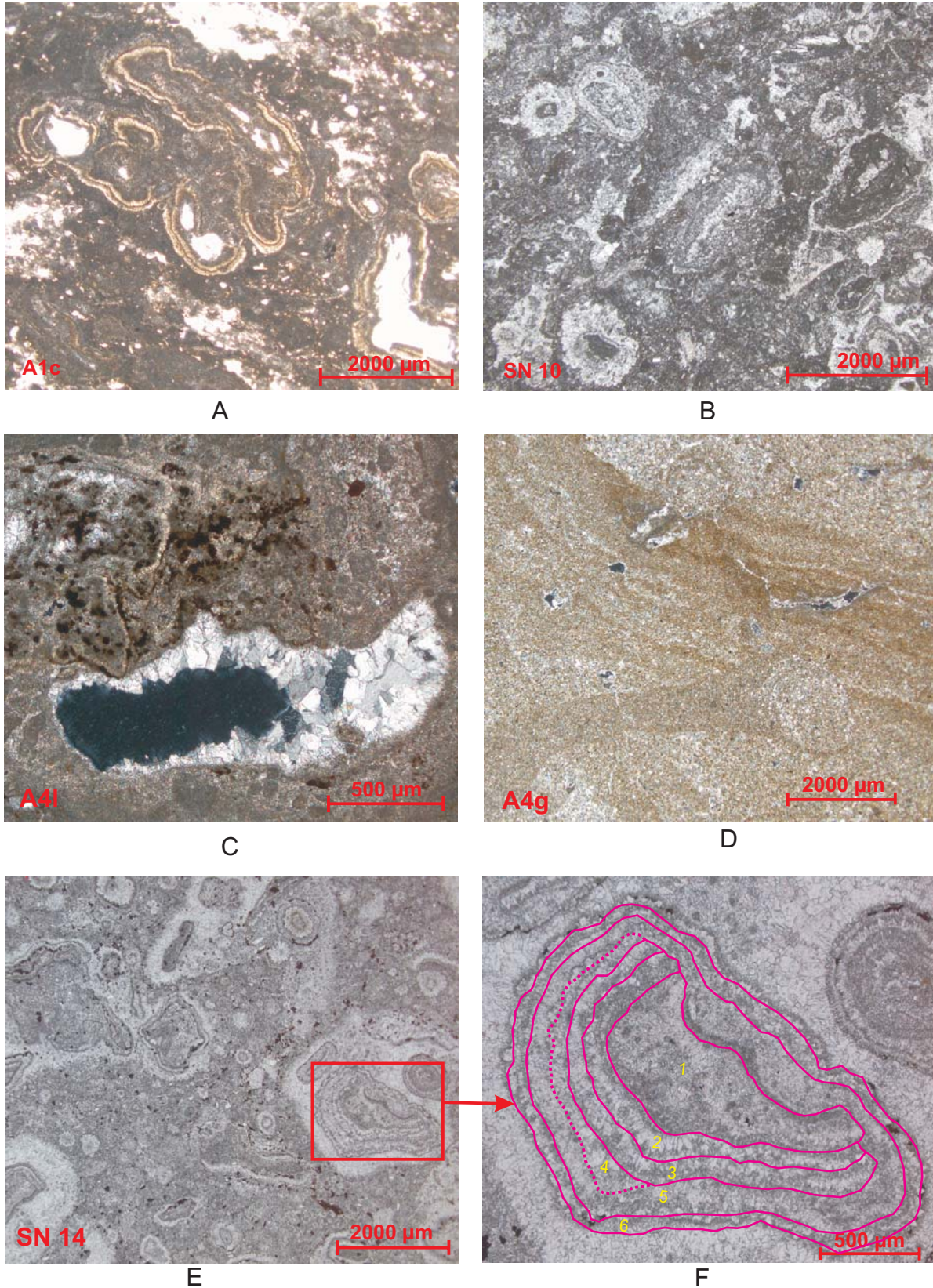
Fig. 5.8: Limestone thin section of the Thakkhola Formation. (A) oncolitic limestone; (B) algal lacuastrine limestone; (C) travertine (laminated micritic layers bordering voids which are partly filled with bladed prismatic calcite cement); (D) intramicrite; (E) oncolitic limestone; (F) growth epidsode of dissolution and fragmentation.
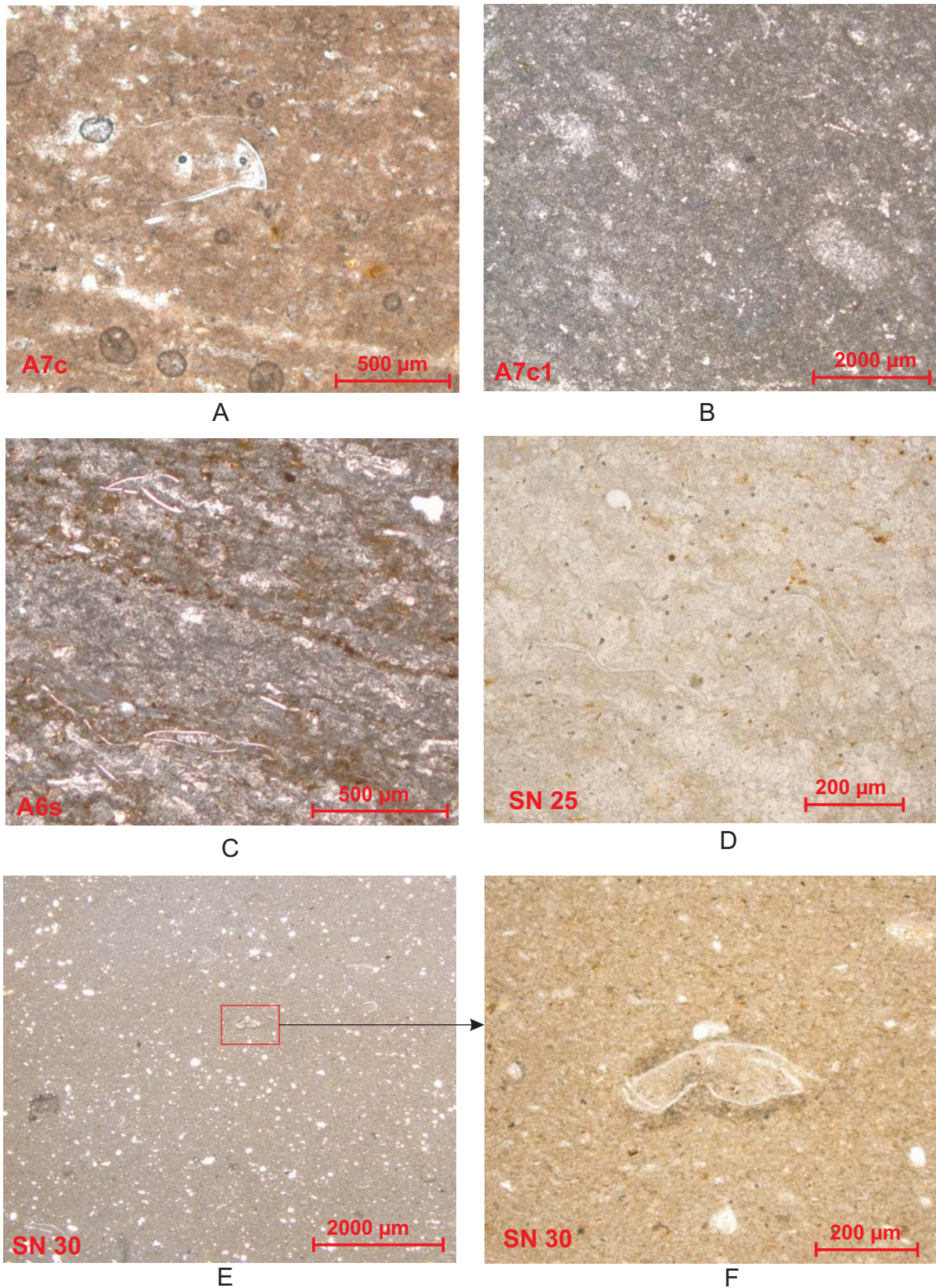
Fig. 5.9: Thin section of limestone of the Tetang Formation. (A) pelletal lacustrine limestone; (B) fine grained limestone; (C) lacustrine limestone with algal structure; (D) lacustrine limestone with algal structure; (E & F) micritic limestone with ostracod.

Table 5.3: Petrographic description, matrix, and bioclast characteristics of the seven carbonate microfacies sub-group recognized in the Thakkhola-Mustang Graben.

Group	Sub-group	Sample number	General Characteristics (classification according to Dunham, 1962 and Folk, 1959)
Shallow-water carbonates	A	A1c, A4i and SN14	Packstone and Oosparite Growth episodes of dissolution and fragmentation is clearly visible in Oncolitic limestone
	B	A4k and SN 9	Wackestone and Intrasparite Carbonate matrix with some clastics, pores are filled with calcite
	C	A4L and SN 10	Wackestone and Biomicrite Rounded to elongated algal mat with fine-grained matrix, charophytes algae.
	D	A4g	Wackestone and Intramicrite Clotted micrite with fenestral fabrics.
Deeper-water carbonates	E	A6u, A7c1, A7c and A6s	Wackestone and Pelmicrite Small peloids are present with some algal structures, fine grained matrix with some ostracoda
	F	SN25 and SN30	Wackestone and Biomicrite Extremely fine-grained matrix with cloudy algal structures. Algal mats are spreading in longitudinal fashion with high compaction.
	G	SN 26	Packstone and biosparite Fine grained matrix with biogenic material with some pellets.

Some carbonates resemble travertine, which is a layered deposit of calcium carbonate with moderate to high primary porosity with some dendritic fabrics (Flügel, 2004) (Fig. 5.8C). All the samples contain siliciclastic material such as a silt fraction whereas clay materials are present in minor amounts. Some fine laminae are present in the limestone of its outcrop.

5.3.4.1.2 Interpretation

Fine laminae in outcrop and dense micrite with some bioclast fragments are interpreted as a low-energy water environment (Abels et al., 2009). Petrographic evidences suggest that shallow water carbonates have undergone little diagenetic alteration with some recrystallization. Some fragmented algal mat suggests that they were transported over a short distance of shallow lake. Oncolites are deposited in the shallow water condition. Shi and Chen (2006) suggested that oncolites deposited in high-energy, wave-agitated reworking and shallow-water (marine) environment. Generally, oncoids originate in

freshwater, brackish water and marine water but better-preserved microstructures and the association is often with terrestrial sediments (Flügel, 2004).

5.3.4.2 Deep-water lake carbonates
5.3.4.2.1 Description
Deep-water carbonates include sub-group E, F and G (Fig. 5.9) of the Tetang Formation and comprise mainly carbonates with a fine-grained micritic matrix and various particles. Very fine-grained micrite containing small peloids with some algal mats. Charophyts algae are badly preserved (Fig. 5.9C and D). The erect and branched thallus is divided into regular succession of nodes with whorls of small branches and internodes (Fig. 5.9C and D). Its steam is replaced by sparite and looks white in thin section (Fig. 4.8D). Some biogenic materials with ostracods are distributed in such kinds of limestone (Fig. 5.9E &F). Sandy calcareous mudstone is very fine-grained consisting of some nodules but quartz is visible as light colored and dark areas are possible of ferric product in thin section (Fig. 5.9B).

5.3.4.2.2 Interpretation
Deep-water lake carbonates are mainly identified by a fine-grained micritic matrix, which proofs deposition below the normal wave base. Abundant charophyte debris in samples suggests that the breakdown of calcareous biogenic material may be the source of micrite in deeper-water lake carbonates. Dean (1981) suggested that deposition of micrite with presence of abundant charophytes is a characteristic of lake sediments. Davis (1900, 1901 and 1903 cited in Murphy and Wilkinson, 1980) suggested that marl accumulation in lake occurs primarily because of the breakup of characean skeleton. He reported that *Chara*, which thickly covered bench slopes, was heavily encrusted with calcium carbonate. Massive micritic lacustrine limestones with absences of internal structure are mainly the result from burrowing of different intensity (Freytet and Verrechia, 2002). Micritic material can be originated from calcareous skeletons, structural parts and/or water product of microorganisms (Kelts and Hsu, 1978). Horizontally oriented bioclasts in some linear fashion are interpreted as a slightly higher energy and deep condition (Abels et al., 2009). Ostracodal micrite is mainly deposited in the cold and relatively stagnant water because of particle settling in quiet waters of hypolimnion (Murphy and Wilkinson, 1980). Presence of ostracods and charophycean algae are characteristic in freshwater, brackish and marine environment (Flügel, 2004). Many researchers used ostracods as a favorite fossil to interpret the paleosalinity because of its occurrence in continental, estuarine, marine and hypersaline water. Peloids are common in both shallow-water and deeper-water carbonates (Flügel, 2004).

5.3.5 Iron-rich carbonate concretions

Iron-rich carbonate concretions occur in some of the layers of the Thakkhola and Tetang formations (Fig. 3.13). Four carbonate and iron nodules were studied by thin section and X-ray diffraction analysis. Growth structures in iron nodules are clearly visible in thin section analysis (Fig. 4.9A). These nodules are brown in color in field but it appears as a dark brown in thin section. Micrite with some microsparite are the enclosing material due to the recrystallization and rare quartz grains in white in thin section (Fig. 4.9A). Carbonate matrix with some clastic grains are present in the carbonate nodules (Fig. 4.9B). Calcite, quartz, muscovite and feldspar are the dominant minerals in these nodules as shows by the X-ray diffraction patter (Fig. 5.11). These carbonate nodules are the product of changing of ferrous iron to the ferric iron and it appears as sediment with mottled pink, purple, red and yellow patches in accumulation of ferric iron whereas grey to white in the depleted in iron (Freytet and Verrechhia, 2002).
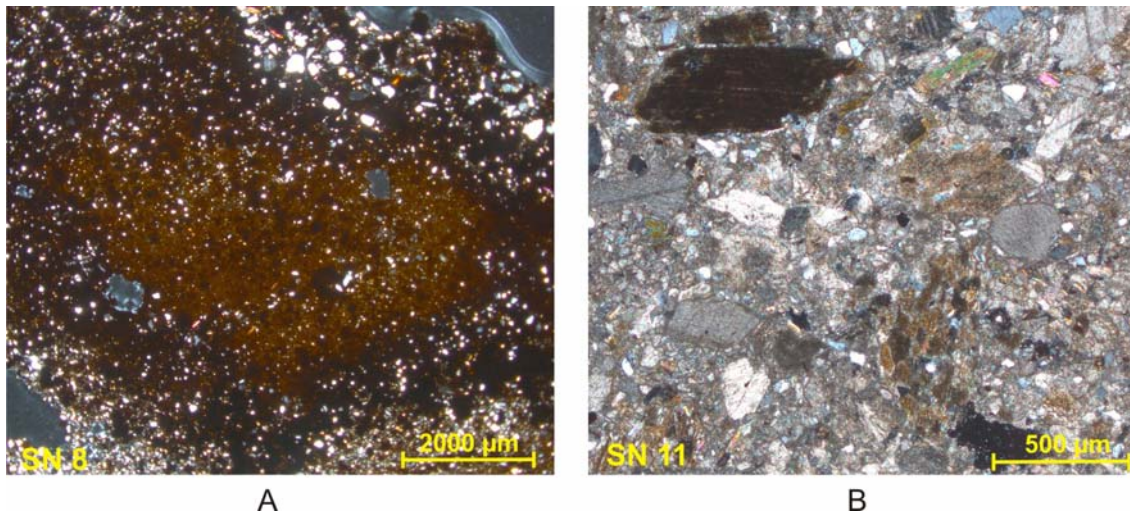
Fig. 5.10: Iron and carbonate nodules found in Thakkhola Formation. (A) Iron nodules in Ghami Khola section, (B) Carbonate nodule in Syanboche Khola section.

5.4 X-ray diffraction analysis

5.4.1 Introduction

X-ray powder diffraction (XRD) is an analytical technique used for phase identification of crystalline material and can provides information on unit cell dimensions. Powder diffraction analysis has the potential to provide a wealth of information on the nature and abundance of all of the other minerals on the sediments. Analysis of whole-rock samples in random powder method often can be applied to any fraction of a sample (Hiller, 2003).
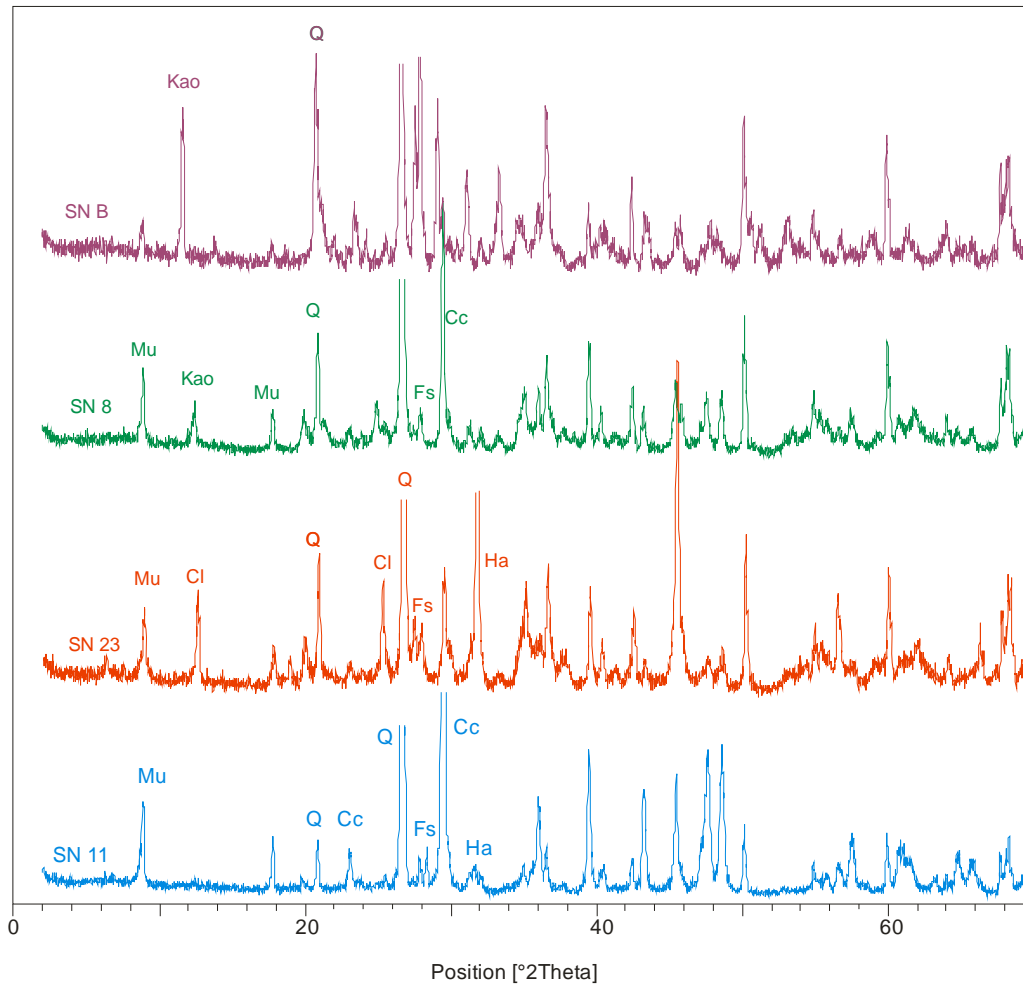
Fig. 5.11: X-ray diffraction patterns of different nodules of Thakkhola and Tetang formations. SNB = Chunker village, SN8 = Ghami Khola section, SN23 = Tetang village, SN11 = Syanboche Khola.

X-ray powder diffraction relies on the preparation of random powder samples in order to obtain the correct relative intensities of all the peaks in the diffraction pattern. X-rays are electromagnetic radiation with typical photons energies in the range of 100 eV-100 keV but only short wavelength x-rays in the range of few angstroms to 0.1 angstrom (1 keV-120 keV) are used. X-rays primarily interact with electrons in atoms. When X-ray photons collide with electrons, some of them will be deflected away. If the wavelength of these scattered x-rays did not change then it has been transferred in the scattering process. Diffracted waves from different atoms can interface with each other and the resultant intensity distribution is strongly modulated by this interaction. Measuring diffraction pattern allows deducing the distribution of atoms in a material. The interaction of the incident rays with the sample produces constructive interface when condition satisfy Bragg's law (1912) (Fig. 5.12).
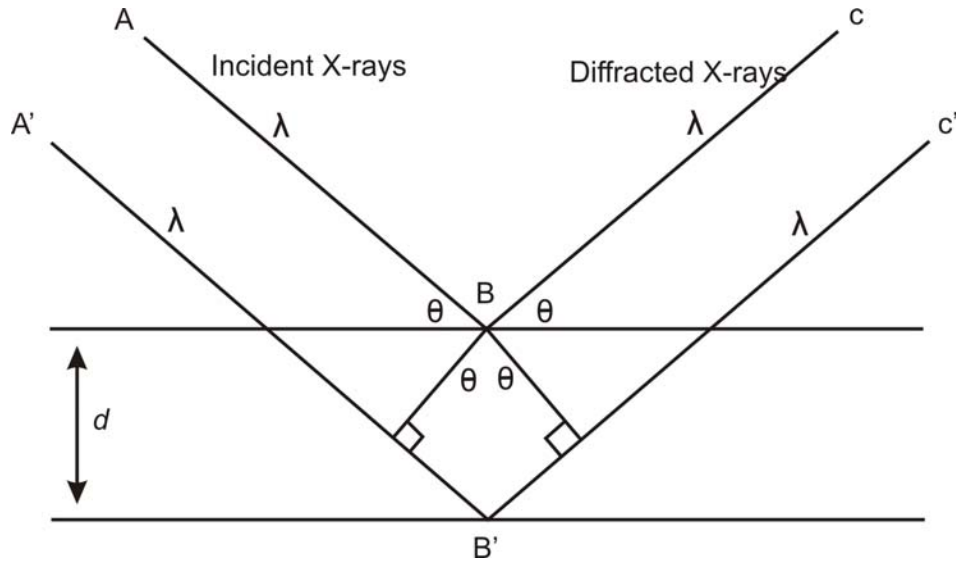
Fig. 5.12: Illustration of Bragg's law

$n\lambda = 2d \sin \theta$

Where, n = integer representing the order of the diffraction peak

    λ = wavelength

    d = inter-lattice plane distance

    θ = scattering angle

Powder XRD is very widely used to study the crystalline domain, which are randomly oriented. The geometry of and X-ray diffractometer is such that the samples rotates in the path of the collimated X-ray beam at an angle θ while the X-ray detector is mounted on an arm to collect the diffracted X-rays and rotates at an angle of 2θ (Fig. 5.13). Goniometer maintains the angle and rotation of sample. When the 2-D diffraction pattern is recorded, it shows concentric rings of scattering peaks corresponding to the various d spacing in the crystal lattice. This technique is very useful to determine unknown solids in geology, environment science, material science, engineering and biology.

5.4.2 Methods

A set of 31 mud and sand samples were collected from different part of Thakkhola-Mustang Graben. Samples were grinded to make fine powder and sieved to obtain much finer than 0.062 mm to avoid fractionation of the minerals. The grinded samples were placed in a sample holder and distributed the powder. The glass slide or metal was used to pack the sample in the cavity firmly enough so that it will not fall out, deform, or slide, but not so firmly that preferred orientation would be produced on the opposite surface.

An additional sample could be used as filler if necessary to fill the cavity. Clip was
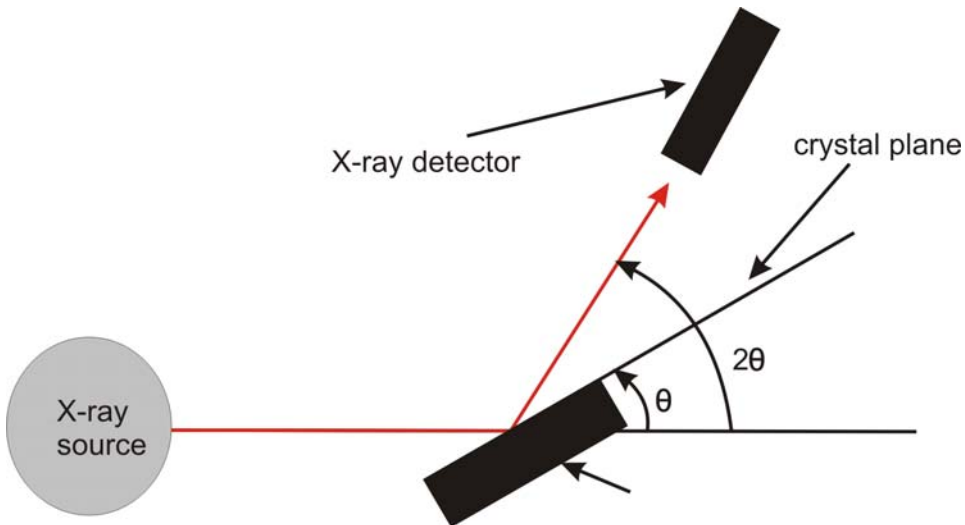
Fig. 5.13: Illustration of X-ray diffraction in one crystal setup

attached to the holder, which would be the back surface of the sample. The holder was carefully lifted. The surface of the sample should be smooth, uniform and flush with the metal surface of the holder and the holder labeled with the pencil. Diffraction data were collected with a Philips diffractometer (PW 3710, goniometer PW 1820), Cu Kalpha radiation (45 kV, 35 mA), and step scan (step size 0.02, 1s per step) (Fig. 5.14 A, B, C, D, E, F & G). The data were collected at 2θ from 2° to 70° angles that are present in the X-ray scan. Oriented samples were analyzed with dry condition and after saturation with ethylene glycol.

5.4.3 Results and discussion

The diffractograms of the samples revealed the presence of quartz, calcite, muscovite, feldspar, chlorite, dolomite, goethite and some clay minerals (Fig. 5.14A, B, C, D, E, F & G). Quartz, feldspar, muscovite and calcite are the dominant minerals among all the samples. The dominance of quartz as well as some amounts of plagioclase and alkali feldspars in all samples reflects the derivation of their detritus from preexisting sedimentary rocks and granitic rocks exposed in the source area. Einsele (1962) described that the preservation and transport of feldspars, especially less stable plagioclase, are indicators of limited chemical weathering condition. Halite is present only in some of the samples of the Tetang Formation (Fig. 5.14G), which shows the presence of salt deposits in the source area or as secondary diagenetic precipitates. Calcite occurs in the suspensions of the river draining basins in arid climatic belts (Konta, 1988) while Einsele (1992) stated that
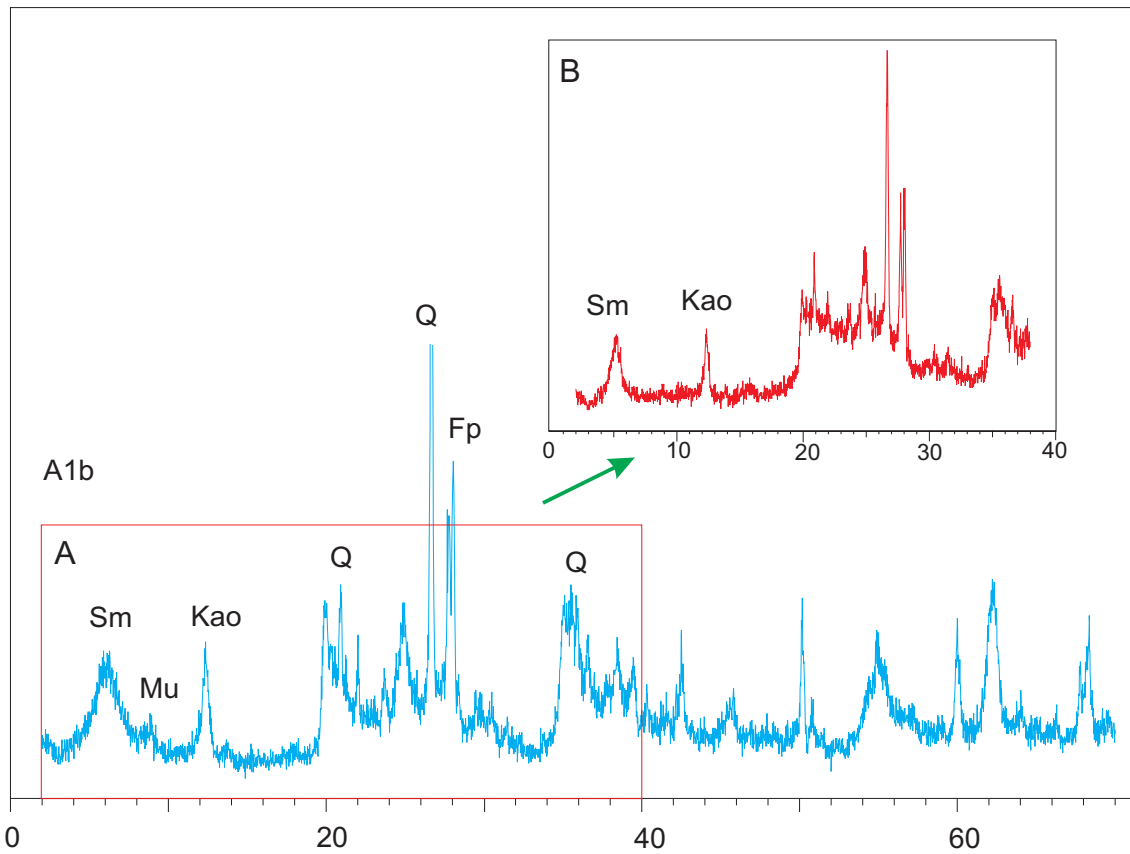
Fig. 5.14: X-ray diffraction pattern of the Thakkhola Formation at Dhi gaon. (A) bulk mineral composition (B) clay fraction after putting the ethylene glycol
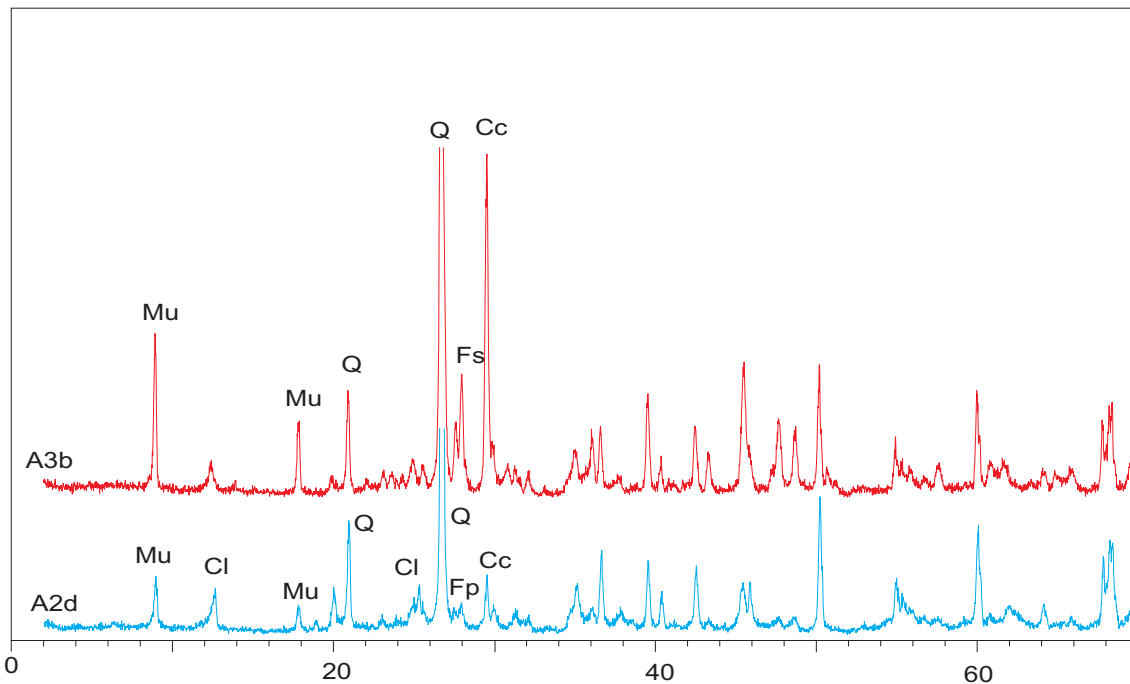
Fig. 5.14C: Thakkhola Formation at Tange gaon (A2d) and Ghiling gaon (A3d).
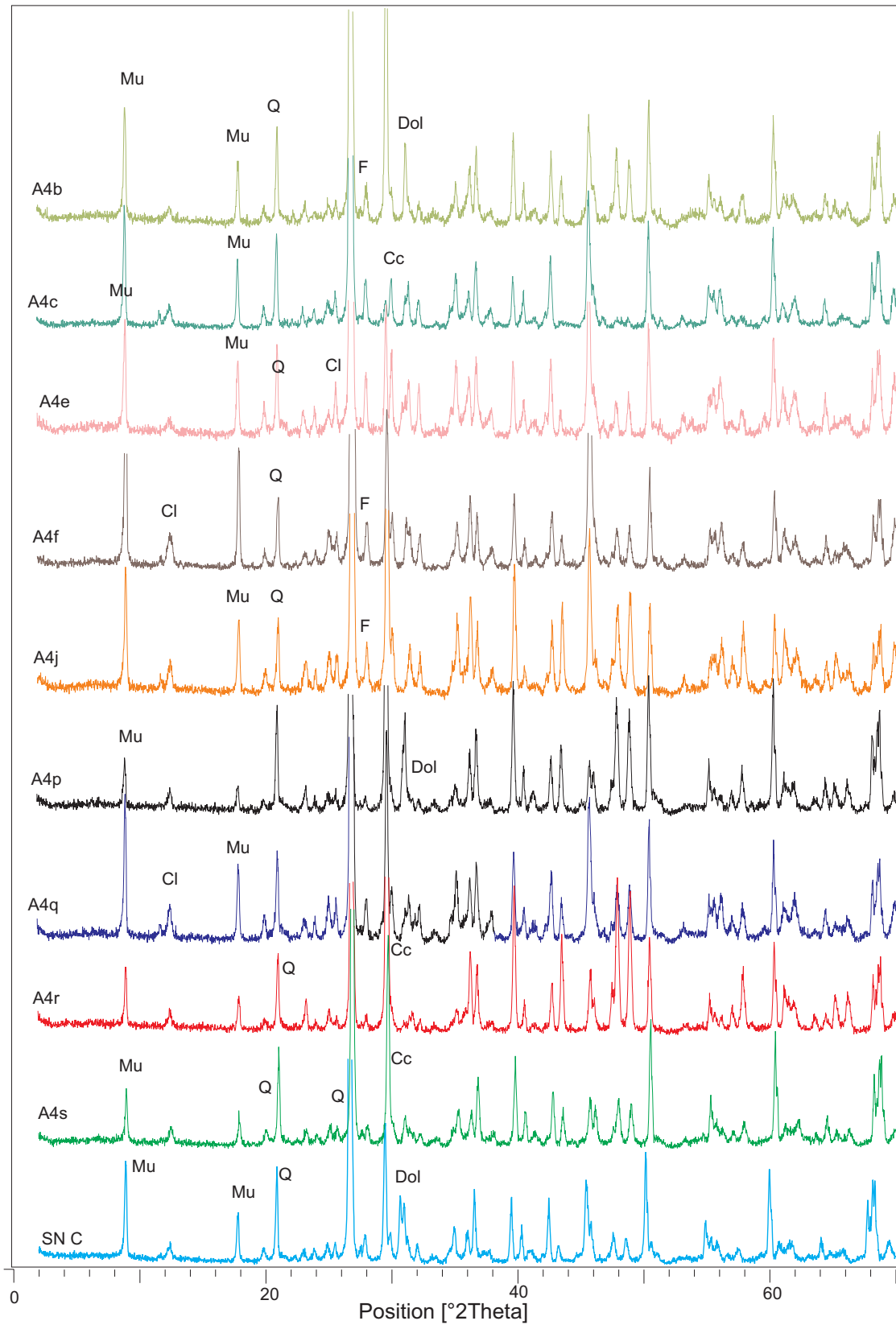
Fig. 5.14D: Thakkhola Formation at Chaile Village.
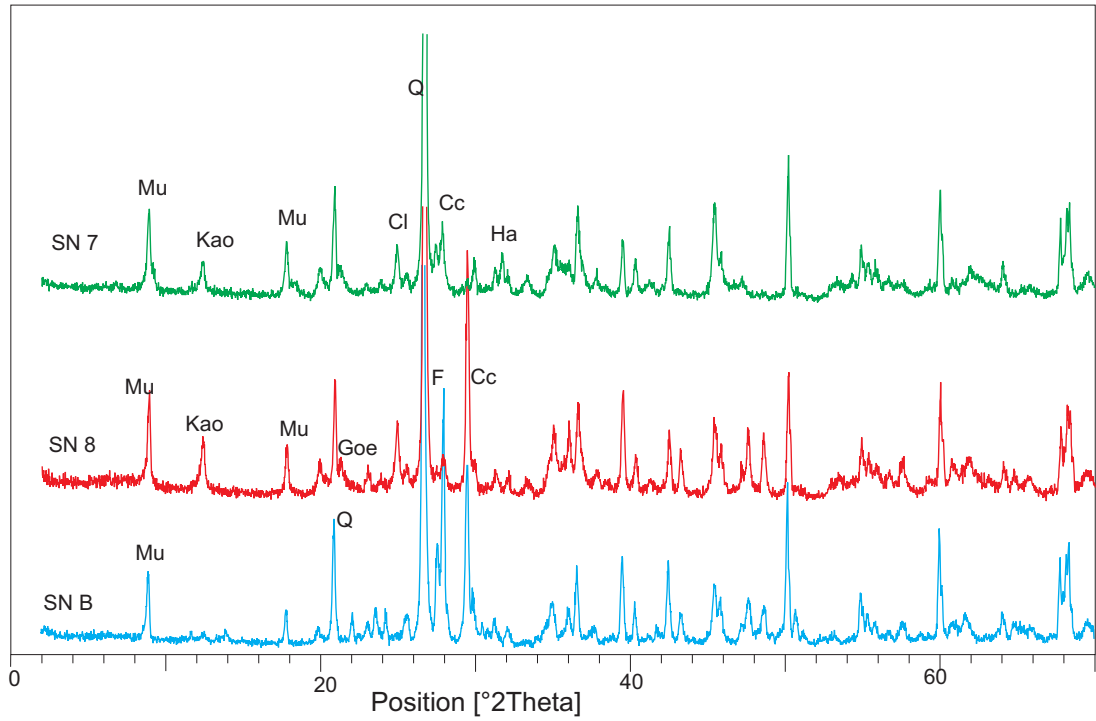
Fig. 5.14E: Thakkhola Formation at Syanboche (SNB), Ghami Khola (SN8) and Dhakmar village (SN 7)
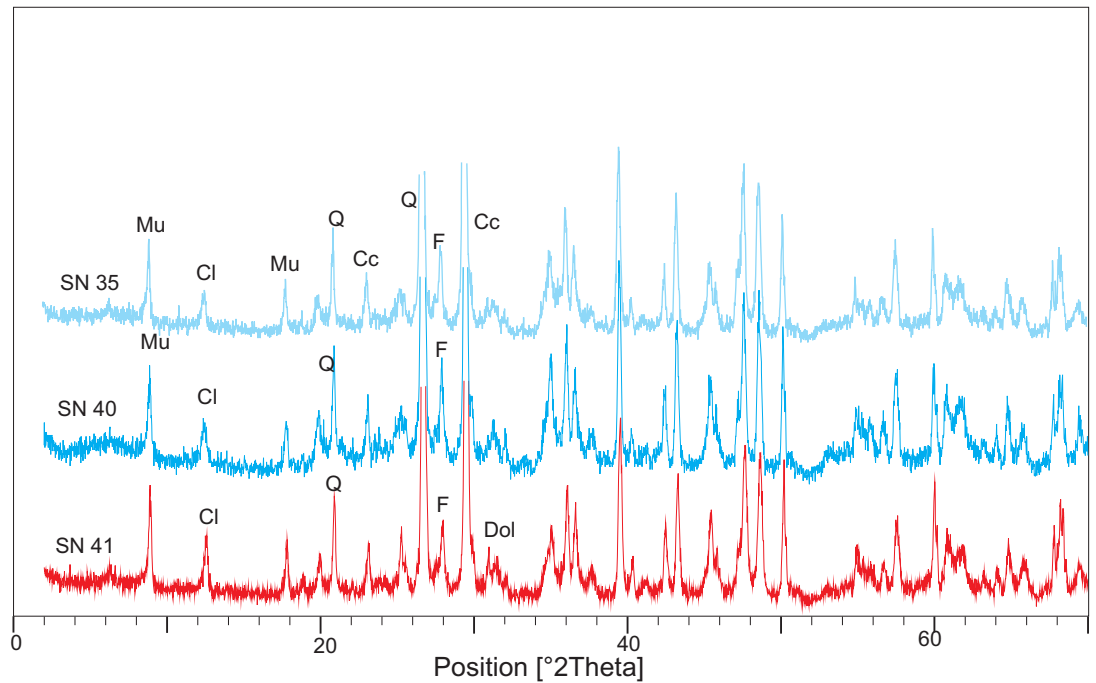
 Fig. 5.14 F: Sammargaon Formation (SN 35) and Marpha Formation at Syang Khola (SN 40), Marpha village (SN 41).
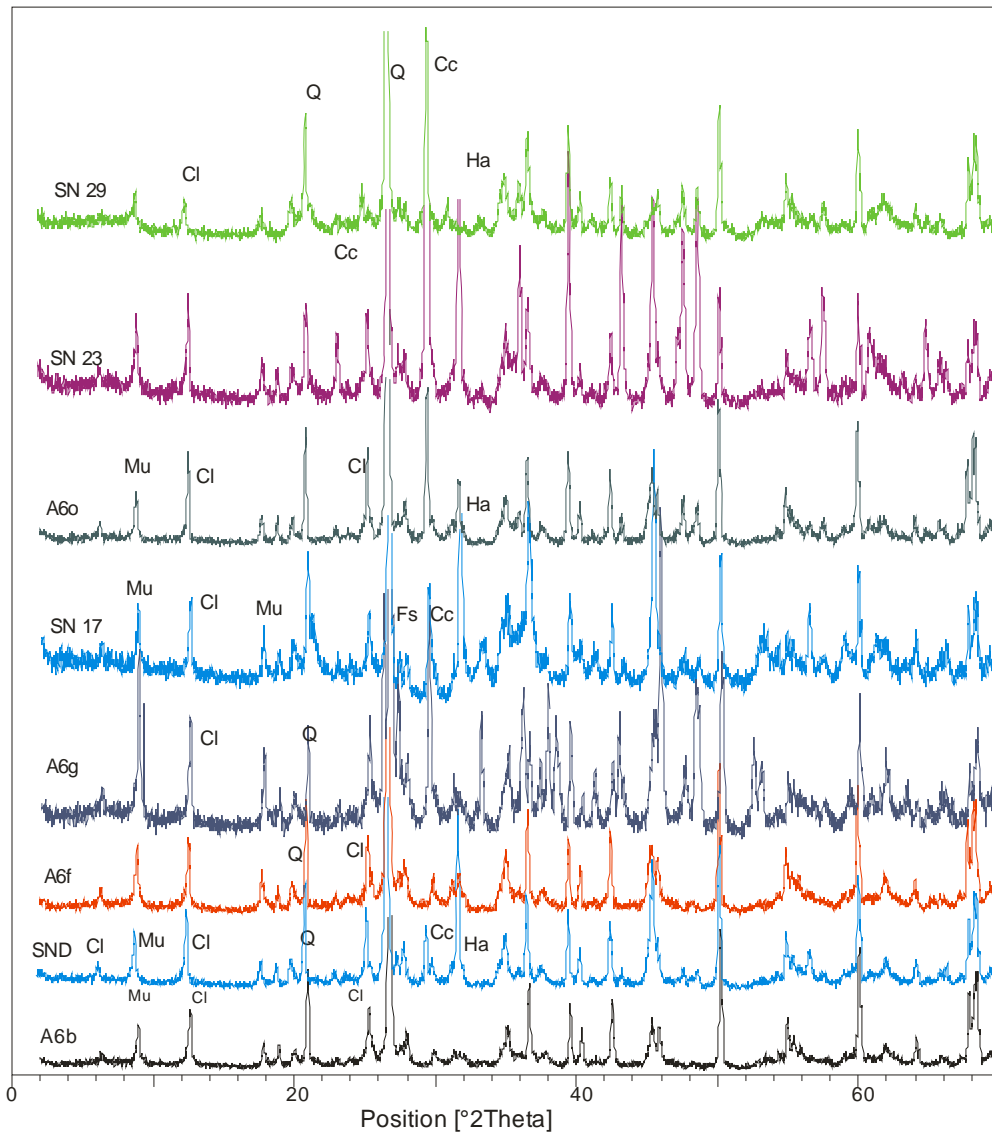
Fig. 5.14G: X-ray diffraction of bulk composition of the Tetang Formation at Tetang village. Sm = smectite, Kao = kaolinite, Q = quartz, Mu = muscovite, F = feldspar, Cc = calcite, Cl = chlorite, Dol = dolomite, Goe = goethite, Ha = halite.

the presence of carbonate minerals in the riverbed is a particularly sensitive indicator of the absence of deeply chemical weathered soils in party of drainage area. Smectite is present in the sample of Dhi gaon area on a considerable manner (Fig. 5.14A & B), which may be derived from all silicate minerals with relatively high concentration of Mg^{2+}, Fe^{2+} and Ca^{2+} cations. Grim (1968) described that when a basic igneous rock contains considerable amounts of magnesium and weathers under conditions of poor drainage or low rainfall in the magnesium is remained in the weathering environment after the breakdown of the parent minerals and smectite will be the alteration product, but

if the rainfall is high and the drainage is good, the magnesium is removed as soon as it is released from the parent minerals and kaolinite will be the weathering product. Barshad (1966) noted that smectite might form in higher content from mafic igneous rocks under higher precipitation regimes than form more siliceous igneous rocks. On the other hand smectite in the Dhi gaon area may come from the Chuck Formation (Fig. 2.4), which consists of volcanic-derived microconglomerates (Colchen, 1986). In addition, Huyghe et al. (2008) suggested that smectite in the fluvial Siwalik sequences formed in plain and low topographic areas less susceptible to erosion. Moreover, Bouquillion et al. (1990) reported that smectite-kaolinite rich clays in the sediments are the evidence of reduced physical erosion of the Himalayan range during the late Miocene and Pliocene time. From the discussion, it is strikingly obvious that all the minerals in the sediments are detritic and must have been derived from the surrounding basement rocks.

CHAPTER SIX
STABLE ISOTOPE ANALYSIS

6.1 Introduction

Several methods have been developed in recent years that allow for quantitative estimation of the past altitude or elevation changes of mountain ranges. These methods have focused on diverse principles such as basalt vesicularity (Sahagian and Maus, 1994), cosmogenic nuclides (Brooke et al., 1995) and paleobotany (Forest et al., 1999). Nowadays, mainly researchers focused on the use of stable isotopes of authigenic minerals to reveal important information about both the magnitude and timing of mountain range elevation change (Chamberlain et al., 1999; Chamberlain and Poage, 2000; Garzione et al., 2000a; Garzione et al., 2000b). Harold Urey (1948) first outlined the idea to use the oxygen isotopic composition of carbonates to deduce the temperature at which the carbonate was deposited. The importance of isotopes in helping to establish the climates of the past is based upon the original work of H.C. Urey and his associates on $^{18}O/^{16}O$ in the 1950s (Epstein et al., 1953). These measurements are now one of the cornerstones of paleocenographic research but not always dominantly for derivation of paleotemperatures - the data are commonly also used for evaluation of polar ice volume.

Determining the links and feedbacks between topography of mountain belts, tectonics, and climate change is an important, yet poorly understood, problem in earth sciences. Surface uplift of large plateaus such as Tibet and the western U.S. Cordillera may have strongly influenced Earth's climate during the Cenozoic by altering large-scale atmospheric circulation patterns (Kutzbach et al., 1989; Ruddiman and Kutzbach, 1990). The values of $\delta^{18}O$ become increasingly depleted with increasing altitude and this effect has been recognized in almost all the major mountain belts of the world (Dansgaard, 1964; Siegenthaler and Oeschger, 1980). This effect results principally from Rayleigh distillation and the depletion of $\delta^{18}O$ in precipitation and vapor as an air mass rises orographically and rains out moisture (Poage and Chamberlain, 2001). Oxygen isotopic ratios from carbonates and the waters from which they precipitate decreases with increasing elevation, making them potentially useful paleoaltimeters (DeCelles et al., 2007). The altitude effect is most often expressed as an isotopic lapse rate and given as a permil change in $\delta^{18}O$ of precipitation per 100 m of elevation. The averaged lapse rates for the North America, Central and South America and Europe grouping are -0.31, -0.27 permil/100m, and -0.24permil/ 100m, respectively while the high altitude grouping including Himalaya has a higher mean isotopic lapse rate of -0.41permil/100m (Poage and Chamberlain, 2001). As a global perspective, Southeast Asia revels the most complex pattern of spatial and temporal distribution of stable isotope composition of precipitation (Araguás and Froehlich, 1998).

Oxygen isotope data from lacustrine carbonates is controlled by lake water isotopic composition and temperature. Lake water composition is in turn responsive to the

isotopic composition of rainfall over the lake basin, which reflects rainfall temperature and atmospheric circulation patterns. These relationships provides a basis for estimating past climate variations from the oxygen isotope composition of carbonates in lake sediment cores.

The $\delta^{13}C$ value of soil carbonate is determined by the local proportion of C_3 and C_4 plants and by the extent of local plant cover where the climate is dry (Quade et al., 1989). Carbon isotopic records in carbonates (limestone and fossils) are of interest to paleoceanographers because they help to understand the functioning of the carbon cycle during earth history and through the carbon cycle of the biosphere. C_3 plants first organic carbon compound made in photosynthesis contains 3 carbon atoms. The carbon isotopic fractionation of such C_3 plants is very large. Therefore, plant material from such plants (including rice, wheat, soybeans and potatoes) has $\delta^{13}C$ values between -23 and -33‰, with an average of about -26‰. Plants that live in dry region (water loss problem) or in salty water (fresh water loss problem) allow them to open the stomata sparingly. This pathway is called the C_4 reaction (first organic compound formed has four carbon atoms). C_4 plants (mostly tropical grasses, salt marsh grasses and corn) are known only since Cenozoic and have been common only since the later part of the Miocene. C_4 plants show less isotopic fractionation of carbon than C_3 plants and have $\delta^{13}C$ values with an average about -13‰, ranging from -9‰ to -16‰ (Thomas, 2008).

6.1.1 Oxygen and Carbon isotope mass spectrometry

The element oxygen occurs as 3 stable isotopes: the common isotope ^{16}O (99.765%), the rare isotope ^{18}O (0.1995%), and the very rare isotope ^{17}O (0.0355%). Usually, the common isotope is lighter than the rare ones. An element must be in the gas phase if we want to measure its isotopic ratios in a mass-spectrometer, and the gas used for analysis of oxygen isotopes is CO_2. A CO_2 molecule can thus have different molecular weights (the parameter measured in a mass-spectrometer) because of the presence of the three stable isotopes of oxygen and two of carbon. The most common configurations of CO_2 are: $^{12}C^{16}O^{16}O$ (molecular weight 44), by far the most common molecule; $^{13}C^{16}O^{16}O$ (molecular weight 45), and $^{12}C^{18}O^{16}O$ (molecular weight 46). The element carbon occurs in two stable isotopes: the common ^{12}C (98.89%), and the rare isotope ^{13}C (1.11%). CO_2 is librated from $CaCO_3$ by dissolution in phosphoric acid (H_3PO_4), which is expressed by following formula.

$$3CaCO_3 + 2H_3PO_4 \rightarrow 3CO_2 + 3H_2O + Ca_3(PO_4)_2$$

These are all molecules that have no or only one of the rare isotopes. Molecules in which two rare isotopes are present are extremely rare, because the probability of pairing two ^{18}O-atoms in one CO_2 molecule by randomly moving atoms is infinitesimally small.

Carbon isotope data from carbonates are usually referred to the PDB (a belemnite, Belmnitella Americana, from the late Cretaceous Pee Dee Formation in South Carolina), as oxygen isotope data from carbonates. In the atmosphere, most carbon atoms occur in carbon dioxide (CO_2). Dissolved in the oceans, most carbon occurs in bicarbonate (HCO_3^-). In the biosphere, carbon occurs in organic matter on the form of organic material and calcium carbonate.

6.2 Materials and Methods

Twenty eight samples of limestones and calcareous clay were collected from the different formations within the Thakkhola-Mustang Graben to study the stable isotopes (Fig. 3.2). Seventeen samples of limestone, calcareous mud and carbonate concretions were collected from different areas of the Thakkhola Formation whereas 10 samples of fine-grained limestone, calcareous clay and calc-sandstone were collected from the Tetang Formation. One paleosol sample was collected from the Marpha Formation. By application of the Müller Gastner Bombe-method (Muller and Gastner, 1971), the percentage of calcium carbonate was measured.

From each bulk rock and soil samples, about 100-250 g powder was used for stable isotope analysis. The powdered samples and standard material were loaded into individual glass vials and placed into a drying oven at 50°C for at least 12h. After sealing with silicon-fluoride and Kel-F septa, the vials were placed into a sample rack of a Micromass Multiprep system. The samples were sequentially reacted by 103 % orthophosphoric acid (H_3PO_4) at a constant reaction temperature of 90°C. The isotopic ratio data were collected by means of a Micromass Optima isotope ratio mass spectrometer at the Center for Earth Sciences, University of Vienna. A few samples were run at the stable isotope lab of the University of Innsbruck, Innsbruck, Austria. The isotope data are reported in delta notation in per mil deviations relative to the international VPDB (Vienna PeeDee Belemnite) carbonate standard. Calibration to the VPDB was done by the carbonate standard NBS-19 for which the isotope ratios relative to VPDB are 1.95 ‰ ($\delta^{13}C$) and -2.20 ‰ ($\delta^{18}O$). The standard deviation (1σ) of NBS-19 standards (n = 15) treated identically to the samples averages 0.04 ‰ for $\delta^{13}C$ and 0.08 ‰ for $\delta^{18}O$.

6.3 Results and Discussions

A variety of factors influences the $\delta^{18}O$ values of carbonates, such as the $\delta^{18}O_{mw}$, evaporation, diagenetic effects, and temperature of calcite/aragonite precipitation. The lake level rises during the high inflow and $\delta^{18}O$ values of the lake water are lowered, and $CaCO_3$ precipitates have a relatively lighter isotopic composition. Evaporation increases the positive value of $\delta^{18}O$ and $CaCO_3$ precipitates shift to a heavier isotopic composition

Table 6.1: Table of stable oxygen and carbon data (see Fig. 3.2 for sample no.). * Values calculated based on lapse rate according to Poage and Chamberlain, 2001.

Sample	δ ^{13} C V-PDB[‰]	δ ^{18} O V-PDB[‰]	CaCO$_3$ %	Longitude	Latitude	Altitude (m)	*Paleoaltitude	Description
A1b	-21.87			E083°52'29.2"	N28°49'01.2"	3283		Organic black clay
A1c	4.6	-18.41	45.00	E083°52'29.2"	N28°49'01.2"	3289	4490	Marl
A2b	-26.64			E083°56'41.9"	N29°00'14.7"	3342		Black clay with fossil
sn09	3.78	-23.26	77.00	E083°50'56.4"	N29°00'49.9"	3707	5674	Fine grained limestone
sn10	6.29	-22.86	95.00	E083°51'00.0"	N29°00'10.5"	3670	5577	Limestone with pebbles
sn11	1.78	-17.37	48.00	E083°50'28.3"	N28°59'28.1"	3689	4237	Carbonate concretion
sn12	3.24	-19.53	63.00	E083°50'28.3"	N28°59'28.1"	3692	4764	Fine grained limestone
A4e1	2.01	-21.52	58.00	E083°48'40.8"	N28°56'22.9"	3471	5249	Coarse grained limestone
A4e			9.00	E083°48'40.8"	N28°56'22.9"	3456		Carbonaceous clay
A4g	0.065	-21.9	47.00	E083°48'40.8"	N28°56'22.9"	3430	5341	Fine grained limestone
sn13	1.92	-21.46	95.00	E083°48'37.0"	N28°56'37.0"	3409	5234	Fine grained limestone
A4i	6.03	-24.61	89.00	E083°48'40.8"	N28°56'22.9"	3390	6002	Fossiliferous limestone
sn14	5.10	-24.96	99.50	E083°48'40.2"	N28°56'22.1"	3392	6088	Fine grained limestone
A4j			27.00	E083°48'40.8"	N28°56'22.9"	3389		Calcareous mud
A4k	8	-23.12	82.00	E083°48'40.8"	N28°56'22.9"	3388	5639	Red limestone
A4L	7.09	-22.26	91.00	E083°48'40.8"	N28°56'22.9"	3387	5429	Fine grained limestone
A4R	-0.62	-19.46	48.00	E083°48'40.8"	N28°56'22.9"	3226	4746	Limestone
sn30	6.44	-19.69	85.00	E083°49'53.7"	N28°54'32.8"	3122	4802	Fine grained limestone
A6u	11.07	-20.33	91.00	E083°49'56.1"	N28°55'35.6"	3118	4959	Laminated limestone
sn25	11.08	-20.18	94.00	E083°49'53.7"	N28°54'32.8"	3107	4923	Fine grained limestone
A6s	10.03	-19.94	91.00	E083°49'56.1"	N28°55'35.6"	3093	4863	Laminated limestone
sn23	3.56	-21.42	33.50	E083°49'53.7"	N28°54'32.8"	3101	5223	calcareous clay
sn24	1.93	-21.39	24.00	E083°49'53.7"	N28°54'32.8"	3100	5217	Calc-Sandstone
A6L	-24.08			E083°49'56.1"	N28°55'35.6"	3042		Black clay with fossil
A7c1	5.58	-22.57	92.00	E083°50'39.4"	N28°53'10.5"	3554	5505	Fine grained limestone
A7c	4.03	-17.64	90.00	E083°50'39.4"	N28°53'10.5"	3524	4302	Fine grained limestone
sn26	6.05	-21.69	99.50	E083°50'39.4"	N28°53'10.5"	3493	5291	Fine grained limestone
sn41	1.58	-13.53	31.00	E083°41'26.4"	N28°45'14.7"	2683	3299	calcareous clay
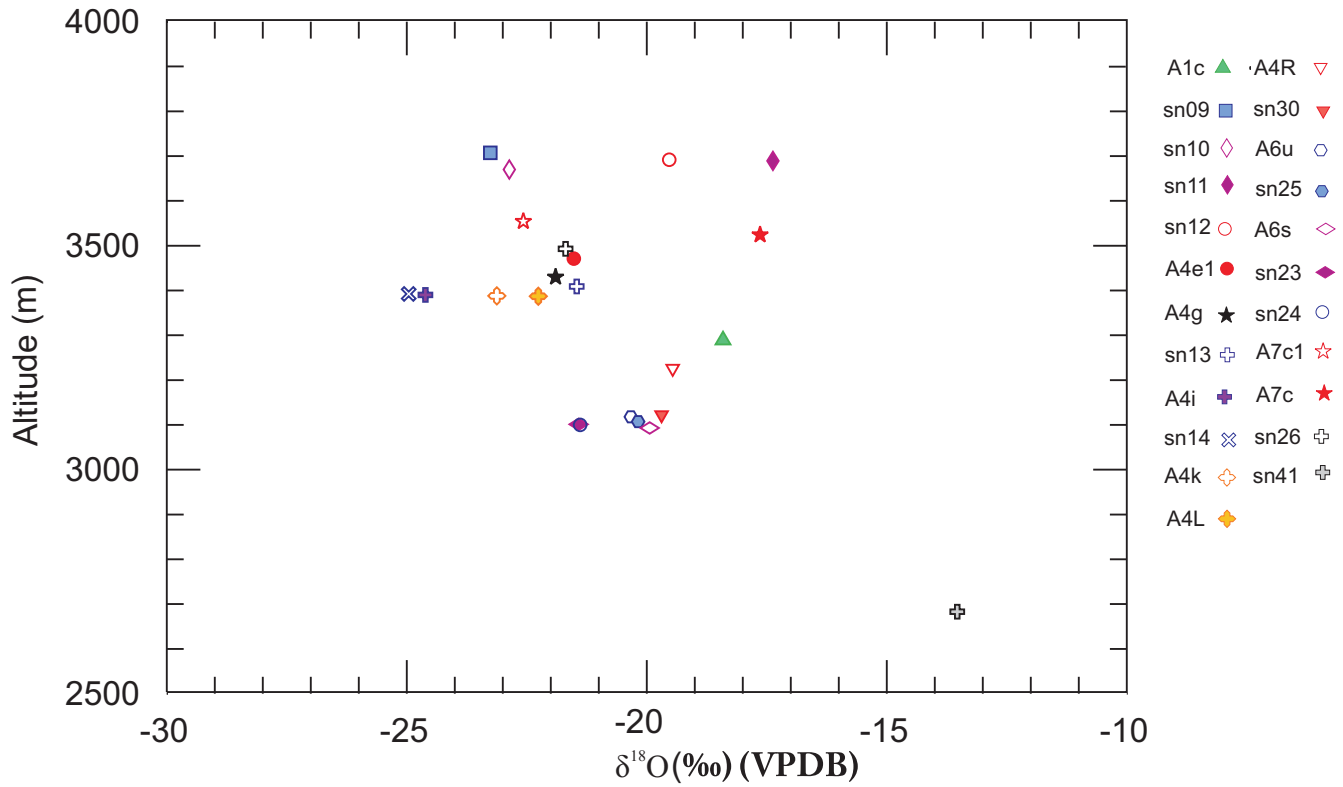
Fig. 6.1: Plot of δ¹⁸O (‰) versus altitude of carbonates within the Thakkhola-Mustang Graben (see Fig. 3.2 for sample location)
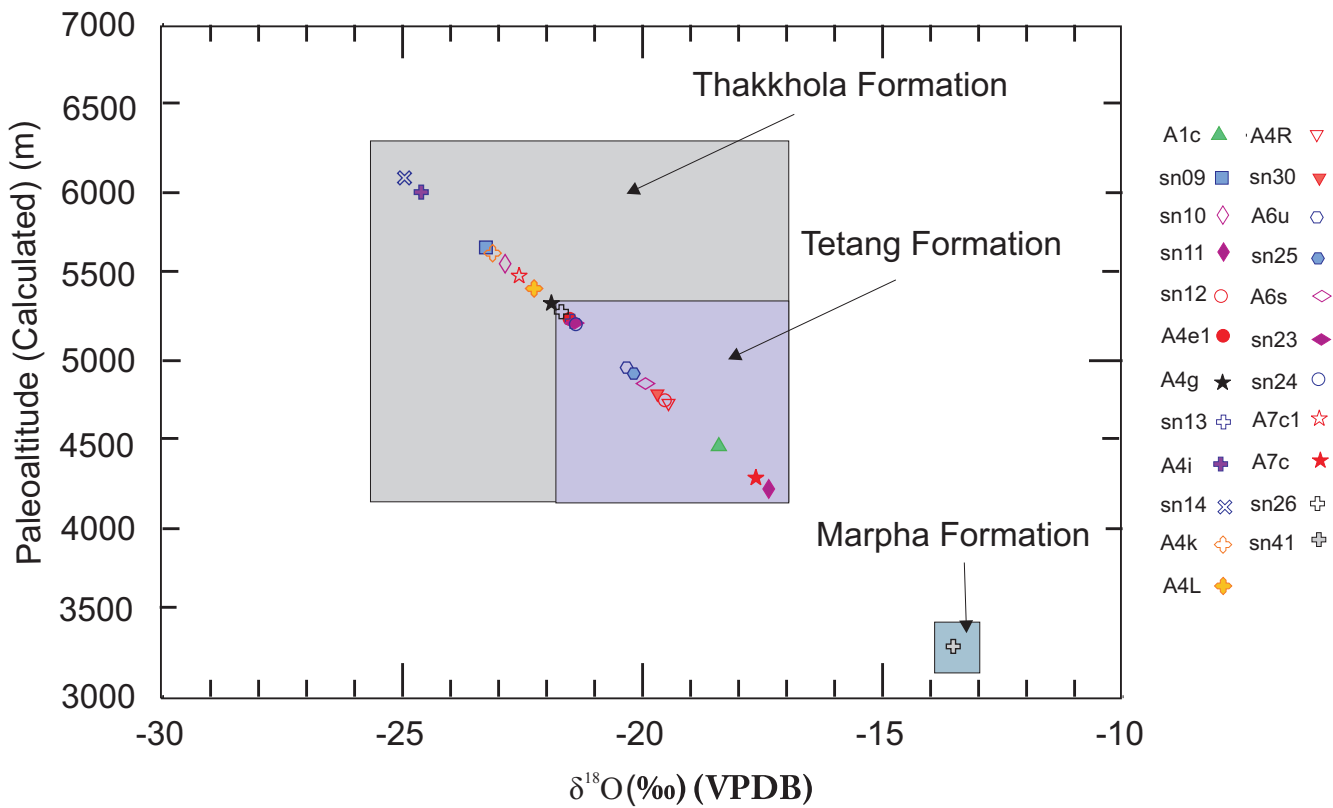
Fig. 6.2: Plot of δ¹⁸O (‰) versus paleoaltitude (calculated) of carbonates within the Thakkhola-Mustang Graben (see Fig. 3.2 for sample location)

88
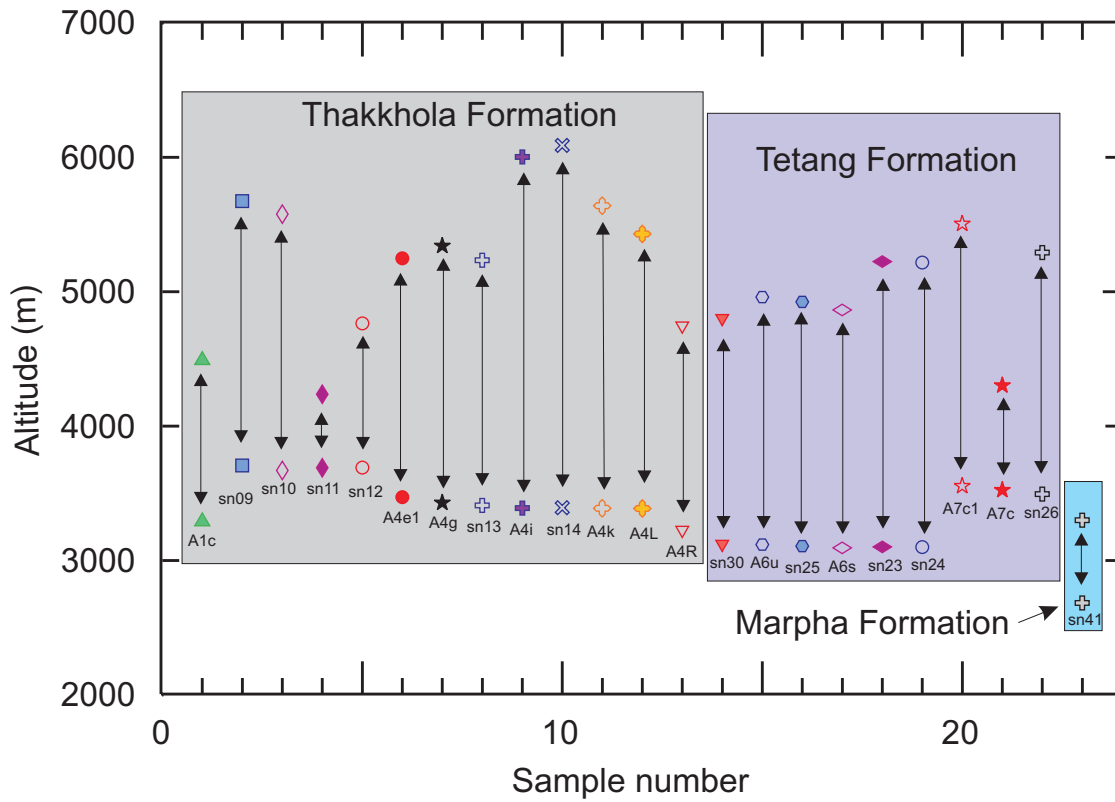
Fig. 6.3: Plot of present altitude and calculated paleoaltitude (-0.41permil/100m from the δ¹⁸O value according to Poage and Chamberlain, 2001) Vs sample no of carbonates Thakkhola-Mustang Graben (see Fig. 3.2 for sample location). Paleoaltitudes are higher than present altitude.
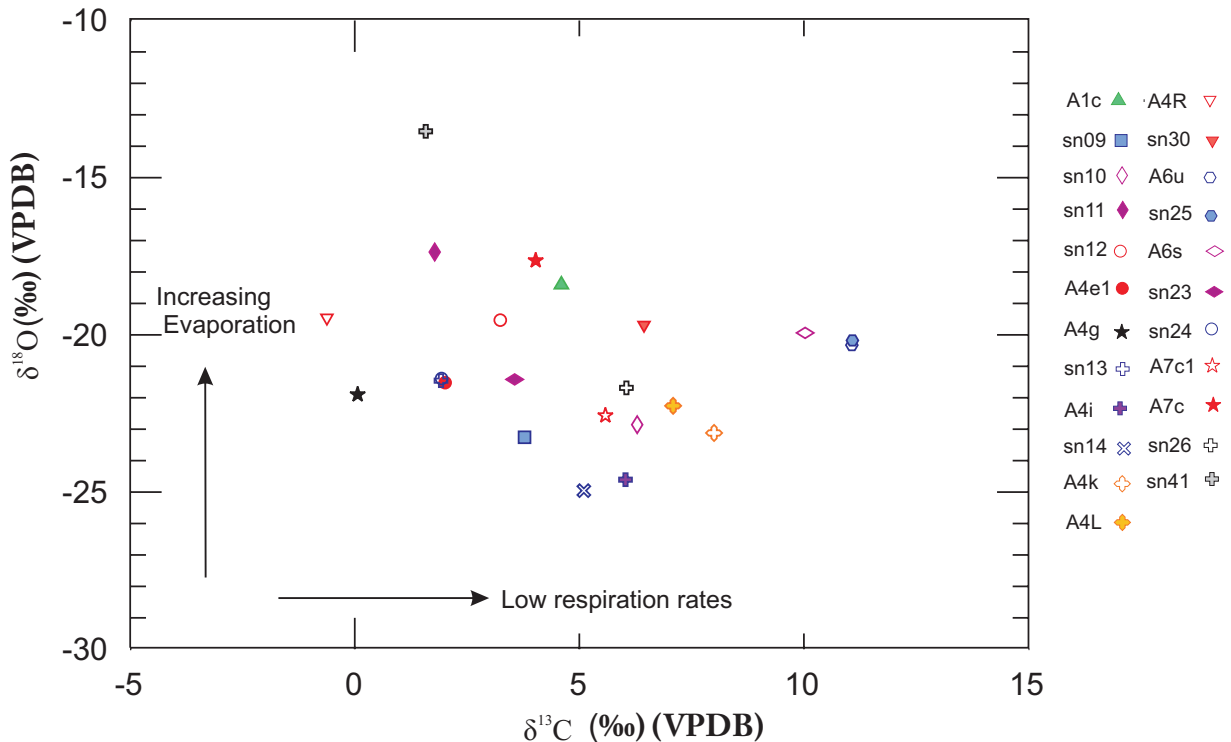
Fig. 6.4: Plot of value δ¹⁸O (‰) Vs δ¹³C (‰) of carbonates of Thakkhola-Mustang Graben (see Fig. 3.2 for sample location)
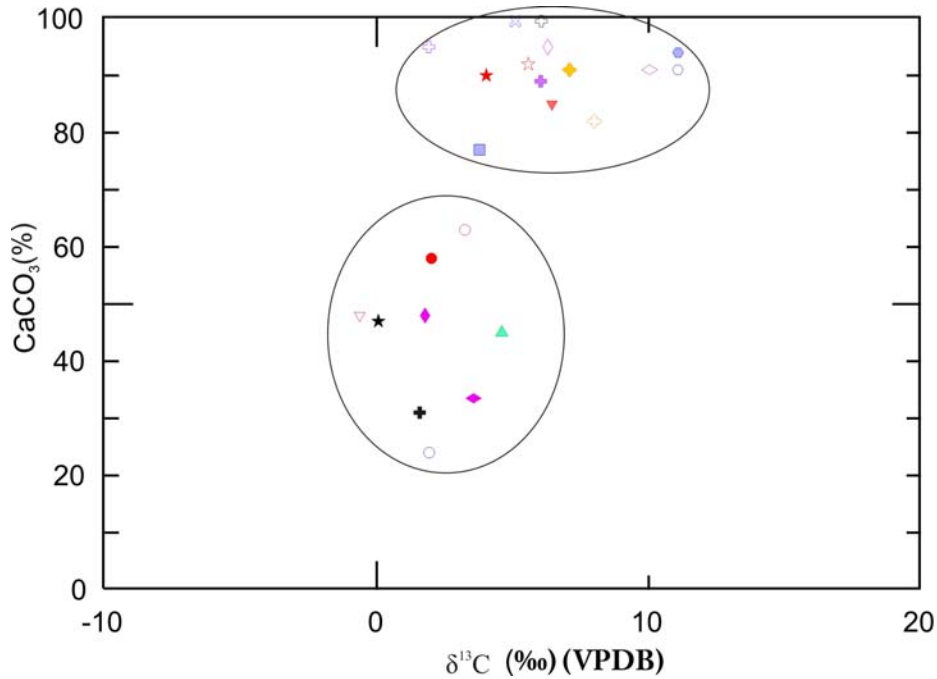
Fig. 6.5: Plot of CaCO₃ (%) Vs value δ¹³C (‰) of carbonates of the Thakkhola-Mustang Graben (see Fig. 3.2 for sample location)

on both oxygen and carbon. Variation on $\delta^{18}O$ and $\delta^{13}C$ shows the fluctuations of the lake water level (inflow and evaporation balance). Carbon and oxygen isotopic compositions of limestone, carbonate concretion and the calcareous clay are listed in the Table 6.1. The $\delta^{18}O$ values vary from -13.5 ‰ (sn 41 Marpha) to -24.96 ‰ (sn 14, Chaile) averaging 19.24 ‰. According to Poage and Chamberline (2001), the isotopic composition of precipitation decreases linearly with increasing elevation in most region of the world except in Himalaya or above 5000 meters because it has been suggested that the high variation may be due to post-depositional changes in snow (Niewodniczanski et al., 1981) or addition of a secondary source of moisture from the upper troposphere (Holdsworth and Fogarasi, 1991). The lapse rate is -0.41 permil/100m (Poage and Chamberlain, 2001) in Himalaya, although low r^2 values of individual studies limit the usefulness of this number. Applying this lapse rate, the paleo-altitude of the Thakkhola-Mustang Graben varies from 3300 (Marpha Formation) to 6087m (Thakkhola Formation) (Fig. 6.2 and 6.3). The isotopic composition of samples taken in the rainshadow of a developing mountain range may be a more sensitive indicator of paleoelevation surface. As a rainshadow develops, increased evaporation may shift the isotopic composition of soil or groundwater to higher $\delta^{18}O$ values, which may also result in underestimation of elevation change (Poage and Chamberlain, 2001).

The value of $\delta^{18}O$ is decreasing with increasing altitude in most of the cases with some exception within small altitude difference (Fig. 6.1). Sample (sn 09) collected at the highest altitude (3707) has more negative value (-23.26 ‰) than the sample (sn 41) with -13.53 ‰ $\delta^{18}O$ value of the lowest altitude at Marpha village (2683). However, the sample of the Chaile section (sn 14) has very negative value. Rowley et al. (2001) calibrated a theoretical relationship based on Rayleigh fractionation; they applied it to sedimentary rocks in the grabens in the southernmost Tibet using the data of Garzione et al., (2000b) and Wang et al. (1996) and reported no change in the elevation since ~10 Ma and their results allow higher estimated of paleo-than present-day elevation. Garzione et al. (2000 a, b) reported already the very negative value of $\delta^{18}O$ of the carbonate in the Thakkhola graben and they inferred that this indicates elevations similar to modern elevation since the late Miocene onset of deposition in the basin.

The stable oxygen isotope composition ($\delta^{18}O$) of a precipitated carbonate depends mainly on the isotope composition, salinity and temperature of the host fluid whereas the stable carbon isotope composition ($\delta^{16}C$) reflects the source of CO_2 for precipitation such as meteoric or sea water, shell dissolution or various biochemical origins including microbial oxidation of organic matter and methane (Friedman et al. 1977; Rankamma. K., 1936 cited in Narayan et al. 2007). Rainwater, derived by evaporation of seawater, is depleted in $\delta^{18}O$ and hence has negative value where as brines are enriched in heavy $\delta^{18}O$ and have a positive value. The range of $\delta^{18}O$ values, however, shows no obvious changes since 10.6 Ma (Tetang formation), which might suggest stronger wet and dry seasonality since that period but the climate was slightly dry because of increasing evaporation in the Marpha period (Fig. 6.4).

Generally, carbonates with a high percentage of $CaCO_3$ have a high $\delta^{13}C$ values (Fig. 6.5). Stable carbon isotopes of lacustrine carbonate of the Tetang Formation have higher values of $\delta^{13}C$ than the Thakkhola and Marpha formations having the values ranging from -24.08 to 11.08 ‰ (Fig.6.4 and 6.5). Very negative values of the organic black clay samples (A6L, A2b and A1b) should have been from the degradation of organic matter in sulfate reducing environments (Irwin et al., 1977). The $\delta^{13}C$ value of other calcareous clay and limestones range from -0.62 to 11.08‰, which are quite higher than other organic black clay samples. Such high $\delta^{13}C$ values strongly indicate that these carbonates formed in the methanogenic zone (Irwin et al., 1977). The $\delta^{13}C$ value of dissolved inorganic carbon (DIC) in lake systems is relatively more enriched than fluvial water that supplies the lake because of the preferential uptake of ^{12}C by photosynthesis organisms in the lake (McKenzie, 1985) and the preferential outgassing of ^{12}C-rich CO_2 from the surface of the lake (Talbot, 1990). The isotopic composition of the DIC is recorded by the primary lake carbonates in the upper water column of the lake at the time of carbonate precipitation. Extremely positive $\delta^{13}C$ values of the carbonates in the Tetang Formation infer that the bottom water conditions were dysaerobic in the lake, leading to the

breakdown of organic matter by bacterial methanogenesis (Garzione et al., 2003). The implication of the high values of $\delta^{13}C$ from the Thakkhola-Mustang Graben is that orographic barriers are in the Himalaya, which was actively growing during Oligocene time and earlier (Hodges, 2000).

The value of $\delta^{18}O$ is almost constant whereas the values of $\delta^{13}C$ varies largely (Fig. 6.4). The diagenesis affected the C isotope composition of carbonate, but had a minimal effect on isotopes because it occurred in the presence of the original pore fluids in the sediments (Talbot and Kelts, 1990). Talbot and Kelts (1990) documented similar observation in the organic rich lake deposits in Ghana. Garzione et al. (2003) studied the isotopes of carbonate in detailed and concluded that the more negative value of the sparite on the eastern part of the Tetang Formation suggest that the sparite formed at a higher temperature then micrite, perhaps after burial of the Tetang Formation.

CHAPTER SEVEN
HEAVY MINERAL ANALYSIS

7.1 Introduction

Heavy mineral analysis is one of the most sensitive and widely used techniques in the determination of provenance of clastic deposits. Heavy minerals are particularly useful in studies of sedimentation related to tectonic uplift. The evolution and unroofing episodes of orogenic belts are faithfully reflected in their foreland belts by clastic sedimentation. However, the composition of heavy mineral assemblages is not only controlled by the mineralogical composition of the source region. Several other processes that operate during the sedimentation cycle (Fig. 7.1) modify the original provenance signal. So that, heavy mineral data from the sediments and sandstone do not solely reflect the composition of the parent rocks. According to Morton and Hallsworth (1999), heavy mineral assemblages are affected by three processes; physical sorting, mechanical abrasion and dissolution. Physical sorting takes place because of the hydrodynamic conditions operative during the transport and depositional stages and controls both absolute and relative abundances of heavy minerals. Mechanical abrasion takes place during transport and it causes grains to diminish in size by a combination of fracturing and rounding.
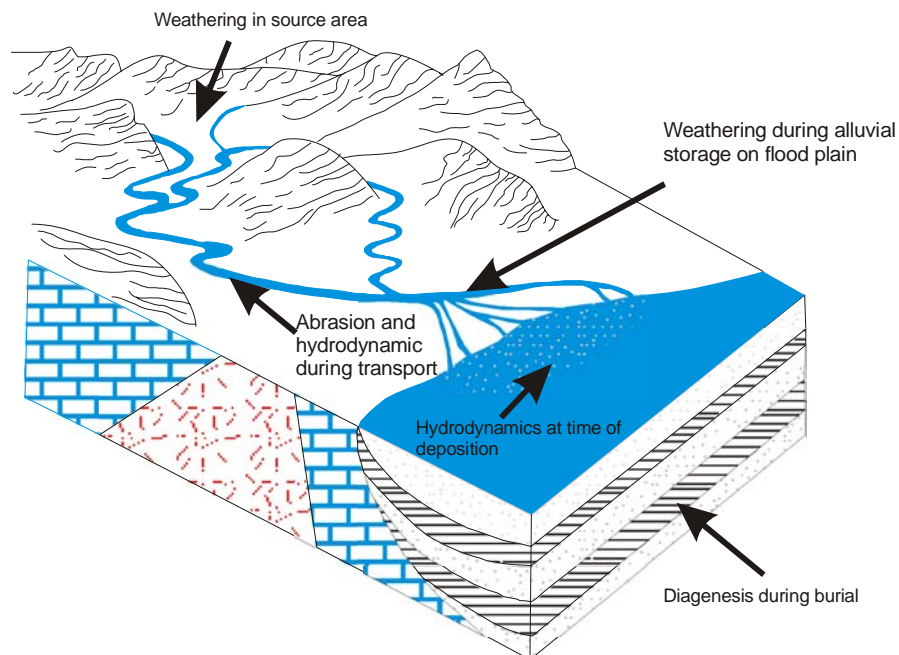
Fig. 7.1: Schematic diagram showing process controlling heavy mineral assemblages in sedimentary succession (modified after Morton and Hallsworth, 1999)

Dissolution causes partial or complete loss of heavy minerals in a variety of geochemical condition at several stages in the sedimentation cycle from weathering at source, sub-aerial exposure in non-marine depositional setting, during burial and finally during weathering at outcrop. Analysis of heavy minerals in basin-fill sequences may thus prove valuable in constraining the structural histories of both the basin and the tectonic hinterlands. From the moment, the minerals are released from their host rocks a series of processes come into effect. Among them, hydraulic factor and post-depositional effects are very important (Mange and Maurer, 1992). The hydraulic factor decides which minerals grains will be deposited under certain hydraulic condition.

7.2 Materials and Methods

Fifty samples were taken for the analysis from different formations of the Thakkhola-Mustang Graben (Table 7.1) (Fig. 5.7A, B, C, D & E). 100 to 200 g of dry crushed sample material was used for the heavy mineral analysis and it yielded sufficient quantity of heavy mineral concentration. The following sequences of treatment were used for the heavy mineral separation:

1. disaggregation of coherent sediments to liberate individual grains;
2. 10% acetic acid (CH_3COOH) was used to acid digestion to eliminate carbonates for 1 week and samples were washed with water to dissolve soluble salts;
3. Removal of organic substances;
4. Samples were sieved with 0.063 mm – 0.4 mm sieve size to extract the retained grain.

5.2.1 Heavy mineral separation

There are many techniques to separate heavy minerals. The choice of techniques used will also have an effect on the quality of the results obtained. Rittenhouse and Bertholf (1942) compared the effectiveness of gravity settling and centrifuge separation. They observed that the weight percentage of heavy minerals concentration obtained by the two methods differ significantly but the number frequencies of the individual heavy mineral are the same in both cases. Therefore, gravity separation method was used on this study. Heavy minerals were separated by using Tetrabromoethane ($Br_2CHCHBr_2$) of 2.96 g/cm^3 density. Acetone (CH_3COCH_3) was used to remove the heavy liquid from the grains. A gravity separation apparatus was used in the Department of Geodynamics and Sedimentology, University of Vienna, Vienna, Austria, that is illustrated by the fig. 7.2. The two funnel were connected by setting up a ring stand with one ring attached in the middle and the other one is on the top. A beaker was placed below the lower funnel. A small piece of rubber tube was connected to the bottom of the lower funnel to collect the heavy liquid into the beaker. A piece of filter paper was then folded and placed into the

lower funnel. This funnel was clamped off at first to prevent flow. Tetrabromoethane was then poured into the top funnel and then the dry sample was added to the heavy liquid. Samples were stirred to ensure there the grains are thoroughly wetted.
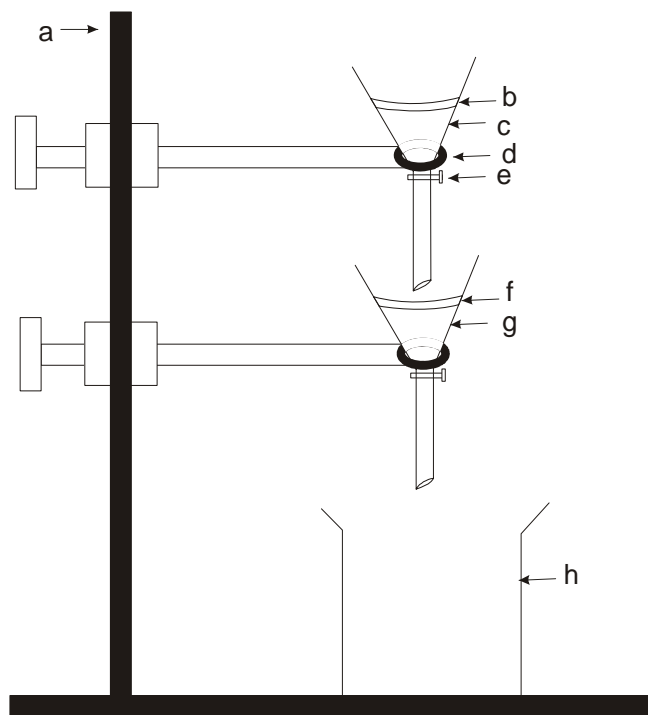
Fig. 7.2: Arrangement of equipment for heavy mineral separation by gravity settling, (a) Retort stand, (b) Position of light minerals, (c) Funnel, (d) Funnel support, (e) Pinch clip, (f) Filter paper, (g) Lower funnel, (h) Collecting beaker.

Samples were stirred time to time by 30 minutes interval for the three hour. After the time had elapsed, the clamp was released from the funnel just long enough for the collected heavy minerals. The Tetrabromoethane then filtered through the paper into the beaker leaving the heavy minerals on the filter paper. The Tetrabromoethane could then be reused. The light fraction was then drained into a second funnel. Both fractions were washed several times thoroughly with a mixture of acetone and Tetrabromoethane and in the end by pure acetone. A collecting bottle for washed fluid was later used for recycling of Tetrabromoethane and filter papers were then removed and replaced. This process was repeated for each of the 50 samples.

Samples were air-dried over night after all samples were separated. The heavy minerals from each sample were then mounted onto a slide using Canada balsam and viewed using a petrographic microscope. With the help of Mange and Maurer's book (1992), each mineral identified by using certain characteristics such as color, shape, and appearance under different lights using the Fleet method (Fleet, 1926). More than 300 grains on each slide were counted and identified as possible from which relative abundances were

calculated. Percentages were then figured and graphs were made showing the composition of each of the sand samples are presented. Several minerals such as opaque minerals, biotite, chlorite were excluded from quantitative examinations.

Non-parametric Spearman Rank correlation (ρ) was used for calculating a correlation because this technique assuming that both variables are independent and compares their rank not the absolute values of the two datasets (Eq. 7.1).

$$\rho = 1 - \frac{6\sum d2}{n(n2-1)} \quad \dots\dots\dots\dots\dots\dots\dots\dots\dots\dots\dots\dots\dots\dots\dots\dots\dots\dots\dots\dots\text{Eq. 7.1}$$

Where, n = the number of values in each data set

        d = different between corresponding ranks

If the tied ranks exist, classic person's correlation coefficient (Eq. 2) between ranks has to be used instead of eq.7.1.

$$\rho = \frac{n(\sum x_i y_i) - (\sum x_i)(\sum y_i)}{\sqrt{n(\sum x_i^2) - (\sum x_i)^2}\ \sqrt{n(\sum y_i^2) - (\sum y_i)^2}}. \quad \dots\dots\dots\text{Eq. 7.2}$$

Where,

        n = the number of values in each data set (same for both sets)

        x_i and y_i = ranks of the corresponding values

7.3 Results and discussions

Only 41 out of 50 samples had enough heavy minerals to count more than 300 grains. The results are given in table 7.1. Nine samples, which had less then 300 heavy mineral grains are presented in the table 7.2. Average heavy mineral concentration encountered in the sections was presented in pie diagrams (Fig. 7.6) and pie diagrams of average values are plotted on the map (Fig. 7.8). They are also presented in the generalized stratigraphy column (Fig. 7.9).

Heavy minerals present in the graben sediments include zircon, garnet, andalusite, kyanite, staurolite, chloritoid, epidote, tourmaline, hornblende, rutile, chrome spinel, apatite and amphibole. The heavy mineral assemblages are in general characterized by predominance of tourmaline followed by zircon, staurolite, apatite, garnet, rutile, epidote, and kyanite whereas lesser amounts of chrome spinel, chloritoid, hornblende and blue amphibole are present. The following discussions of the heavy minerals distribution are based on the results obtained from the microscopic investigation.

Staurolite

High reliefs combined with shades of yellow or yellowish brown and distinct pleochroism are the diagnostic characteristics of staurolite with average value of 12.6%. It is a typical mineral of intermediate metamorphism (Fig. 7.5C). It is negatively

Table: 7.1: Heavy mineral composition (more than 300 countable grains) of the Thakkhola and Tetang formations (expressed in grain %)

Abbreviations: ZIR-zircon, GAR-garnet, AND-andalusite, KYA-kyanite, STA-staurolite, CTD-chloritoid, EPI-epidote, TOU-tourmaline, HOR-hornblende, RUT-rutile, CRS-chrome spinel, APA-apatite, AMP-amphibole, SD-Standard deviation

Lomanthang

Sample	ZIR	GAR	AND	KYA	STA	CTD	EPI	TOU	HOR	RUT	CRS	APA	AMP	Total
SN 3	0.9	3.7	0.0	0.0	0.0	0.0	0.0	95.4	0.0	0.0	0.0	0.0	0.0	100.0

Dhigaon

Sample	ZIR	GAR	AND	KYA	STA	CTD	EPI	TOU	HOR	RUT	CRS	APA	AMP	Total
A1a	14.0	14.8	5.4	0.0	6.6	0.0	0.0	32.7	0.8	3.1	0.0	22.6	0.0	100.0
A1e	7.7	11.2	3.1	0.0	7.7	0.0	0.4	53.8	0.8	1.9	0.0	13.5	0.0	100.0
A1f	0.3	6.1	15.0	0.0	3.2	0.0	1.1	64.9	0.8	1.1	0.0	7.7	0.0	100.0
Average	7.3	10.7	7.9	0.0	5.8	0.0	0.5	50.5	0.8	2.0	0.0	14.6	0.0	100.0
SD	6.9	4.4	6.3	0.0	2.4	0.0	0.5	16.4	0.0	1.0	0.0	7.5	0.0	

Tangegaon

Sample	ZIR	GAR	AND	KYA	STA	CTD	EPI	TOU	HOR	RUT	CRS	APA	AMP	Total
A2a	6.0	28.7	2.4	0.0	25.1	0.0	0.0	28.7	0.0	3.2	0.0	6.0	0.0	100.0
A2c	37.5	6.3	0.0	0.0	18.8	0.0	0.0	25.0	0.0	0.0	0.0	12.5	0.0	100.0
Average	21.7	17.5	1.2	0.0	21.9	0.0	0.0	26.8	0.0	1.6	0.0	9.2	0.0	100.0
SD	22.3	15.9	1.7	0.0	4.5	0.0	0.0	2.6	0.0	2.3	0.0	4.6	0.0	

Ghiling gaon

Sample	ZIR	GAR	AND	KYA	STA	CTD	EPI	TOU	HOR	RUT	CRS	APA	AMP	Total
A3a	4.4	11.5	1.2	0.0	16.5	0.0	0.0	58.3	0.0	0.0	0.0	5.0	3.1	100.0
A3d	0.0	3.2	3.9	0.0	5.0	1.4	0.0	79.6	2.9	0.0	0.0	3.9	0.0	100.0
A3e	2.3	34.4	2.3	0.0	39.2	0.0	0.0	21.2	0.0	0.0	0.0	0.6	0.0	100.0
Average	2.2	16.4	2.5	0.0	20.3	0.5	0.0	53.0	1.0	0.0	0.0	3.2	1.0	100.0
SD	2.2	16.1	1.4	0.0	17.4	0.8	0.0	29.5	1.7	0.0	0.0	2.3	1.8	

Syanboche-Vena trail near Syanboche Khola.

Sample	ZIR	GAR	AND	KYA	STA	CTD	EPI	TOU	HOR	RUT	CRS	APA	AMP	Total
SN 12	2.7	3.6	0.0	0.0	12.5	0.0	0.9	51.8	0.0	0.0	0.0	28.6	0.0	100.0

Chaile gaon

Sample	ZIR	GAR	AND	KYA	STA	CTD	EPI	TOU	HOR	RUT	CRS	APA	AMP	Total
A4d	4.6	2.6	0.0	0.0	2.3	0.0	0.0	56.0	1.0	2.6	0.7	30.3	0.0	100.0
A4f	3.1	3.4	13.5	0.3	1.7	0.8	0.0	68.2	0.3	0.0	0.0	8.7	0.0	100.0
A4h	50.7	1.5	2.2	1.5	5.1	0.0	0.0	30.1	0.0	4.4	0.0	4.4	0.0	100.0
SN 13	3.3	0.5	0.2	0.0	0.0	0.0	0.0	56.5	0.0	5.4	3.9	28.9	1.2	100.0
A4m	17.3	0.3	0.0	0.3	0.3	0.0	0.0	80.0	0.0	0.6	0.0	1.2	0.0	100.0
A4n	10.3	0.0	0.0	0.0	1.3	0.0	0.0	87.1	0.0	0.0	0.0	1.3	0.0	100.0
A4o	12.7	0.3	0.0	0.0	0.6	0.0	0.0	86.3	0.0	0.0	0.0	0.0	0.0	100.0
A4p	6.7	0.9	0.0	0.0	0.3	0.0	0.0	85.4	0.3	0.0	0.0	6.4	0.0	100.0
A4s	10.8	0.3	0.3	0.3	2.0	0.0	0.0	83.7	0.0	0.3	0.0	2.3	0.0	100.0
A4t	15.8	0.0	0.3	0.0	0.9	0.0	0.0	80.5	0.0	0.6	0.0	1.8	0.0	100.0
A4u	9.9	0.0	0.0	0.0	0.9	0.0	0.0	83.6	0.0	1.8	0.0	3.8	0.0	100.0
Average	**13.2**	**0.9**	**1.5**	**0.2**	**1.4**	**0.1**	**0.0**	**72.5**	**0.1**	**1.4**	**0.4**	**8.1**	**0.1**	**100.0**
SD	**13.3**	**1.1**	**4.0**	**0.4**	**1.4**	**0.3**	**0.0**	**18.1**	**0.3**	**1.9**	**1.2**	**10.9**	**0.4**	

Tetang Village

Sample	ZIR	GAR	AND	KYA	STA	CTD	EPI	TOU	HOR	RUT	CRS	APA	AMP	Total
A6a	18.9	2.9	0.4	0.8	3.3	0.0	0.0	66.8	0.0	0.0	0.0	7.0	0.0	100.0
A6c	11.4	8.6	0.0	0.0	1.4	0.0	0.0	76.4	0.0	0.0	0.0	2.1	0.0	100.0
A6d	35.5	1.8	0.0	0.0	2.1	0.0	0.0	57.9	0.0	0.6	0.0	2.1	0.0	100.0
A6i	14.0	1.7	0.0	0.0	1.4	0.0	0.0	77.8	0.0	1.4	0.0	3.8	0.0	100.0
SN 32	25.9	6.5	0.0	0.0	0.0	0.0	0.0	48.1	0.0	0.0	0.0	19.4	0.0	100.0
A6m	10.0	7.5	0.0	0.0	5.0	0.0	0.0	67.5	0.0	7.5	0.0	2.5	0.0	100.0

Sample	ZIR	GAR	AND	KYA	STA	CTD	EPI	TOU	HOR	RUT	CRS	APA	AMP	Total
A6n	16.0	0.3	0.0	0.0	1.5	0.0	0.0	78.8	0.0	3.4	0.0	0.0	0.0	100.0
SN 31	15.7	11.8	0.0	0.0	0.0	0.0	5.9	51.0	0.0	3.9	0.0	11.8	0.0	100.0
A6p	35.4	1.8	0.0	0.0	0.0	0.0	0.0	61.0	0.0	1.8	0.0	0.0	0.0	100.0
SN 23	12.7	17.5	0.0	6.3	7.9	0.0	0.0	34.9	0.0	0.0	0.0	20.6	0.0	100.0
SN 24	8.9	2.1	0.0	0.0	0.0	0.0	5.2	69.1	0.0	3.1	0.0	11.6	0.0	100.0
A6r	17.3	3.3	0.0	0.0	2.3	0.5	0.0	73.4	0.0	0.0	0.0	3.3	0.0	100.0
A6z2	46.2	2.6	3.3	0.0	1.1	0.0	0.0	42.1	0.0	3.3	0.0	1.5	0.0	100.0
Average	**20.6**	**5.3**	**0.3**	**0.6**	**2.0**	**0.0**	**0.9**	**61.9**	**0.0**	**1.9**	**0.0**	**6.6**	**0.0**	**100.0**
SD	**11.6**	**5.0**	**0.9**	**1.8**	**2.3**	**0.1**	**2.1**	**14.2**	**0.0**	**2.3**	**0.0**	**7.1**	**0.0**	

Dhinkyo Khola

Sample	ZIR	GAR	AND	KYA	STA	CTD	EPI	TOU	HOR	RUT	CRS	APA	AMP	Total
SN 27	1.8	23.8	1.2	8.5	45.1	0.0	1.2	11.0	0.0	0.0	0.0	7.3	0.0	100.0
A7a	1.6	10.1	1.6	0.0	63.6	0.0	0.0	22.5	0.0	0.0	0.0	0.6	0.0	100.0
A7b	1.0	16.1	0.3	0.0	58.6	0.0	0.0	21.7	0.0	0.0	0.0	2.3	0.0	100.0
A7d	0.6	7.9	0.9	0.0	4.0	0.0	0.0	76.6	0.0	0.0	0.0	10.0	0.0	100.0
Average	**1.3**	**14.5**	**1.0**	**2.1**	**42.8**	**0.0**	**0.3**	**32.9**	**0.0**	**0.0**	**0.0**	**5.1**	**0.0**	**100.0**
SD	**0.6**	**7.1**	**0.5**	**4.3**	**27.1**	**0.0**	**0.6**	**29.6**	**0.0**	**0.0**	**0.0**	**4.4**	**0.0**	

On the left side of the Kaligandaki River towards Tanbe from the Chhuksang gaon

Sample	ZIR	GAR	AND	KYA	STA	CTD	EPI	TOU	HOR	RUT	CRS	APA	AMP	Total
SN33	**32.4**	**8.3**	**5.6**	**1.9**	**0.0**	**0.0**	**1.9**	**26.9**	**0.0**	**4.6**	**0.0**	**18.5**	**0.0**	**100.0**

Syang Village

Sample	ZIR	GAR	AND	KYA	STA	CTD	EPI	TOU	HOR	RUT	CRS	APA	AMP	Total
SN 37	4.4	3.9	0.6	0.0	21.6	0.0	19.1	25.5	0.0	1.9	0.6	22.4	0.0	100.0
SN 38	22.3	8.0	5.1	1.1	5.1	4.6	2.3	24.0	0.6	2.9	10.3	13.7	0.0	100.0
Average	**13.4**	**5.9**	**2.8**	**0.6**	**13.4**	**2.3**	**10.7**	**24.7**	**0.3**	**2.4**	**5.4**	**18.1**	**0.0**	**100.0**
SD	12.6	2.9	3.2	0.8	11.6	3.2	11.9	1.0	0.4	0.6	6.9	6.2	0.0	
Total average	**14.5**	**8.7**	**2.4**	**0.6**	**12.56**	**0.3**	**1.4**	**46.1**	**0.2**	**1.6**	**0.5**	**11.1**	**0.1**	**100.0**

Table: 7.2: Heavy mineral composition (less than 300 countable grains) of the Thakkhola and Tetang formations

Abbreviations: ZIR-zircon, GAR-garnet, AND-andalusite, KYA-kyanite, STA-staurolite, CTD-chloritoid, EPI-epidote, TOU-tourmaline, HOR-hornblende, RUT-rutile, CRS-chrome spinel, APA-apatite, AMP-amphibole, SD-Standard deviation

(a) expressed in grain number

Sample	ZIR	GAR	AND	KYA	STA	CTD	EPI	TOU	HOR	RUT	CRS	APA	AMP	Total
A3c	1	1	1	0	0	0	0	30	0	0	0	0	0	33
A4a	4	0	0	0	0	0	0	60	0	4	0	0	0	68
A4b	2	0	0	0	0	0	0	51	0	2	0	0	0	55
A4c	2	0	1	0	3	0	0	50	1	0	0	0	0	57
A4v	0	0	0	0	0	0	0	17	0	0	0	1	0	18
A6b	16	0	1	0	0	0	0	29	0	0	0	0	0	46
A6c	3	0	0	0	0	0	0	37	0	0	0	0	0	40
A6e	7	0	0	0	0	0	0	17	0	0	0	0	0	24
A6j	0	0	0	0	0	3	0	7	0	2	0	0	0	12

(b) expressed in grain %

Sample	ZIR	GAR	AND	KYA	STA	CTD	EPI	TOU	HOR	RUT	CRS	APA	AMP	Total
A3c	3.0	3.0	3.0	0.0	0.0	0.0	0.0	90.9	0.0	0.0	0.0	0.0	0.0	100.0
A4a	5.9	0.0	0.0	0.0	0.0	0.0	0.0	88.2	0.0	5.9	0.0	0.0	0.0	100.0
A4b	3.6	0.0	0.0	0.0	0.0	0.0	0.0	92.7	0.0	3.6	0.0	0.0	0.0	100.0
A4c	3.5	0.0	1.8	0.0	5.3	0.0	0.0	87.7	1.8	0.0	0.0	0.0	0.0	100.0
A4v	0.0	0.0	0.0	0.0	0.0	0.0	0.0	94.4	0.0	0.0	0.0	5.6	0.0	100.0
A6b	34.8	0.0	2.2	0.0	0.0	0.0	0.0	63.0	0.0	0.0	0.0	0.0	0.0	100.0
A6c	7.5	0.0	0.0	0.0	0.0	0.0	0.0	92.5	0.0	0.0	0.0	0.0	0.0	100.0
A6e	29.2	0.0	0.0	0.0	0.0	0.0	0.0	70.8	0.0	0.0	0.0	0.0	0.0	100.0
A6j	0.0	0.0	0.0	0.0	0.0	25.0	0.0	58.3	0.0	16.7	0.0	0.0	0.0	100.0

Table 7.3: Rank correlation coefficient of heavy minerals of the Thakkhola Formation.

Abbreviations: ZIR-zircon, GAR-garnet, AND-andalusite, KYA-kyanite, STA-staurolite, CTD-chloritoid, EPI-epidote, TOU-tourmaline, HOR-hornblende, RUT-rutile, CRS-chrome spinel, APA-apatite, AMP-amphibole. Significant rank correlation coefficients are in bold figures

Thakkhola Formation: Chaile (n = 11)

	ZIR	GAR	AND	KYA	STA	CLO	TOU	HOR	RUT	CRS	APA	AMP
ZIR	1.000	**-0.390**	0.000	**0.463**	0.193	**-0.500**	0.073	**-0.613**	0.079	**-0.512**	**-0.709**	**-0.400**
GAR		1.000	**0.362**	**0.346**	0.151	**0.481**	**-0.605**	**0.675**	0.098	**0.394**	**0.672**	0.116
AND			1.000	**0.551**	**0.502**	**0.545**	**-0.466**	-0.095	0.165	-0.147	**0.283**	0.109
KYA				1.000	**0.502**	**0.545**	**-0.466**	-0.095	0.165	-0.147	**0.283**	0.109
STA					1.000	0.167	**-0.289**	0.156	0.108	-0.052	0.167	**-0.509**
CLO						1.000	**-0.200**	**0.382**	**-0.358**	-0.148	**0.300**	-0.100
TOU							1.000	**-0.214**	**-0.763**	**-0.526**	**-0.636**	**-0.300**
HOR								1.000	-0.183	**0.386**	**0.659**	-0.191
RUT									1.000	**0.593**	**0.451**	**0.512**
CRS										1.000	**0.674**	**0.593**
APA											1.000	**0.400**
AMP												1.000

Tetang Formation: Tetang Village (n= 12)

	ZIR	GAR	AND	KYA	STA	CLO	EPI	TOU	RUT	APA
ZIR	1	**-0.413**	**0.221**	-0.112	**-0.205**	0.129	**-0.326**	**-0.267**	**-0.208**	**-0.337**
GAR		1.000	-0.044	**0.355**	**0.214**	0.044	**0.226**	**-0.545**	**-0.218**	**0.599**
AND			1.000	**0.604**	**0.311**	-0.091	-0.134	-0.044	**-0.317**	0.131
KYA				1.000	**0.602**	-0.134	-0.198	**-0.414**	**-0.468**	**0.474**
STA					1.000	**0.222**	**-0.525**	-0.007	**-0.247**	-0.012
CLO						1.000	-0.134	**0.218**	-0.317	-0.044
EPI							1.000	-0.156	**0.479**	**0.393**
TOU								1.000	0.196	**-0.56**
RUT									1.000	**-0.283**
APA										1.000
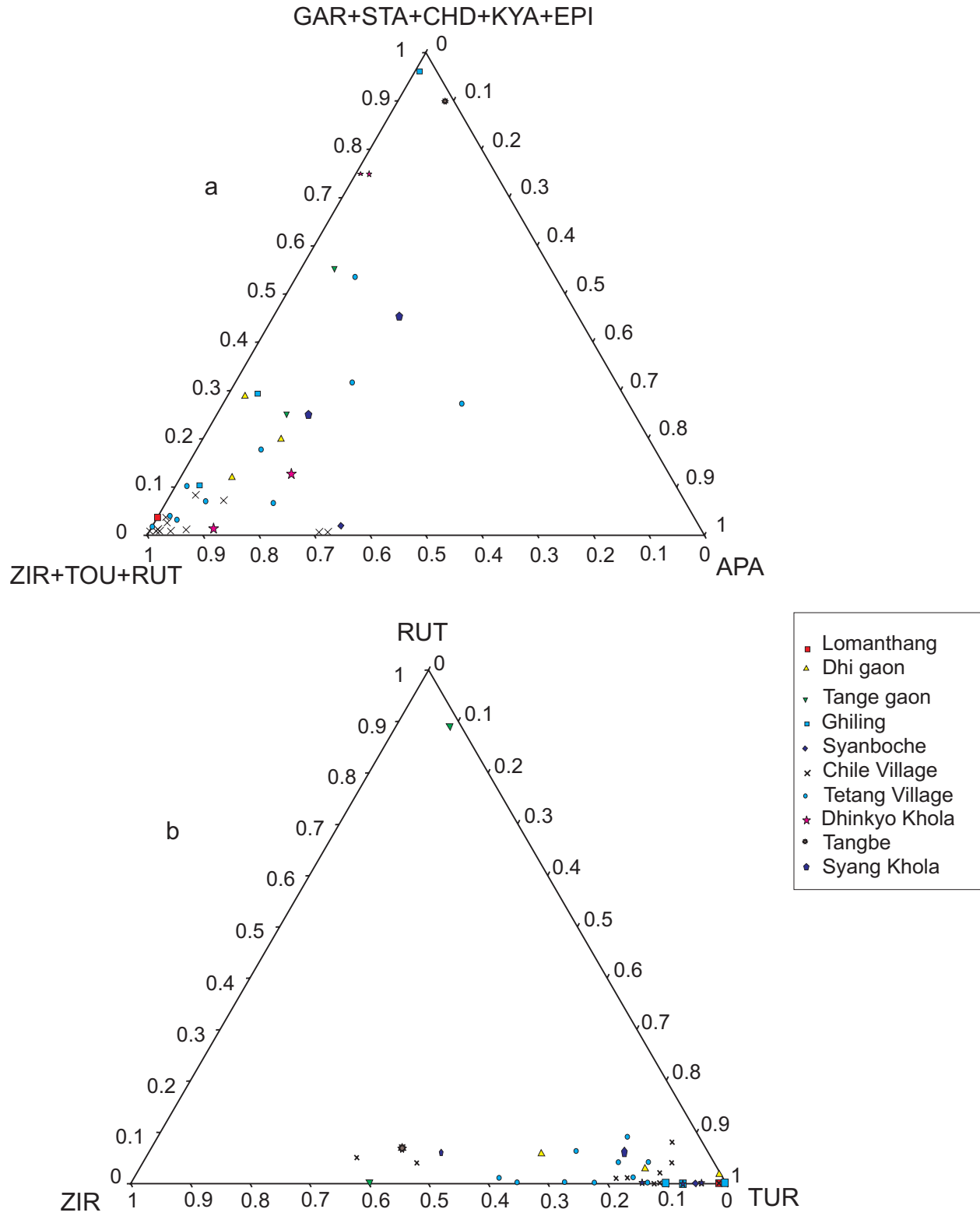
Fig. 7.3: Triangular plots

a. Triangular plots of GAR+STA+CHD+KYA+EPI (garnet+staurolite+choloritoid+kyanite+epidote)
-ZIR+TOU+RUT (zircon+tourmaline+rutile)-APA (apatite), b.Triangular plots of ZIR-TOU-RUT.
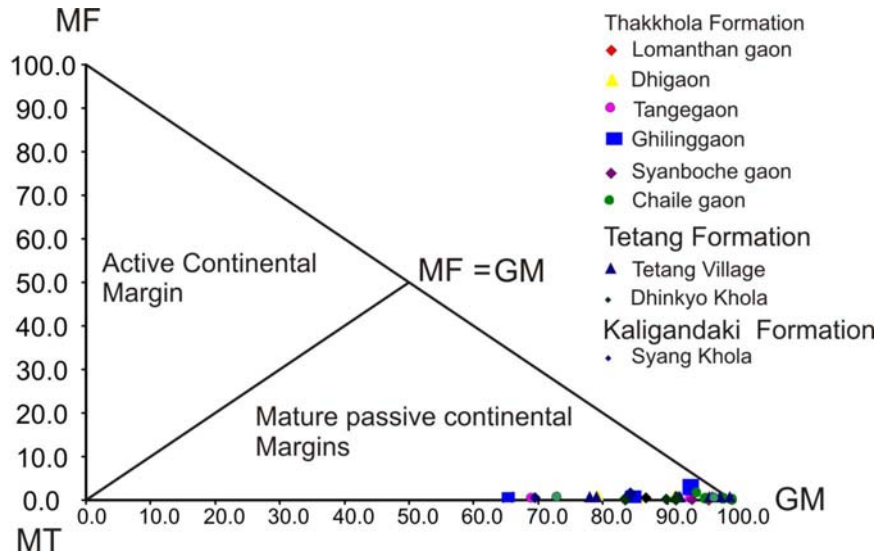
Fig. 7.4: GM-MT-MF plot for the heavy minerals of the graben (diagram of Nechaev and Isohording, 1993). MT= Total content of garnet, epidote, amphibole; GM= Total content of zircon, andalusite, kyanite, staurolite, tourmaline; MF= hornblende

correlated with ampbiboles (r = -0.509) and positively correlated with kyanite (r = 0.605) in the Tetang Formation.

Apatite

It is identified by moderately high relief and lack of color with weak birefringence (Fig. 7.5B). Apatite is present in almost all samples with an average value of 11.1%. It shows positively correlation with garnet (r = 0.672) and negatively correlation with tourmaline (r = -0.636).

Garnet

The garnets are colorless in most of the cases or pale pinkish and characterized by their high relief with an isotropic feature (Fig. 7.5). It is found in most of the samples with an average value of 8.7%. It shows negative correlation with tourmaline (r = -0.605) and (r = -0.545) in Thakkhola and Tetang formations respectively.
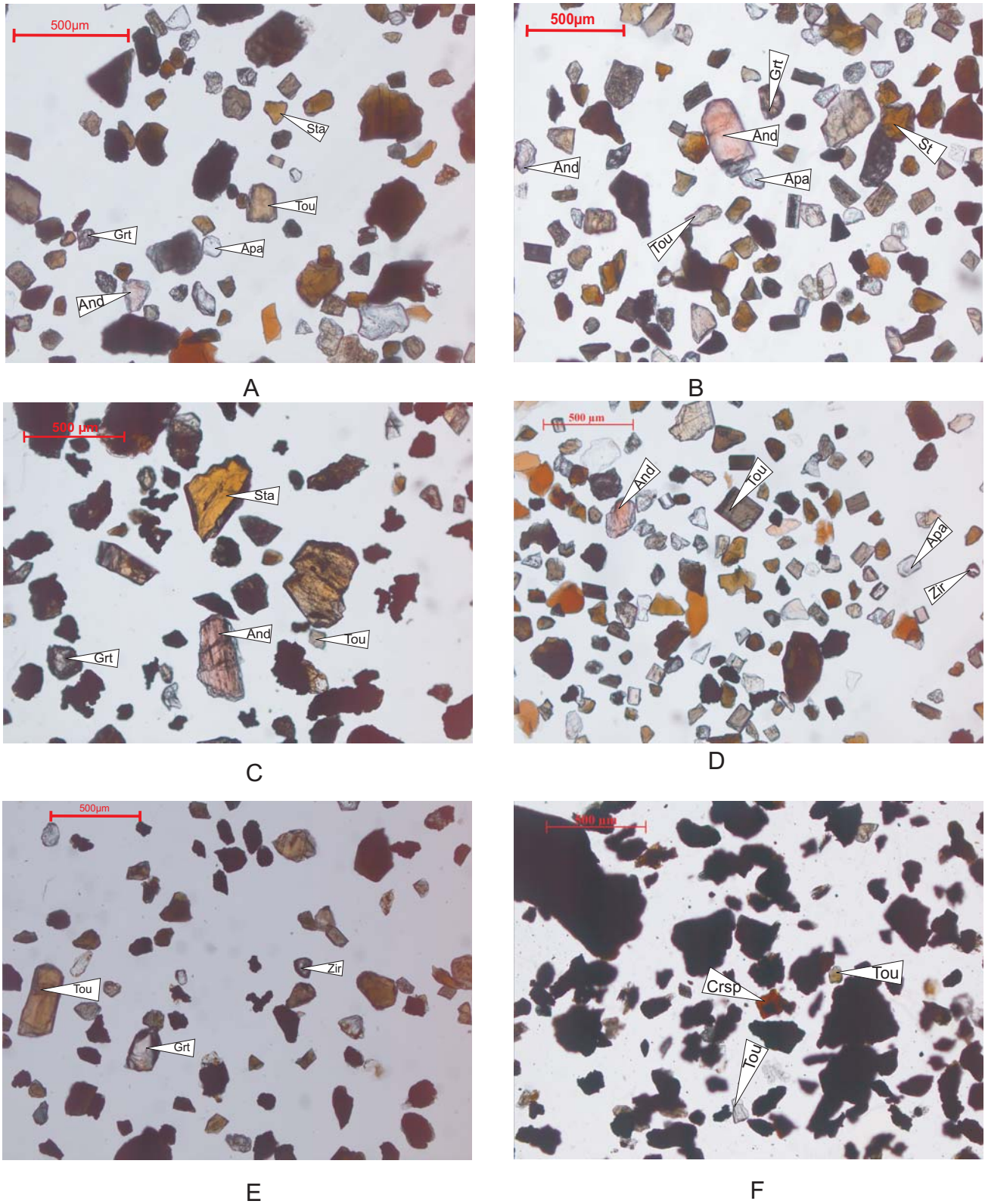
Fig. 7.5: Phtotomicrographs of heavy minerals in plane polarized light. (A & B) Dhi section, (C) Ghiling village, (D) Chaile village, (E) Dhinkyo Khola, (F) Syang Khola. Tourmaline (TOU), garnet (Grt), apatitie (Apa), andalusite (And), staurolite (Sta), zircon (Zir), chrome spinel (Crsp).
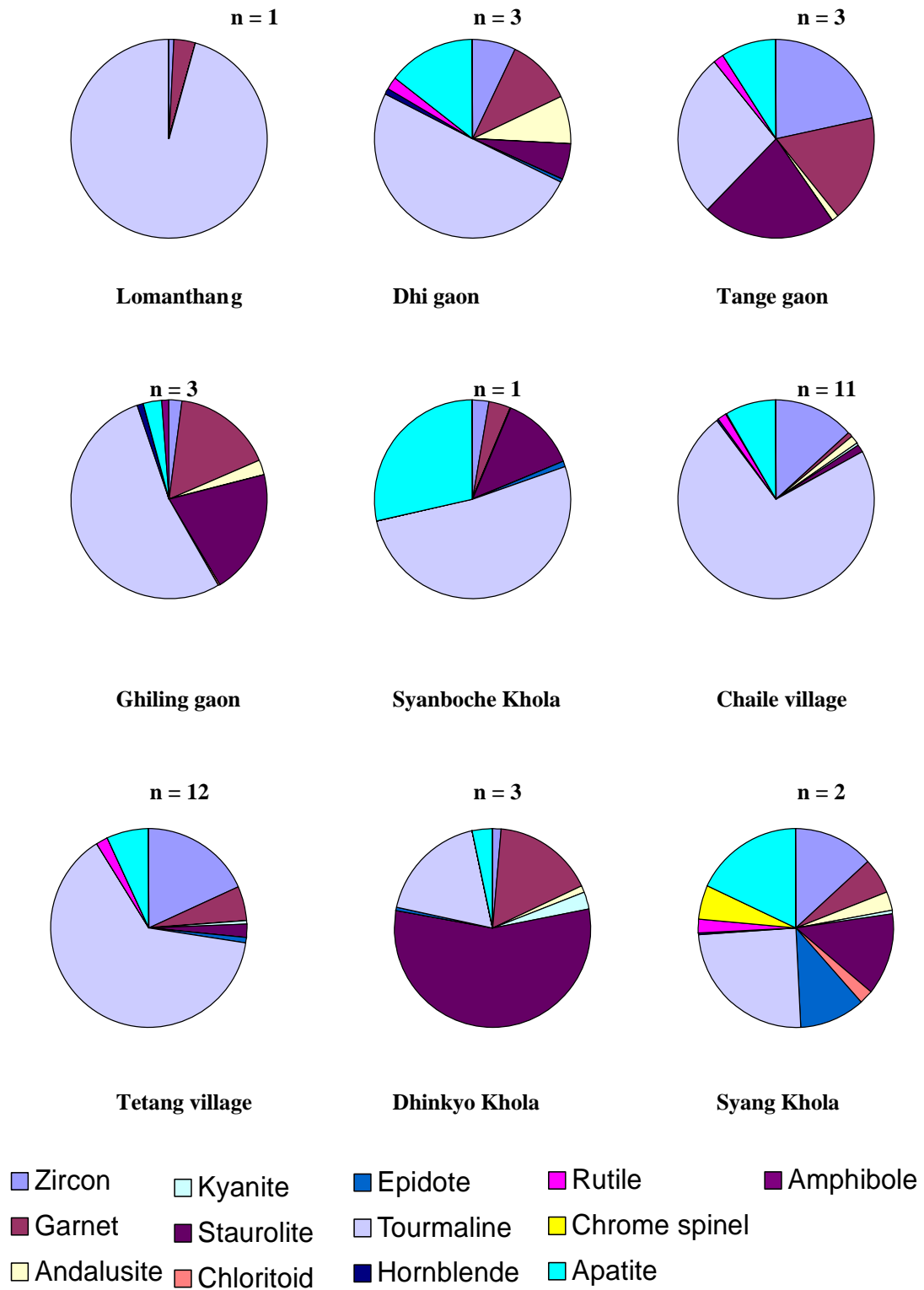
**Fig. 7.6: Pie diagrams of average heavy mineral assemblage in different areas within the graben.
n = number of grains.**
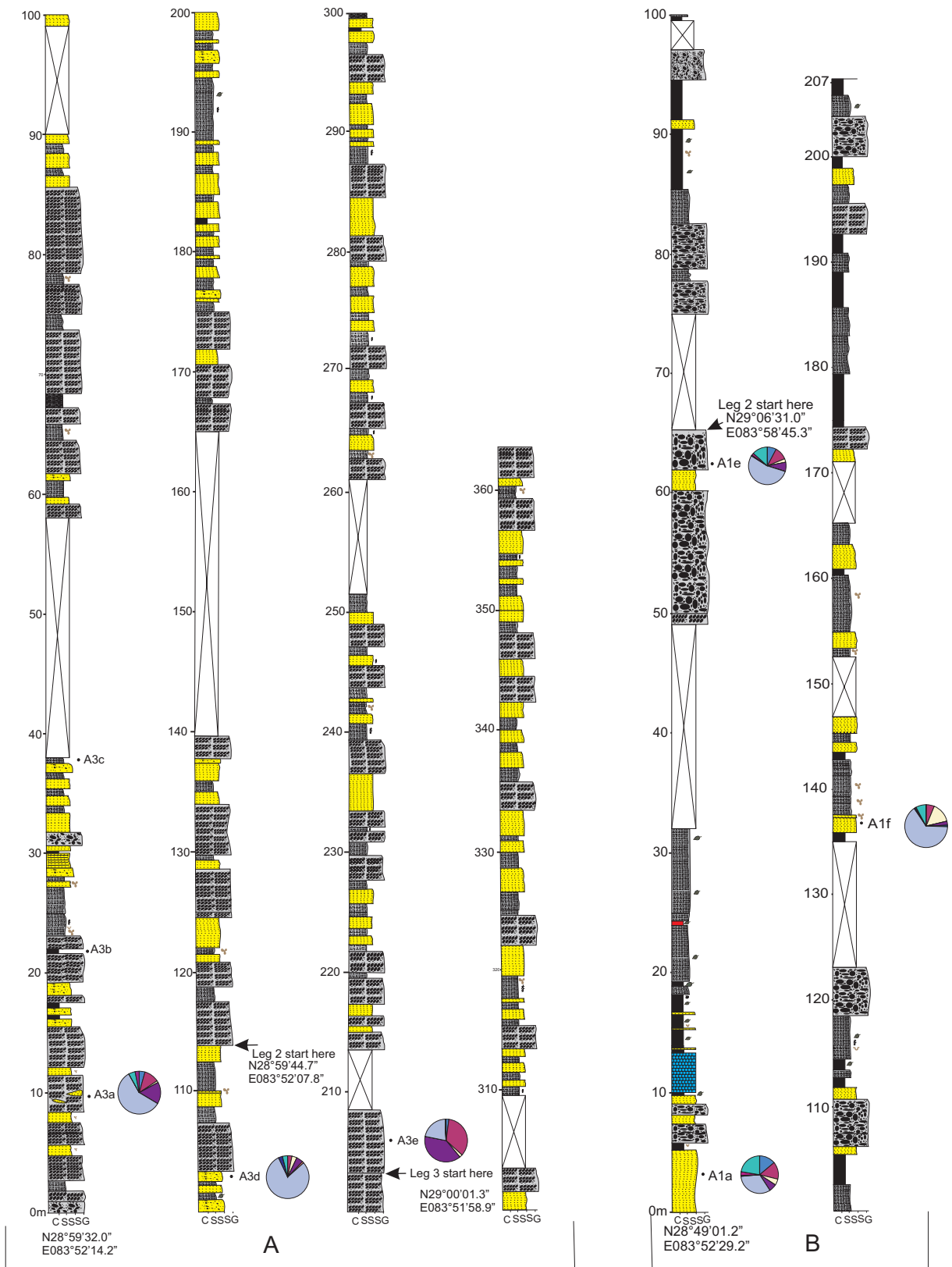
Fig. 7.7: Columnar section of measured sections with heavy minerals. Thakkhola Formation at (A) Ghiling gaon, (B) Dhi gaon.
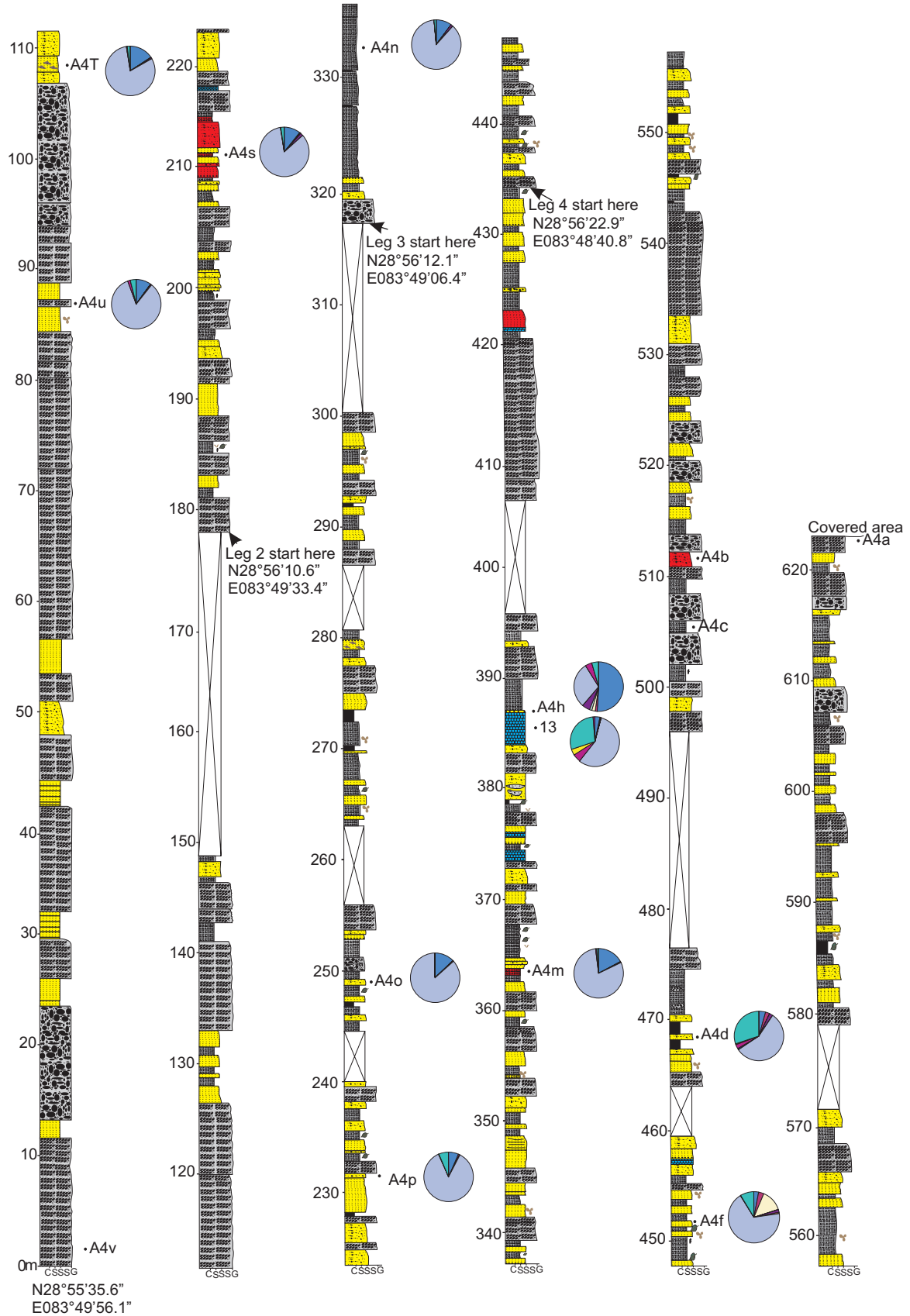
Fig. 7.7 (continued) (C) Chaile village
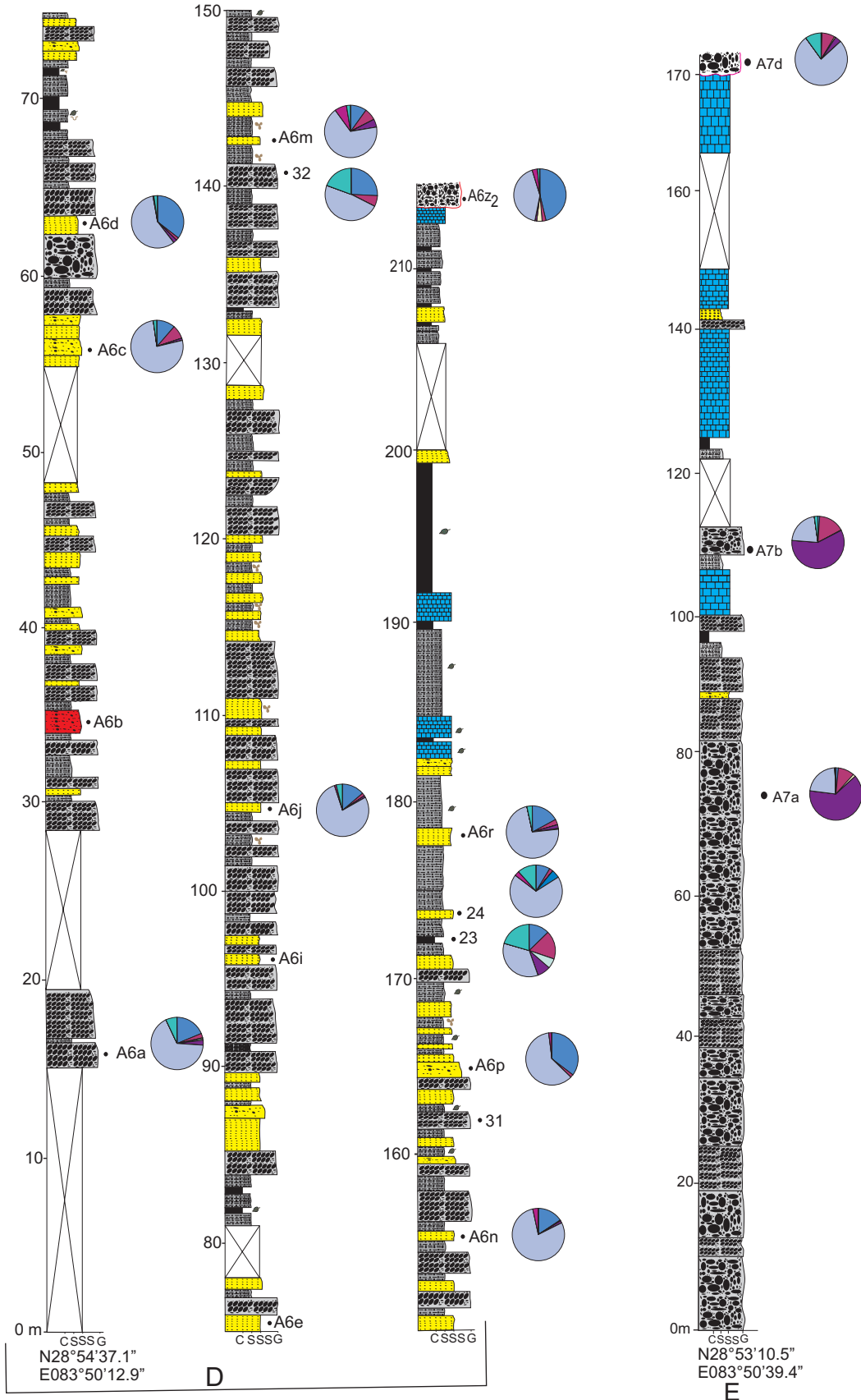
Fig. 7.7 (continued) Tetang Formation at (D) Tetang village, (E) Dhikyo Khola

Legend

Columnar sections

- Siltstone
- Limestone
- Sandstone
- Mudstone
- Pebbly sandstone
- Covered area
- Massive conglomerate
- Imbricated conglomerate
- Sand lense in conglomerate
- Conglomerate lense in sandstone
- Cross bedding
- Concretion
- Plant fossil
- Bioturbation
- Root fragments
- Unconformity
- Horizontal Stratification

•A4c Heavy mineral sample

C S SS G
Clay Silt Sandstone Gravel

Pie chart (Heavy mineral)

- Zircon
- Garnet
- Andalusite
- Kyanite
- Staurolite
- Apatite
- Amphibole
- Chrome Spinel
- Choloritoid
- Epidote
- Tourmaline
- Hornblende
- Rutile

Fig. 7.7 (continued) (F) Legend for columnar sections of measured sections in the Thakkhola-Mustang Graben
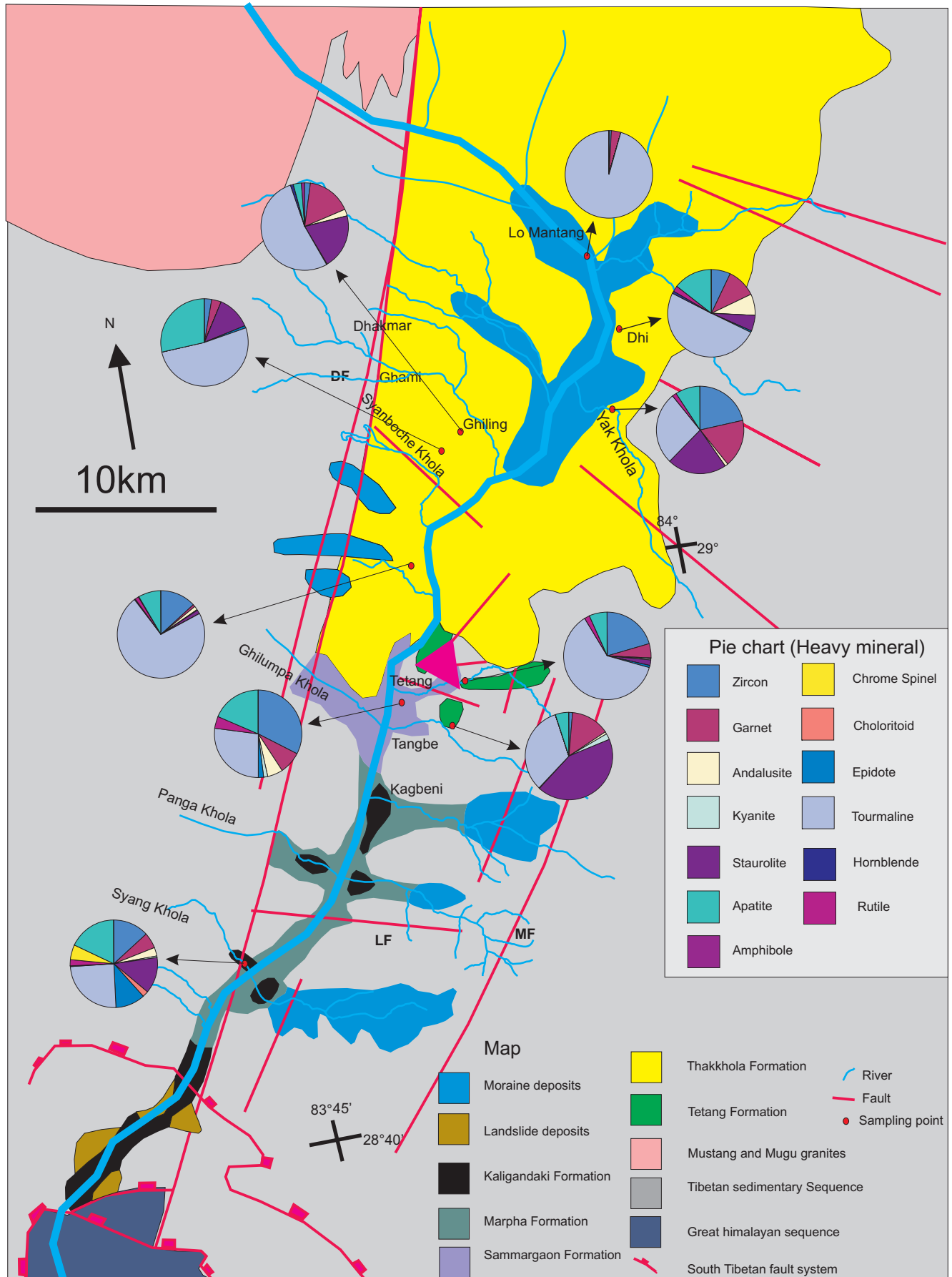
Fig. 7.8. Heavy mineral distribution map in the Thakkhola-Mustang Graben 110

Andalusite

Distinctive reddish pleochroism with moderate relief distinguishes andalusite from other minerals. Andalusite is present in most of the samples of the Thakkhola Formation whereas it is rarer in the Tetang Formation (Table 7.1). It represents a temperature-dominated region and it is common in gneisses and schists.

Rutile

It is diagnosed by its very high relief, deep colors, pleochroism and extreme birefringence (Fig. 7.5) with an average value of 1.6%. It shows negative correlation with tourmaline. It is generally a widespread accessory mineral in metamorphic rocks, particularly in schists, gneisses and amphibolites.

Epidote

Epidote is characterized by high relief, green colors and pleochroism as well as irregular morphology. High amounts of epidote are present in the Kaligandaki Formation at Syang Khola but fewer amounts in Dhi gaon section (Table 7.1).

Kyanite

Kyanite as a typical mineral of pressure-dominated metamorphism and is characterized by bladed or prismatic grains and the combination of perfect cleavage and parting together with a large extension angles (Fig. 5.5). Kyanite is observed in minor amounts with an average of 0.6%. Kyanite is present in high amounts in the Dhinkyo Khola section (8.5%). Kyanite positive correlation with staurolite (r = 0.602) and is negatively correlated with rutile (r = -0.468) in the Tetang Formation.

Chrome spinel

Chrome spinels are observed in 4 samples out of 41 samples with very low average value of 0.5 % and is characterized by its dark reddish brown to clove brown, very sharp angular and irregular fragments. It shows the conchoidal breakage pattern and is truly isotropic. Detrital chrome spinel is an indicator mineral for ophiolite complexes (Pober and Faupl, l988).

Chloritoid

It is diagnosed by platy habit, relatively high relief and low birefringence with gray color that is a product of low- to lower- medium-grade metamorphism. It is generated by the

regional metamorphism of pelitic sediments. It is present only in few samples with average value of 0.3 % (Table 7.1).

Hornblende

Hornblendes are characterized by prismatic morphology and their bluish green color and pleochroism (Fig. 7.5). Hornblende was found in 8 samples out of 41 samples but in fewer amounts with average value of only 0.2 %. High percentage of hornblende is present in Dhi gaon (Table 7.1). Hornblende is a typical mesometamorphic mineral.

Blue Amphibole

Amphibole was identified by its remarkable blue color, cleavage and conspicuous pleochroism. It was found only in two samples in Chaile and Ghiling gaon sections (Table 7.1). It is frequent mineral in high-pressure belts.

7.4 Heavy mineral assemblages

Although heavy mineral assemblages contain a variety of mineral species but they rarely constitute more than 1% of the total volume of sediments (Singh et al., 2004). The results are plotted as average heavy mineral compositions on pie chart (Fig. 5.6). Comparing these results, the assemblages of Lomathang are quite different from others because most of the heavy minerals are tourmaline (95 %). Staurolite is present in high percentage in Dhinkyo Khola whereas the samples from the Syang Khola are very rich with diverse heavy minerals. A broad range of metamorphic source rocks are reflected in the characteristic heavy mineral assemblages (Fig. 7.3a) (Table 7.4), which suggest unroofing of the orogenic belts in the higher areas like the Himalaya. The possible sources of garnet and staurolite are mica schist complexes and related metamorphic rocks (Füchtbauer, 1964). Tourmaline is mostly brown colored with euhedral shape, which indicates a low-grade metamorphic provenance (Singh et al., 2004). Tourmaline is the predominant mineral among the ZTR suites (Fig. 7.3b). Chloritoid and epidote were contributed from the low-grade metamorphic series whereas gneisses, granitoid rocks and some reworked sediments are possible sources of stable minerals like zircon, tourmaline, rutile and apatite. The kyanite is contributed from the high-pressure and kyanite-grade metamorphic rocks in the catchment. Presence of andalusite shows also a high-grade metamorphic provenance. Sorkhabi and Arita (1997) suggested that biotite-garnet grade to staurolite grade of metamorphism and kyanite grade of metamorphism is indicative of middle almandine amphibolite facies. Apatite is believed to be derived from biotite-rich rocks (Faupl et al., 1998) but it is a common accessory mineral in virtually all igneous and many metamorphic rocks (McConnell, 1973; Nash, 1984 and Chang et al., 1998) and is therefore not an especially specific provenance indicator mineral.

The presence of small amounts of chrome spinel indicates the subordinate existence of ophiolite complexes in the source area and they are believed to be associated with suture belts. Zimmerle (1984) showed that a marked increased of "detrital brown spinel" in a succession marks the stratigraphic interval that records the beginning of processes that expose and progressively erode obducted ophilitic mafic-ultramafic complexes (Table 7.4).

Table: 7.4. Possible sources of heavy mineral

Heavy minerals	Source
Andalusite	High grade metamorphic rocks
Kyanite, staurolite, garnet	Medium grade metamorphic rocks
Tourmaline, chloritoid,epidote	Low grade metamorphic rocks
Zircon, tourmaline, rutile, apatite	Granite and gneisses eg. Mustang and Mugu granite
Chrome spinel	Ophiolitic complex
Epidote, blue-green amphibole	Mafic ophiolite sequences
Apatite	Biotite rich rocks

However, the low amounts of chrome spinels recorded compared to other orogenic basins (Faupl and Pober, 1988) may indicate a reworking of older ophiolite-derived sediments. Chloritoid is most common in low-to-medium-grade metapelites and occurs in metasediments and meta basalts with ophilotic affinities and in pelitic blueschists (Mange and Morton, 2007). Epidote and blue-green amphibole may be related to the mafic ophiolite sequences but epidote is very common in the sedimentary records. Presence of blue amphiboles refers the existence of high pressure/low temperature metamorphic rocks in addition those types of rocks were reported along the Indus suture zone in Ladakh, NW Himalayas (Honegger et al., 1989).

Minerals are categorized in three groups such as GM, MT and MF according to Nechaev and Isohording (1993) and plotted in the right angle triangle (Fig. 7.4). The GM suit is characterized by zircon, tourmaline, staurolite and less commonly sillimanite, andalusite, monazite and kyanite (indicative of granitic and silicic metamorphic complexes). The MT suite is in basic metamorphic minerals such as pale-colored and blue-colored amphiboles, epidote and garnet and the MF suites indicated mafic minerals like olivine, iddingsite, all pyroxene and green-brown hornblende. All the heavy minerals occupy the passive continental margin field of the Nechaev and Isohording (1993) diagram. Therefore, heavy minerals from the Thakkhola-Mustang Graben are similar to the passive margin heavy mineral setting according to this classification (Fig. 7.4). Singh et al. (2004) also suggested that the heavy minerals from Upper Siwalik and recent Cenozoic sedimentary
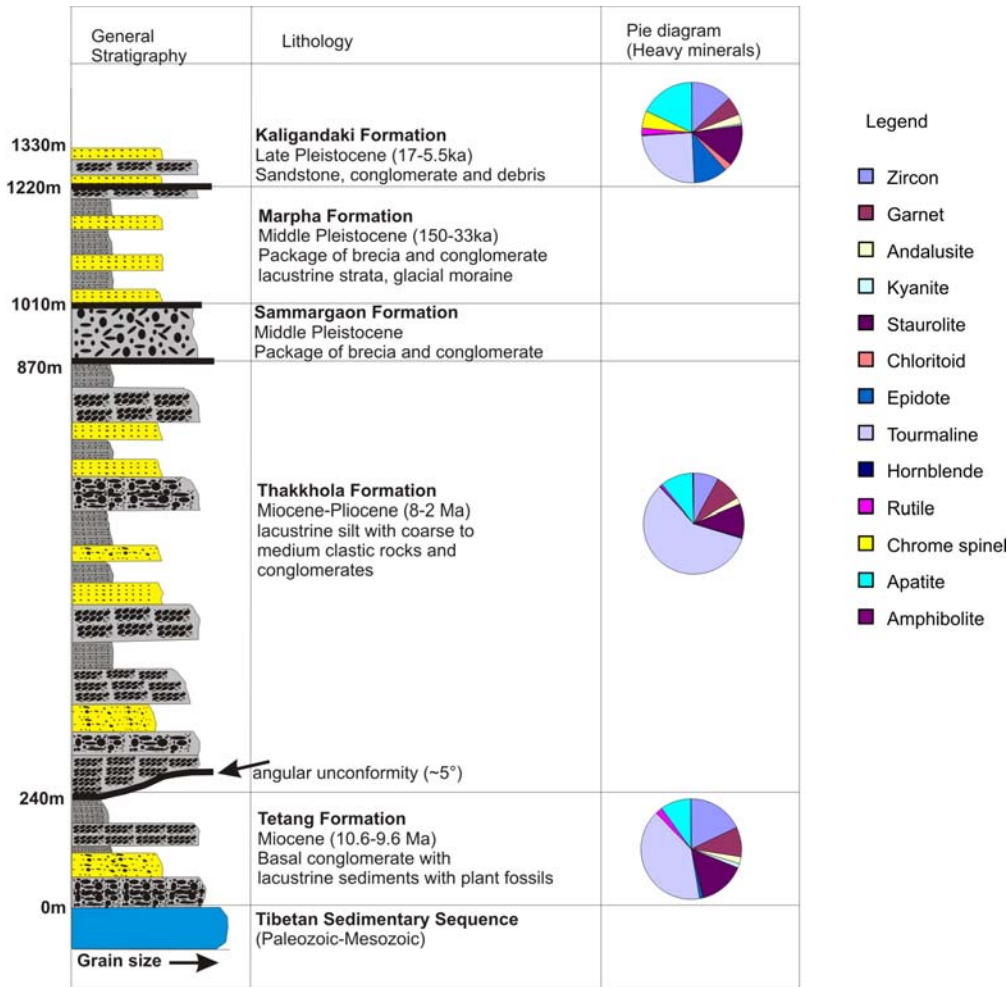
Fig. 7.9: Generalized stratigraphy of the Thakkhola-Mustang Graben fill with representation of heavy mineral in pie diagram.

rocks of the foreland basing of the Himalaya derive mainly from a passive continental margin setting. Essentially two kinds of local sources (types) for the sediments are found in the Thakkhola-Mustang Graben (Fig. 7.10A). The sediments in the Lomanthang and Tangegaon of the Thakkhola Formation show almost exclusively medium/high grade metamorphism whereas the other places of Thakkhola and Tetang formations are more or less similar having a mixture of high and low-grade metamorphism with predominance of high/medium-grade metamorphic rocks in the source area. Again, the youngest Kaligandaki Formation gives the other end, in having more low-grade than high-grade source rocks than all the other (older) localities (Fig. 7.10B). This can be interpreted as an evolution from slightly higher grade (Gar+And+Kya) in Thakkhola and Tetang formations to slightly lower grade metamorphics (Kaligandaki Formation). This does not indicate successive exhumation of a lower-to-higher grade metamorphic unit but maybe a change in source area to more (local) lower grade units. Apatite and ZTR are probably not significant but a little more apatite in the Kaligandaki Formation may point to shorter
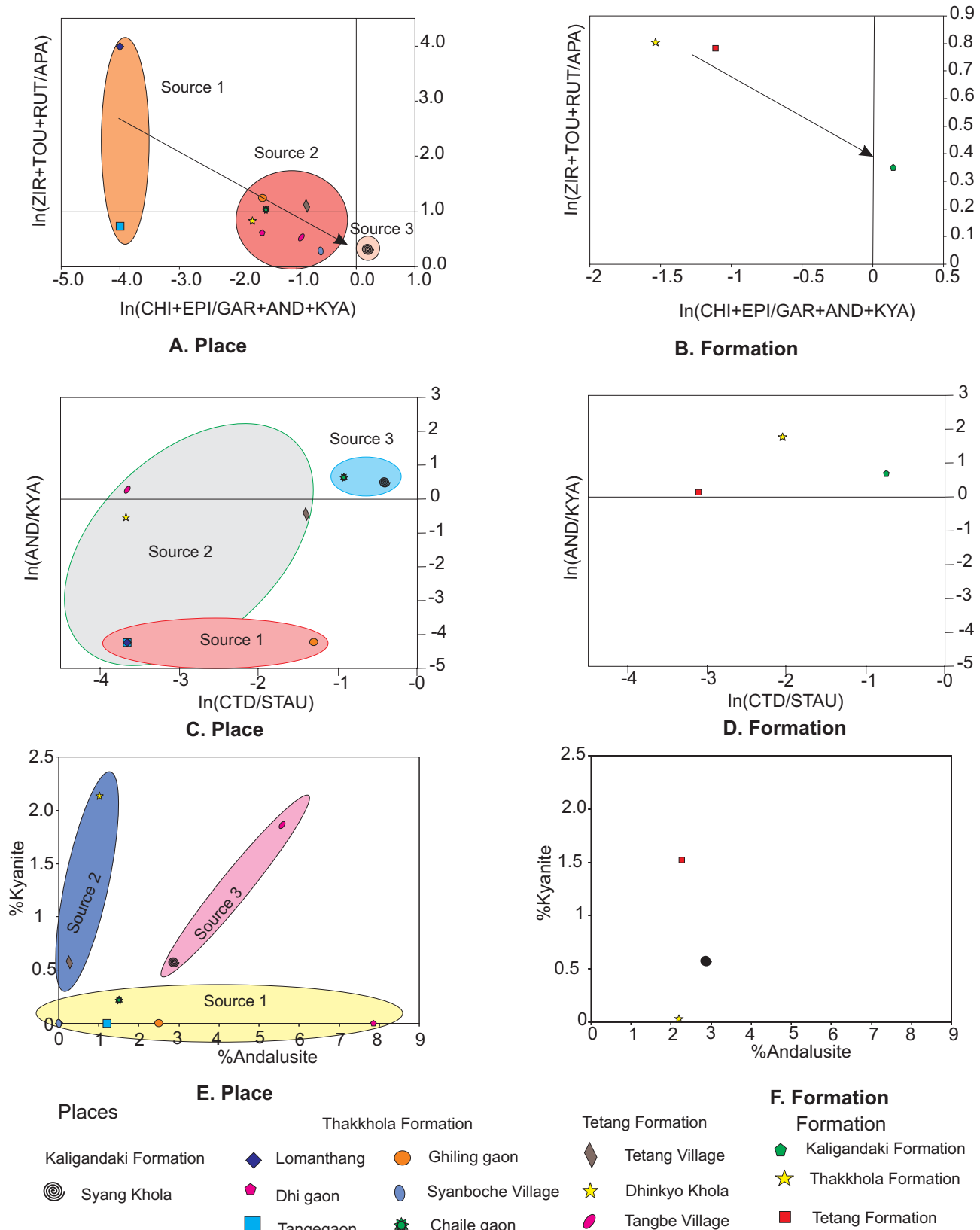
Fig. 7.10: Logratio diagram of the heavy mineral with different reations. (A&B) stable/unstable minerals on y axis Vs medium/high grade of metamorphism on X axis, (C&D)low/high pressure (AND/KYA) Vs low/high metamorphism (CTD/STAU) and (E&F) %Kyanite (high pressure metamorphism) Vs %Andalusite (low pressure or contact metamorphism).

transport than the others or may indicate influence from the local glacial transport. The sediments from the northern side of the Thakkhola Formation show low-pressure metamorphism and/or contact metamorphism provenance because of the presence of andalusite whereas high grade of metamorphic sediments found in the Tetang Formation that is confirmed by presence of high percentages of staurolite (Fig. 7.10C). All types of metamorphic sediments were found in Chaile and Syang Khola area. Percentage of high pressure/high grade minerals (kyanite >andalusite) are more in Tetang Formation than the Thakkhola Formation (Fig. 7.10E), which suggest that sediments in the Tetang Formation came from the high metamorphic source area.

7.5 Conclusions

Mostly following major rock complexes were exposed in the source area:

1. A low to high-grade metamorphic rock complexes comprising mica schists and related metamorphic rocks were present on the source area. Chloritoid and epidote shows the low-grade metamorphic terrain. It is very hard to define the exact grade of metamorphic rock without studying the chemical composition of the heavy minerals. Kyanite and garnets shows the variety of grade while staurolite shows the intermediate grade of metamorphism. Traces of andalusite and amphibole suggest the high grade of metamorphic rocks.

2. Presence of stable mineral like zircon, rutile and apatite clearly refer to the granitoid source terrain. These minerals may come from Mustang and Mugu granites.

3. Ultramafic rocks seem to have been a minor influence because of low amounts of chrome spinel. Chrome spinel is associated with the ophiolite complexes (Zimmerle, 1984) but the low amounts may derive from reworked older sediments. Mafic rocks indicated by the presence of epidote and hornblende.

4. Nechaev and Isohording (1993) diagram indicates a passive margin setting according to the classification.

CHAPTER EIGHT
POLLEN ANALYSIS

8.1 Introduction

Palynology is the study of the fossil palynomorphs, including pollen, spores, dinoflagellate cysts, acritarchs, chitinozoans and scolecodonts together with particular organic matter and kerogen found in sedimentary rocks and sediments. The palynomorph is the geological term used to describe a particle of size between 5 and 500 µm found in the sedimentary rock deposits and composed of organic material like chitin, pseduchitin and sporopollenin. The term "palynology" is derived from the Greek verb *palynein,* which means to spread or strew around - pollen grains and spores are indeed often dispersed by the wind or by insects or other animals and by water. Hyde and Williams introduced the term palynology in 1944 following correspondence with the Swedish geologist Antevs in the pages of the Pollen Science Circular.

Palynology has wide application in the earth and natural sciences. It can be used to correlate and provide relative ages for layers of rock, mainly oil exploration, vegetation distribution and climate changes in the past and past vegetation particularly of the Quaternary period in the different parts of the world. Stratigraphic changes in pollen assemblages are assumed to record changes in vegetation, which in turn provide information about changes in species distribution, providing climate, human activities and cultural resources. Most of the early studies of Quaternary pollen sequences focused on bog sediments (Erdtman, 1931, 1943; Cain, 1939) but within the past 30 years lake sediments have emerged as a primary source of Quaternary pollen data. Lake sediments are especially well suited because the sediments in a lake build up over time and the sequences of samples from the bottom to the top of a core provides details of vegetation change over time. Spores and pollen indicate the presence of source vegetation because they originate almost on the continent and plants, which are sensitive indicators of continental environments (Alfred, 2007). Quaternary scientists focused to study the pollen grains for different purpose because they occur in sedimentary rocks of all ages and from many different sedimentary and biological environments, in higher abundance than that of other fossils and represent fast evolution of plants. Several processes influence the relationship between vegetation and pollen assemblages including pollen production, dispersal, deposition, preservation and identification (Fagerlind, 1952; Webb and McAndrews, 1976) and these processes are in turn governed by a wide range of array of factors ranging from physical and chemical to biological.

8.2 Structure and terminology of pollen grain and spores (after Punt et al., 2007)

The entire wall of a pollen grain or spore is called *Sporoderm* (Fig. 8.1). The surface relief or topography of a pollen grain or spores is called the *Sculpture*. The outer layer

of a palynomorph, which is highly resistant to strong acids and bases, is called *Exine*. There are two different systems used to describe the exine stratification (Fig. 8.1). Pollen exines are generally preserved in peat and sediments even when almost all other organic constituents are reduced to structureless and indefinable structures. In a typical exine, it is possible to distinguish between two main layers; the outer layer is *Ectexine* (Fægri, 1956) and the inner layer is *Endexine* (Erdtman, 1943). A complete ectexine is regarded as a three layered structure, in which the granules form small columns, *collumellae* and the outer and inner stratum are called respectively *tectum* and *foot layer*. If the tectum covers most of the grain, it is called *tectate*. The inner layer forms a microscopically homogenous continuous membrane with few, if any, morphologic developments except for those connected with apertures. Recent investigations by means of electron microscopy have indicated the presence of various layers in the endexine, others are only found close to the apertures.
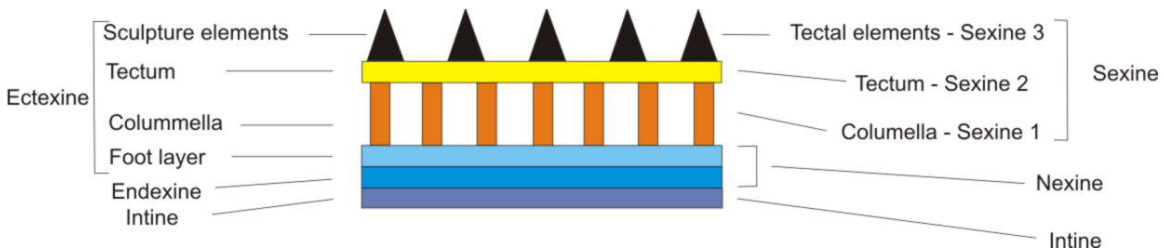
Fig. 8.1: Two different systems used to describe the exine stratification (redrawn after Punt et al., 2007)

Alveolate: Describing a type of ectexine/sexine structure, in which the infratectal layer is characterized by partitions forming compartments of irregular size and shape (*e.g. Pinus*).
Annulus: An area of the exine surrounding a pore that is sharply differentiated from the remainder of the exine, either in ornamentation or in thickness.
Aperture: A specialized region of the sporoderm, that is thinner than the remainder of the sporoderm and generally differs in ornamentation and/or structure. Aperture are described as simple if they are present only one wall layer, or compound if they affect more than one layer of the wall. Various types of aperture are recognized based on their shape such as colpus, laesura, pore, sulcus, ulcus etc.
Apex: A general term applied for the tip of an organ. In fossil spores applied to the tip or corner of a trilete spores.
Aspisdate: A prominently protruding thickening of exine around a pore.

Apolar: Describing pollen and spores without distinct polarity.

Alveolate: Describing a type of sexine/ectexine structure, in which the infratectal layer is characterized by partitions forming compartments of irregular size and shape.

Bilateral: Describing pollen and spores having a single principle plane of symmetry.

Bisaccate: Describing pollen with sacci.

Cingulum: A thick outer structure of a spore that projects at the equator, but does not extend over the distal or proximal face.

Columella: A rod like element of the ectexine/sexine, supporting either a tectum or caput. (pl. columellae)

Corpus: The body of a saccate pollen grain or camerate spore.

Discordant pattern: A pattern in a tectate pollen grain in which the arrangement of the columellae is different from that of the elements on the tectum.

Distal: A common descriptive term used in contrast to proximal, applied in palynology to features on the surface that face outward in the tetrad stage.

Distal face: The part of a palynomorph that faces outwards the centre of the tetrad, between equator and distal pole.

Distal pole: The centre of the surface of the distal face.

Echinate: Pollen and spores with an ornamentation comprising spines longer than 1 µm.

Ectexine: The outer part of the exine. Ectexine consists of foot layer, columella, tectum and sculpture elements.

Ectoaperture: An aperture in the outer layer of the sporoderm.

Endexine: The inner part of the exine.

Endoaperture: An aperture in the inner layer of the sporoderm often the inner aperture of the compound aperture.

Endospore: The innermost layer of a spore wall.

Equator: The dividing line between the distal and the proximal face of a pollen grain or spore.

Equatorial diameter: A line, lying in the equatorial plane, perpendicular to the polar axis and passing through it.

Equatorial outline: General description of the equator when a pollen grain is seen in polar view.

Equatorial plane: The plane perpendicular to the polar axis and lying midway between the poles.

Equatorial view: The view of a pollen grain or spore where the equatorial plane is directed towards the observer.

Exine: The outer layer of the wall of a palynomorph, which is highly resistant to strong acids and bases, and is composed primarily of sporopollenin.

Exospore: The outer layer of a spore wall.

Foveola: A feature of ornamentation consisting of more or less rounded depressions or lumina more than 1µm in diameter. The distance between foveolae is greater than their breadth.

Furrow: A common word for an elongate aperture.

Granule: General word for a small rounded element.

Leptoma: A thin area at the distal pole of a pollen grain, presumed to function as an aperture.

Laesura: The arm of a proximal fissure or scar of a spore.

Lobate: Describing an equatorially aperturate pollen grain with a lobed shape in polar view.

Margo: An area of exine around an ectocolpus that is differentiated from the remainder of the sexine, either in ornamentation of by difference in thickness.

Mesocolpium: The area of a pollen grain surface delimited by lines between the apices of adjacent colpi or margins of adjacent pores.

Monolete: Describing a spore with a single laesura.

Monosaccate: Describing a pollen grain with a single saccus.

Murus: A ridge that is part of the ornamentation and, for example, separates the lumina in a reticulate pollen grain or the striae in striate pollen grain (pl. muri).

Nexine: The inner, non-sculptured part of the exine, which lies below the sexine.

Oblate: Describing the shape of a pollen grain or spore in which the polar axis is shorter than the equatorial diameter.

Palynofacies: The assemblages of phytoclasts found in particular sediment, such as palynomorphs, wood fragments and cuticles.

Palynology: The study of pollen and spores and of other biological materials that can be studied by means of palynological techniques.

Palynomorphs: A general term for all entities found in palynological preparations.

Panto-aperturate: Describing a pollen grain with apertures spread over the surface sometimes forming a regular pattern.

Perforate: A general adjective indicating the presence of holes, applied in palynology to holes less than 1µm in diameter and generally situated in tectum.

Polar view: A view of a pollen grain or spore in which the polar axis is directly towards the observer.

Pore: A general term, applied in palynology to a circular or elliptic aperture with a length breadth ratio less than two.

Prolate: Describing the shape of a pollen grain or spore in which the polar axis is larger than the equatorial diameter.

Proximal face: The part of a palynomorph, which faces towards the centre of the tetrad, between equator and proximal pole.

Proximal pole: The centre of the proximal face.

Psilate: Describing a pollen or spore with a smooth surface.

Reticulum: A network-like pattern consisting of lumina or other spaces wider than 1µm bordered by elements narrower than the lumina.

Rugulate: Describing a type of ornamentation consisting of elongated sexine element more than 1µm long, arranged in an irregular pattern that is intermediate between striate and reticulate.

Saccus: An expanded sac formed by a local separation within the exine of a pollen grain and at least partly filled with an alveolate infrastructure.

Sculpturing: The surface relief, or topography, of a pollen grain or spore.

Sexine: The outer, sculptured layer of the exine, which lies above the nexine.

Spheroidal: Describing the shape of a pollen grain or spore in which the polar axis and the equatorial diameter are approximately equal.

Spine: A general term applied in palynology to long tapering pointed elements.

Tectum: The layer of sexine, which forms a roof over the columellae.

Tetrad: A general term for a group of four pollen grains or spore, either as dispersal unit or as a developmental stage.

Tricolpate: Describing pollen grains with three ectocolpi, three compound apertures or three pores.

Trilete: Describing a spore with laesurae, thus showing a trilete mark.

Trilete mark: The triradiate mark of a trilete spore.

Verruca: A wart-like sexine element, more than 1µm wide, that is broader than it is high and is not constricted at the base.

Vestibulum: A separation between two layers of the exine forming a cavity between the inner and outer pores. (*e.g. Betula*)

8.3 Material and Methods

300-400 g of silty clay to clay was collected for each of 26 samples from different layers of the Thakkhola and Tetang formations (Fig. 8.2 & 8.3). Samples were taken in the first phase for a preliminary examination to find out pollen-bearing horizons. Detailed pollen samples were taken in a second field sampling campaign (Table 8.1). Pollen and spores were generally not well preserved in the sediments because they were broken while handling with hair needle.
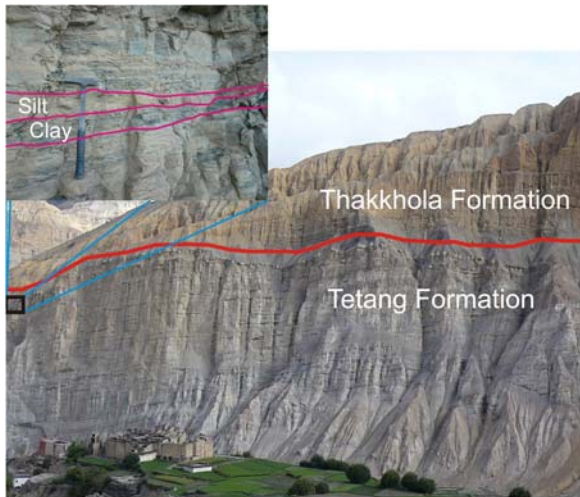
Fig. 8.2: Exposure of Tetang Formation (214m) located at the Tetang village. Alternation of medium sand, silt and silty clay in the inset.

Fig.8.3: Exposure of Thakkhola Formation located at the Chaile village. Alternation of medium sand, silt and silty clay with massive to imbricated conglomerate beds.

8.3.1 Preparation of samples

The methodology developed by Zetter (1989) and described in detail by Zetter and Ferguson (2001) was followed for the pollen extraction (Fig. 8.4). Each sample was cleaned by scrapping with a knife to avoid the contamination from the recent pollen on the surface. Some samples were crushed in a mortar to make powder (Fig. 8.4). Samples were boiled with hydrochloric acid (HCl) for few minutes to remove the carbonates and residue was transferred into copper pan for boiling with hydrofluoric acid (HF) to remove the silicates. HF is very poisonous and dangerous. So that, chemical preparation was done under a fume cupboard with a mask and special rubber gloves. The samples were then transferred to a large polyethylene jar containing three to four liters of water and sediments were allowed to settle down. After that, settled samples were boiled with conc. HCl to avoid the formation of fluorite. Then, the samples were kept for decantation. After settled down, the residue samples were transferred to a hard glass test tube and washed with water three times centrifuging it at 1500 rpm before the acetolysis. Samples were now transferred to a test tube and glacial acetic acid (about 1.5 cm in test tube) added, which is followed by of freshly prepared solution of saturated sodium clolorate ($NaClO_3$) (ca. 3 cm in test tube) and few drops of conc. HCL. The test tube was stirred by glass rod and transferred in a beaker with boiling water in an upright position for 3-5 minutes. The test tube was then centrifuged at 2000 rpm for 30 second after cooling and the liquid fraction was decanted. The sample was washed with water and centrifuged three times to eliminate remaining chemicals. To remove the water, the samples were washed with glacial acetic acid. Precaution should be taken to make the acetolysis because it is very corrosive   and   explosive   if   it   came   to   contact   with   water.   This

Fig. A   Fig. B   Fig. C   Fig. D

Fig. I   Fig. H   Fig. G   Fig. F   Fig.E

Fig. J   Fig. K   Fig. L   Fig. M   Fig. N

Fig. R   Fig.Q   Fig. P   Fig. O

124
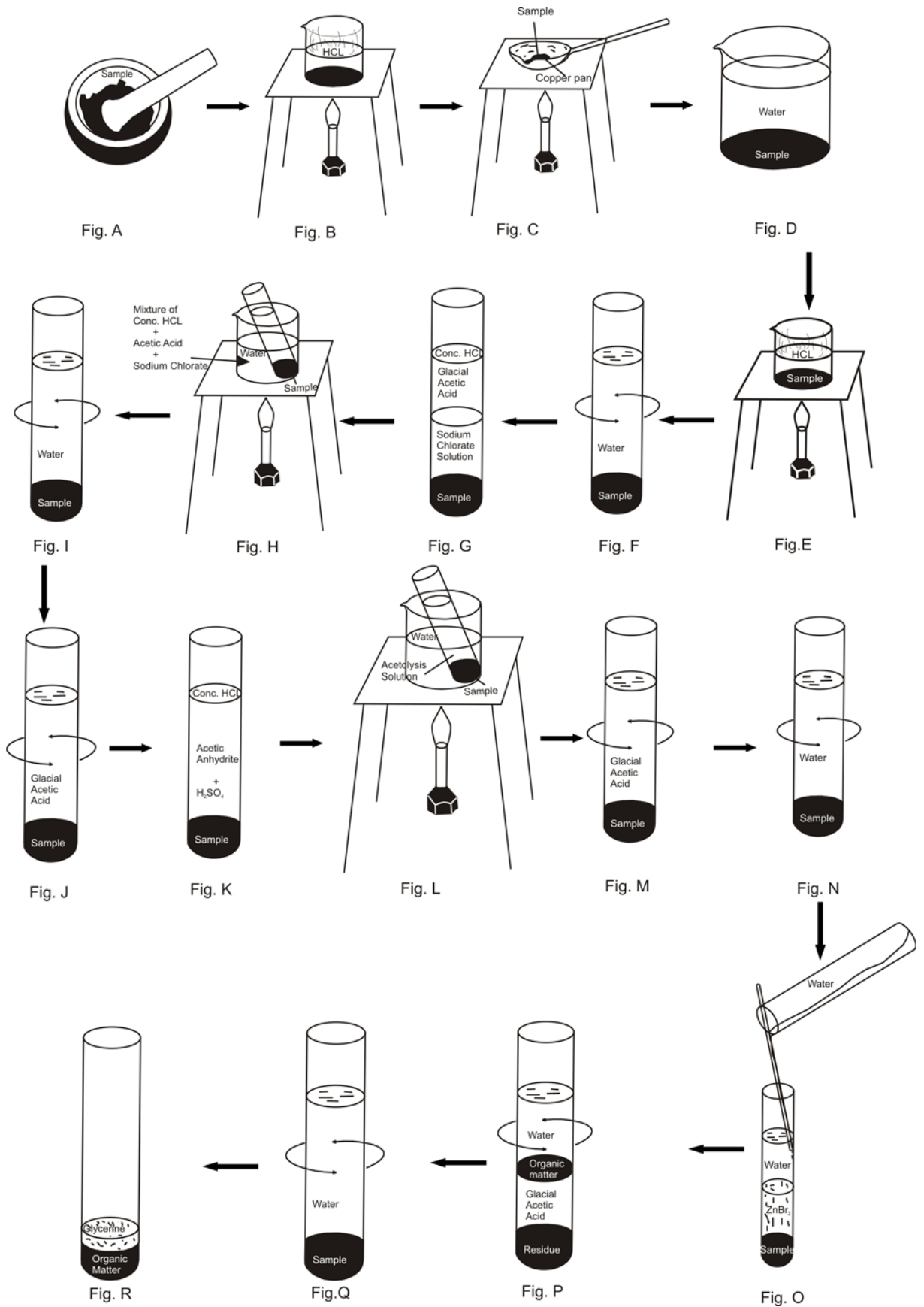
Fig. 8.4: Preparation of pollen sample Fig. A: Grinding of sample in a mortar to make a fine power, Fig. B: Boiling sample with conc. HCL, Fig. C: Boiling of sample with HF in a copper pan. Fig. D: Beaker containing water for decantation of sample, Fig. E: Boiling of sample with conc. HCL to remove fluorite, Fig. F: Collection of residue by washing with water and centrifuging, Fig. G: Mixing of sample with NaClO$_3$ + conc.HCL+ acetic acid, Fig. H: Boiling the mixture of NaClO$_3$ + conc. HCL+ acetic acid, Fig. I: Washing with water and centrifuging, Fig. J: Washing with glacial acetic acid and centrifuging, Fig. K: Mixing sample with acetic anhydride and conc. H$_2$SO$_4$, Fig. 12: Hot water bath, Fig. L: Washing with glacial acidic acid and centrifuging, Fig. M: Washing with water and centrifuging, Fig. O: Treatment with heavy liquid and water, Fig. P: Centrifuging the sample for the separation of the organic matter, Fig. Q: Washing the organic residue with water and centrifuging, Fig. R: Collecting the extracted residue in glycerin for microscopic study.

solution was made by mixing of nine parts of acetic anhydride and one part of conc. sulphuric acid (H$_2$SO$_4$) (Erdtman, 1954). The samples were treated with acetolysis solution and placed in warm water bath for 3-4 minutes. Samples were removed from the bath and allowed to cool and the residues were washed and centrifuged once with glacial acetic acid and three times with water. Zinc Bromide (ZnBr$_2$) was added to the test tube containing the residue. Few drops of water were poured in the test tube without mixing with the heavy liquid. Then, the test tube was centrifuged at 3000 rpm for one minute and a layer of organic suspension was appeared at the boundary. That organic suspension was transferred in to the clean test tube leaving the mineral fraction and liquid. The organic materials were washed with water twice and remaining material was put on the glycerin for the microscope study.

8.3.2 Light microscopy (LM)

With a pipette, a drop of the organic residue was transferred to a glass slide. The slide was examined under the light microscope using 10x, 20x, 40x, 60x and 80x objectives after distributing the uniformly on the glass slide. Possible pollen grains up to 400 were counted by moving the slides from left to right. Interesting pollen grains were brushed to the edge of the glycerin with the hair needle and they were transferred to another glass slide with a fresh drop of glycerin for photography under the light microscope. With the help of the hair needle, the pollen was oriented in equatorial and polar view or desired position. Photographs were taken by using digital camera and photos were transferred in computer.

8.3.3 Scanning electron microscopy (SEM)

After examining under the LM and taking LM photographs, the same pollen grain was brought to the edge of the glycerin. The SEM stub was kept under a binocular microscope. Pollen grains were transferred to a SEM stub by the help of hair needle to which a drop of absolute ethanol (99%) had been dropped with a pipette simultaneously Fig. 8.5).Glycerin should be removed from the pollen grain before examining under the

Table 8.1: Description of samples with pollen and organic residue (See Fig. 3.2 for location)

SN	Sediment	Pollen and organic residue	Location
SN1	Organic clay	very low concentration of pollen	Fig. 3.2B(Thakkhola Fm)
SN2	Organic clay	Low concentration of pollen	Fig. 3.2B (Thakkhola Fm)
SN4	Organic clay	very low concentration of pollen	Fig. 3.2B (Thakkhola Fm)
A1b	Black clay	black and dark brown plant fragments, no pollen	Dhi section (Thakkhola Fm)
A2b	clay	brown plant fragments and tissues in different size>10μ are dominant, different species of pollen and spores	Tange section (Thakkhola Fm)
A2d	Silty clay	debris only, no pollen/spores	Tange section (Thakkhola Fm)
A3b	Black clay with plant fossil	small debris, no pollen	Ghiling section (Thakkhola Fm)
A4f	Organic clay	no pollen	Ghiling section (Thakkhola Fm)
A4c	Carbonaceous clay	pollen/spores more frequent, bisaccate pollen are absolutely dominant, not very good preserved	Chaile section (Thakkhola Fm)
A6f	Organic clay	Black to dark brown debris (unstructured components), very fine disseminated debris, much smaller than 10 μ, no pollen	Tetang village (Tetang Fm)
A6g	Black clay	Small debris, no pollen	Tetang village (Tetang Fm)
SN15	Organic clay	No pollen, organic fragments	Tetang village (Tetang Fm)
SN 16	Clay and wood	A lot of woody plant fragments	Tetang village (Tetang Fm)
SN 18	Organic clay	No pollen, More mineral fragments than organic particles in the residue	Tetang village (Tetang Fm)
A6l	black clay	debris 30-50μ, no pollen	Tetang village (Tetang Fm)
SN 21	Organic clay	No pollen	Tetang village (Tetang Fm)
A6o	Clay with plant fossil	small debris, no pollen	Tetang village (Tetang Fm)
A6q	Clay with plant fossil	very small debris, some bigger fragments, few pollen/ spores, not good preserved	Tetang village (Tetang Fm)
SN 28	Organic clay	More pollen than in the other samples, but not good preserved. Pollen of conifer trees are dominant (bisaccate pollen grains)	Tetang village (Tetang Fm)
A6t	Black clay	small debris, few bisaccate pollen, no good preserved	Tetang village (Tetang Fm)
A6v	Black clay	small debris, brown band black, bisaccate pollen (*Pinus, Picea*) more frequent than A6t, not good preserved	Tetang village (Tetang Fm)
A6w	Organic clay	small debris, few pollen	Tetang village (Tetang Fm)
A6x	Organic clay	small debris, few pollen	Tetang village (Tetang Fm)
A6y	black clay	pollen/spores more frequent, bisaccate pollen are absolutely dominant, not very good preserved	Tetang village (Tetang Fm)
A6z	Black clay	very small debris, no pollen	Tetang village (Tetang Fm)
A6z1	black clay	few pollen, not good preserved	Tetang village (Tetang Fm)

SEM. After removing glycerin, the SEM stub was placed in a BIORAD Sputter Coater for four minutes to coat with gold. Then after, the SEM stub will put inside and pollen grains were examined with Jeol 6400 Scanning Electron Microscope at 10 kV with different magnification and orientation. Digital photographs were taken in desired magnification and transferred in to the computer. Pollen grains were identified and presented in graphical as well as in plate with the help of the LM and SEM photographs
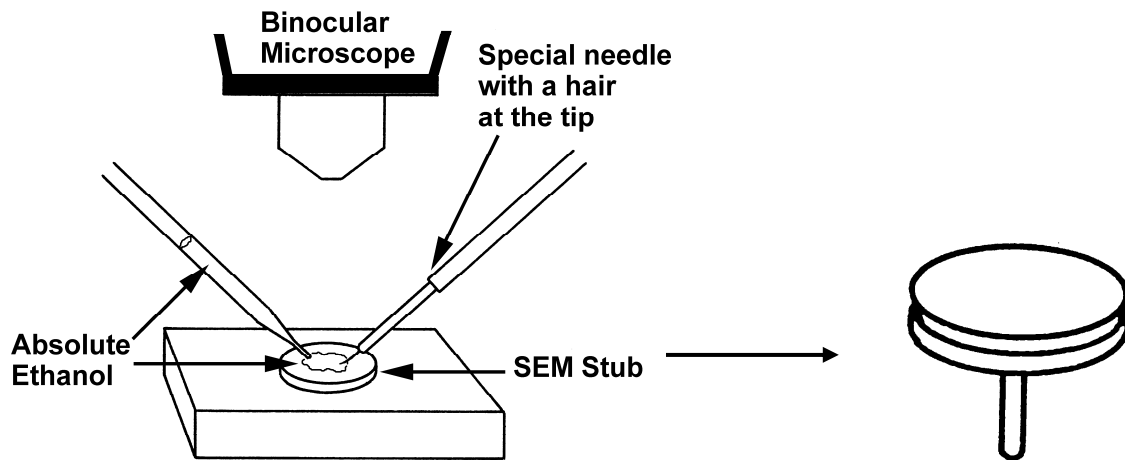
Fig. 8.5: Preparation of pollen for SEM study (after Ferguson et al., 2007)

8.4 Identifications and descriptions

Pollen records from the Tetang Formation and the Thakkhola Formation are identified under LM and SEM. High quality photographs (LM and SEM) were prepared and compared with modern pollen data records. The high quality photographs, particularly SEM images, are essential for comparison with other fossil microfloras, even or in particular, when the material is not yet botanically identified (Hofmann and Zetter, 2001). Plates are presented in appendix I.

8.4.1 Pteridophytes
LYCOPODIACEAE

<div align="center">

Lycopodiaceae sp.
Plate I. Fig. 1-2

</div>

Shape: sub-angular.
Size: 80 µm
Aperture: Trilete.
Exospore: 1 µm, pseudo-reticulate, chambers fused to form 'honey-comb' like structure.

POLYPODIACEAE

Polypodium sp.
Plate I. Fig. 3

Shape: Elliptical
Size: 70µm
Aperture: Monolete
Exospore: 2-3 µm, regulate and spiny. The spines are blunt and irregularly distributed.

PTERIDACEAE

Pteris sp.
Plate I. Fig. 4

Shape: Sub-angular
Size: 40µm
Aperture: Trilete
Exospore: regulate in distal pole, rugulae often fused to each other to form irregular depressions in between them, cingulum psilate.

8.4.2 Gymnosperms
PINACEAE

Abies sp.
Plate II. Fig. 6

Shape: Bisaccate
Size: 130 µm
Exine: in proximal part of corpus is thick and coarsely regulate. Corpus attached to the upper half of the sacci.

Keteleeria sp.
Plate II. Fig. 7

Shape: Bisaccate
Size: 40-50 µm, corpus 40, sacci 22 µm
Corpus is rugulate and rough. The outline of the sacci in the polar view is discontinuous with the outline of the corpus.

Picea sp.

Plate II. Fig. 8

Shape: Bisaccate

Size: 150 µm

Corpus faintly and finely verrucate regulate and perforate. Sacci is finely alveolate. Sacci attached almost along full width of the corpus.

Pinus sp.
Plate II. Fig. 9

Shape: Bisaccate

Size: 45-53 µm, corpus 43, sacci 23 µm

Corpus is rugulate and rough. In LM, leptoma present small verrucae. Sacci attached almost along full width of the corpus. The outline of the sacci in the polar view is discontinuous with the outline of the corpus. Therefore, the grain seems to consist of three distinct oval parts.

Tsuga sp.
Plate II. Fig. 10

Shape: Monosaccate, oblate, circular in polar view.

Size: 76 µm

Corpus verrucate to regulate, foveolate and echinate. Saccus are echinate and folded.

8.4.3 Angiosperms
FAGACEAE

Quercus sp.
Plate II. Fig. 11 and Plate III. Fig. 12

Shape: Prolate, circular and lobate in polar view.

Size: 22 µm in polar axis and 21 µm in equatorial axis.

Aperture: Tricolporate, colpi relatively broad.

Exine: 1-1.25 µm thick, tectum consists of very small (< 1µm), randomly oriented and uniformly distributed rods.

Fagus sp.
Plate III. Fig. 13

Shape: Lobate in polar view.

Size: 33µm in polar axis and 24 in polar view.

Aperture: Tricolporate, colpi relatively broad.

Exine: 2-2.5 µm thick, tectum consists of uniformly distributed randomly oriented rods.

Fagaceae ?
Plate III. Fig. 14

Shape: Spheroidal in equatorial view, sub triangular in polar view.

Size: 32 µm in polar axis, equatorial view is 21 µm.

Aperture: Tricolporate

Exine: 2-2.5 µm thick, tectum consists of uniformly distributed rods, randomly oriented.

JUGLANDACEAE

Juglans sp.
Plate III. Fig. 15

Shape: Oblate, (sub spheroidal to spheroidal) and circular.

Size: 41-43 µm.

Aperture: Pantoporate, pores aspidate, circular rarely oval, 2-3 µm.

Exine: 2µm, sexine is thicker than nexine, tectum is microechinate.

BETULACEAE

Alnus sp.
Plate IV. Fig. 16

Shape: Oblate, penta-angular in polar view.

Size: 35-40 µm

Aperture: Pentaporate, pori vestibulum type, neighbouring pori connected by archs or bands of nexinous thickening.

Exine: 1.5 µm, tectum consists of irregular regulate with very small spinules. Sexine slightly thicker than nexine.

Betula sp.
Plate IV. Fig. 17

Shape: Oblate, triangular in polar view.
Size: 29 µm
Aperture: Triporate occasionally tetraporate, pores circular and vestibulum type, sexine with tectum clearly thickest at the apex, vestibulum forming a well-defined annulus.
Exine: 2 µm, sexine consists of irregular regulae with very small spinules.

TILIACEAE

Tilia sp.
Plate IV. Fig. 18

Shape: Triangular to rounded in the polar view and oblate in the side view.
Size: 35 µm
Aperture: Tricolporate
Exine: Three very short oval furrows, each containing an elliptical pore, which are surrounded by coarse areas. A network pattern tapers to the equator and there are small polar meshes.

SALICACEAE

Salix sp.
Plate IV. Fig. 19

Shape: Prolate, reticulate
Size: 20-25 µm
Aperture: Tricolporate
Exine: The reticulation decreases in size near the furrow, often producing a psilate margo parallel to the furrow. The lumina generally decrease in size at the poles.

ACERACEAE

Acer sp.
Plate V. Fig. 20

Shape: Prolate
Size: 26-30 µm
Aperture: Trocolpate.
Exine: Fine rugulate-striate sculpture

OLEACEAE

Fraxinus sp.
Plate V. Fig. 21-22

Shape: Prolate, circular in polar view.
Size: Polar axis 17 µm and equatorial axis 14 µm.
Aperture: Tricolporate, colpi are long, small circular endoaperture.
Exine: 1µm, sexine thicker than nexine, tectum reticulate, lumina are heterobrochate, triangular to polygonal in shape, muri with a fine ring-like ornamentation.

Ligustrum sp.
Plate V. Fig. 23

Shape: Sub prolate
Size: Polar axis is 22 µm and equatorial axis 20 µm.
Aperture: Tricolporate
Exine: 1.2 µm, sexine is thicker than nexine, reticulate, beterobrochate, muri are smooth, lamina with rudimentary columellae.

CARYOPHYLLACEAE

Caryophyllaceae gen. indet.
Plate VI. Fig. 24

Shape: Spheroidal
Size: 28-30 µm.
Aperture: Pantoporate, pori circular, diameter ca. 2 µm.
Exine: 2 µm, sexine as thick as exine, sexine perforated, spinulate, pore membrane spinulate.

ROSACEAE

Rosaceae gen. indet.
Plate VI. Fig. 25-26

Shape: Oblate spheroidal, triangular in polar view.
Size: Polar axis in 23 µm and equatorial axis is 16 µm.
Aperture: Tricolporate, colpi long.
Exine: 1-1.5 µm, sexine is thicker than nexine, striate, striations sometimes joined with each other and variable in size.

VITAEAE

Parthenocissus sp.
Plate VI. Fig. 27 and Plate VII. Fig. 28

Shape: Prolate, semiangular in polar view.
Size: Polar axis is 38 µm and equatorial view is 29 µm.
Aperture: Tricolporate
Exine: 1.5 µm, sexine thicker than nexine, micrireticulate to perforate and sparsely covered by granules.

CHENOPODIACEAE

Chenopodiaceae gen. indet.
Plate VII. Fig. 29

Shape: Spheroidal
Size: 28 µm
Aperture: Pentoporate, pore circular.
Exine: 1 µm, sexine thicker than nexine, sexine spinulate, perforate, mesoporium raised above pori, pore membrane spinulate, granulate.

PLANTAGINACEAE

Plantago sp.
Plate VII. Fig. 30

Shape: Spherical
Size: 20 µm
Aperture: Pantoporate, diameter of pore 2-3 µm.
Exine: 1 µm, Pores are surrounded by a thickened, projecting ring known as annulus, and with an operculum. Network of small hills and valleys, with large irregular verrucae.

POACEAE

Poaceae gen. indet.
Plate VII. Fig. 31

Shape: Spheroidal
Size: 21 µm
Aperture: Ulcerate, pore annulate, diameter of pore 2-3 µm.
Exine: 1 µm, sexine as thick as nexine, microverrucate with small spiny elements especially at the edges of the microverrucae.

COMPOSITAE

Tubiflorae Compositae gen. indet.
Plate VIII. Fig. 32

Shape: Spheroidal, circular in polar view.

Size: 22 µm

Aperture: Tricolporate

Exine: 4 µm, sexine than nexine, sexine microreticulate and spiny, spines 1-2 µm with relatively large perforations.

Tubiflorae Compositae gen. indet.
Plate VIII. Fig. 33

Shape: Sub-prolate to prolate.

Size: 25 µm

Aperture: Tricolporate

Exine: 5-6 µm (with spines), sexine thick, sexine perforate and echinate, the basal part of spine broadly perforate with perforations of various shape and sizes, surface granulate, spines 2-3 µm in length.

Tubiflorae Compositae gen. indet.
Plate VIII. Fig. 34

Shape: Prolate, circular in polar view.

Size: 20 µm

Aperture: Tetracolporate

Exine: 4 µm, sexine much thicker than, nexine, tectum perforate, spiny, the base of the spine with larger perforations, surface granulate.

Tubiflorae Compositae gen. indet.
Plate VIII. Fig. 35

Shape: Prolate to circular

Size: 18 µm

Aperture: Tricolporate

Exine: 7 µm, sexine much thicker at mesocolpium forming a crown, microreticulate, spiny, micro-reticulate, lumina 0-1 µm.

ASTERACEAE

Artemisia sp.

Plate IX. Fig. 36

Shape: Prolate circular in polar view, lobate
Size: 22 µm
Aperture: Tricolporate, colpi nearly as long as polar axis.
Exine: 3 µm, sexine much thicker than nexine, distinctly stratified, sexine in mesocolpium thicker than in the colpi area forming margo, sexine microechinate and granulate, granules uniformly distributed between the spinules.

Undetermined
Plate IX. Fig. 37

Shape: Spheroidal in equatorial view, sub triangular in polar view.
Size: 25 µm in polar axis, equatorial view is 22 µm.
Aperture: Tricolporate
Exine: 1-2 µm thick, tectum is granules uniformly distributed between the spinules.

8.5 Pollen assemblages

More than 19 families and genera of pollen were identified from all of the samples. A high percentage of grassland taxa and a low percentage of temperate forest taxa characterize the pollen assemblages.

8.5.1 Tetang Formation

Of seventeen samples collected from the Tetang Formation at Tetang area, pollen were found only in seven samples. All samples were carbonaceous clay with plant fossils in some samples (Table 8.1). Sediments display a higher percentage of *Pinus*, *Quercus* and *Keteleeria* with *Abies* and *Tsuga* and low concentration of *Betula* and *Juglans*. The upper horizon of the Tetang Formation is dominantly lacustrine sediments, which are rich in pollen. Coniferous pollen grains (*Pinus)* are dominant in these horizons (A6y). However, pollens were not preserved in large number and it is impossible to make a detailed pollen diagram.

8.5.2 Thakkhola Formation

Nine samples were studied from the Thakkhola Formation but pollens were present only in five samples (Table 8.1). Most of the samples are organic-rich clay but some of them are silty clay.
Two samples are rich in pollen in the Thakkhola Formation. One sample taken from the Chaile section (A4c) is very pollen rich. This sample is characterized by the presence of Angiosperms and Gymnosperms pollen. Varieties of pollen are found in this sample.

Pinus, Quercus, Tsuga, Fagus, Juglans, Betula, Tilia, Salix, Acer, Fraxinus and *Plantago* are the dominant pollen grains in the Chaile section.

Spores are found in the sample taken from Tange section (A2b). Lycopodiaceae, Polypodiaceae and Pteris families dominate the spores. Most dominant pollen grains are *Pinus* sp*., Quercus, Plantago, Poaceae,* Compositae and *Artemisia* in the Tange section (Appendix I).

8.6 Discussions

Sporopollen includes arboreal taxa (such as *Pinus, Betula, Keteleeria, Juglans, and Quercus*), shrub taxa (such as Oleaceae) and herbaceous taxa, which are mainly Chenopodiaceae, *Artemisia*, Poaceae, *Compositae* and Rosaceae. The palynofloras of the Thakkhola Formation and the Tetang Formation indicate that paleotemperature is the key factor in controlling long-term trend and fluctuations in the Neogene vegetation in the Thakkhola-Mustang Graben. *Pinus* is usually over-represented because of its high pollen production and long distance dispersion (Denton and Karlen, 1973 and Wang and Wang, 1983) and the percentage of *Pinus* below 10% are insignificant (Fægri and Iverson, 1989). Therefore, they are generally regarded as being exotic. Howerver, coniferous pollen grains dominate the pollen assemblage in the upper horizons of the Tetang Formation. It can be inferred that the altitude is higher than present time during deposition of the Tetang Formation. The presence of *Keteleeria* in Tetang Formation may indicate a warm climate but it can be reworked from the older sediments. Yoshida et al. (1984) suggested the dry climate during the deposition of Tetang Formation based on the high percentage of *Ephedra* spores.

Betula, Quercus and *Juglans* are very sensitive to humidity and their pollen contents increase with rainfall (Sun et al., 1996). Therefore, the presence of these taxa in the Thakkhola-Mustang Graben indicates temperate forest increased significantly, implying a relatively humid climate, especially for the Tetang Formation. The presence of high percentages of Plantago, Poaceae, *Artimisia* and Chenopodiaceae in the Thakkhola Formation indicate a more arid climate. They show that mostly steppe vegetation was dominant during the deposition time of Thakkhola Formation. This steppe vegetation might be caused by the Himalayan barrier. The uplift of the Tibetan Plateau could exert a profound effect upon atmospheric circulation and environmental changes of Asia. It would form a water vapor barrier, so that the water vapor carried by the south west monsoon could not reach the Tibetan Plateau (Ruddiman and Kurzbach, 1989), leading to the decrease of rainfall and gradual vegetational change to arid grasslands in the Thakkhola-Mustang Graben. A precise biostratigraphic classification with pollen in the studied samples is not possible because there are not index fossils.

CHAPTER NINE
DISCUSSIONS

Several models for the tectonic formation of sedimentary basins and their evolution in time and space have been proposed by Dickinson (1974 and 1976), Kay (1951), Bally and Snelson (1980), Miall (1984), Klein (1987) and Kinsman (1975), especially for half-graben or symmetrical graben and rifts. In this work, a half-graben model is attributed to the Thakkhola-Mustang Graben because of the presence of only one clearly visible master fault, i.e. the Dangardzong fault on the western boundary (Fig. 3.22 and 9.1) and the general geometry of the sedimentary fill of the basin. A minor fault, the Muktinath Fault, is present at the eastern side but it is not clearly visible in the field in the Muktinath area. In this area, only some minor fault related structures could be detected in the field (Fig. 3.23). Chamlagai and Hayashi (2005) carried out a numerical simulation of the Thakkhola-Mustang Graben and deduced that the Dangardzong Fault did not only contribute a major role but numerous other factors contribute to development of the graben.

India-Eurasia continental collision began around 45-55 Ma ago with the closure of the Neotethys Ocean. The great crustal thickness of the Himalaya and Tibet resulted from the convergence of India and Eurasia and their collision. Many thrusts and faults were developed after the collision and they divided the Himalaya into many longitudinal slabs. The Miocene Siwalik is separated from Lesser Himalaya by the Main Boundary Thrust (MBT) and the Main Frontal Thrust (MFT). The Main Central Thrust (MCT) was active during ~ 22 Ma, which separates Lesser Himalaya from Greater Himalayan Crystalline. The South Tibetan Detachment System (STDS) juxtapose the Greater Himalayan Crystalline against lower-grade Tethyan shelf deposits. The hanging wall of the STDS was deformed at ~22 Ma (Hodges et al. 1996; Coleman, 1998). The exposed detachment fault along the STDS in Gonto-La was active at 12.4 ± 0.4 Ma but the relationship of the STDS to this body remains uncertain (Edwards and Harrison, 1977). STDS and Indus Tsangpo Suture Zone (ISTZ) bound Tibetan Tethys sedimentary sequences on south and north, respectively. STDS is a system of normal–dipping, east-striking and predominately extensional structures exposed at the crest of the Himalaya along east-west (Burchfiel et al. 1992; Valdia, 1989) (Fig. 9.1A). The Thakkhola-Mustang Graben developed in different successive stages on top of the Tibetan Tethys sedimentary rocks (Fig. 9.1). Different basin fill sedimentary sequences developed in different time interval and thus indicate a complex basin evolution.

The Miocene Tetang Formation is the oldest formation in the Thakkhola-Mustang Graben, which was deposited just above the Cretaceous basement at ca 11-9.6 Ma (Garzione et al., 2000) (Fig. 9.1B). It was deposited mostly in the southeastern part of the

graben near Tetang village and Dhinkyo Khola section. A clearly seen unconformity with onlap geometry characterizes the contact between this formation and the Cretaceous substratum in the Tetang area (Fig. 3.8). Mainly Mesozoic and Paleozoic clasts are found in the conglomerate beds with absence of granite clasts in these conglomerate beds (Fig. 4.14). Thus, either Mugu and Mustang granites had not yet started to be eroded at this time or the material derived from them was not transported to the depositional area of the graben. The thick conglomerate succession with Mesozoic clasts suggests local high-relief topography and a provenance from the eastern margin of the basin (Fig. 9.1B) as Mesozoic outcrops are mainly concentrated on the eastern side of the basin. The thickness of the Tetang Formation increases abruptly towards west in outcrop scale (Fig. 3.8). Paleocurrent directions from the imbricated pebbles suggest that the sediments were derived from the surrounding rocks, mainly to the west, which indicates the presence of the main master fault of the basin at the western margin already during the time of deposition of the Tetang Formation. Sediments were deposited in different paleoenvironments including alluvial fan, braided river system, fluvio-lacustrine, lacustrine and flood plains. The upper portion of the Tetang Formation was dominated by fine-grained laminated carbonate deposits with some fossils (Fig. 5.9 & 5.10) and thus testifies for a decrease in the relief and the formation of a lacustrine environment. Carbonates display high variety of δ^{13}C values ranging from -24.08 to 11.08 ‰ (Table 6.1). These results are similar to those of Garzione et al. (2003). Extremely positive δ^{13}C values of the carbonate in the Tetang Formation infer that the bottom water conditions were dysaerobic in the lake, leading to the breakdown of organic matter by bacterial methanogenesis (Garzione et al., 2003). Many synsedimentary small-scale faults are present within this formation, which indicate the synsedimentary activity of east-west extension (Fig. 3.20). Parts of the accommodation space for the deposition of sediments in this formation was probably also created as a response to normal faulting and footwall uplift associated with STDS because Garzione et al. (2003) did not find strong evidences for syndepositional faulting.

After the deposition of the Tetang Formation, these strata were rotated ~ 5° westward down before the deposition of the Thakkhola Formation. Consequently, these two formations are separated by an angular unconformity which can be seen only in Tetang area and Dhinkyo Khola area. This angular unconformity records a temporal gap of $\geq$ 2.5 Ma, beginning at ca. 9.6 Ma and ending at 7 Ma (Garzione et al., 2000a). The basal imbricated conglomerate sequence of Thakkhola Formation rests upon the lacustrine deposits of the Tetang Formation (Fig. 3.7). Renewed coarse conglomerate deposition may be attributed to a reactivation of fault systems and formation of high relief. Granite clasts were recorded for the first time, indicating the unroofing of the Mugu and Mustang granites in the source area for this formation.

The Thakkhola Formation is distributed mostly in the northern part of the basin starting from Tetang area up to Lomangthang. Its western proximity is bounded by Dangardzong fault (Fig. 9.1C) and it forms the main phase of half-graben deposition. Alluvial fan, braided river system, fluvio-lacustrine and lacustrine paleoenvironments were dominant in this formation. Paleocurrent directions indicate that the sediments were derived from the north ranging from NW to NE. Pebbles in Dhi and Tange gaon show SW-directed paleoflow, which suggests a northeastern provenance. Sediments were transported from NW and NE to the centre part of the basin. Clast compositions are composed of sandstone, quartzite, shale, mudstone, carbonate and granites. Paleozoic and Mesozoic basement rocks are responsible for these clasts. The conglomerate layers in Chaile have 0.5 and 10 m thickness, which shows that the channel size of flow of the Paleo-Kaligandaki River was similar in magnitude to the present Kaligandaki River. The presence of granite clasts in the Thakkhola Formation indicate that the Mustang and Mugu granites of age 17.6 ± 0.3 Ma dated by Th-Pb monazite (Harrison et al., 1997) had been already brought to the surface and were starting to be eroded before the deposition of the Thakkhola Formation. There are different carbonate layers deposited in different intervals, which shows that a periodic damming of the Paleo-Kaligandaki River and formation of a lake. The clast sizes in sediments are influenced also by local fan systems, e.g. there are large clasts present at the southwestern margin of the basin along the (active) Dangardzong fault and significant smaller pebbles at the northeastern margin of the basin in the Dhi area. The number of silt layers increases. It indicates that the velocity and capacity of the river(s) was strong in the central part of the basin compared than northern edge of the basin.

The Sammargaon and Marpha formations in the southern (lower) part of the basin were deposited during Pleistocene times (Fig. 9.4). The Sammargaon Formation is associated with glacial moraines and it is a glacio-fluvial package deposited during the middle Pleistocene glaciation (Fort et al., 1982). The Marpha Formation is made up by a thick pile of fine-grained sandstone and siltstone with some conglomerate beds. It is best exposed at the Marpha village. Fort et al. (1982) correlate the lowermost Marpha Formation to the uppermost part of the Sammargaon Formation based on the association of the Marpha Formation with an underlying glacial till but some other researchers (Iwata, 1984; Yoshida et al., 1984) assigned a late Pleistocene age based on magnetostratigraphic studies and moraines. The Kaligandaki Formation was deposited with a cut and fill relations to these formations and represents the youngest fill of the Thakkhola-Mustang Graben.

These Pleistocene-Holocene formations were deposited by the damming of the paleo Kaligandaki River. However, there are no strong evidences to prove the cause of damming. Tectonic landslides, glaciers or seismic activity are the main possibilities. Iwata (1984) stated that large-scale landslides occurred around Larjung before the Last
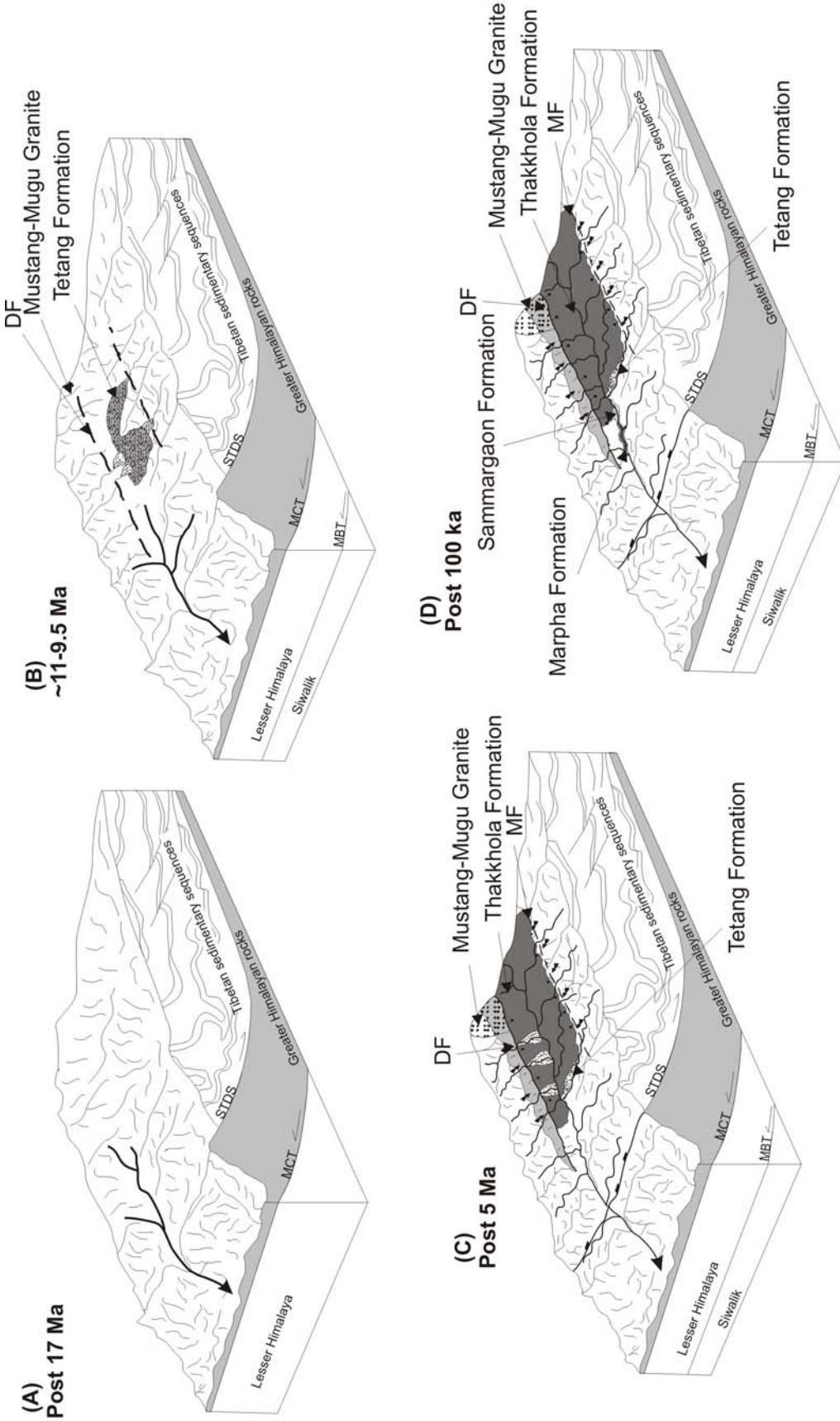
Fig. 9.1: Paleogeographic reconstruction of Early Miocene to Late pleistocene basin reconstruction in Thakkhola-Mustang Graben (Age taken from different authors: see in text). DF = Dangardzong Fault, MF = Muktinath Fault

Interglacial period was responsible for the damming of the river and the formation of the Paleo Marpha Lake. Some evidence by structural and thermochronological data suggests growth of structures south of the Thakkhola-Mustang Graben that could have caused structural damming. Activation of Main Central Thrust (MCT), South Tibetan Detachment System (STDS) and Dangardzong Fault (DF) could make the structural dam by either headward erosion through the Greater Himalayan south of STDS or rupture of detachment system and Higher Himalaya by the Dangardzong fault.

CHAPTER TEN
CONCLUSIONS

The Thakkhola-Mustang Graben lies in the central part of the Nepal Himalaya. The graben is filled by more than 850 m of continental deposits of alluvial fan, braided river and lacustrine origin. Detail field study as well as laboratory studies of deposits of the Thakkhola-Mustang Graben lead to the following conclusions:

- Based on lithostratigraphic investigations, mapping and section logging, the Thakkhola-Mustang Graben sediments are divided in to five formations: the Tetang Formation, the Thakkhola Formation (Miocene-Pliocene), the Marpha Formation, the Sammargaon Formations (Plio-Pleistocene) and the Holocene Kaligandaki Formation.

- The sediments are classified into three lithofacies associations containing 12 lithofacies with six architectural elements. The lithofacies associations are (1) matrix-rich conglomerate-gravelly sandstone association, (2) matrix-rich conglomerate with sandstone and mudstone and (3) massive siltstone with mudstone, alternating with carbonate layers. This investigation revealed that the sediments were deposited in alluvial fan, lacustrine, braided river and glacio-fluvial environments.

- Lacustrine carbonates are deposited within the Thakkhola and Tetang formations in different lithostratigraphic sequences and the percentage of $CaCO_3$ in limestone samples of both Thakkhola and Tetang formations ranges from 24 to 99.5 whereas in the calcareous clays it ranges from 4 to 48. Limestone microfabrics are classified into two groups with seven sub-groups based on petrographic study of texture and structures. The first group includes shallow water lacustrine carbonate microfacies while a second group includes deep-water lacustrine carbonate microfacies.

- The $\delta^{18}O$ values of carbonates in the Thakkhola-Mustang Graben ranges from -13.5‰ to -24.96 ‰. These values are similar to those of modern meteoric values of that area. They suggest that the southern Tibetan Plateau attained its current elevation already prior to east-west extension. Based on the lapse rate, the inferred paleoaltitude of the Thakkhola-Mustang Graben varies from 3300 (Marpha Formation) to 6087m (Thakkhola Formation). Stable carbon isotopes of lacustrine carbonates from the Tetang Formation have higher values of $\delta^{13}C$ than those of the Thakkhola and Marpha formations and range from -24.08 to 11.08 ‰. High $\delta^{13}C$ values strongly indicate that these carbonates were formed in a methanogenic zone.

- Paleocurrent data of imbricated conglomerates from all formations of the basin show a generally southward paleoflow direction. At Dhi and Tange, the Thakkhola Formation consists of clasts derived mainly from the Mesozoic rock exposed to the east. In the Ghiling, Dhakmar and Chaile areas, the Thakkhola Formation is represented by a mixture of clasts from Paleozoic, Mesozoic and Tertiary rocks. They indicate a paleoflow from north and west. The conglomerates of the Tetang Formation comprise mostly Mesozoic rock clasts showing an eastern provenance.

- Heavy mineral analysis indicates that low-to high-grade metamorphic complexes comprising micaschists and related metamorphic rocks were the primary source. The presence of andalusite and amphiboles suggest a source of high-grade metamorphic rocks whereas stable minerals like zircon, rutile and apatite refer to a granitoid source terrain and/or reworking of sediments. The presence of chrome spinel indicates a minor influence of ultramafic rocks whereas the heavy minerals like epidote and hornblende point out to a mafic rock source.

- The palynological study shows that the sediments contain pollens dominantly of alpine trees such as *Pinus, Picea Tsuga, Keteleeria* and *Quercus* with some steppe elements like *Artemisia, Compositae, Chenopodiaceae, Plantago* and *Poaceae* indicating dry climate during the sediment deposition. Consequently, it is presumed that the paleoclimate during the evolution of the Thakkhola-Mustang Graben was significantly warmer than the present-day climate.

- The sedimentary infill of the Thakkhola-Mustang Graben and the tectonic structure point to a half-graben model for the basin. The main synsedimentary active boundary fault was the north-south striking Dangardzong fault at the western margin whereas the eastern margin shows only minor fault activity during the deposition of the Tetang and Thakkhola formations.

References

Abels, H.A., Aziz, H.A., Calvo, J.P., and Tuenters, E., 2009. Shallow lacustrine carbonate microfacies document orbitally paced lake-level history in the Miocene Teruel Basin (North-East Spain), Sedimentology, vol. 56, pp. 399-419.

Amatya, K. M. and Jnawali B. M., 1994. Geological map of Nepal. Scale: 1:1,000,000, Published by Department of Mines and Geology, Kathmandu, Nepal

Araguás L.A., and Froehlich, K., 1998. Stable isotope composition of precipitation over Southeast Asia, Journal of Geophysical Research, vol. 103, no. D22, pp. 28721-28742.

Armijo, R., Tapponnier, P., and Han, T., 1989. Late Cenozoic right-lateral strike-slip faulting in southern Tibet, Journal of Geophysical Research, vol. 94, pp. 2787-2838.

Armijo, R., Tapponnier, P., J.L., and Han, T.L., 1986. Quaternary extension in southern Tibet: Field observation and tectonic implications, Journal of Geophysics Research, vol. 91, pp. 13803-13872.

Auden, J.B., 1935. Traverses in the Himalaya, Record of the Geological Survey of India, vol. 69 (2), pp. 123–167.

Bally, A. W., and Snelson, S., 1980, Realms of subsidence, Canadian Society of Petroleum Geologists Memoir, vol. 6, pp. 9-75.

Barshad, I., 1966. X-ray analysis of soil colloids by the modification salt paste method, National conference on clay and clay minerals proceeding, vol. 5, pp. 350-364.

Bashyal, R.P., 1998. Petroleum exploration in Nepal, Journal of Nepal Geological Society, vol. 18, pp. 19-24.

Bassoullet J. P., Enay, R. and Mouterde, R., 1986. La marge nord-himalayenne au Jurassique. Sc. Terre, Mém., n. 47, pp. 43-60. 2 fig., Nancy.

Bassoullet, J.P. and Mouterde, R., 1977. Les formations sédimentaires Mésozoïques du domain Tibetain de l'Himalaya du Népal. Ecologie et géologie de l'Himalaya, Coll. Int. C.N.R.S., vol. 268, pp. 53–60.

Bathrust, R.G.C., 1975. Carbonate Sediments and their Diagenesis, Amsterdam, Elsevier, 658 p.

Blair, T.C., 1999. Sedimentary processes and facies of the water laid Anvil Spring Canyon alluvial fan, Death Valley, California, Sedimentology, vol. 46, pp. 913-940.

Blair, T.C., and McPherson, J.G., 1994. Alluvial fans and their natural distinction from rivers based on morphology, hydraulic processes, sedimentary processes, and facies assemblages, Journal of Sedimentary Research, vol. A 64, pp. 450-489.

Blatt, H., Middleton, G., and Murray, R., 1980. Origin of sedimentary Rocks, 2nd edition, 782 p, New Jersey, Prentice-Hal.

Blisniuk, P., Hacker, B.R., Glody, J., Ratschbacher, J., Bi, S., Wu, Z., McWilliams, M.O. and Calvert, A., 2001. Normal faulting in central Tibet since at least 13.5 Myr ago, Nature, vol. 412, pp. 628-632.

Bodenhausen, J. W. A., De Booy, T., Egeler, C. G. and Nijhuis, H. J., 1964. On the geology of central west of Nepal. A preliminary note, Rep. 22nd International geologic congress, pt. 11, pp. 101-122, 5 fig., Delhi.

Bodenhausen, J.W.A., De Booy, T., Egeler C.G. and Nijhuis, H.J., 1964. On the Geology of central west Nepal, A preliminary note, Rep. 22nd International geologic congress, pt. 11. pp. 101-122, 5 fig., Delhi.

Bordet, P., Colchen, M., and Le Fort, P., 1975. In: Recherché géologi- ques dans l'Himalaya du Népal région du Nyi-Shang, Paris Editions du Centre National de la Recherche Scientifique, Paris, 138 p.

Bordet, P., Colchen, M., Krummenacher, D., Le Fort, P., Mouterde, R., Rèmy, J.M., 1971a. Recherches géologiques dans l'Himalaya du Népal région de la Thakkhola, Paris, Editions du Centre National de la Recherche Scientifique, Paris, 275 p.

Bordet, P., Colchen, M., Krummenacher, D., Le Fort, P., Mouterde, R., Remy, M., 1971. Recherches géologiques dans l'Himalaya du Nepal, region de la Thakkhola. C.N.R.S., Paris. Pp. 1–279.

Bordet, P., Colchen, M., Le Fort, P., 1971b. Esquisse géologique du Nyi-Shang (Népal central) au 1/75000, Paris Editions du Centre National de la Recherche Scientifique, Paris.

Bordet, P., Colchen, M., Le Fort, P., Mouterde, R. and Rèmy, M., 1967. Données nouvelles sur la géologie de la Thakkhola (Himalaya du Nepal), Bull. Soc. Géol. France, s. 7, vol. 9, pp. 883–896.

Bouquillon, A., France-Lanord, C., Michard, A., and Tiercelin, J.J., 1990. Sedimentology and isotopic chemistry of the Bengal Fan sediments: the denudation of the Himalaya. Leg 116, Proceedings of the Ocean Drilling Program, Scientific Results, vol. 116, pp. 43-58.

Brook, E.J., Brown, E.T., Kurz, M.D., Ackert, R.P., Jr., Raisbeck, G.M., and Yiou, F., 1995. Constraints on age, erosion and uplift of Neogene glacial deposits in the Transantarctic Mountains determined from in situ cosmogenic ^{10}Be and ^{26}Al, Geology, vol. 23, pp. 1063-1066.

Burchfiel, B.C., Chen, Z., Hodges, K.V., Liu, Y., Royden, L.H., Deng, C. and Xu, J., 1992. The south Tibetan Detachment System Himalayan orogen. Extension contemporaneous with and parallel to shortening in a collisional mountain belt, Special paper Geological Society of America, vol. 269, 41p.

Cain, S.A., 1939. Pollen analysis as a paleo-ecological research method. Botanica Review, vol. 5, pp. 627-54.

Chamberlain, C.P, and Poage, M.A., 2000. Reconstructing the paleotopography of mountain belts from the isotopic composition of authigenic minerals, Geology, vol. 28, pp. 115-118.

Chamberlain, C.P., Poage, M.A., Craw, D., and Reynolds, R.C., 1999. Topographic development of the Southern Alps recorded by the isotopic composition of authigenic clay minerals, South Island, New Zealand, Chemical Geology, vol. 155, pp. 279-294.

Chamlagain, D. and Hayashi, D., 2005. Fault development in the Thakkhola half Graben: insights from numerical simulation. Bulletin Faculty of Science, University of Ryukyus, No. 79, pp. 57-90.

Chamlagain, D. and Hayashi, D., 2006. Numerical Modeling of Graben Faults with Special Reference to Thakkhola Half Graben, central Nepal Himalaya, Himalayan Geology, vol. 27 (2), pp. 95-110.

Chang, L.L. Y., Howie, R.A., Zussman. J., 1998. Rock forming minerals volume 5B: Non-silicates: Sulphites, Carbonates Phosphates and Halides. 2nd ed. Geological Society, London, 383 p.

Chetri, M. 2005. Status, Habitat use and Conservation of Tibetan Gazelle in Dhalung Rangeland, Upper Mustang, National Trust for Nature Conservation, Annapurna Conservation Area Project, Upper Mustang Biodiversity Conservation Project.

Clift, P.D., Giosan, L., Blusztajn, Campbell, I.H., Allen, C., Pringle, M., Tabrez, A.R., Danish, M., Rabbani, M.M., Alizai, A., Carter, A., and Lückge, A., 2008. Holocene erosion of the Lesser Himalaya triggered by intensified summer monsson, Geology, vol. 36 (1), pp. 79-82.

Colchen, M., 1980. Evolution paléogéographique et structurale du fossé de la Thakkhola-Mustang (Himalaya du Népal): Implications sur l'histoire récent de la chaine himalayenne, Paris, Computes Rendus des Academie des Sciences, vol. 290, pp. 311-324.

Colchen, M., 1999. The Thakkhola-Mustang Graben in Nepal and the Late Cenozoic extension in the Higher Himalayas, Journal of Asian Earth Sciences, Vol. 17, pp. 683-702.

Colchen, M., Le Fort, P., and Pécher, A. 1980. Carte géologique Annapurna-Manaslu-Ganesh, Himalaya du Népal Echelle 1:200,000, Centre National de la Recherche Scientifique, Paris.

Colchen, M., Le Fort, P., and Pecher, A., 1986. Recheches geologiques dans I'Himalaya du Nepal, Annupurna-Manasalu-Ganesh Himal, Paris, Editions du C. N.R.S, Paris, 136 p.

Coleman, M., and Hodges, K., 1995. Evidence for Tibetan plateau uplift before 14 Myr ago from a new minimum age for east-west extension, Nature, vol. 374, pp. 49-52.

Coleman, M.E, 1998, U-Pb constraints on Oligocene-Miocene deformation and anatexis within the central Himalaya, Marsyandi valley, Nepal. American Journal of Science, vol. 298, pp. 553-571.

Cowardin, L.M., Carter, V., Golet, F.C., and LaRose, E.T., 1979. Classification of wetlands and deepwater habitats of the United States. Office of Biological Services, Fish and Wildlife Service. US Department of Interior, Washington, DC, United States, 131 p.

Crook, K.A.W., 1974. Lithogenesis and geotectonics: the significance of compositional variation in flysisch arenites (graywackes), in modern and ancient geosynclinals sedimentation. SEPM, Special publication, vol. 19, pp. 304-310.

Dansgaard, W., 1964. Stable isotopes in precipitation. Tellus. vol. 16 (4), pp. 436-468.

Dasgupta, P., 2007. Facies characteristics of Talchir Formation, Jharia Basin, India: Implications for initation of Gondwana sedimentation, Sedimentary Geology. vol. 185, pp. 59-78.

Davis, C.A., 1900. A contribution to the natural history of marl, Journal of Geology, vol. 9, pp. 485-497.

Davis, C.A., 1901. A second contribution to the natural history of marl, Journal of Geology. Vol. 10, pp. 491-497.

Davis, C.A., 1903. Contribution to the natural history of marl, Rep. Geol. Surv. Mich., vol. 8, pp. 65-99.

Dean, W.E, 1981. Carbonate minerals and organic matter in sediments of north temperate hard-water lakes, In F.G. Ethridge and T.M. Flores [eds.], Recent and ancient non-marine depositional environment: Models for exploration, SEPM Special Publication, vol. 31, pp. 213-231.

DeCelles, P. G., Robinson, D. M., Quade, J., Ojha, T. P., Garzione, C. N., Copeland, P., and Upreti, B. N., 2001. Stratigraphy, structure, and tectonic evolution of the Himalayan fold-thrust belt in western Nepal, Tectonics, vol. 20, pp. 487-509.

DeCelles, P.G., Quade, J., Kapp, P., Fan, M., Dettman, D.L., and Ding, L., 2007. High and dry in central Tibet during the Late Oligocene, Earth and planetary Science Letters, vol. 253, pp. 389-401.

Denton, G.H., Karlen, W., 1973. Holocene climatic variations-their pattern and possible cause, Quaternary Research, vol. 3, pp. 155-205.

Dhital, M.R., Gajurel, A.P., Pathak, D., Paudel, L.P., Kizaki, K., 1995. Geology and structure of the Siwalik and Lesser Himalaya in the Surai Khola–Bardanda area, Mid Western Nepal, Bulletin of Department of Geology Tribhuvan University, vol. 4, pp. 1–70.

Dickinson, W.R., 1974. Plate tectonics and sedimentation. Society of Economic Paleontologists and Mineralogists, Special publication, vol. 22, pp. 1-27.

Dickinson, W.R., 1976. Plate tectonic evolution of sedimentary basins. American Association of Petroleum Geologists Continuing Education Course Notes Series, vol. 1, 62p.

Dickinson, W.R., 1985. Interpreting provenance relations from detrital modes of sandstones; In: Provenance of Arenites (ed.), G. Zuffa (Dordrecht: D. Reidel Pub. Co.), pp. 333–362.

Dickinson, W.R., and Suczek, C.A., 1979. Plate tectonics and sandstone compositions, American Association of Petroleum Geologists Bulletin, vol. 63, pp. 2164-2182.

Dickinson, W.R., Beard, L.S., Brakenridge, G.R., Erjavec, J.L., Ferguson, R.C., Inman, K.F., Knepp, R.A., Lindberg, F.A., and Ryberg, P.T., 1983. Provenance of North American Phanerozoic sandstones in relation to tectonic setting, Geological Society of American Bulletin, vol. 94, pp. 222–235

Dott, R.H. Jr., 1964. Wacke, greywacke, and matrix-what approach to immature sandstone classification? Journal of Sedimentary Petrology, vol. 34, pp. 625-632.

Dunham, R.J., 1962. Classification of carbonate rocks according to depositional texture, in; Ham, W.E. (ed.), classification of carbonate rocks, American Association of Petroleum Geologist Memoir, pp. 108-121.

Edwards, M.A, and Harrison, T. M., 1997, When did the roof collapse? Late Miocene N-S extension in the High Himalaya revealed by Th-Pb monazite dating of the Khula Kangri granite, Geology, vol. 25, pp. 543-546.

Egger, J., Bajrachaya, S. Egger, U., Heinrich, R., Reuder, J., Shayka. P., Wendt. H. and Wirth, V., 2000. Diurnal winds in the Himalayan Kali Gandaki Valley. Part I: Observations, American Meteorological Society, vol. 128, pp.1106-1122.

Einsele, G., 1992. Sedimentary Basins, Springer Verlag, Berlin, 648p.

Epstein, S., Buchsbaum, R., Lowenstam, H.A., and Urey, H.C., 1953. Revised carbonate-water isotopic temperature scale, Geological Society of America Bulletin, vol. 64, pp. 1315-1326.

Erdtman, G., 1954. An introduction to pollen analysis. Chronica Botanica Company, Waltham, Mass., USA, 239p.

Erdtman, O.G.E., 1931. Pollen-statistics: a new research method in paleo-ecology. Science, vol. 73, pp. 399-401.

Erdtman, O.G.E., 1943. An Introduction to pollen analysis. Waltham, Mass.239p.

Fægri, K. and Iversen, J., 1989. Textbook of pollen analysis, John Wiley & Sons, 328 p. Fægri, K., 1956. Recent trends in palynology. Bot. Rev. 22, pp. 639–664.

Fægri, K., 1956. Recent trends in palynology. Bot. Rev., vol. 22, pp. 639–664.

Fagerlind, F., 1952. The real significance of pollen diagram. Botaniska Notiser, vol. 105. pp. 184-224.

Faupl, P., Pavlopoulos, A. and Migiros, G., 1998. On the provenance of flysch deposits in the External Hellenides of mainland of Greece: results from heavy mineral studies, Geological Magzine. 135, pp. 421-442.

Ferguson, D.K., Zetter, R., Paudayal, K.N., 2007. The need for the SEM in paleopalynology. Systematic Paleontology, C.R. Palevol. 6, pp. 423-430.

Fleet, W.F. 1926. Petrological notes on the Old Red Sandstones of the West Midlands, Geological Magazine, vol. 65, pp. 6-8.

Flügel, E., 2004. Microfacies of carbonate rocks: Analysis, Interpretation and Application, Spinger-Vetlag, Berlin Heidelberg, 976 p.

Folk, R.L., 1959. Practical petrographic classification of limestones, American Association of Petroleum Geologist Bulletin, vol. 43, pp. 1-38.

Forest, C.E., Wolfe, J.A., Molnar, P., and Emanuel, K.A., 1999. Paleoaltimetry incorporating atmospheric physics and botanical estimates of paleoclimate. Geological Society of America Bulletin, Vol. 111, pp. 497-511.

Fort, M, 1980. Les formations quaternaires lacustres de la Basse Thakkhola (Himalaya du Nèpal): intèrèt palèogèographique, nèotectonique et chronologique- C.R. Ac. Sc., Paris, 280, pp.171-174.

Fort, M., 1976. Quaternary deposits of the middle Kali Gandaki Valley (central Nepal) Himalayan Geology, vol. 6, pp. 449-507.

Fort, M., 1989. The Gongba conglomerates: Glacial or tectonic? Zeitschrift für Geomorphologie, vol. 76, pp. 181-194.

Fort, M., 2000. Glaciers and mass wasting processes: their influence on the shaping of the Kali Gandaki valley (higher Himalaya of Nepal, Quaternary International, vol. 65/66 pp. 101-119.

Fort, M., Freytet, P., and Colchen, M., 1982. Structural and sedimentological evolution of the Thakkhola Mustang Graben (Nepal Himalaya). Z. für Geomorph. Suppl. Bd 42, pp. 75-98.

Frank, W., and Fuchs, G., 1970. Geological investigations in western Nepal and their significance for the geology of the Himalayas, Geologischen Rundschau, vol. 59, pp. 552-580.

Freytet, P., and Plaziat, J.C., 1982. Continental carbonate sedimentatiton and pedogenesis: Late Cretaceous and Early Tertiary of southern France, Contributions to Sedimentology, vol. 12, pp. 1-213.

Freytet, P., and Verrechhia, E.P., 2002. Lacustrine and palustrine carbonate petrography: an overview, Journal of Paleolimnology, vol. 27, pp. 221-237.

Friedman, I., and O'Neil, J.R., 1977. Compilation of stable isotope fractionation factors of geochemical interest. In: M. Fleischer, Editor, Data of Geochemistry (6th edition ed.), U.S. Geological Survey Professional Paper 440-KK, 6th ED., Reston, VA.

Fuchs, G. and Poudel, L.P., 1998. Note on the Tethyan sedimentary series of the Manaslu region (northern Nepal), Jahrbuch der Geologischen Bundesanstalt-A 141, pp. 45-50.

Fuchs, G., 1964. Note on the geology of the Palaeozoics and Mesozoics of the Tibetan zone of the Dolpo region (Nepal- Himalaya), Sonderabdruck aus den Verhandlungen der Geologischen bundesanstalt 1, pp. 6-9.

Fuchs, G., 1974. On the geology of the karnali and Dolpo regions, west Nepal, Mitteilugen der Geologischen Gesellschaft in Wien, 66-77, Band, pp. 21-32.

Fuchs, G., 1977. The geology of Karnali and Dolpo regions, western Nepal. Jb. Geol. Bundesanst., vol. 120, n. 2, pp. 165-217, 13 pl., 35 fig., Wien.

Fuchs, G., Widder, R.W. and Tuladhar, R., 1988. Contributions to the geology of the Annapurana range (Manang area, Nepal), Jahrbuch der Geologischen Bundesanstalt-A Wein 131, 593-607.

Füchtbaur, H., 1964. Sedimentpetrographische Untersuchungen in der äöteren Mollase nördlich der Alpen.- Eclogene Geol. Hel, vol. 57, pp. 157-298.

Gadstein, M., Rad, U. V., Gibling, M. R., Jansa, L. F., Kaminski, M. A., Christians, I. L., Ogg, J. G., Rohl, U., Sarti, M., Thurow, J. W., Westermann, G. E. G. and Widemann, J., 1992. The Mesozoic continental margin of central Nepal, Germany, Hannover, pp. 1-141.

Gaetani, M., and Garzanti, E., 1991. Multicyclic history of the northern Indian continental margin (NW Himalaya), American Association of Petroleum Geologist Bulletin, vol. 75, pp. 1427-1446.Tulsa.

Gaetani, M., Casnedi, R., Fois, E., Garzanti, E., Jadoul, F., Nicora, A. and Tintori, A., 1986. Stratigraphy of the Tethys Himalya in Zanskar, Ladakh – Initial report, Riv. It. Paleont. Strat., n. 4, pp. 443-478, 16 fig., Milano.

Gansser, 1964. Geology of the Himalayas Interscience Publ. Wiley, London, 289 p.

Garzanti, E., and Frette, M. P., 1991. Stratigraphic succession of the Thakkhola Region (central Nepal), comparison with the northwestern Tethys Himalaya, Riv. It. Paleont. Strat., vol. 97, n.1, pp. 3-26.

Garzanti, E., Baud, A., and Mascle, G. (1987). Sedimentary record of the northward flight of Indian and its collision with Eurasia, Geodinamica Acta, vol.1, n. 4/5, pp. 87-102, 13 fig. Paris.

Garzione, C.N., DeCelles, P.G., Hodkinson, D.G., Ojha T.P. and Upreti, B.N., 2003. East-west extension and Miocene environmental change in the southern Tibetan plateau: Thakkhola graben, central Nepal, Geological Society of America Bulletin, vol. 115; no.1; pp. 3-20

Garzione, C.N., Dettman, D.L., Quade, J., DeCelles, P.G., and Butler, R.F., 2000a. High times on the Tibetan plateau: Paleoelevation of the Thakkhola graben, Nepal, Geology, vol. 28, pp. 339–342.

Garzione, C.N., Quade, J., DeCelles, P.G., and English, N.B., 2000b. Predicting paleoelevation of Tibet and the Himalaya from $\delta^{18}O$ vs. altitude gradients in meteoric water across the Nepal Himalaya, Earth and Planetary Science Letters, vol. 183, pp. 215–229.

Gierlowski-Kordesch, E.H., 1998. Carbonate deposition in as ephemeral siliclastic alluvial system: Jurassic Shuttle Meadow Formation, Newark Supergroup, Hartford basin, USA, Paleogeography, Paleoclimatology, Paleoecology, vol. 140, pp. 160-184.

Godin, L., 2003. Structural evolution of the Tethyan sedimentary sequence in the Annapurna area, Central Nepal Himalaya, Journal of Asian Earth Sciences, vol. 22, pp. 307-328.

Gradstein, F.M., Gibling, M.R., Jansa, L.F, Kaminski, M.A., Ogg, J.G., Sarti, M., Thurow, J.W., von Rad, U. and Westermann, G.E.G., 1989. Mesozoic stratigraphy of Thakkhola, central Nepal, Centre for Marine Geology, Dalhousie Univ, Halifax, Nova Scotia, Spec. Rep. No 1: 114 pp

Gradstein, F.M., von Rad, U, Gibling, M.R., Jansa, L.F., Kaminski, M.A., Kristiansen, I.L., Ogg, J.G., Rthl, U., Sarti, M., Thurow, J.W., Westermann, G.E.G., and Wiedmann, J., 1992. Stratigraphy and depositional history of the Mesozoic continental margin of central Nepal, Geol. Jb Reihe B 77, pp. 3-14.

Grim, R.E., 1968. Clay Mineralogy, 2nd, McGraw-Hill, New York, 597 p.

Hagen, T., 1959. Geologie de la Thakkhola (Nepal), Eclog. Geol.Helv.52/2, pp.709-719.

Hagen, T., 1968. Report on the Geological Survey of Nepal Volume, 2. Geology of the Thakkhola including adjacent areas, Zürich Mémoires de la Societe Helvétique des Sciences Naturelles LXXXVI/2, 160.

Hagen, T., 1969. Report on the Geological Survey of Nepal, vol. 1. Preliminary Reconnaissance, Druk von Art. Institut. orell Füssli Agi Zürich, Kommissionverlag von Gerbüder Fretzag , Zürich .

Harrison, T.M., Copeland, P., Kidd, W.S.F., and Lovera, O., 1995. New insights into the origin of two contrasting Himalayan granite belts, Geology, vol. 25, pp. 899-902.

Harrison, T.M., Lovera, O.M., and Grove, M., 1997. New insights into the origin of two contrasting Himalayan granite belts, Geology, vol. 25, pp. 899-902.

Hiller, S., 2003. Quantitative analysis of clay and other minerals in sandstones by X-ray powder diffraction, Int. Assoc. Sedimentol. Spec. Publ., vol. 34, pp. 213-251.

Hodges, K.V, Parrish, R. R., Serle, M. P., 1996, Tectonic evolution of the central Annapurna Range, Nepalese Himalayas, Tectonics, vol. 25, pp. 1264-1291.

Hodges, K.V., 2000. Tectonics of the Himalaya and southern Tibet from two perspectives, Geological Society of America Bulletin, vol. 112, pp. 324-350.

Hofmann, C. C. and Zetter, R., 2001. Palynological investigation of the Krappfeld area, Palaeocene/Eocene, Carinthia (Austria). Palaeontographica, Abt. B. Bd. 259, 47-64.

Holdsworth, G., and Fogarasi, S., 1991. Variation of the stable isotopes to water with altitude in the Saint Elias Mountains of Canada, Journal of Geophysical Research, vol. 96, pp. 7483-7494.

Honegger, K., Fort, Le P., Mascle, G. & Zimmermann, J.L., 1989. The blueschists along the Indus Suture Zone in Ladakh, NW Himalaya, Jour. Metamorphic Geol., vol. 7, pp. 57-72.

Hurtado, J.M., Hodges K.V. and Whipple, K.X., 2001. Neotetonics of the Thakkhola graben and implications of recent activity on the south Tibetan Fault system in the central Nepal Himalaya, Geological Society of America Bulletin, vol. 113, no.2, pp. 222-240.

Hurtado, J.M., Hodges K.V. and Whipple, K.X., 2001. Neotetonics of the Thakkhola graben and implications of recent activity on the south Tibetan Fault system in the central Nepal Himalaya. Geological Society of America Bulletin, vol. 113, no.2, pp. 222-240.

Huyghe, P., Guilbaud, R., Bernet, M., and Gajurel, A.P., 2008. Significance of the clay mineral distribution in the fluvial sediments of the Neogene Himalayan Foreland Basin (central Nepal), 23rd Himalayan-Karakoram-Tiber workshop (extended abstracts), Himalayan Journal of Sciences, vol. 5 (special issue), pp. 100.

Hyde, H.A. and Williams, D.A., 1944. The right word. Pollen Science Circular. No. 8, p. 6.

Irwin, H., Curtis, C., Coleman, N., 1977. Isotopic evidence for the source of diagenetic carbonate during burial of organic-rich sediments, Nature, vol. 269, pp. 209-213.

Iwata, S., 1984. Geomorphology of the Thakkhola–Muktinath region, Central Nepal, and its late Quaternary history, Geographical Reports of Tokyo Metropolitan University, vol. 19, pp. 25–42.

Iwata, S., Yamanaka, H., and Yoshida, M., 1982. Glacial landforms and river terraces in the Thakkhola region, central Nepal, Journal of Nepal Geological Society, vol. pp. 81–94.

Jarvis, A., Reuter, H. I., Nelson, A., and Guevara, E., 2006. Hole-filled seamless SRTM data V3, International center for Tropical Agriculture (CIAT), available from http://srtm.csi.cgiar.org.

Jo, H.R., Rhee, C.W., Chough, S.K., 1997. Distinctive characteristics of a stream flow-dominated alluvial fan deposits: Sanghori area, Kyongsang Basin (Early Cretaceous), southern Korea, Sedimentary Geology, vol. 110, pp. 51-79.

Johnson, A. M., 1970. Physical Processes in Geology, Freeman Copper, San Francisco. 577 p.

Johnson, A. M., 1984. Debris flow, I: Brunsden, D., Prior, D. B. (Eds), Slope Instability. Wiley, Chichester, pp. 257-261.

Johnson, M.N., Opeyke N.D., Johnson G.D., Lindsay E.H. and Tahirkiheli R.A.K., 1982. Magnetic polarity stratigraphy and ages of siwalik group rocks of the potwar plateau, Pakistan, Paleogeography, Paleoclimatology, Plaeoceology, vol. 27, pp. 17-42.

Johnson, N.M., Opdyke, N.D., Johnson, G.D., Lindsay, E.H., and Tahirkherli, R.A.K., 1982. Magnetic polarity stratigraphy and ages of Siwalik Group rocks of the Potwar, Pakistan, Palaeogeography, Palaeoclimatology, Palaeoecology, vol. 37, pp. 17–42.

Kapp, P., and Guynn, J.H., 2004. Indian punch rifts Tibet, Geology, vol. 32, pp. 993-996.

Kay, M., 1951. North American geosynclines. Geological Society of America Memoir, vol. 48, 143p.

Kelts, K., and Hsu, K.J., 1978. Freshwater carbonate sedimentation, in, Lerman, A., Ed., Lakes: Chemistry, Geology, Physics, Spinger-Verlag, New York, pp. 295-323.

Kinsman, D.J.J., 1975. Rift valley basins and sedimentary history of trailing continental margins, in Fischer, A.G., and Judson, S., eds., Petroleum and global tectonics: Princeton, New Jersey, Princenton, University Press. pp. 83-126.

Klein, G. D., 1987, Current aspects of basin analysis. Sedimentary Geology, vol. 50, pp. 95-118.

Konta, J., 1988. Minerals in Rivers, Mitt. Geol.-Paläont. Inst. Univ. Hamburg, SCOPE/UNEP, Sonderband., vol. 66, pp. 341-365.

Kutzbach, J. E., Guetter, P. J., Ruddiman, W. F., and Prell, W. L., 1989. Sensitivity of climate to late Cenozoic uplift in Southeast Asia and the American West; numerical experiments, Journal of Geophysical Research, vol. 94, pp. 18393–18407.

Le Fort, P. 1975. Himalayas: The collided range, Present Knowledge of the continental arc, American Journal of Science, vol. 275-A, pp. 1-44.

Le Fort, P. 1981. Manaslu Leucogranite: A collision Signature of the Himalaya, A Model for its Genesis and emplacement, Journal of Geophysical Research, vol. 86, pp. 10545-10568.

Le fort, P., and France-Lanord, C., 1994. Granites from Mustang and surrounding regions, central Nepal, Nepal Geological Society Journal, vol. 10, pp. 79-81.

Mange, M.A. and Maurer, H.F.W., 1992. Heavy minerals in Color, Chapman and hall, 147 p.

Mange, M.A. and Morton, A.C. 2007. Geochemistry of heavy minerals, Developments in Sedimentology, vol. 58. pp. 345-391.

McConnel, D., 1973. Apatite-its crystal chemistry, mineralogy, utilization and geologic and biologic occurrences, Spinger.Verlag, New York, pp. 111.

McKenzie, J.A., 1985. Carbon isotopes and productivity in the lacustrine and marine environment. In: Stumm, W. (Ed.), Chemical Processes in Lakes, Wiley, New York, NY, pp. 99– 118.

Miall, A. D., 1984. Principles of sedimentary basin analysis. New york, Springer-Verlag, 490p.

Miall, A. D., 1985. Architectural-element analysis: a new method of facies analysis applied to fluvial deposits. Earth Science Review, vol. 22, pp- 261-308.

Miall, A. D., 1996. The geology of fluvial deposits, Springer-Verlag, Berlin, 581 p.

Molnar, P. and Tapponnier, P., 1978. Active tectonics of Tibet, Journal of Geophysical Research, vol. 52, pp. 107–114.

Molnar, P., 1984. Structure and tectonics of the Himalaya: Constraints and implications of Geophysical data, In Annu. Rev. Earth Planet. Sci., vol.12, pp. 489-426.

Molnar, P., 1986. The Geologic history and structure of the Himalaya, American scientist, vol. 74, pp. 144-154.

Molnar, P., and Tapponnier, P., 1978. Active tectonics of Tibet, Journal of Geophysics Research, vol. 83, pp. 5361-5375.

Morton, A.C., and Hallsworth, C.R., 1999, Processes controlling the composition of heavy mineral assemblages in sandstone. Sedimentary Geology, vo., 124, pp. 3-29.

Mugnier, J.L, Leturmy, P., Mascle, G., Huygle, P., Chalaron, E., Vidal, G., Husson, L. and Delcaillau, B., 1999. The siwalik of Western Nepal: I. geometry and kinematics, Journal of Asian Earth Sciences, vol. 17 (5-6), pp. 629-642.

Müller, G. and Gastner, M., 1971. The "Karbonat-Bombe", a simple device for the determination of the carbonate content in sediments, soils and other materials, N. Jb. Miner. Mh., H. 10, pp. 466-469.

Murphy, D.H., and Wilkinson, B. H., 1980. Carbonate deposition and facies distribution in a central Michigan marl Lake, Sedimentology, vol. 27, pp. 123-135.

Nakayama, K., Ulak, P.D., 1999. Evolution of fluvial style in the Siwalik Group in the foothills of the Nepal Himalaya, Sedimentary Geology, vol. 125, pp. 205-224.

Narayanan, V., Anirudhan, S., and Grottoli, A.G., 2007. Oxygen and carbon isotope analysis of the Miocene limestone of Kerala and its implications to paleoclimate and its depositional setting, Current Science, vol. 93, No.8, pp. 1155-1159.

Nash, W.P., 1984. Phosphate minerals in terrestrial igneous and metamorphic rocks. In: Nriagu J. O., Moore, P. B. (Eds), Phosphate of the 6th Petroleum Geology Conference, Geological Society of London, pp. 957-967.

Nechaev, V.P., and Isohording, W.C., 1993. Heavy mineral assemblages of continental margins as indicators of plate tectonics environment, Journal of Sedimentary Petrology, vol. 63, pp. 1110-1117.

Niewodniczanski, J., Grabczak, J., Baranski, L., and Rzepka, J., 1981. The altitude effect on the isotopic composition of snow in high mountain, Journal of Glaciology, vol. 27, pp. 99-11.

Ogg, J.G., and von Rad, U., 1994. The Triassic of the Thakkhola (Nepal) II: Paleoaltitudes and Comparison with other Eastern Tethyan Margins of Gondwana, Geol. Rundsch, vol. 83, pp. 76-106.

Opdyke, N.D., Johnson, G.D., Lindsay, E.H., and Tahirkheli, R.A.K., 1982. Paleomagnetism of the Middle Siwalik Formations of northern Pakistan and rotation of the Salt Range Decollement, Palaeogeography, Palaeoclimatology, Palaeoecology, vol. 37, pp. 1–15.

Paul, K. and Guynn, J.H., 2004. Indian punch rifts Tibet, Geological Society of America vol. 32, no.11, pp. 993-996

Platt, J.P. and England, P.C., 1994. Convective removal of lithosphere beneath mountain belts: Therman and mechanical consequences, American Journal of Science, vol. 294, pp. 307-336.

Poage, M.A., and Chamberlain, C.P., 2001. Empirical relationships between elevation and the stable isotope composition of precipitation and surface waters: considerations for studies of paleoelevation change, American Journal of Sciences. vol. 301, pp. 1-15.

Pober, E. & Faupl, P., 1988. The chemistry of detrital chromian spinels and its implications for the geodynamic evolution of the Eastern Alps. geol. Runds., vol. 77, pp. 641-670.

Punt, W., Hoen, P.P., Blackmore, S., Nilsson, S., and Thomas, A. L., 2007. Glossary of pollen and spore terminology. Review of Palaeobotany and Palynology, vol. 143, pp.1-81.

Quade, J., Cerling, T.E., and Bowman, J., 1989. Development of Asian monsoon revealed by marked ecological shift during latest Miocene in northern Pakistan, Nature, vol. 342, pp 163-166.

Ramos-Guerrero, E., Berrio, I., Fernos, J. J., and Moragues, L., 2000. The middle Miocene Son Verdera lacustrine-lacustrine system (Santa Margalida Basin, Mallorca). In: Gierlowski-Kordesch, E. H., Kelts, K. R., (Eds), Lake Basins through Space and Time, American Association of Petroleum Geologists Studies in Geology, vol. 46, Tilsa, pp. 441-448.

Rankamma, K., 1963. Progress in Isotope Geology, John Wiley, New York, p. 705.

Rees, A. I., 1965. The use of anisotropy of magnetic susceptibility in the estimation of sedimentary fabric, Sedimentology, vol. 4, pp. 257-271.

Rittenhouse, G., and W. E. Bertholf, Jr., 1942. Gravity versus centrifuge separation of heavy minerals from sands, Journal of Sedimentary Petrology, vol. 12, pp. 85-89.

Rothery, D.A., and Drury, S.A., 1984. The neotectonics of the Tibetan plateau, Tectonics, vol. 3, pp. 19–26.

Rowley, D.B., Pierrehumbert, R.T., and Currie, B.S. 2001. A new approach to stable isotope-based paleoaltimetry: implications for paleoaltimetry and paleohypsometry

of the High Himalaya since the Late Miocene, Earth Planetary Science Letters*,* vol. 188, pp. 253-268.

Ruddiman, W.F, and Kutzbach, J.E., 1989. Forcing of late Cenozoic northern hemisphere climate by plateau uplift in southern Asia and The American west. Journal of Geophysical Research, vol. 94, pp. 18409-18427.

Ruddiman, W.F., and Kutzbach, J.E., 1990. Late Cenozoic uplift and climate change: Transactions of the Royal Society of Edinburgh, Earth Sciences, vol. 81, pp. 301–314.

Sah, R.B., Ulak, P.D., Gajurel, A.P., and Rimal, L.N., 1994. Lithostratigraphy of Siwalik sediments of Amlekhganj–Hetauda area, sub-Himalaya of Nepal, Himalayan Geology. vol. 15, pp. 37–48.

Sahagian, D.L., and Maus, J.E., 1994. Basalt vesiculatiry as a measure of atmospheric pressure and paleoelevation, Nature, vol. 372, pp. 449-451.

Saijo, K., and Tanaka, S., 2002. Paleosols of middle Holocene age in the Thakkhola basin, central Nepal, and their paleoclimatic significant, Journal of Asian Earth sciences, vol. 21, pp. 323-329.

Scholle, P.A., 1978. A color illustrated guide to constituents, texture, cements and porosities of sandstones and associated rocks, American Association of Petroleum Geologists, (AAPG Memoir 28), 201p.

Schwab, F.L., 1975. Framework mineralogy and chemical composition of continental margin-type sandstone, Geology, vol., pp. 487-490.

Serle, M.P., Windley, B.F., Cward, M.P., Cooper, D.J.W., Rex, A.J., Rex, D., Tingdong, L., Xuchang, X., Jan, M.Q, Thakur, V.C., and Kumar, S., 1987. The closing of Tethys and the tectonics of the Himalaya, Geological Society of America Bulletin, vol. 98, n.6, pp. 678-701, 7 figs. Boulder.

Sharma, C.K., 1977. Geology of Nepal, Educational Enterprises, Kathmandu, 164 p.

Shi, G.R., and Chen, Z.Q, 2006. Lower Permian oncolites from South China: Implications for equatorial sea-level responses to Late Palaeozoic Gondwana glaciation, Journal of Asian Earth Sciences, vol., 26. pp. 424-436.

Siegenthaler, U., and Oeschger, H., 1980. Correlation of ^{18}O in precipitation with temperature and altitude, Nature, vol. 285, pp. 189-223.

Singh, B.P., Pawar, J.S., and Karlupia, S.K., 2004. Dense mineral data from the northwest Himalayan foreland sedimentary rocks and recent river sediments: evaluation of the hinterland, Journal of Asian Earth Sciences, vol. 23, pp. 25-35.

Smith, N., D., 1972. Some sedimentological aspects of planar cross-stratification in a sandy braided river, Journal of Sedimentary Petrology, vol. 42, pp. 624-634.

Sohn, Y. K., Thee, C. W., Kim, B. C., 1999. Debris flow and hyperconcentrated flood-flow deposits in an alluvial fan, northwestern part of the Cretaceous Yongdong Basin, Central Korea. J. Geol., vol. 107, pp. 107-132.

Sorkhabi, R. B., Arita, K., 1997. Towards a solution for the Himalayan puzzle: mechanism of inverted metamorphism constrained by the Siwalik sedimentary records, Current Science, vol. 72 (11), pp. 862-873.

Stoliczka, A., 1966. Summary of the geological observation during a visit to the provinces Rupshu Karnag, South Ladakh, Zanskar, Sumdo and Dras of western Tibet, Mem. Geol. Survey India, vol. 5, pp. 337-354, Calcutta.

Sun, X.J., Wang, F.Y., Song, C.Q., 1996. Pollen-climate response surfaces of selected taxa from Northern China, Science in China, Series D 39 (5), pp. 486-493.

Talbot, M.R., 1990. A review of the paleohydrological interpretation of carbon and oxygen isotopic ratios in primary lacustrine carbonates. Chemical Geology, vol. 80, pp. 261– 279.

Talbot, M.R., and Kelts, K., 1990. Paleolimnological signatures from carbon and oxygen isotopic ratios in carbonates from organic carbon-rich lacustrine sediments. Lacustrine Basin Exploration: case Studies and Modern Analogs, AAPG Memoir, vol. 50, pp. 99–112.

Tapponnier, P., Zhiqin, Xu., Roger, F., Meyer, B., Arnaud, N., Wittlinger, G. and Jingsui, Y., 2001. Oblique stepwise Rise and Growth of the Tibet plateau, Science, vol. 294, pp. 167-177.

Tater, J.M., 1968. Ammonites from Muktinath area, Kathmandu, Department of Mine and geology, pp.1-10.

Thomas, E., 2008. http://ethomas.web.wesleyan.edu/ees123/carboniso.htm

Tokuoka, T., Takayasu, K., Yoshida, M. and Hisatomi, K., 1986. The Churia (Siwalik) Group in the Western part of the Arung Khola area, West Central Nepal, Mem. Fac. Shim. Univ., vol. 22, pp. 131–143.

Traverse, A., 2007. Paleopalynology. Topics in Geobiology, vol. 28. 813 p.

Tucker, M.E., 1981. Sedimentary Petrology, In: An introduction. New York. 252 p.

Ullah, K., Arif, M., and Shah, M.T., 2006. Petrography of Sandstones from the Kamlial and Chinji Formations, southwestern Kohat Plateau, NW Pakistan: Implications for Source Lithology and Paleoclimate, Journal of Himalayan Earth Sciences, vol. 39, pp. 1-13.

Upreti, B.N. 1996. Stratigraphy of the western Nepal Lesser Himalaya: a synthesis, Journal of Nepal Geological Society, vol. 13, pp. 11-28.

Upreti, B.N. 1999. An overview of the stratigraphy and tectonics of the Nepal Himalaya, Journal of Asian Earth Sciences, vol. 17, pp. 577-606.

Upreti, B.N. and Le Fort, P. 1999. Lesser Himalayan crystalline nappe of Nepal: Problems of their origin, Geological Society of America Special Paper, vol. 328, pp. 225-238.

Urey, H.C., 1948. Oxygen isotopes in nature and in the laboratory, Science, vol. 108. pp. 489-496.

Valdia, K.S, 1989, Trans-Himadri intracrustal fault and basement upwards south of the Indus-Tsangpo Suture Zone, Progress in Physical Geography, vol. 26, 3, pp. 360-399.

Von Rad, U., Dürr, S.B., Ogg, J.G., and Widermann, J., 1994. The Triassic of the Thakkhola (Nepal) I: stratigraphy and paleoenvironment of a northeast Gondwanan rifted margin, Geol Rundsch, vol. 83, pp. 76-106.

Wang, F.B., Li, S.F., Shen, X.H., Zhang, J., and Yan, G. 1996. Formation, evolution and environmental changes of the Gyirong Basin and uplift of the Himalaya. Science in China (Series D)*,* vol. 39, pp. 401-409.

Wang, K.F., Wang, X.Z., 1983. Palynology Conspectus. Beijing University Press, Beijing.

Waterhouse, J.B., 1966. Lower Carboniferous and Upper Permian brachiopods from Nepal, Jb. Geol. Bundesanst Sonderbd., vol. 12, pp. 5- 99.

Waterhouse, J.B., 1978. Permian brachiopod and mollusca from north-west Nepal. Paleontographica Abteilung A. 160, pp. 1-175.

Webb, T., III and McAndrews, J.H., 1976. Corresponding patterns of contermporary pollen and vegetation in central North America, Geological Society of America memoir, vol. 145, pp. 267-299.

Yin, A., 2000, Mode of Cenozoic east-west extension in Tibet suggesting a common origin of rifts in Asia during the Indo-Asian collision, Journal of Geophysical Research, vol. 105, N.B9, pp. 21745-21759.

Yin, A., Kapp, P., Murphy, M., Manning, C.E., Harrison, T.M., Ding, L., Deng., X., and Wu, C., 1999. Evidence for significant late Neogene east-west extension in north Tibet, Geology, vol. 27, pp. 787-790.

Yoshida, M., Igarashi, Y., Arita, K., Hayashi, D., and Sharma, T., 1984. Magnetostratigraphy and pollen analytic studies of the Takmar series, Nepal Himalayas, Journal of Nepal Geological Society, vol. 4,   pp. 101-120 (Special Issue).

Zetter, R., 1989. Methodik und Bedeutung einer routinemäßig kombinierten lichtmikroskopischen und rasterelektronenmikroskopischen Untersuchung fossiler Mikrofloren, Cour. Forschungsinst. Senckenb. vol. 109 , pp. 41–50.

Zetter, R., Ferguson, D.K., 2001. Trapaceae pollen in the Cenozoic, Acta Palaeobot. vol. 41, pp. 321–339.

Zimmerle, W., 1984. The geotectonic significance of detrial brown spinel in sediments, Mitteilungen aus dem Geologisch-Paläontologischen Institute der Universtät Hamburg, vol. 56, pp. 337-360.

Appendix
Plate I-Plate IX
(Pollen records from the Tetang and Thakkhola formations)

EXPLANATION OF PLATE
PLATE I

Fig. 1.   **Lycopodiaceae, LM**
Fig. 2.   **Lycopodiaceae, SEM**
Fig. 3.   **Polypodiaceae, LM**
Fig. 4.   **Polypodiaceae, LM**
Fig. 5.   **Pteris sp., LM**

1

— 10 μm

2

20 μm

3

— 10 μm

4

— 10μm

5

— 10μm
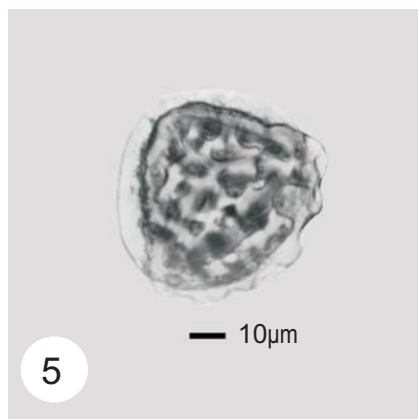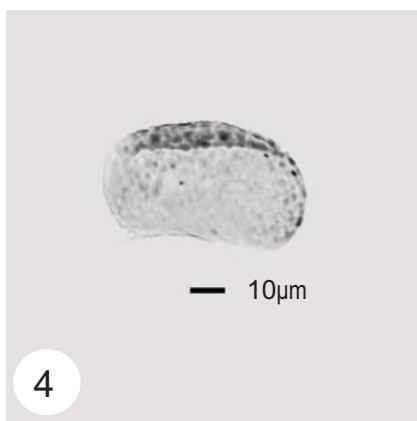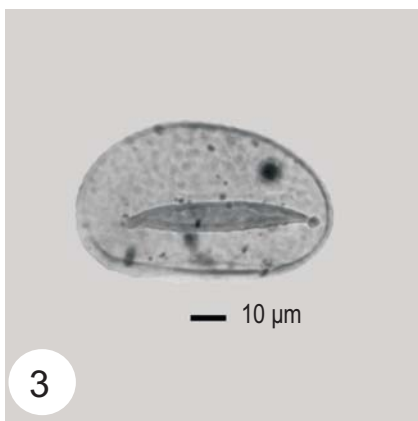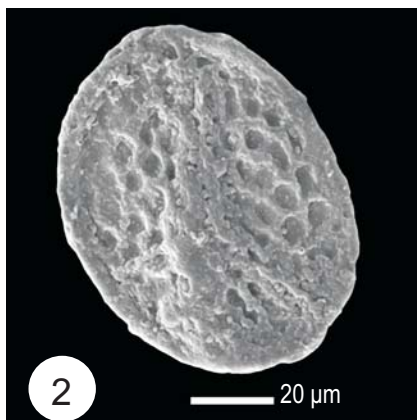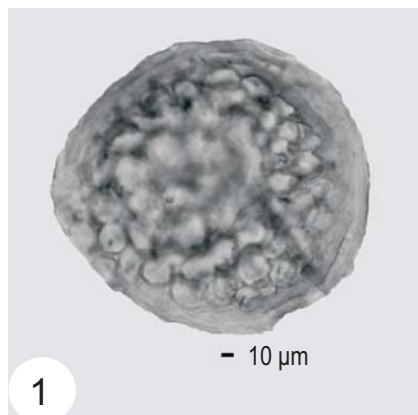
PLATE I

EXPLANATION OF PLATE
PLATE II

Fig. 6.	*Abies sp*.
Fig. 7.	*Keteleeria sp.*
Fig. 8.	*Picea* **sp., Equatorial view**
Fig. 9a.	*Pinus* **sp., Equatorial view, LM X 600**
Fig. 9b.	*Pinus* **sp., Polar view, LM X 600**
Fig. 9c.	*Pinus* **sp., Polar view, SEM**
Fig. 9d.	*Pinus* **sp., Detaile view of tectum, SEM**
Fig. 10a.	*Tsuga* **sp., Polar view, LM X 600**
Fig. 10b.	*Tsuga* **sp., Polar view, SEM X 1400**
Fig. 10c.	*Tsuga* **sp., Detail view of Tectum, SEM X 4300**
Fig. 11a.	*Quercus* **sp., Equatorial view, LM X 600**
Fig. 11b.	*Quercus* **sp., Polar view, LM X 600**
Fig. 11c.	*Quercus* **sp., Polar view, SEM X 2500**
Fig. 11d.	*Quercus* **sp., Detail view of Tectum, SEM X 14000**

6

7

8

9a

9b

9c

9d

10a

10b

10c

11a

11b

11c

11d
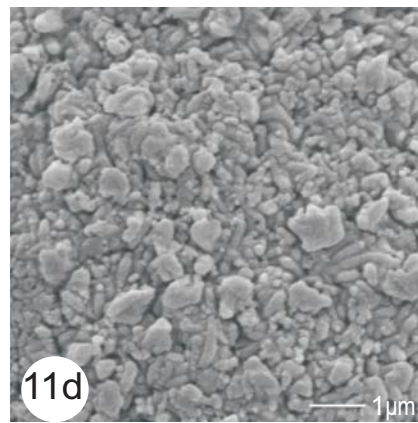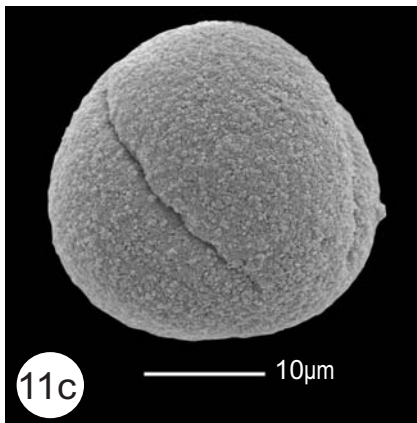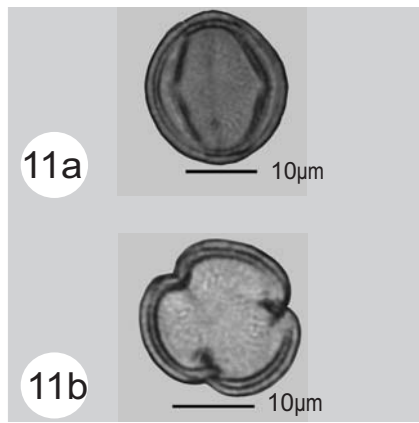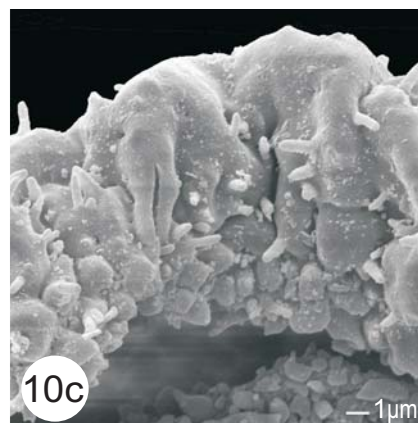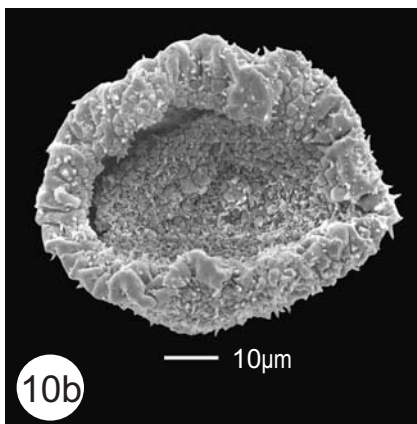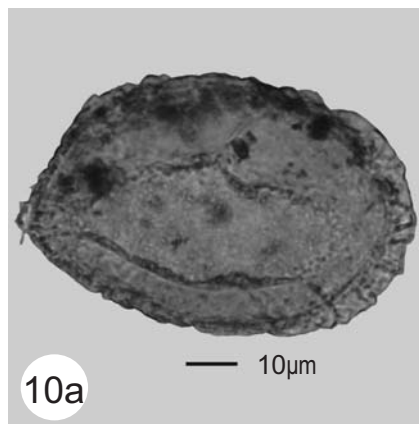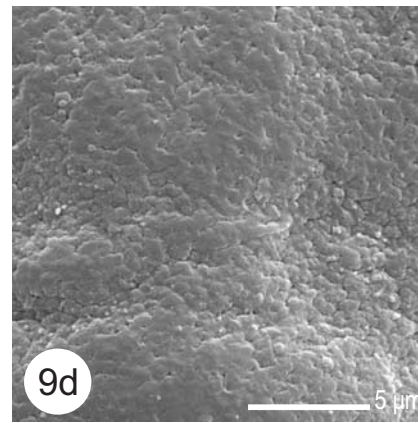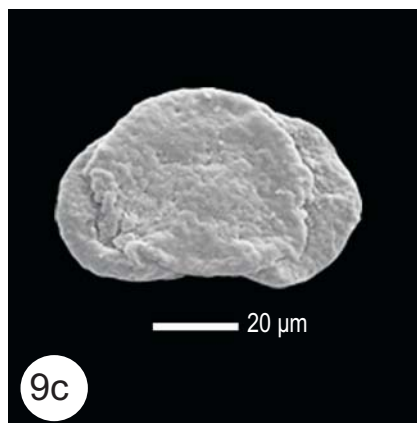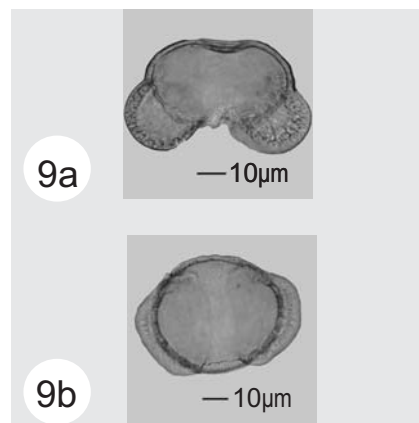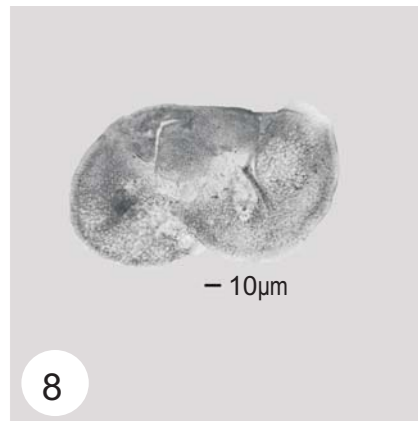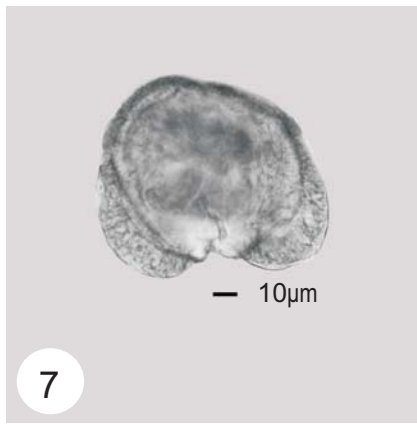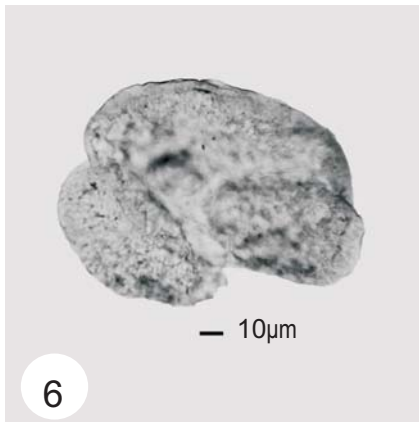
PLATE II

EXPLANATION OF PLATE
PLATE III

Fig. 12a.   *Quercus* **sp., Equatorial view, LM X 600**
Fig. 12b.   *Quercus* **sp., Polar view, LM X 600**
Fig. 12c.   *Quercus* **sp., Polar view, SEM X 3000**
Fig. 12d.   *Quercus* **sp., Detail view of Tectum, SEM X 14000**
Fig.. 13a.   *Fagus* **sp., Equatorial view, LM X 600**
Fig. 13b.   *Fagus* **sp., Polar view, LM X 600**
Fig. 13c.   *Fagus* **sp., Equatorial view, SEM X 2200**
Fig. 13d.   *Fagus* **sp., Detail view of Tectum, SEM X10000**
Fig. 14a.   **Fagaceae (?), Equatorial view, LM X 600**
Fig. 14b.   **Fagaceae (?), Equatorial view, SEM X 2700**
Fig. 14c.   **Fagaceae (?), Detail view of Tectum, SEM X 14000**
Fig. 15a.   *Juglans* **sp., LM X 600**
Fig. 15b.   *Juglans* **sp., SEM X 1900**
Fig. 15c.   *Juglans* **sp., Detail view of Tectum, SEM X 10000**

12a   10µm

12b   10µm

12c   10µm

12d   1µm

13a   10µm

13b   10µm

13c   10µm

13d   1µm

14a   10µm

14b   10µm

14c   1µm

15a   10µm

15b   10µm

15c   1µm
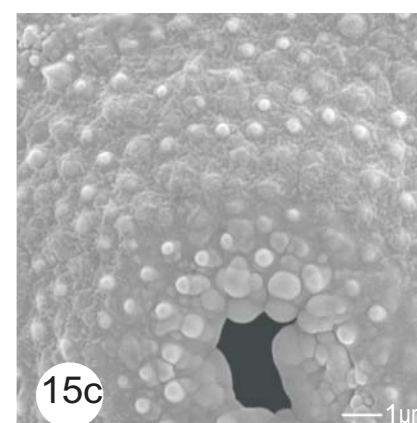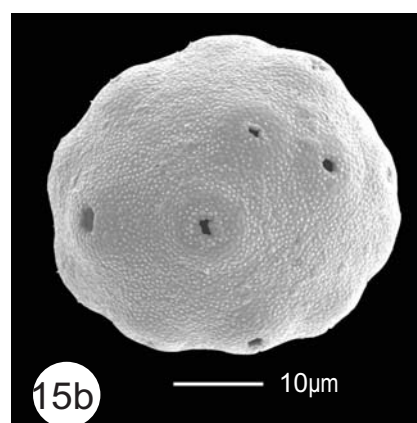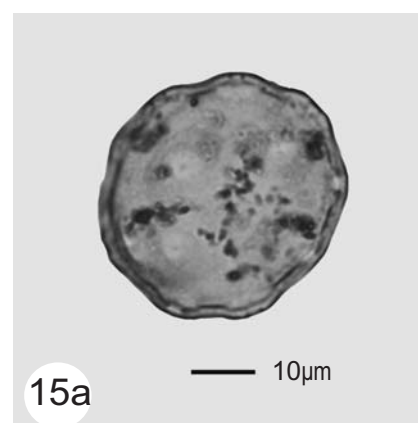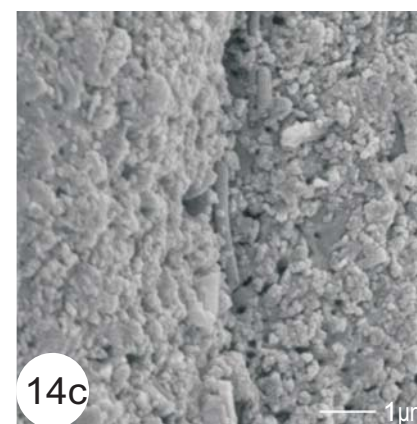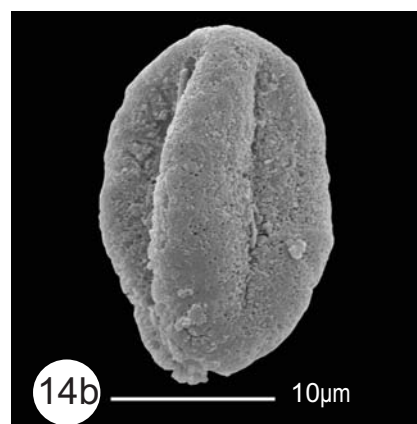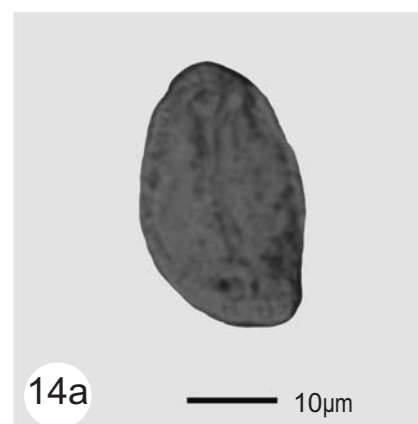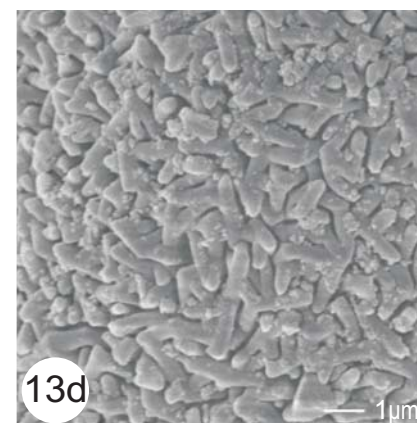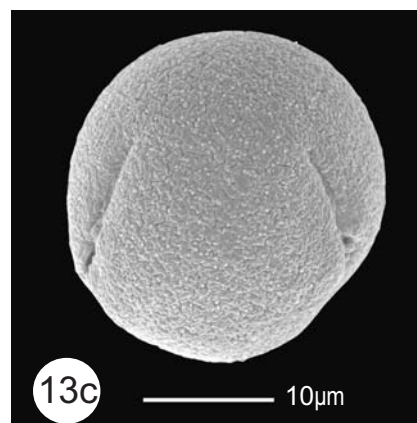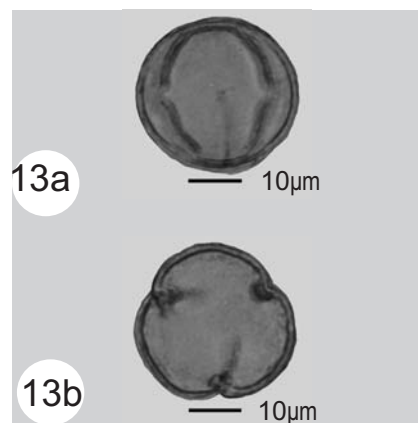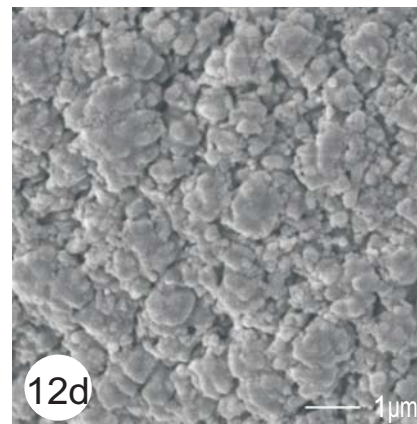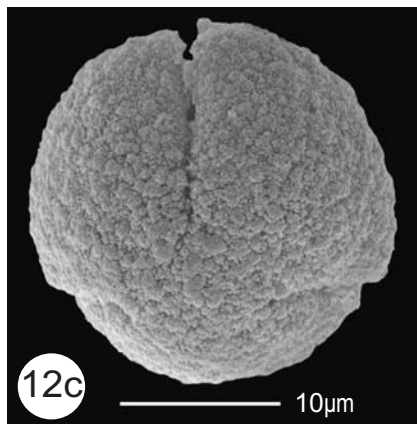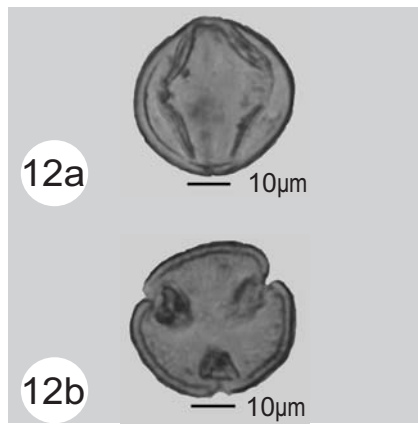
PLATE III

EXPLANATION OF PLATE
PLATE IV

Fig. 16a.   *Alnus*.sp., Polar view, LM X 600
Fig. 16b.   *Alnus* sp., Polar view, SEM X 3700
Fig. 16c.   *Alnus* sp., Detail view of Tectum, SEM X 14000
Fig. 17a.   *Betula* sp., Polar view, LM X 600
Fig. 17b.   *Betula* sp., Polar view, SEM X 4000
Fig. 17c.   *Betula* sp., Detail view of Tectum, SEM X 14000
Fig. 18a.   *Tilia* sp., Polar view, LM X 600
Fig. 18b.   *Tilia* sp., Polar view, SEM X 2000
Fig. 18c.   *Tilia* sp., Detail view of Tectum, SEM X 10000
Fig. 19a.   *Salix* sp., Equatorial view, LM X 600
Fig. 19b.   *Salix* sp., Polar view, LM X 600
Fig. 19c.   *Salix* sp., Equatorial view, SEM X 3300
Fig. 19d.   *Salix* sp., Detail view of Tectum, SEM X 17000

16a   — 10μm

16b   — 10μm

16c   — 1μm

17a   — 10μm

17b   — 10μm

17c   — 1μm

18a   — 10μm

18b   — 10μm

18c   — 1μm

19a   — 10μm

19b   — 10μm

19c   — 10μm

19d   — 1μm

PLATE IV
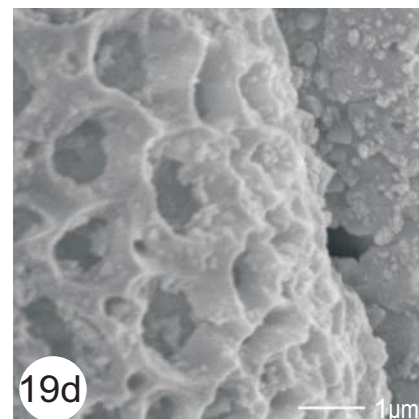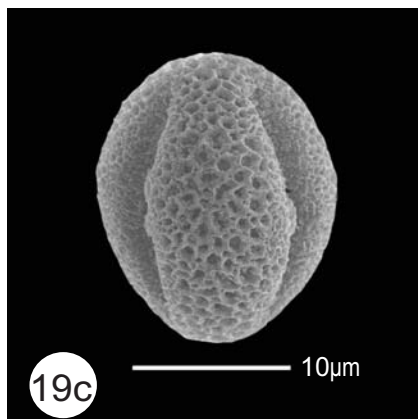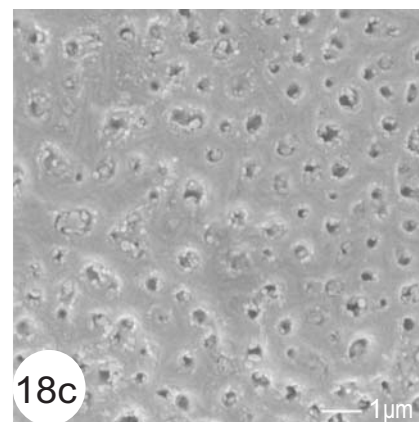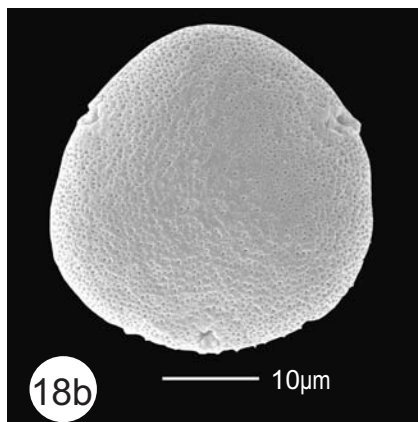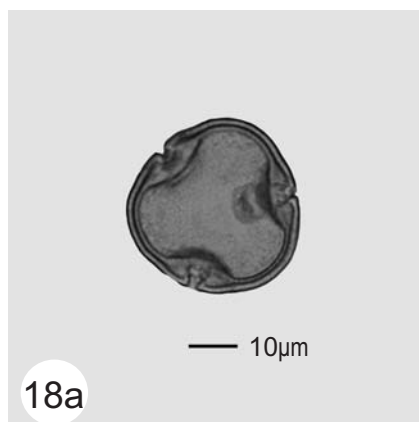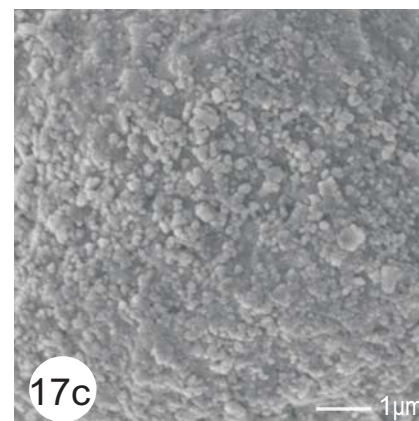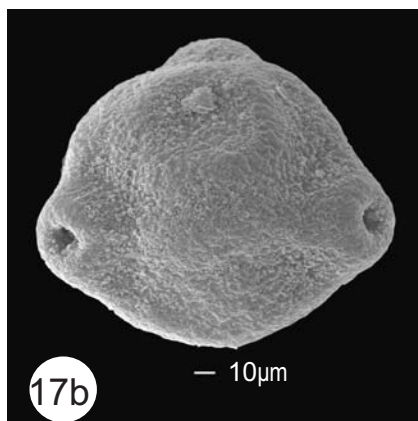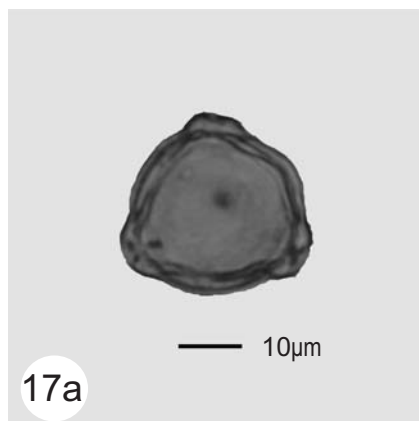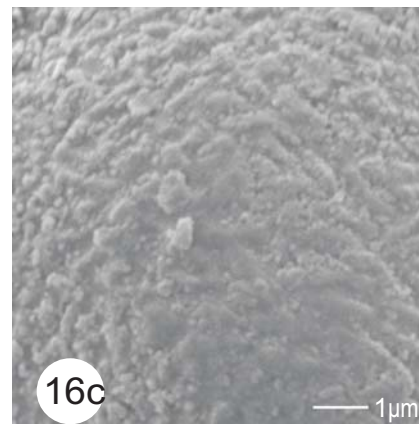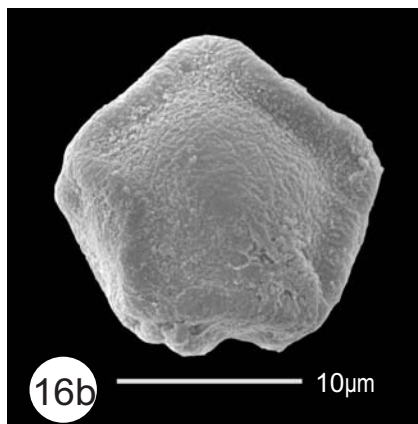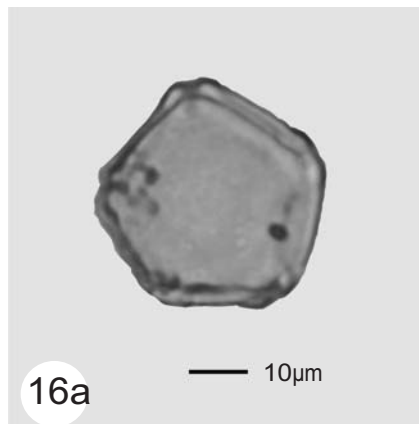
EXPLANATION OF PLATE

PLATE V

Fig. 20a.   *Acer* sp., Polar view, LM X 600

Fig. 20b.   *Acer* sp., Equatorial view, SEM X 3000

Fig. 20c.   *Acer* sp., Detail view of Tectum, SEM X 14000

Fig. 21a.   Oleaceae (Fraxinus), Polar view, LM X 600

Fig. 21b.   Oleaceae, Equatorial view, SEM X 3000

Fig. 21c.   Oleaceae, Detail view of Tectum, SEM X 10000

Fig. 22a.   Oleaceae (Fraxinus), Equatorial view, LM X 600

Fig. 22b.   Oleaceae, Polar view, LM X 600

Fig. 22c.   Oleaceae, Polar view, SEM X 2500

Fig. 22d.   Oleaceae, Detail view of Tectum, SEM X 14000

Fig. 23a.   Oleaceae (Ligustrum), Equatorial view, LM X 600

Fig. 23b.   Oleaceae, Polar view, LM X 600

Fig. 23c.   Oleaceae, Equatorial view, SEM X 3300

Fig. 23d.   Oleaceae, Detail view of Tectum, SEM X 14000

20a

20b 10µm

20c 1µm

21a 10µm

21b 10µm

21c 1µm

22a 10µm

22b 10µm

22c 10µm

22d 1µm

23a 10µm

23b 10µm

23c 10µm

23d 1µm
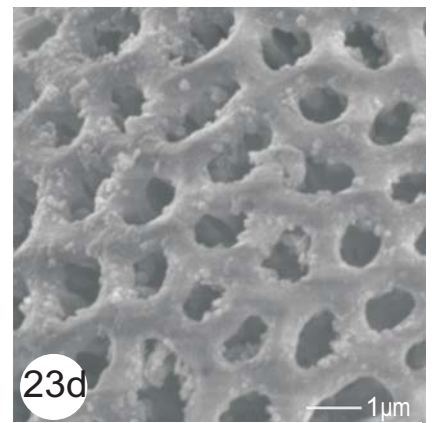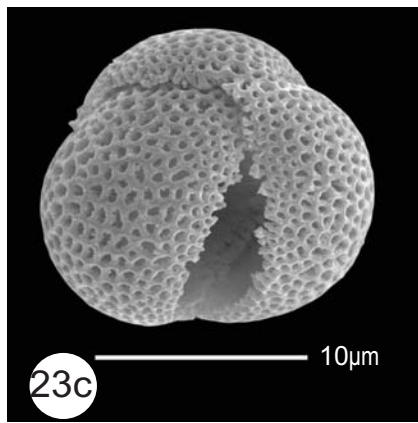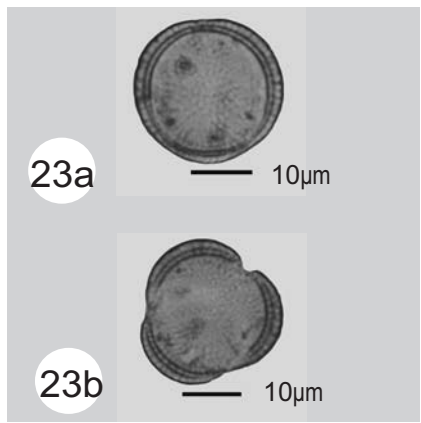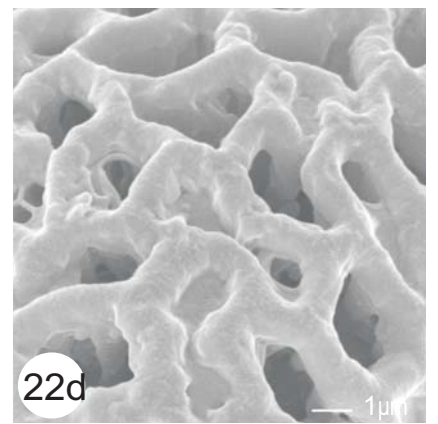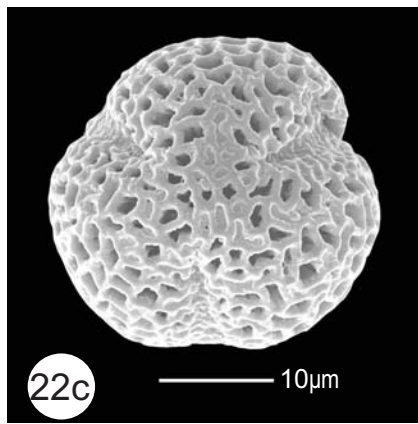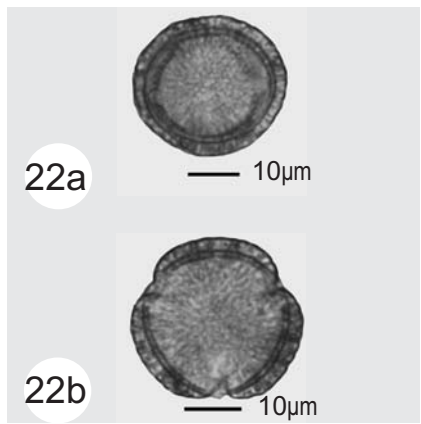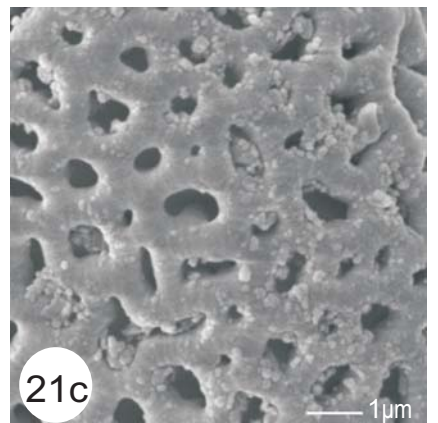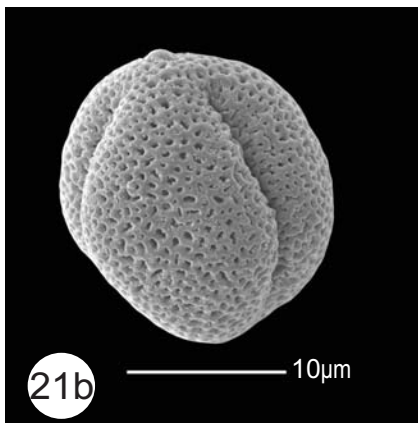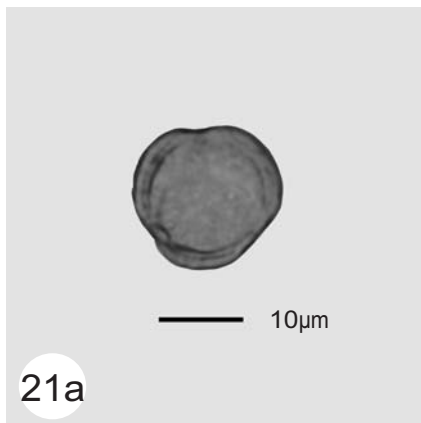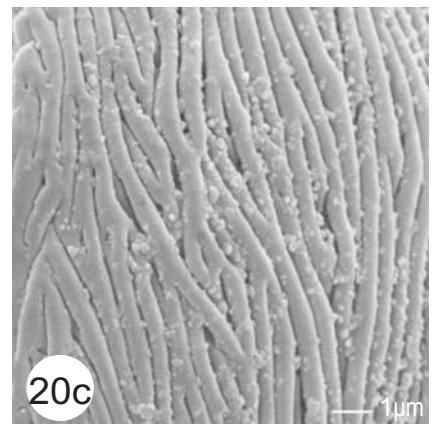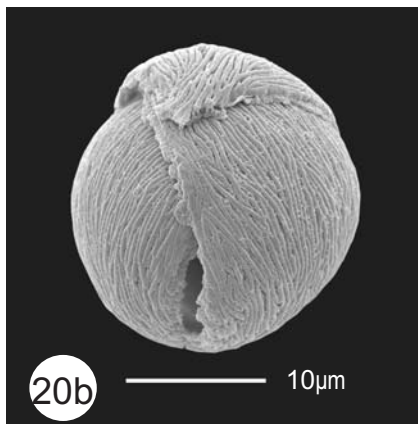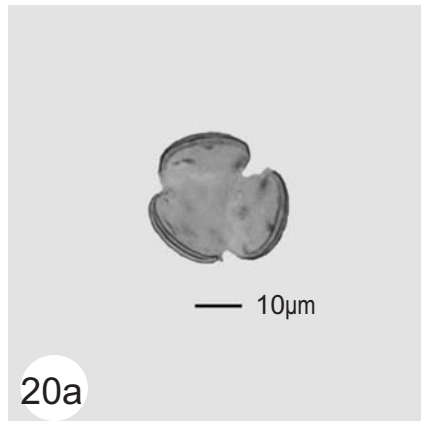
PLATE V

EXPLANATION OF PLATE
PLATE VI

Fig. 24a.   **Caryophyllaceae, LM X 600**
Fig. 24b.   **Caryophyllaceae, SEM X 4300**
Fig. 24c.   **Caryophyllaceae, Detail view of Tectum, SEM X 10000**
Fig. 25a.   **Rosaceae, Polar view, LM X 600**
Fig. 25b.   **Rosaceae, Equatorial view, SEM X 3300**
Fig. 25c.   **Rosaceae, Detail view of Tectum, SEM X 14000**
Fig. 26a.   **Rosaceae, Equatorial view, LM X 600**
Fig. 26b.   **Rosaceae, Polar view, LM X 600**
Fig. 26c.   **Rosaceae, Equatorial view, SEM X 2700**
Fig. 26d.   **Rosaceae, Detail view of Tectum, SEM X 14000**
Fig. 27a.   **Parthenocissus sp., Equatorial view, LM X 600**
Fig. 27b.   **Parthenocissus sp., Polar view, LM X 600**
Fig. 27b.   **Parthenocissus sp., Equatorial view, SEM X 2000**
Fig. 27d.   **Parthenocissus sp., Detail view of Tectum, SEM X 8500**

24a — 10μm

24b — 10μm

24c — 1μm

25a — 10μm

25b — 10μm

25c — 1μm

26a — 10μm

26b — 10μm

26c — 10μm

26d — 1μm

27a — 10μm

27b — 10μm

27c — 10μm

27d — 1μm
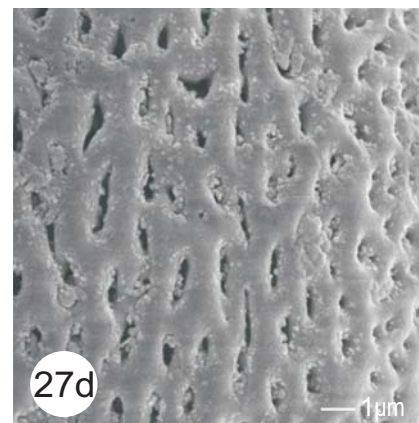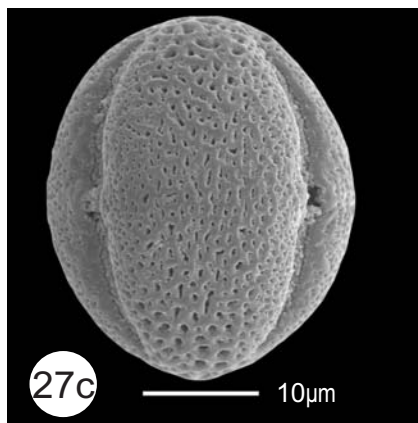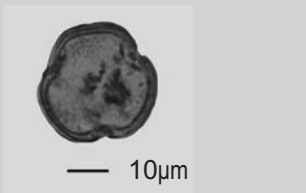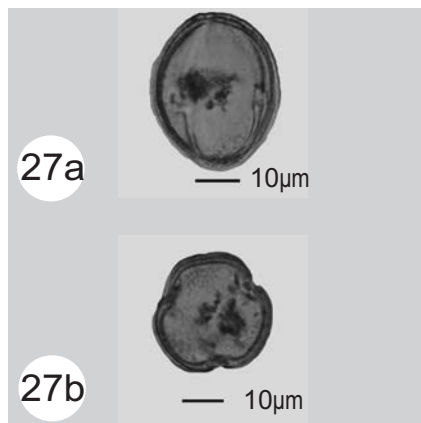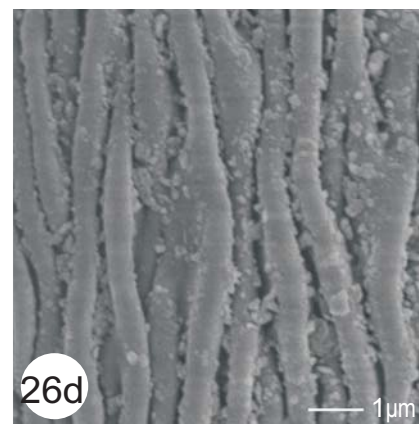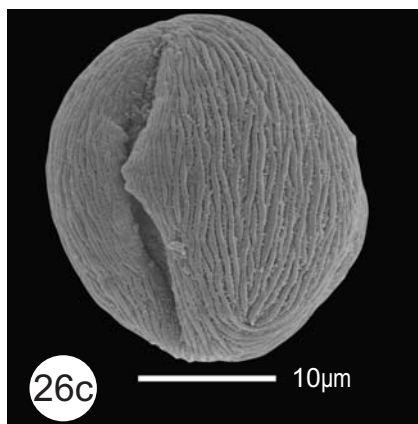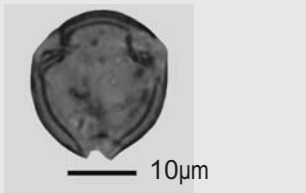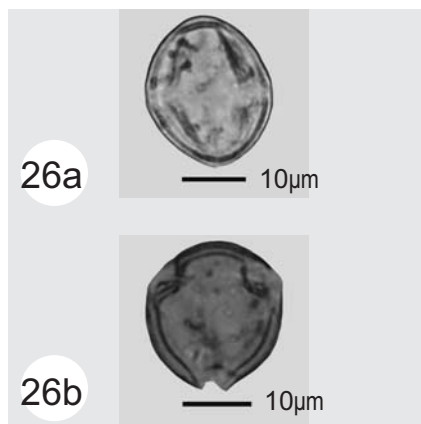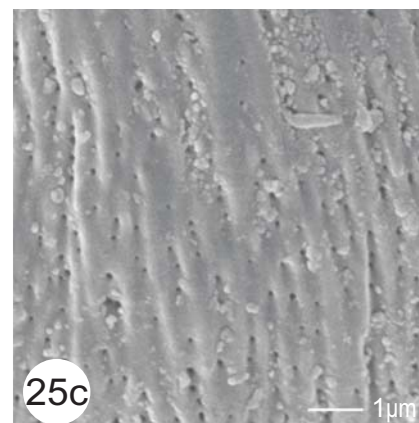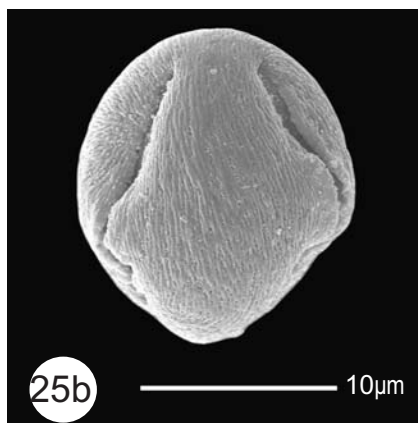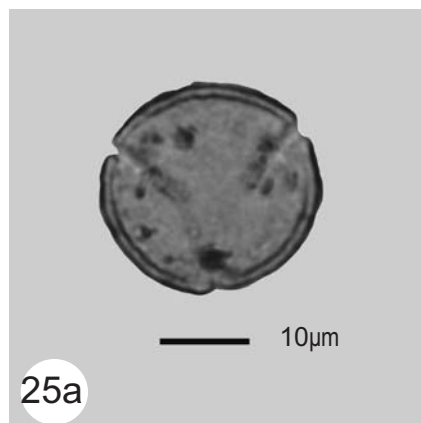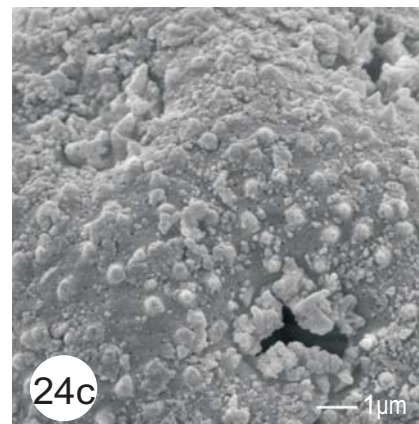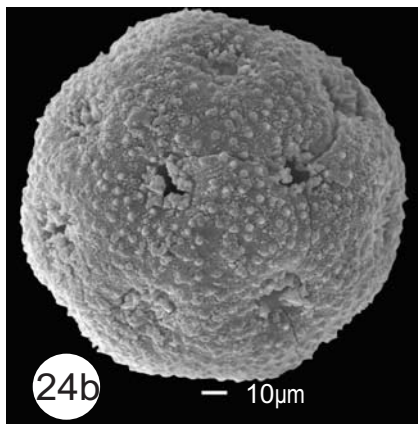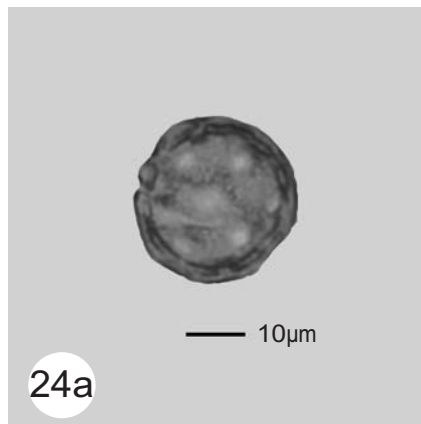
PLATE VI

EXPLANATION OF PLATE
PLATE VII

Fig. 28a.	**Vitaceae (?), Equatorial view, LM X 600**
Fig. 28b.	**Vitaceae (?), Polar view, LM X 600**
Fig. 28c.	**Vitaceae (?), Equatorial view, SEM X 2000**
Fig. 28d.	**Vitaceae (?), Detail view of Tectum, SEM X 10000**
Fig. 29a.	***Chenopodiaceae*, LM X 600**
Fig. 29b.	***Chenopodiaceae*, SEM X 3500**
Fig. 29c.	***Chenopodiaceae*, Detail view of Tectum, SEM X 14000**
Fig. 30a.	***Plantago* sp., LM X 600**
Fig. 30b.	***Plantago* sp., SEM X 3500**
Fig. 30c.	***Plantago* sp., Detail view of Tectum, SEM X 10000**
Fig. 31a.	**Poaceae, LM X 600**
Fig. 31b.	**Poaceae, SEM X 3500**
Fig. 31c.	**Poaceae, Detail view of Tectum, SEM X 10000**
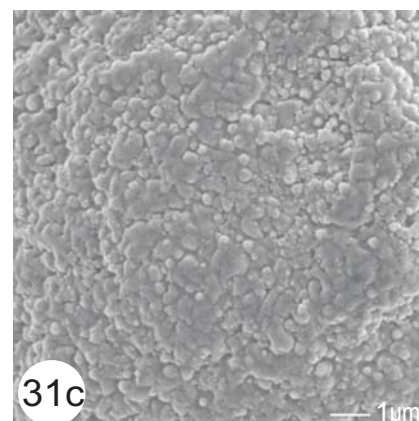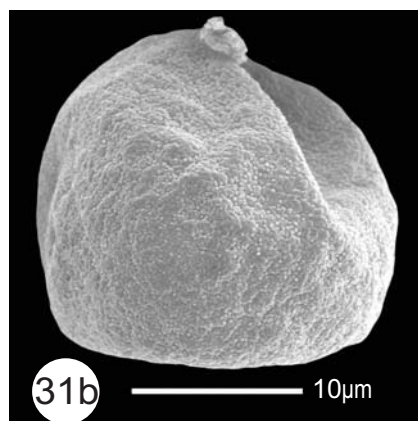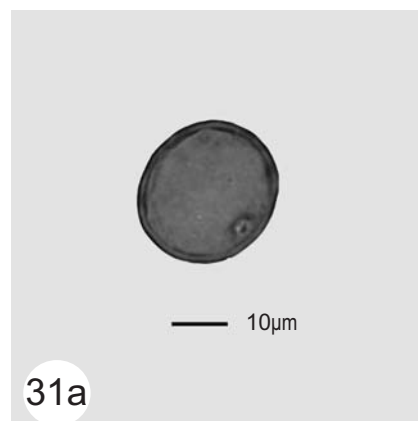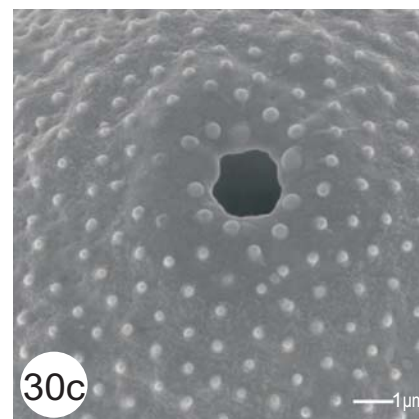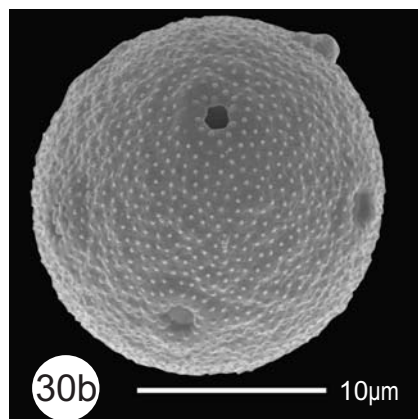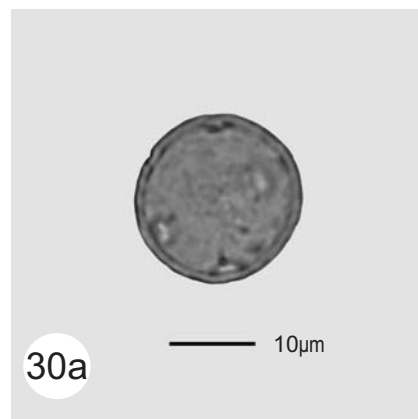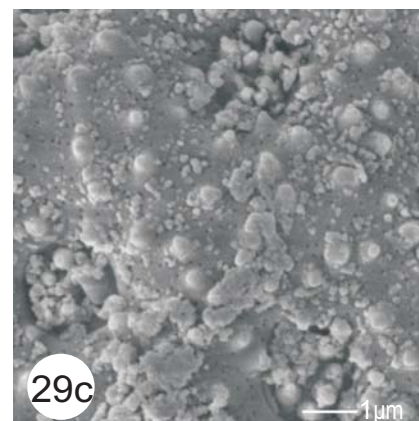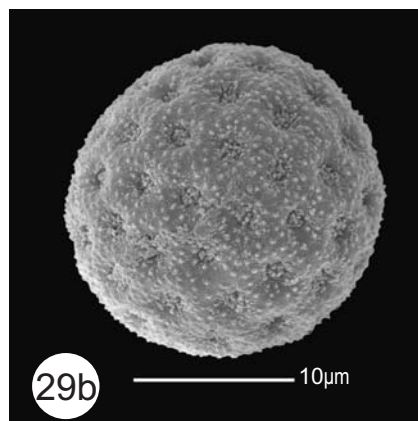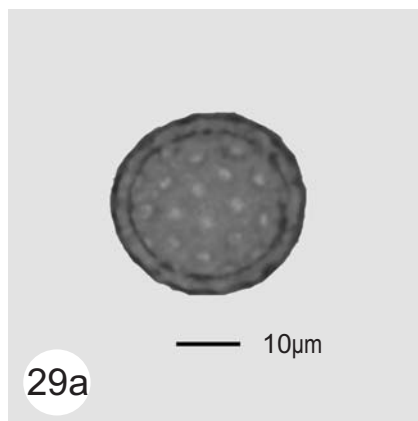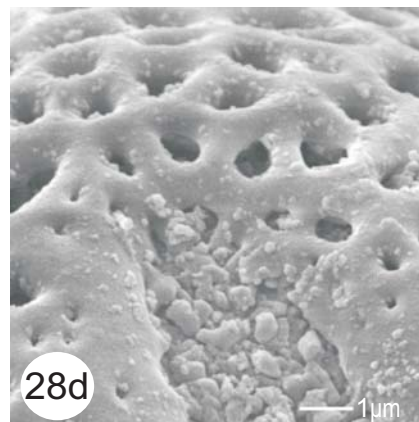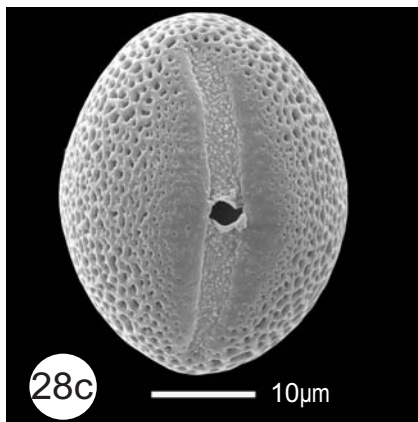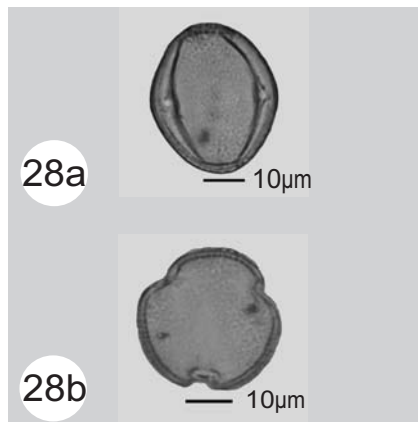
PLATE VII

EXPLANATION OF PLATE
PLATE VIII

Fig. 32a.　　　**Compositae, Polar view, LM X 600**
Fig. 32b.　　　**Compositae, Polar view, SEM X 3500**
Fig. 32c.　　　**Compositae, Detail view of Tectum, SEM X 8500**
Fig. 33a.　　　**Compositae, Equatorial view, LM X 600**
Fig. 33b.　　　**Compositae, Equatorial view, SEM X 2300**
**Fig. 33c.**　　　**Compositae , Detail view of Tectum, SEM X 10000**
Fig. 34a.　　　**Compositae, Polar view, LM X 600**
Fig. 34b.　　　**Compositae, Polar view, SEM X 3300**
Fig. 34c.　　　**Compositae, Detail view of Tectum, SEM X 10000**
Fig. 35a.　　　**Compositae, Polar view, LM X 600**
Fig. 35b.　　　**Compositae, Equatorial view, SEM X 4300**
Fig. 35c.　　　**Compositae, Detail view of Tectum, SEM X 14000**

32a

32b

32c

33a

33b

33c

34a

34b

34c

35a

35b

35c

PLATE VII
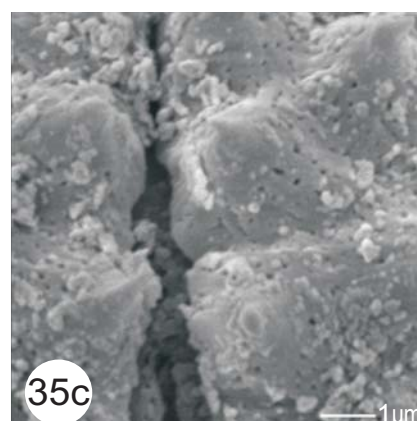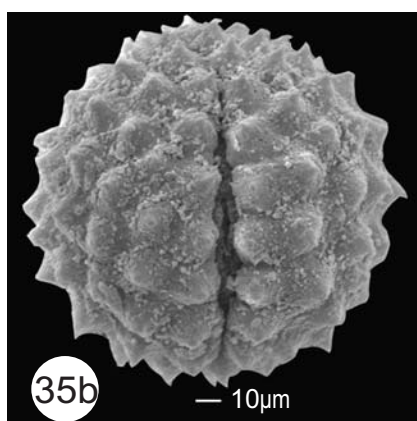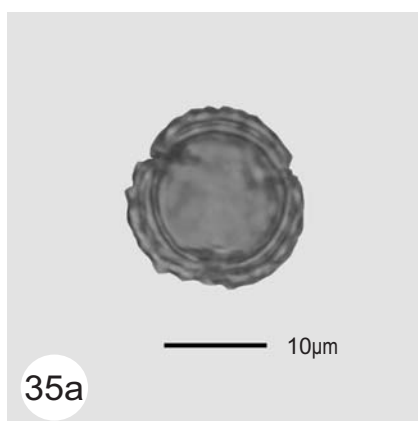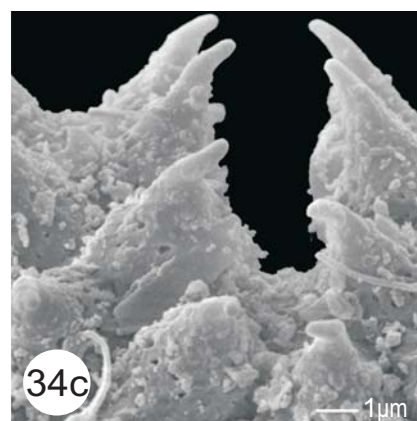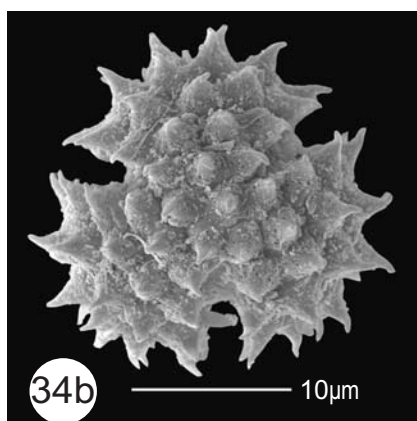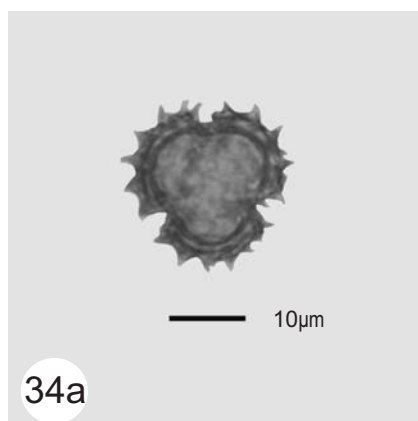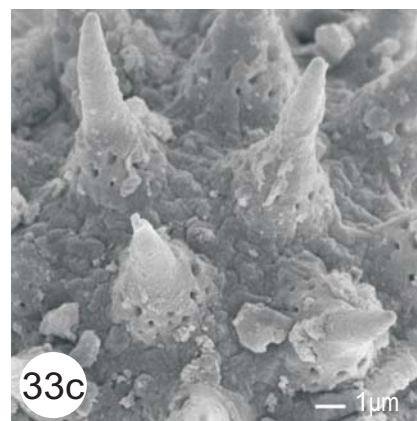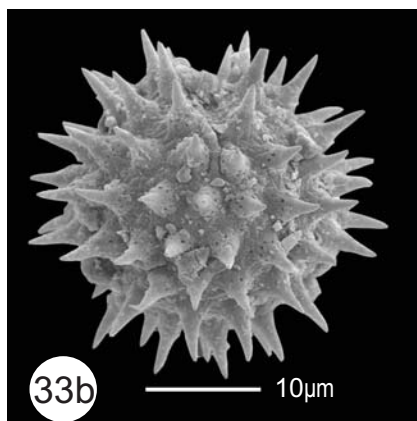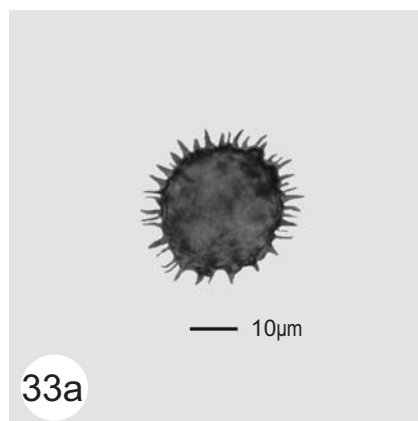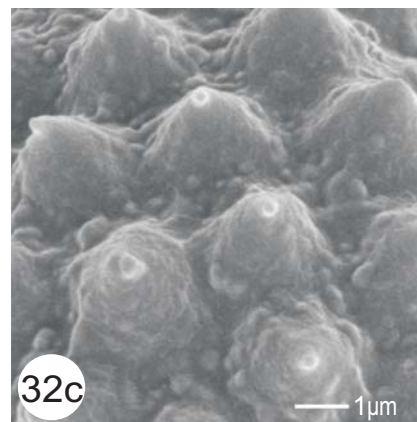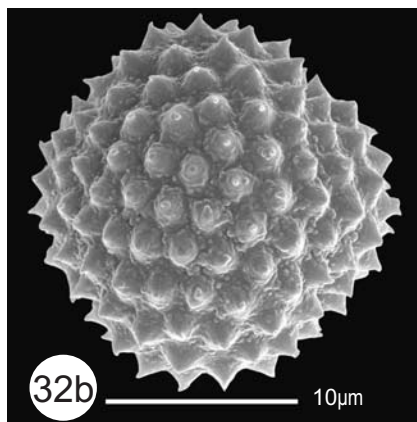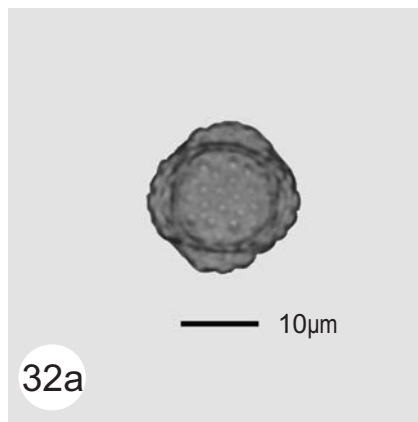
EXPLANATION OF PLATE
PLATE IX

Fig. 36a.   *Artemisia* **sp.,**
Fig. 36b.   *Artemisia* **sp., Polar view, SEM X 4500**
Fig. 36c.   *Artemisia* **sp., Detail view of Tectum, SEM X 14000**
Fig. 37a.   **Unidentified, Polar view, LM X 600**
Fig. 37b.   **Unidentified, Detail view, SEM X 2500**
Fig. 37c.   **Unidentified, Detail view of tectum, SEM X 14000**

36a

10µm

36b ⎯10µm

36c 1µm

37a 10µm

37b 10µm

37c 1µm

PLATE IX
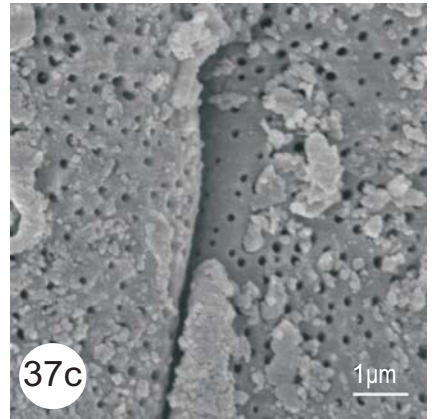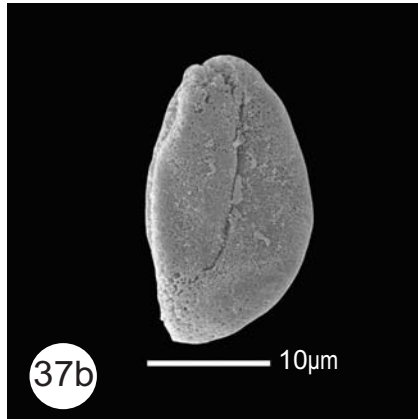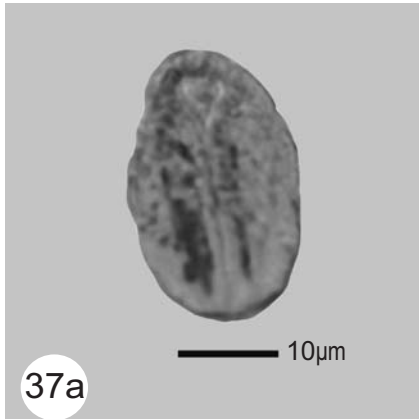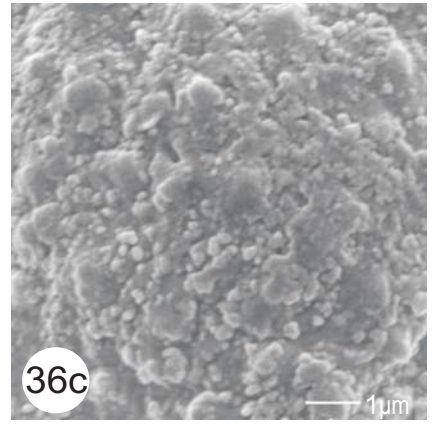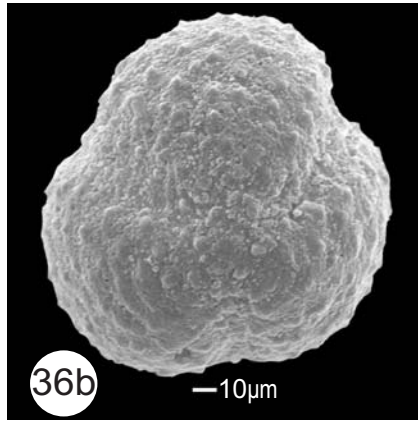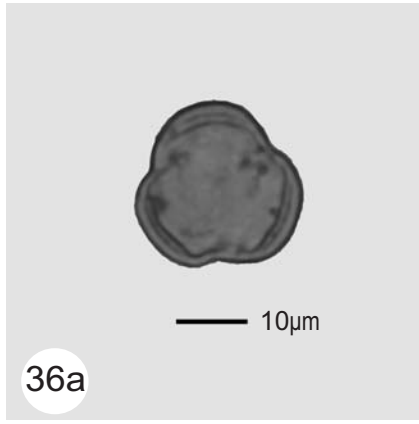
Curriculum Vitae

Personal data

Name:	Basanta Raj Adhikari, M.Sc.
Permanent address:	Lekhanath-10, Begnas, Kaski, Nepal
Date of Birth:	11-30-1980
Nationality:	Nepali
Email:	basanta58@yahoo.com
Personal web page:	http://basantarajadhikari.webs.com

Education:

1986-1996:	Secondary School, Shree Ananda Jyoti Secondary School, Begnas, Kaski
1996- 1998:	Intermediate in Science, Prithivi Narayan Campus, Pokhara, Nepal.
1998- 2001:	Bachelor's degree in science with major geology, botany and Zoology, Tri-chandra Multiple Campus, Nepal.
2001-2003:	Master's degree in Geology with major mapping and analysis, Central Department of Geology, Tribhuvan University.
Oct. 2006-Dec.2009:	PhD thesis in Department of Geodynamics and Sedimentology, University of Vienna, Austria supervised by Ao. Prof. Dr. Michael Wagreich in topic "Sedimentology and Basin analysis of Thakkhola-Mustang Graben, central Nepal"

Research Interest:

Basin analysis
Sedimentology
Himalayan Tectonics
Paleoclimate

Publications

Paper

Adhikari, B. R., and Tamrakar, N. K., 2006, Bank instability and erosion problems of Bishnumati River, Kathmandu, Nepal, Nepal Geological Society, vol. 34, pp.109-116.

Abstracts

Adhikari, B. R., and Tamrakar, N. K., 2005, Bank instability and erosion problems of Bishnumati River, Kathmandu, Nepal," Journal of Nepal Geological Society, Abstract volume, (Vol. 32, Special Issue, Abstract volume).

Adhikari, B. R., and Wagreich, M., 2008, Sedimentation in the Cenozoic Thakkhola-Mustang Graben (central Nepal), Geophysical Research Abstracts, Vol. 10, EGU2008-A-01618, EGU General Assembly, Vienna, Austria.

Adhikari, B. R., and Wagreich, M., 2008, Palustrine limestone in the sedimentary succession of the Cenozoic Thakkhola-Mustang Graben (central Nepal), Journal of Alpine Geology, Vol. 49, pp 1-127 (3), Vienna, Austria.

Adhikari, B. R., and Wagreich, M., 2009, Provenance analysis of Neogene sediments in the Thakkhola-Mustang Graben (central Nepal), Geophysical Research Abstracts, Vol. 11, EGU 2009-2842, EGU General Assembly, Vienna, Austria.

Article

Adhikari, B. R., 2001, Topography of the Ocean Floor, GEOWORLD.